University of Nevada, Reno

Synthesis, Characterization, and Screening of Signal Peptide Dependent Inhibitors of the Sec61 Channel

A dissertation submitted in partial fulfillment of the

requirements for the degree of Doctor of Philosophy in

Cellular and Molecular Biology

by

Ryan Olsen

Dr. Thomas W. Bell/Dissertation Advisor

December 2023

THE GRADUATE SCHOOL

We recommend that the dissertation
prepared under our supervision by

Ryan Olsen

entitled

Synthesis, Characterization, and Screening of Signal Peptide Dependent Inhibitors of the Sec61 Channel

be accepted in partial fulfillment of the
requirements for the degree of

Doctor of Philosophy

Thomas Bell, Ph. D.
Advisor

David Aucoin, Ph.D.
Co-advisor

Wesley Chalifoux, Ph.D.
Committee Member

Robert Ryan, Ph.D.
Committee Member

Yftah Tal-Gan, Ph.D.
Graduate School Representative

Markus Kemmelmeier, Ph.D., Dean
Graduate School

December, 2023

Abstract

The classic approaches to medicinal chemistry have been greatly successful for the production of therapeutics in modern times. The most successful approach has been using small molecules to target proteins to disrupt their function. Most of these therapeutic targets fall in a narrow range of protein classes and have left many potential therapeutic targets without successfully developed drugs. New approaches will be necessary to fill this need. The Sec61 translocon channel located in the ER membrane provides a passageway for entry into the ER lumen or integration into the ER membrane for a large percentage of human proteins. A few compounds have been discovered to block translocation of proteins through this channel, but most are not specific and too toxic for development into drugs. Cyclotriazadisulfonamide (CADA) is so far the most specific inhibitor of the Sec61 mediated translocation owing largely to its unique ability to bind specific amino acid residues with the hydrophobic α-helical H-region of signal peptides. Signal peptides (SPs) are unique tags on the N-terminus of proteins which target them to the Sec61 channel for translocation. The purpose of this dissertation was to synthesize new CADA analogues with improved potency, explore the mechanism of action of TL020 towards reduction of HBV replication, and develop novel screening platforms for CADA analogues.

The strength of the dipole moment in its sidearm constituents has been shown to correlate with potency, likely owing to this specific interaction with the SP. Towards the first goal, nine new CADA analogues were synthesized with strong dipole moments in their sidearms to make highly potent CADA analogues. New and previously synthesized compounds were tested for their drug like properties of solubility, membrane permeability, and toxicity. CADA and its analogues are currently being developed as novel therapeutic agents for several diseases

including infection by hepatitis B virus (HBV). Towards the second goal, the effects on protein and mRNA expression levels of the potent CADA analogue, TL020, were explored on liver cells in an attempt to better understand the specificity and anti-HBV mechanism of action. Owing to the unique mechanism of CADA analogues it was necessary to develop novel screening assays to expand the list of disease targets for CADA analogues. Towards the third goal, cell-based assays were developed in 96-well plate format for finding potent drugs for SARS-CoV-2 and preterm labor. CADA has opened up a new window of possibilities for medicinal chemistry and it is possible that many other conditions can be targeted in the future by this novel approach.

Acknowledgements

It is important to acknowledge the many people whose support has made this dissertation possible. It is with great pleasure that I remember all those who have graciously helped me over this time. Dr. Thomas W. Bell is my advisor who has shown me the care, support, and dedication required to bring a student to the level of knowledge and skill I am at today. It is undoubtedly that without his kindness and knowledge that I would never have been successful in my pursuit of a Ph.D. His support means the world to me and I am fortunate that he has supported me throughout this time.

Dr. Amarawan Intasiri has been instrumental in my development and success. She has worked with me in the lab from the very beginning and has been a wealth of knowledge. Her dedication to the projects and development of procedures as well as her careful analytical approach has taught me lifelong lessons that I will continue to use throughout my career. For all that she has done I am forever grateful.

My committee members Dr. David Aucoin, Dr. Wes Chalifoux, Dr. Robert Ryan, and Dr. Yftah Tal-Gan have remained a source of inspiration. These are great researchers who lead the way by example and I am glad to have them as members of my committee. When needed they have been there for me with advice in many aspects, and without this guidance I would have been lost.

I would like to express my gratitude to the multiple labs and lab members that were available to assist me when expertise and equipment was needed from outside. Dr. Robert Ryan, Irina Romenskaia, Dr. Subhash Verma, Dr. Timsy Uppal, Kabita Adhikari, Dr. Ian Buxton, Dr. Scott Barnett, Dylan Saxon, Dr. Christine Krieger, Dr. Marvin Gershengorn, and Dr. Massimo D'Agostino were all instrumental to my success at different points. All were such helpful and

knowledgeable people and have made my research not only possible, but have been a joy to work with. I would also like to thank the UNR proteomics center, genomics center, and bioinformatics center. The contribution to my work has been substantial from these centers.

Importantly I would like to thank all the members of Dr. Bell's lab who have helped me in countless ways while I have been here. Thanks to Dr. Azizul Islam, Dr. Topprasad Kapri, Dr. Jhonnathan Brawley, Yetunde Oyasakin, Supadach Pretprawnon, Sagar Gyawali, Gilbert Ganschow, and Bradford Adams. You all have helped me in the lab unmeasurably, but even more importantly have touched my heart and will remain with me forever.

Table of Contents

List of Tables

List of Figures

List of Schemes

Chapter 1: Introduction

Section 1: Medicinal Chemistry

Medicinal chemistry is a discipline that draws from a broad range of scientific fields of study and as such requires an interdisciplinary approach. The general goal of medicinal chemistry is to design and synthesize compounds which will have a beneficial effect on the body of a person or other organism. At the center of medicinal chemistry is organic chemistry, but it is also necessary to test, develop, and optimize the compounds after they have been synthesized. As such medicinal chemistry also draws heavily on knowledge and techniques in biochemistry, molecular biology, and pharmacokinetics amongst many others. It is important to bring a broad perspective to the study of medicinal chemistry. A drug interacts with the various cellular components such as the nucleic acids, lipids, carbohydrates, inorganic molecules, and proteins in different ways to produce changes to the structures and functions or degradation of these components. Additionally, these components may degrade or change the structure of the drug itself further altering the way it interacts with the components of the cell. This makes the study of medicinal chemistry complex and quite interesting. Common targets in medicinal chemistry will be covered below with the intention of highlighting not only the successes, but also understanding the gap left for novel drug mechanisms. CADA represents an opportunity for partially filling this gap. CADA is part of a novel class of Sec61 inhibitors with vast pharmaceutical potential grouped together by their mechanism of action which involves binding to the Sec61 protein conducting channel in the endoplasmic reticulum (ER) membrane, blocking translocation, and typically resulting in protein degradation. Of this novel class CADA is the most specific known to date. CADA is also the only compound in this class that has so far been

shown to interact specifically with the SPs of target proteins which is a major factor in the selectivity of CADA and its many analogues.

1.1 Drug Targets: Nucleic Acids

A very important component of the cell is nucleic acid. Nucleic acid polymers are the informational carrying molecules in the cells. The polymers come in two basic varieties, either DNA or RNA. DNA holds the information to synthesize RNA which holds the information to synthesize proteins. In addition, RNA can perform several important structural and catalytic roles. The genetic information which is passed from one cell or organism to another from one generation to the next is carried in the more stable DNA, while RNA serves as a short-term intermediate between DNA and protein. This multilevel chain provides multiple opportunities for regulation and fine-tuning of gene expression.[1] It also provides multiple opportunities for different varieties of drugs. Drugs that interact with nucleic acids for their desired mechanism of action come in a variety of forms. Planar aromatic/heteroaromatic compounds can intercalate between the layers of the DNA double helix base-pairs and interfere with replication and transcription of the DNA with toxic consequences. Alkylating agents use electrophilic functional groups to form cross-links with the nucleophilic nitrogen atoms on adenine, guanine, or cytosine nucleotides. Unfortunately, they tend to have poor selectivity due to alkylation of nucleophilic groups in proteins. Chain cutting compounds react with a nucleophile to create an aromatic diradical species which then reacts with the DNA, in turn creating a radical species on the DNA which then reacts with oxygen to cleave the DNA chain. Due to their toxicity, compounds which target DNA are generally used as anticancer or antibiotic agents.[2] This is an important lesson in medicinal chemistry; off-target effects and lack of specificity for the desired target tend to have

toxic or otherwise undesirable consequences, which limits the application of an otherwise clinically useful drug.

Drugs that tend to have better specificity are those that target complexes of DNA and protein such as the topoisomerase poisons and nucleotide or nucleoside analogues. By targeting complexes involving proteins, medicinal chemists can take advantage of higher degree of structural variation in proteins to tune specificity. Topoisomerase enzymes relieve the tension that builds up in DNA as it is unwound during replication and transcription. Quinolones and fluoroquinolones are examples of antibacterial drugs which target bacterial topoisomerases.[3] The largest class of antiviral drugs function by mimicking nucleic acids and being incorporated into a growing DNA chain during polymerization by the targeted polymerase enzyme. Once incorporated into the chain, they cause issues such as chain termination due to lacking the necessary 3'-OH group in the sugar moiety or an accumulation of mutations due to modifications of the nucleobase. Nucleos(t)ide analogs have been highly successful as antiviral drugs, but one major issue is the high mutation rate of viruses, which allows them to develop resistance to these drugs. While well-known as antiviral agents, these drugs are also effective antimicrobials and anticancer agents. Nucleoside analogs consist of either the ribose or 2-deoxyribose sugar moiety attached to a purine or pyrimidine base through a β-N-glycosidic bond, while nucleotide analogs include a 5' phosphate ester moiety. Modifications in either the sugar or nucleobase moieties of the naturally occurring nucleos(t)ides is used to produce potent antiviral drugs. The sugar moiety has been changed in therapeutic agents by modification of its substituents, changing the ether oxygen to another atom (carbon, nitrogen, phosphorous, or sulfur), addition of heteroatoms to the ring, changing the ring size or opening of the ring. The nucleobase has been changed in a variety of ways as well including halogenation and purine modification. Often these drugs contain

multiple modifications to achieve the desired effect. Additionally, these drugs are delivered as prodrugs in order to increase stability and membrane permeability. The active form of the drugs are the nucleotide triphosphates, but this group is not very stable, and the charges prevent it from crossing through the cell membrane and into the cell. A nucleoside lacks a phosphate ester moiety and requires a series of three phosphorylation events by nucleoside kinase, nucleoside monophosphate kinase, and nucleoside diphosphate kinase, in that order. The first phosphorylation is rate-limiting and as such nucleotide monophosphate prodrugs with protecting groups have been designed to become deprotected once in the cell and rapidly converted into the active nucleotide drug.[4] The issues of membrane permeability and stability are other important concepts for a good medicinal chemist to keep in mind when designing a drug. Cellular membranes are composed of lipids, which will be explored next. Due to their connection with other drugs that reduce protein levels within the cell, compounds that target specific sequences of DNA or RNA to reduce expression levels of targeted proteins will be discussed at the end of this section.

1.2 Drug Targets: Lipids

Lipids are another important component of cells. Cells contain thousands of varieties of lipids and invest significant energy in their synthesis.[5] Lipid-targeting drugs are not very common, but there are some examples. General anesthetics may alter cells membrane signaling potential through hyperpolarization. The exact mechanism is unclear, but what is clear is that the resting potential is reduced, which makes it less sensitive to stimulus and harder to reach the action potential threshold.[6] Additionally, there are antifungals and antibiotics, such as amphotericin B and gramicidin A, respectively, which take advantage of differences in lipid composition between target cells and mammalian cells to specifically insert into cell membranes

of target cells and cause pores, which kill the cells as their contents leak out.[2] Despite not being common targets for the mechanism of action of drugs, lipids are crucial for the functioning of cells, as is obvious from the lethal nature of drugs such as amphotericin B on their target cells. Lipids serve as energy storage and signaling molecules, and form the lipid bilayer membranes surrounding and within cells.[5] The importance of lipids to medicinal chemistry goes beyond their potential as drug targets as lipid membranes create the boundary between the inside and outside of the cell, as well as boundaries within cells. This importance should be clear from the previous discussion of the need for nucleos(t)ide analog prodrugs to cross the cell membrane. Whether or not a drug is able to pass through cellular membranes or accumulate within them affects their distribution within cells and the body as whole. This distribution affects a drug's ability to encounter and interact with its primary target as well as its overall stability within the body. Drug distribution is another important concept to medicinal chemists.

Lipids form the cell membrane of all cell types, but in addition eukaryotic cells are characterized by containing membrane bound organelles such as the nucleus, mitochondria, chloroplasts, and the endoplasmic reticulum (ER). The complex compartmentalization of eukaryotic cells allows for segregation of chemical and biochemical reactions. This increases efficiency, allows spatiotemporal control of the release of reaction products, and protects biological products such as DNA or proteins.[5] These functions are demonstrated well by the ER membrane which is of central importance to cellular compartmentalization. The lumen of the ER functions as a reservoir for Ca^{2+} ions with a concentration 10,000 times higher than that of the cytosol. The coordinated release of these ions can serve as an important regulatory and signaling mechanism with various outcomes depending on cell type and timing. However, these sequestered ions also serve important functions within the lumen of the ER as they are required

for the activity of various chaperones and enzymes within the ER. The ER serves as the site for synthesis of roughly one-third of the proteins produced in the cell[7] as well as synthesis of lipids and carbohydrates.[5] Protein-conducting channels like Sec61 in the ER membrane are important in aiding the protein synthesis and localization at the ER membrane.[7] This is a complex and important process that has thus far generally escaped the attention of the medicinal chemistry community. Exploring a group of drugs, specifically CADA compounds, that target the Sec61 channel will be the focus of this dissertation and much more detail on this will be covered later. The lumen of the ER provides a protected environment for proteins to fold properly and for larger protein complexes to assemble. The lumen of the ER contains an elevated concentration of glutathione, which maintains an oxidative environment in the lumen compared to the reducing environment of the cytosol. This oxidizing environment is necessary for the proper formation of disulfide bonds and folding of proteins. The Ca^{2+} ions in the lumen also help to maintain this oxidizing environment, as a depletion of Ca^{2+} ions will shift the lumen to a reducing environment.[7] Protein synthesis at the ER membrane and modulation of this process will be covered in depth in later sections. For now, it is pertinent to discuss proteins as drug targets.

1.3 Drug Targets: Proteins

Proteins are in fact the most popular target for drugs and as such warrant considerable attention. Proteins play many important functional roles in the cell such as structural proteins, enzymes, receptors, transport proteins, and signaling molecules. Each of these protein types can be targeted by a variety of different mechanisms. For example, viral capsid proteins are structural proteins which self-aggregate to form a shell that encases viral genomes and other proteins to produce viral particles that can leave one cell and infect another. Once inside a newly infected cell the capsid proteins must disassemble to allow the release of the viral genome.[8] Both

assembly and disassembly may be targeted by drugs such as the novel class of promising anti-HBV drugs termed capsid assembly modulators (CAMs) that exhibit a variety mechanisms including premature disassembly, rapid assembly that doesn't allow enough time for the pre-genomic RNA to be encapsidated, or incorrect assembly into defective particles.[9] It is commonly regarded that this approach would work best in combination with the current standard of care antiviral nucleos(t)ide analogs.[9–11] Structural proteins in general tend to be difficult to target, and there are not many examples of drugs that target structural proteins. One reason for this is that structural proteins make protein-protein interactions (PPIs) as demonstrated by the case of capsid proteins that self-aggregate to build a protective shell. PPIs are challenging to disrupt because they occur over a much larger surface area than traditional small molecule inhibitors, the surface area is generally highly hydrophobic and flat ("slippery"), and the two protein surfaces tend to have strong binding affinity for each other.[12] The discussion of proteolysis targeting chimeras (PROTACs) later in this section will cover a more promising technique for targeting structural proteins, but for now the focus will turn to more traditional protein targets of medicinal chemistry efforts, enzymes and receptors.

Enzymes

Enzymes are important targets for medicinal chemists and there are many ways in which a medicinal chemist can disrupt the function of enzymes. Natural substrates bind to a groove or cleft on the enzyme known as the active site, and this binding occurs through intermolecular interactions (ionic bonds, hydrogen bonds and dipole-dipole, ion-dipole, van der Waals or hydrophobic interactions). This provides a much more targetable area for small molecule binding compared to the large and "slippery" binding sites of PPIs. The enzyme functions as a catalyst for a specific reaction by reducing the activation energy because it stabilizes the transition state

between reactants and products. Inhibitors of enzymes can be categorized in several different ways. They may be covalent or non-covalent, may be reversible or irreversible, may bind to the active site or an allosteric site (a site other than the active site), and may be competitive, noncompetitive, uncompetitive, or mixed.[2] In the case of competitive inhibition, which is by far the most common, the substrate and the inhibitor cannot bind to the enzyme at the same time. Conversely the binding of a noncompetitive inhibitor does not affect the affinity of the substrate for the enzyme. Uncompetitive inhibition occurs when the inhibitor can only bind to the enzyme-substrate complex. Typically, all non-covalent inhibitors are considered reversible while covalent inhibitors can be reversible or irreversible. Additionally, noncompetitive inhibitors always bind to allosteric sites. Other than that, an enzyme may fall into any combination of these categories.[13] The following section will discuss these various categories and give some examples of inhibitors with such characteristics.

One example of a non-covalent, competitive inhibitor that binds the active site is the angiotensin converting enzyme (ACE) inhibitor, captopril, used to treat high blood pressure (hypertension).[14] ACE is a metalloproteinase that cleaves the C-terminal 2 amino acids from its substrates using zinc in its active site as a cofactor. Using a previously synthesized weak inhibitor (succinyl-L-proline) as a starting point, captopril was designed by several iterations of synthesis and testing of analogs in a rational fashion (**Fig. 1.1**). By changing a carboxylic acid group in a succinyl-L-proline to a thiol group (which could make a stronger ion-ion interaction with zinc in the active site) the IC_{50}

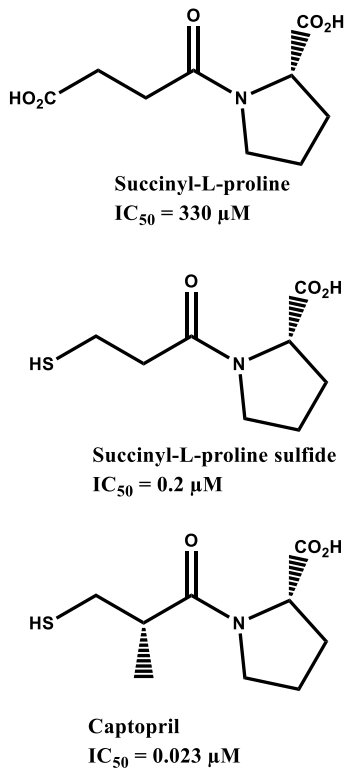

Figure 1.1: ACE inhibitors. Structures of a series rationally designed ACE inhibitors.

(the concentration of drug required to inhibit enzymatic activity by 50%) went from 330 μM to just 0.2 μM. The activity was further improved by addition of a methyl group (which could make hydrophobic interactions with a previously empty pocket in the active site) to give captopril with an IC_{50} of 0.023 μM.[15] This shows that by understanding the available intermolecular interactions and the shape of a desired binding site medicinal chemists can design highly active inhibitors. While typical competitive inhibitors bind to active sites, allosteric competitive inhibition is possible. However, allosteric inhibition will be discussed in the context of other types of inhibition.

Allosteric binding sites are locations other than the active site where drugs may bind and cause a structural change that affects the ability of the active site to perform its catalytic function. Noncompetitive inhibitors bind to an allosteric site and causes inhibition by disrupting either the catalytic mechanism or sterically blocking access to or release from the active site. By definition, the binding of the inhibitor should not reduce the affinity of the substrate for the enzyme; however, this is next to impossible in reality.[13] If the allosteric site is so close to the active site such that binding of a small molecule would sterically block the substrate from reaching the active site, it is likely that the induced fit of inhibitor binding would affect the nearby active site. For the case of a more distant allosteric site that affects the catalytic mechanism there is a similar difficulty. An enzyme binds to its substrate in an induced fit, that is it undergoes a conformational change to maximize the binding interactions with the substrate. This induced fit involves the “largescale” movement of amino acid backbones and is “slow”, on the millisecond timescale. The enzyme must hold the substrate for a fraction of a millisecond in the correct orientation for catalysis. The enzyme and substrate undergo a further change to form the transition state (at which point there is an equal probability of moving towards either products or

reactants). This change involves stochastic atomic level vibrations on the femtosecond timescale. The inhibitor could not possibly be affecting this stochastic search at a distant site. That means a true noncompetitive inhibitor would have to affect the first phase such that the enzyme favors an induced fit for a different orientation with the natural substrate that nonetheless binds with equal affinity.[16] The reality for allosteric inhibitors is that they cause mixed inhibition of competitive and non-competitive modes.[2] Although it is reasonable enough to accept that a small change in orientation might have a much larger effect on catalysis than affinity and there are several accepted examples of purely noncompetitive inhibitors. Non-nucleoside reverse transcriptase inhibitors (NNRTIs) against HIV provide an example of a generally accepted noncompetitive inhibitor.[2,17] NNRTIs all share the same allosteric binding site, which is 10 Å from the active site.[18] Binding causes several conformational changes in the complex active site with multiple effects leading to a complex and unclear mechanism of inhibition that may involve multiple contributions.[17] Certain studies revealed improved binding of the substrate deoxynucleotide triphosphate (dNTP)[19] (a clear deviation from the definition of non-competitive inhibitors) and other studies revealed that the dNTP is not correctly positioned for the reaction to occur.[20,21] Indeed, it appears that the change in binding position does affect the binding affinity as expected. While the term may not reflect reality perfectly, it is still useful for understanding the mechanism of drugs which exhibit some degree of noncompetitive inhibition.

Another type of inhibitor with an even more dubious existence in pure form is the uncompetitive inhibitor. Uncompetitive inhibitors bind to the enzyme-substrate complex and disrupt the catalytic mechanism.[2] An advantage of uncompetitive inhibitors is that their potency increases as substrate accumulates, which is opposed to competitive inhibitors that become less effective as substrate accumulates. In metabolic pathways, the substrate accumulates as an

enzyme is inhibited so this would make an uncompetitive inhibitor seem advantageous. However, there are very few known examples of natural uncompetitive inhibitors and medicinal chemists don't seem to have been very successful in developing synthetic ones.[22] It has been suggested that uncompetitive inhibition may have toxic consequences and there is strong selective pressure against the evolutionary development of natural uncompetitive inhibitors. Additionally, it has been suggested that the mechanism itself is simply highly unlikely.[23] On the other hand, it has also been suggested that a typical high throughput screen (HTS) is biased against discovery of these types of inhibitors and a change of assay conditions could produce hits with an uncompetitive inhibitory mechanism.[22] Nonetheless, amongst other inhibitors some NNRTIs have elements of uncompetitive inhibition[17] and it is a useful term for understanding the complicated mechanisms of certain inhibitors.

Returning to competitive inhibitors affecting the active site, medicinal chemists can take advantage of the way enzymes work as catalysts to design highly potent drugs. As previously mentioned in the discussion of non-competitive inhibitors, after binding to a substrate in an induced fit the enzyme-substrate complex is in the right orientation such that the transition state can be reached through atomic level stochastic vibrations.[16] Transition state analogues resemble the substrate transition state and are capable of binding so strongly (six orders of magnitude more strongly than the substrate), using only non-covalent interactions, that they act like irreversible inhibitors.[2,16] It is interesting to note that while the natural transition state is dynamically transient, the transition state analogs optimized interaction distances and angles and form additional strong interactions (not seen in the induced fit binding of the natural substrate) that hold them in a thermodynamically stable state.[16] The first step in the cleavage of an amide bond involves attack of a nucleophile on the carbonyl carbon to form a high-energy tetrahedral

intermediate. To further improve the ACE inhibitory activity of captopril, mentioned earlier, in another analog the -CH_2SH group was replaced with an amine followed by an sp3 hybridized carbon with tetrahedral geometry to mimic the transition state of the reaction (**Fig. 1.2**). This analog, enalaprilat, has an IC_{50} of 0.0012 μM (compared to 0.023 μM for captopril).[13] Similar transition state inhibitors have also seen success as antivirals by targeting viral proteases, such as for HIV[24] and SARS-CoV-2.[25] This is a powerful approach to make strong binding interactions, yet some transition states are not easy to mimic with stable compounds and some enzymes such as those with limited catalytic rate enhancement are resistant to this approach.[16] Fortunately, more methods are available to medicinal chemists.

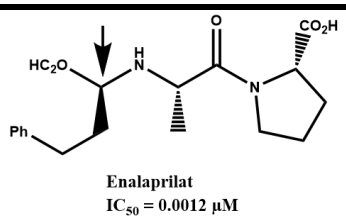

Enalaprilat
IC_{50} = 0.0012 μM

Figure 1.2: Enalaprilat. Structure of a potent ACE transition state inhibitor. The arrow points to the sp3 hybridized carbon that mimics the transition state.

Another powerful approach to making inhibitors with strong affinities for their target is the use of covalent inhibitors. These covalent inhibitors may bind reversibly or irreversibly to the target protein.[26] Typically, a covalent bond is formed by an electrophilic functional group on the drug which reacts with nucleophilic amino acids, usually serine or cysteine.[2] The concern for irreversible inhibitors is that they will exhibit high toxicity due to reaction with off-target nucleophiles. Additionally, they may not be well suited for use in chronic diseases due to a high chance of the resulting drug-enzyme adduct causing an adverse immune response. As such over 50% of irreversible inhibitors are used to treat cancer and microbial infections.[27] Although outnumbered by the noncovalent inhibitors, one of the most used drugs in existence, aspirin, demonstrates the medicinal utility of covalent inhibitors. Owing to the concerns of toxicity, the rational design of these types of drugs has generally been avoided by the pharmaceutical industry. Historically, almost all first-in-class covalent drugs were discovered before their

mechanism was known. Nonetheless, useful drugs such as aspirin, penicillin, clopidogrel (Plavix), lansoprazole (Prevacid), and esomeprazole (Nexium) have had major impacts in medicine.[26,28] One approach to the design of covalent inhibitors is the mechanism-based approach, where the drug creates a covalent bond to one of the enzyme's catalytic residues. One example of this is in the case of the coronavirus main protease (M^{pro}) or 3C-like protease (3CLpro). Using a hexapeptide substrate analog with a chloromethyl ketone "warhead" (functional group capable of making a covalent bond with the target nucleophilic amino acid), a drug was designed to target the catalytically conserved cysteine residue of coronavirus M^{pro} proteases. These drugs were used against SARS-CoV-1 and human rhinovirus (HRV) and were later used for the design of potent SARS-CoV-2 M^{pro} inhibitors. These drugs lack a high degree of specificity and as such can end up targeting unintended enzymes with similarly conserved active sites. Eventually an analog with a nitrile warhead was used. The nitrile warhead produces a thioimidate adduct which can undergo thiol elimination, making the covalent bond reversible (**Fig. 1.3**). This optimized reversible inhibitor, Paxlovid (nirmatrelvir co-administered with cytochrome P450 inhibitor, ritonavir, to increase stability), showed potent anti SARS-CoV-2 activity and safety in human trials.[29,30] Paxlovid was authorized for emergency use in the treatment of COVID-19 by the FDA. While reversible inhibitors alleviate some of the issues

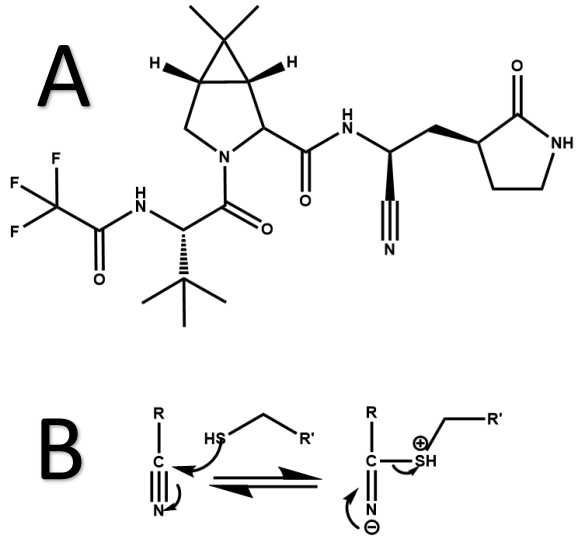

Figure 1.3: Nirmaltrelvir. A) Structure of the reversible covalent inhibitor, nirmaltrelvir. B) Mechanism of reaction of the nitrile warhead with the thiol group of cysteine to produce the thioimidate adduct. The elimination mechanism is shown on the thioimidate adduct.

with toxicity, if they target highly conserved catalytic residues, as in the mechanism-based approach, they will still suffer from disagreeable off-target affects, albeit to a lesser extent.

The strategy of designing covalent inhibitors has gotten new life and has recently become quite popular with a change of strategy. Instead of targeting the highly conserved amino acids involved in the catalytic mechanism of enzymes, medicinal chemists have turned to focusing on poorly conserved amino acids not involved in catalysis. These compounds are dubbed targeted covalent inhibitors (TCIs).[26,28] Although the terminology is new, the mechanism is not. Aspirin, first marketed in 1899, binds the active site of cyclooxygenase enzymes (COX-1 and COX-2) such that its acetyl group is placed in proximity to a non-catalytic serine residue on the enzyme. The serine residue attacks the carbonyl carbon of aspirin. Resulting acetylation of the serine residue blocks the active site for COX-1 or changes the activity for COX-2.[31] Of course, the elucidation of this mechanism occurred much later than aspirin's initial discovery and use. The most popular approach has been to design TCIs starting with a proven reversible compound and adding a covalent warhead. The most popular warheads are Michael acceptors (usually α,β-unsaturated amides) that target non-catalytic cysteines.[26] Two advantages of targeting non-catalytic residues are greatly reducing the chances of toxic off-target reactions and expanding the scope beyond only targeting the active site of enzymes to their allosteric sites and to proteins other than enzymes.[26,28] Good examples of this are the hepatitis C virus (HCV) protease inhibitors that were designed based on the reversible covalent inhibitor, telaprevir. Instead of targeting a catalytic serine residue shared with many human proteases, analogs were designed to target a unique cysteine residue in the active site by using an acrylamide motif as a Michael acceptor. Additionally, tyrosine kinases, such as epidermal growth factor receptor (EGFR), fibroblast growth factor receptors 1-4 (FGFR 1-4), and Bruton's tyrosine kinase (BTK) have

been popular and successful cancer targets using this approach.[32] While EGFR and FGFR 1-4 are kinase enzymes (and the drugs just discussed target the enzymatic activity) they are also receptors, this demonstrates how proteins can fulfil multiple functions at the same time and can be targeted by different approaches. Drugs that target receptor activity will now be discussed.

Receptors

Protein receptors are highly important drug targets. Receptors bind with signaling molecules (also called ligands), typically resulting in downstream signaling cascades that amplify and refine the signal for a specific response. This communication is essential and ubiquitous in the body, allowing cells to work together in a coordinated fashion to achieve vital functions including muscle contraction,[33] digestion,[34] respiration,[35] growth, development,[36] thinking,[37] and immune responses.[38] The ubiquitous and vital nature of signaling demonstrates the importance of receptors as drug targets. Additionally, many receptors are proteins that span the cellular membrane with domains on both sides. The cell membrane presents a hydrophobic barrier that separates the aqueous environments of the extracellular space and the interior of the cell. Targeting cell-surface receptors is advantageous for the drug development process as there is one less barrier between the drug and its site of action.[2] G-protein coupled receptors, kinase-linked receptors, ion channel receptors, and intracellular receptors are examples of some of the important types of receptors that have been targeted successfully by medicinal chemists. The importance of receptors to medicinal chemistry warrants further consideration.

Drugs affect receptors in two basic ways. Antagonists bind to receptors and lock them into inactive conformations. Agonists, on the other hand, bind to receptors and lock them into active conformations. Like with substrates at the active site of an enzyme, ligands cause an induced fit when they bind to the binding pocket of a receptor. As a ligand enters the binding

pocket the correct positioning of its functional groups attracts the nearby functional groups in the binding pocket, which causes a conformation change in the receptor. Other parts of the receptor must shift in turn to minimize the strain induced by change in the binding site, and this modulates the activity of the receptor.[2] To design an agonist, medicinal chemists often use the concept of a pharmacophore, that is having functional groups capable of making the necessary interactions in the correct positioning to mimic the natural signaling molecule.[39] However, mimicry is not necessary as there are other amino acids that provide other possibilities for interactions to get the same effect. The design of antagonists is similar, except one needs to adjust the spacing between critical functional groups or generally add/remove extra bulk in the molecule, so that it binds more strongly with the shape of the binding pocket in the inactive conformation of the receptor.[2] This describes inhibitors acting at the ligand binding site, but like enzymes, inhibitors of receptors may also act at allosteric sites to either enhance or interrupt the effects of the natural signaling molecules. Most receptor targeting drugs are simple agonists or antagonists that target the binding site; yet, due to the increased selectively and associated reduced toxicity, allosteric modulators are growing in popularity.[40,41] Furthermore, there are partial agonists which bind to the active site and produce a weaker response while preventing the natural signaling molecule from producing a full response.[42] Finally, there are inverse agonists which are essentially antagonists which work on receptors that are partially active even in the lack of the natural signaling molecule.[2] Some examples of these different types of drugs will be explored in the following discussion.

It has been estimated that roughly 35% of approved drugs target G protein-coupled receptors (GPCRs).[43] After binding to a ligand, the GPCR undergoes a conformational change which exposes a binding site on the cytoplasmic side of the membrane. This allows for binding

to a particular G-protein. G-proteins are a diverse group of membrane-bound proteins made of three subunits (α, β, and γ) that share the feature of binding guanosine diphosphate (GDP) in the resting state and once bound to the receptor-ligand complex exchanging GDP for GTP. Binding of GTP causes the release of the G-protein in separate pieces (the α subunit and the βγ-dimer) from the complex. The receptor-ligand complex is then free to activate more G-proteins in a similar fashion. The α subunit and the βγ-dimer then go on to stimulate or inhibit other enzymes or receptors such as adenylate cyclase, ion channels, or phospholipase C. Each of these has further downstream targets until eventually the desired response is achieved. Once activated, each enzyme in the cascade activates multiple downstream targets before being deactivated.[2] Going from a small number of the initial signaling molecules to a rapid and large response demonstrates signal amplification that is typical of receptor proteins. It also demonstrates the power of targeting receptors, as a small amount of drug can have a dramatic effect.

A lot can be learned about the design of GPCR targeting drugs from the study of the opioid receptors, which come in three main types: mu (μ), kappa (κ), and delta (δ). Morphine is an agonist for these receptors, and unfortunately it is most active for the μ receptor which is associated with a strong analgesic (pain relieving) effect, but also respiratory depression, euphoria, and addiction. While the κ and δ receptors produce more mild analgesic effects, they also have less severe side effects.[44] The syntheses of morphine analogs illustrates how a lead compound can be optimized for improved activity and pharmacokinetic properties. Morphine is a molecule with 5 connected rings containing a phenol group and a protonated tertiary amine which are the key functional groups that interact with the binding site and produce the pharmacophore (**Fig. 1.4**). The pharmacophore can be described as the appropriately spaced hydrogen bond acceptor, aromatic ring, and cationic group. The addition of a hydroxyl group

between two of the rings (oxymorphone) or replacement of the N-methyl group with an N-phenylethyl group (N-phenylethylmorphine) improved potencies by factors of 2.5 and 14, respectively. These groups in these specific locations allow for new and favorable interactions with the binding site for improved affinity. While the N-phenylethyl extends an aromatic ring into a hydrophobic binding region available in the active conformation, replacement with a shorter N-allyl group (naloxone and nalorphine) positions a hydrophobic group in the right place to bind to this hydrophobic binding region when it is shifted and collapsed in the inactive conformation. N-allyl analogues are potent antagonists of μ receptors and are capable of reversing overdoses. Interestingly, the position of this hydrophobic binding region varies slightly between μ and κ receptors, such that nalorphine is antagonistic for μ receptors, but agonistic towards κ receptors. Unfortunately, this also produces hallucinogenic and psychological side effects.[2] Further modification focused on

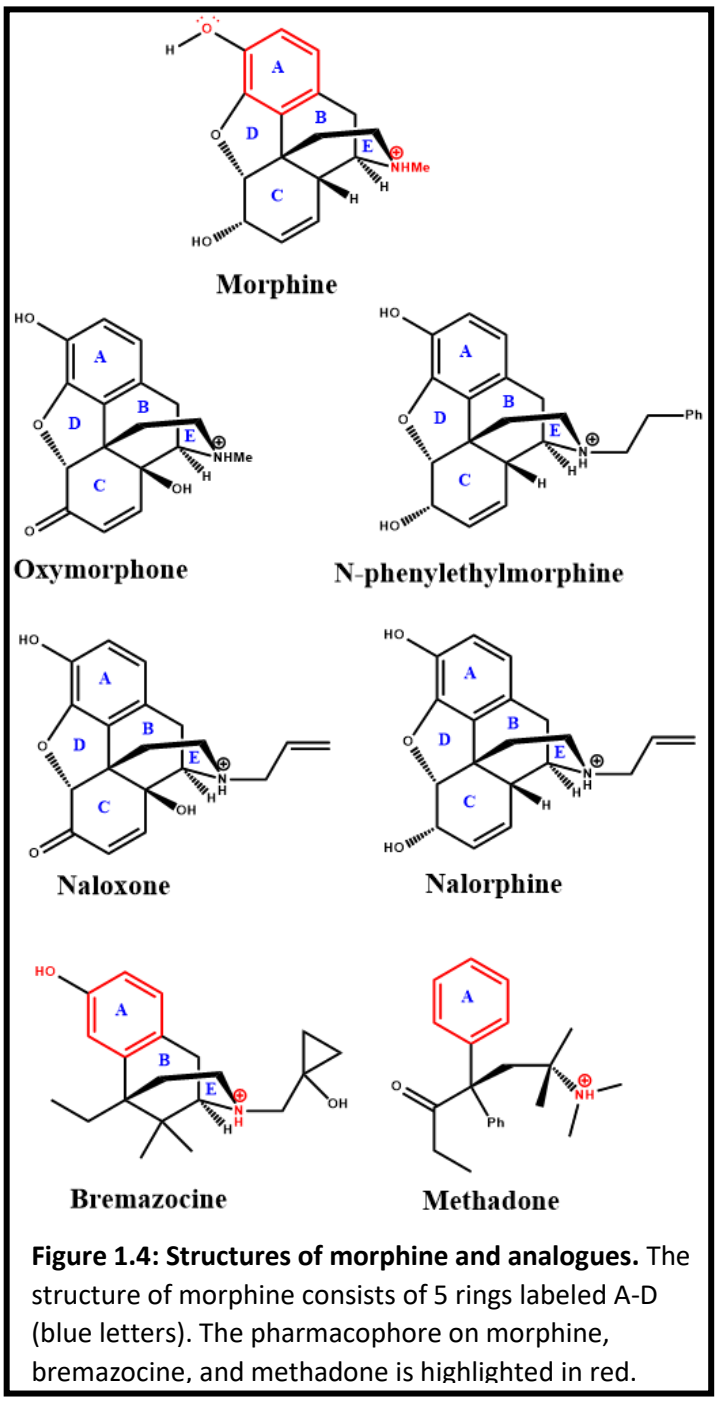

Figure 1.4: Structures of morphine and analogues. The structure of morphine consists of 5 rings labeled A-D (blue letters). The pharmacophore on morphine, bremazocine, and methadone is highlighted in red.

reducing the complexity of the structure while maintaining the basic pharmacophore, although the phenolic hydroxyl proved not to be essential. The reduction in complexity made for cheaper and more facile synthesis and the discovery of highly potent analogs. The D ring includes an oxygen bridge, which proved not to be essential to activity. Its removal improved oral bioavailability and increased the half-life of analogues such as levorphanol.[45] Further simplification down to a three ring structure led to the discovery of bremazocine, which is 200 times more potent than morphine, non-addictive and doesn't produce respiratory depression. Simplification by removing rings while maintaining the pharmacophore continued all the way to analogues that only contain the aromatic A ring of morphine and still retain potent opioid receptor activity.[2] This shows how one can use a known drug that binds a certain receptor as a starting point to optimize the activity and/or reduce the complexity of the original molecule.

Some receptor binding drugs act as antivirals and may escape the standard classification as agonist or antagonist. Viruses enter cells by hijacking the receptors on cell surfaces and modifying the normal function of the receptor so that is used by the virus as an entry receptor. The sodium taurocholate cotransporting polypeptide (NTCP) which is expressed on hepatocytes is normally responsible for the uptake of bile acids into the cell is also used by HBV and HDV as an entry receptor. Myrcludex B is a drug that mimics the viral peptide, which binds to NTCP, blocks the virus from binding, and subsequently prevents it from infecting the cell. While myrcludex B also acts as an antagonist for the receptor and inhibits NTCP mediated bile acid uptake[46], there are cyclosporin derivatives which have been shown to be highly effective at blocking HBV binding and entry without affecting bile acid uptake.[47] This shows that there are many different and creative ways to develop drugs when one understands both the biological and chemical aspects behind a particular illness.

Ion Channels

Ion channels as a group may be second only to G-protein-coupled receptors (GPCRs) as membrane protein targets for FDA-approved drugs.[41] Ion channel receptors (such as ligand-gated ion channels) are made up of five membrane spanning subunits that form pores in lipid bilayer membranes, such as the cellular membrane. Different channels allow for the passage of specific ions across the membrane. A typical ion channel will be closed in its resting state, preventing the passage of ions. When its cognate signaling molecule binds to the binding site, it switches to an open conformation and can allow thousands of ions to pass through, which in turn interact with and typically activate other proteins on the other side of the membrane. Once activated, these proteins often activate other proteins in a cascade where the signal is further amplified.[2] An example of a useful partial agonist is that of varenicline (Chantrix), which helps users quit smoking. By partially activating neuronal nicotinic acetylcholine receptors (nAChRs) the drug allows for increased dopamine levels to counteract the drop in dopamine associated with smoking cessation. Additionally, by blocking the nicotine from activating the receptor it reduces the "rewarding" release of large amounts of dopamine when users give in to the urge to smoke. Varenicline was discovered by screening a targeted library of analogues of the known nAChR partial agonist (-)-cytisine and by carrying out structure activity relationships (SARs) studies.[42] Interestingly, while it has been suggested that partial antagonism may arise from the drug having variable binding orientations within the binding site, crystal structures revealed similar binding poses and conformation changes for both nicotine and varenicline, leaving the nature of the partial antagonism a mystery.[48] A later study shed some light on this mystery when it was discovered that varenicline may antagonistically interact with allosteric sites on certain nAChR

subtypes. This could be a mechanistic explanation for the partial agonism, but further validation is required.[49]

Another type of ion channel (not considered receptors) are the voltage-gated ion channels which are respond to changes in membrane potential to either open or close.[50] Because they are gated by changes in membrane potential, they lack a ligand binding site, which makes rational design of drugs challenging. This limits drugs to binding poorly defined allosteric sites or to binding within channel causing a blockade. As such, identification and validation of lead compounds targeting such proteins has been challenging.[51] Additionally, a major drawback for channel blockers is they often lack specificity between channel subtypes.[41] Advances in the use of fluorescent dyes in HTS cell based assays has led to some success. The Nav1 channels are interesting targets for treating neuropathic pain. A HTS platform screen of approximately 200,000 compounds against Nav1.8 yielded only one viable lead, N-{[2′-(aminosulfonyl)biphenyl-4-yl]methyl}-N′-(2,2′-bithien-5-ylmethyl)succinamide (BPBTS), for optimization by medicinal chemistry. This compound was a channel blocker which lacked specificity and had a poor pharmacokinetic profile. Medicinal chemists were able to improve on the pharmacokinetic profile in further analogues. It took further improvements in screening technology and the development of an ultra HTS (UHTS) screening platform to find a class of channel blockers with defined SARs. Some of these compounds had improved specificity for channel subtypes.[48] The issue with this approach is that it requires the synthesis of large libraries for screening instead of guided drug design based on knowledge of a targeted binding site with known ligands as a starting point.

1.4 Novel Strategies

Scientist have discovered many different drugs with a variety of structures and mechanisms over the years, and many have been left out from the above descriptions. As discussed, proteins are the most common target. In fact, most drug targets are members of one of the following five protein families: GPCRs, ion channels, kinases, nuclear hormone receptors or proteases.[52] Traditional approaches focused on inhibiting or activating the function of a particular protein by a strong binding interaction with a small molecule. This has been successful for many drug targets, but many clinically important targets have been identified which resist this approach. For example, drugs have not been developed for targeting many potential therapeutic targets lacking well defined active or binding sites or with binding sites, that are typically too large for a small molecule to significantly perturb the interaction (such as for PPIs).[53] In fact, less than 20% of the predicted therapeutic targets have FDA drugs targeting them.[54] Antibody and other peptide/protein therapeutics have been developed that have higher molecular weights and come with advantages such as high affinity and specificity over traditional small molecules. However, their application thus far has been limited by membrane permeability, stability, and bioavailability.[55,56] As opposed to targeting the activity of proteins, another approach is modulation of the amount of a particular protein. Besides expanding to new therapeutic targets which old approaches failed to find drugs for, this approach has other potential advantages. This may improve upon drug-resistance or dependence issues which occur with traditional activators or inhibitors. Depending on the target and technique, this approach may also be able to improve upon selectivity and the effects can be rapidly reversable which may reduce toxicity. Additionally, these approaches provide many opportunities for academic research and improving our understanding of some poorly understood yet vital cellular

processes.[57] There are a few different techniques that have become popular for modulating protein levels.

Therapeutic Nucleic Acids

Therapeutic nucleic acids come in a variety of flavors based on the nature of the compounds and mechanism of action. These approaches are relatively new to medicine and have traditionally suffered from rapid nuclease degradation, unfavorable immunological side effects, and difficulty of delivery. *Ex vivo* approaches involve transduced stem cells or T cells which are transplanted into patients. The *in vivo* approaches have seen advancements in stability, immunogenicity, and delivery which has allowed for some major success stories.[58] Antisense oligonucleotides (ASOs) are single-stranded polymers consisting of analogs of deoxynucleotides which bind to pre-mRNA or mRNA and regulate protein synthesis through a variety of mechanisms.[59] ASO's don't require a specialized delivery carrier and the oligonucleotides are highly chemically modified.[58] GalNAc-siRNA conjugates consist of double stranded RNA which silence genes through interaction with the RNA-induced silencing complex (RISC).[59] By conjugating siRNA to GalNAc the conjugates are targeted to the asialoglycoprotein receptor (ASGPR) which internalizes the conjugate by clathrin-dependent receptor-mediated endocytosis. Both a limitation (in scope) and an advantage (in specificity) to this approach is that ASGPR is largely limited to hepatocytes. Another delivery platform is the use of lipid nanoparticles (LNPs). LNPs protect nucleic acids from degradation, can target nucleic acids to specific cell types, and provide a route for these highly charged molecules to cross the lipid membrane barrier of the cell wall. A well-known example of LNP use is with the COVID-19 mRNA vaccines, although the mRNA vaccines produce proteins rather than disrupting their synthesis.[58] Additionally, the mRNA used in the COVID-19 vaccines uses chemically modified nucleotides

to improve translation efficiency and reduce activation of the innate immune response.[60] Lastly there are gene therapy approaches such adeno-associated virus (AAV) which opens many possibilities including modulating protein expression, transcription of non-coding RNA, and repair of DNA mutations. Due to low efficacy, immunotoxicity, genotoxicity, and societal concerns these approaches have largely been limited to a few applications.[58] CRISPR is another gene therapy approach which has shown promise and made big and controversial news when a scientist (without proper approval) in China used the technology on human embryos which were implanted, and the mother gave birth to HIV resistant twins due to their edited genomes. For now, CRISPR is largely used as a research tool. Generally, it is not considered safe enough for most therapeutic applications, largely owing to the irreversible nature of its effects and unpredictable off-target effects.[61] It seems that there may be a big future for therapeutic nucleic acids and much of this, though not all, is related to shutting down the production of specific proteins. This shows how this can be a powerful approach, but there are other mechanisms one can use to achieve this end while avoiding some of the pitfalls of nucleic acids.

PROTACS

A small molecule approach for modulating protein levels is the use of proteolysis-targeting chimeras (PROTACs). This is also a rather new medicinal approach, but it is receiving a lot of attention with its promise for drugging targets that were once considered undruggable. PROTACs are molecules which link the desired target protein to an E3 ubiquitin ligase (E3) and result in the degradation of the target protein.[62] As such they consist of a warhead that targets the desired protein, a linker, and a ligand for the desired E3. A nice benefit is that the PROTAC itself avoids degradation and is free to target more of the same target for degradation such that a single compound can affect many targets. Another benefit which is important is that high binding

affinity is not required, allowing for targeting of non-traditional binding sites on a protein surface. This essentially opens the entire protein surface for targeting as a binding site. This allows for selection of more unique areas allowing for improved selectivity. It also greatly expands the scope of potential targets beyond those with natural ligand binding sites (enzymes and receptors), garnering much excitement in the field of PPIs.[56,61] PROTACs have major promise to target the previously undruggable targets as well as for overcoming resistance mutations in cancer.[63] The design of the warheads is like the design of traditional small molecules that bind to target sites; however, the linker and chosen E3 are also important and complicate rational design. Currently the design of effective linkers is a challenge as the field is still developing and originally this was relegated to trial and error. Deep learning and molecular simulations are starting to replace the inefficient trial and error model.[64] The choice of E3 ligand, which determines which E3 is recruited, has been shown to affect specificity and effectiveness. It has been shown that what is more important than simply the affinity of the warhead for the target is the stability of the target:PROTAC:E3 ternary complex.[65] While excitement in the field is obvious, many authors seem to ignore the limitations of PROTACs. As can be seen above the design is complicated by the importance of all three regions in determining the overall action of the compound. Additionally, the necessity of these three different regions inevitably makes for a bulky compound which complicates synthesis and is a detriment to important drug-like properties such as permeability and oral bioavailability.[56,66] Importantly, certain types of proteins are not yet suited for degradation by PROTACs. For example, protein targets need to contain ubiquitination sites to be targeted for degradation by the proteasome.[67] Also, cell-surface proteins are difficult to target because the degradation machinery is intracellular.[62] So while PROTACs

and therapeutic nucleic acids have shown some promise there is still plenty of room for other techniques to fill the gaps for un-drugged therapeutic targets.

Inhibitors of Protein Biogenesis

While therapeutic nucleic acids act at a stage before protein synthesis and PROTACs work at a stage after protein synthesis, there is also the possibility of drugs acting during the protein synthesis step. This warrants the mention of the class of highly successful antibiotics which target ribosomes (the protein synthesis machinery). In fact, over half of the available anti-infective drugs target ribosomes. While the ribosomes of bacteria and humans are different enough to target bacterial ribosomes over human ribosomes with specificity, these drugs lack specificity in the sense that they generally stop ribosomes from synthesizing all proteins equally, which makes them highly toxic to bacterial cells.[68] As previously mentioned, large subset of proteins pass through the Sec61 channel during or soon after synthesis. The Sec61 channel is a pore in the ER membrane that allows for passage into the lumen or incorporation in the membrane of the ER for client proteins. The proteins then may be sent to the cell surface or other intracellular locations.[69] A new strategy for drug design is to target the Sec61 channel which results in improper localization, folding, and post-translation modification and eventual degradation of Sec61 clients. While many of the drugs which target the Sec61 channel lack specificity for the client proteins, CADA compounds have been shown to be surprisingly and extraordinarily selective.[70] The focus of this dissertation will be on the study CADA compounds. Before ending this introductory discussion on medicinal chemistry and getting into the details of CADA compounds, it is worth looking more closely at the therapeutic gap available for such compounds.

Opportunities

Current data indicates that there are roughly 4,500 genes known to be associated with human disease which gives a huge amount of opportunity for drug development. FDA approved medicines only target 750 of these.[54] Furthermore, given the problem of resistance mutations (particularly for targets of infectious agents and cancers) even protein targets with well-established medications may benefit from new drugs with different mechanisms of action.[63] Simply put, there is a huge unmet need for drugs with novel mechanisms capable of targeting pharmaceutically relevant proteins. CADA compounds are limited to proteins that contain signal peptides or transmembrane domains that target them to the Sec61 channel in the ER. This is about a third of the proteins in eukaryotic cells.[71] A PROTAC's efficiency of degradation is highly dependent on cellular location owing to the need for the targeted protein to encounter the degradation machinery. Generally, the cytosol and nucleus have been described as favorable locations for PROTAC targets, while membrane bound targets are a grey area and other cellular locations such as the Golgi or ER lumen may be unfavorable.[67] While it appears that PROTACs can still target these locations in some cases it tends to be less efficient and success is highly variable depending on PROTAC design and the target protein.[72] Fortunately, CADA compounds are well positioned to target the proteins which are in these less accessible locations as most of them pass through the Sec61 channel on their way to these locations.[69] The development of CADA compounds still needs work to fully demonstrate the potential, but it is clear that there is room for CADA compounds to make a significant mark on the medicinal chemistry landscape.

Section 2: Protein Synthesis

The proper regulation of protein expression is critical to the functioning of our cells and bodies. Regulation is an incredibly complex process that occurs at every step of protein expression. The structure of the DNA, transcription of DNA to pre-mRNA, processing of pre-

mRNA to mature mRNA, transport of mRNA from the nucleus, stability of the mRNA, translation of mRNA to protein, translocation, post-translational modification of the proteins, protein stability, and protein transport all represent points of regulation[1]. While translocation is often overlooked and likely the most poorly understood of these processes, it is the step that is targeted by CADA compounds this will be the focus of this section. Although CADA compounds have been shown to reduce protein levels by disrupting the translocation of a specific subset of proteins, this doesn't mean that every observed effect on proteins in cells is due to that single mechanism. It is important to understand that disturbances in any of the above-mentioned processes will also affect a given protein.

The complex and important function of protein synthesis is achieved by the action of ribosomes. In eukaryotes, the ribosome is a massive complex of 79 ribosomal proteins (RPs) and four ribosomal RNAs (rRNAs) which make up the 40S and 60S subunits. During synthesis the subunits combine to make the 80S ribosome. The pre-40S and pre-60S subunits are assembled in subnuclear compartments called nucleoli then exported to the cytoplasm where they become the mature 40S and 60S subunits; this process takes all three types of RNA polymerases and over 150 other proteins.[73] One estimate attributes 60% of cellular energy expenditure to ribosome production.[74] Protein synthesis can be broken down to four steps: initiation, elongation, termination, and recycling.[75] Initiation is the rate limiting step in protein synthesis; therefore, of these four steps, regulation of initiation is typically used to control the amount of all proteins, subsets of proteins, or specific proteins that are made. Regulation at an earlier step is more energetically favorable as it doesn't waste resources on unneeded proteins; however, regulation at later steps can be used as a more rapid response to changing conditions. Once in the cytoplasm, the coordination of 9 or more eukaryotic initiation factors (eIFs) and several auxiliary

factors help assemble the 80S ribosome with the mRNA initiator codon based paired with initiator tRNA (Met-tRNA^{Met}) placed in the P-site of the ribosome. The more common mechanism of initiation involves scanning of the 5' untranslated region (5' UTR) while a secondary mechanism involves the use of internal ribosome entry sites (IRES) and doesn't rely on the 5' UTR. Regulatory mechanisms that affect the eIFs, such as phosphorylation or degradation, have very broad effects on protein synthesis.[76] However, it is important to note that different sets of eIFs are used in the scanning mechanism verses the IRES mechanism of initiation. Proteins under the control of these different mechanisms will be affected differently by the regulatory mechanisms targeting eIFs that are not common to the two initiation mechanisms. A more sequence specific type of regulation involves RNA-binding proteins that will affect synthesis of only the subset of proteins that come from mRNAs with the requisite motif. This motif is more often found in the 3' UTR as opposed to the 5' UTR, but in general this type of regulation seems to be involved in development processes as opposed to response to stimuli. The most specific regulation involves base pairing of a miRNA with a specific target site in the 3' UTR. This binding recruits an argonaute (AGO) protein which subsequently recruits the protein, GW182. The result is repression of translation and an accelerated rate of degradation for the targeted mRNA.[76]

Once protein synthesis is initiated, elongation occurs. Regulation of elongation typically refers to the speed of elongation (or synthesis). Synthesis may be slowed such that it influences protein folding, localization, or even to cause a shift in the reading frame to produce a different protein altogether. mRNA secondary structures, rare codons, or by binding of the signal recognition particle (SRP) before entering the Sec61 channel are all mechanisms of slowing elongation to regulate protein synthesis. Regulation of the termination step usually refers to the

read through of a stop codon to produce a C-terminally extended protein.[75] The regulation of the recycling step on the other hand, has been shown to have the potential to affect protein levels in conjunction with reduced ribosome levels but this seems to be less common or at least less well understood.[77] Reduced ribosome levels have been observed in response to many stresses, including heat shock, serum starvation, and toxicity induced by trivalent arsenic which may be related to improper protein folding. Under such stress conditions, reduced ribosome levels are correlated with simultaneous inhibition of initiation of translation by the phosphorylation of eIF2α.[78,79] This coordinated reduction of ribosome levels, initiation of translation, and ribosome recycling may be an important regulatory mechanism at play in response to toxic levels of CADA compounds.

Section 3: Membrane Translocation and Integration

The membranes surrounding and within cells represent a barrier to the passage of molecules such as proteins. Each membrane creates a unique environment with a distinct set of proteins both within the compartment created by the membrane and the membrane itself (**Fig. 1.5**). For proteins to be inserted into or pass through membranes typically they must contain organelle-specific targeting signals. Targeting signals or signal sequences tend to have little sequence homology but share a distinctive set of physiochemical properties. The general sequence of events is that the targeting signal is first

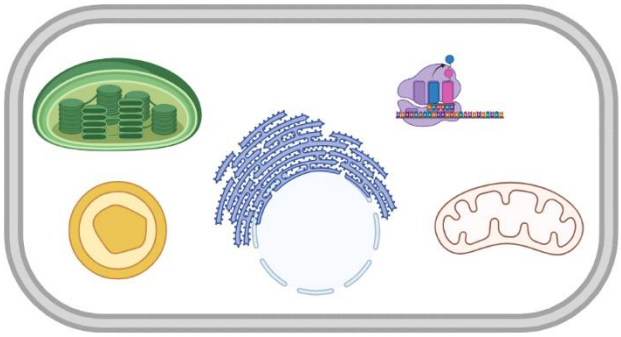

Figure 1.5: Membranes within cells. Ribosomes (dark purple) synthesize proteins in the cytosol of cells. Chloroplasts (green), mitochondria (light purple), peroxisomes (orange), the ER (dark blue), and nucleus (light blue), are all enclosed by lipid membranes that contain protein conducting channels. Additionally, the cell itself is enclosed by one or two membranes (grey) which contain protein conducting channels.

recognized by a soluble signal receptor which brings the complex to a membrane-associated receptor. In the case of signal-gated channels, the membrane channel is present in the membrane in a closed state and passage of the signal sequence to the channel opens the channel for passage of the protein through or into the membrane. Signal-gated translocons tend to have smaller pore sizes and accept proteins with minimal to no secondary structure. The correct signal sequence will gate or open the channel either laterally for integration into the membrane or vertically for passage across the membrane. Alternatively, for signal assembled channels, localization of the signal at the membrane triggers assembly of a multimeric channel around the protein which can be released across or into the membrane. In the case of both signal-gated and signal-assembled translocons, each binding event is more energetically favored than the previous, which pushes the process in the right direction. The process can occur during or after protein synthesis, known as co- or post-translational translocation, respectively.[80] In co-translational translocation synthesis may be slowed or stalled once the signal sequence is recognized by a soluble receptor giving the ribosome nascent chain complex time to dock onto the channel before resuming synthesis, which threads the protein through the channel.[81] A tight seal between the ribosome and channel along with the energy of GTP hydrolysis by the ribosome during synthesis drives the nascent chain through the channel in co-translational translocation.[80,82] In post-translational translocation, chaperones are often involved in maintaining proteins in an unfolded state so they can be threaded through the channel, but other proteins may need to fold prior to passage through a larger channel complex. ATP hydrolysis or membrane potential are common methods for driving proteins through the channel during post-translational translocation.[80] The adenosine triphosphate binding cassette (ABC) transporter superfamily uses ATP hydrolysis to transport a wide variety of substrates across membranes. Some of them transport peptides, but since most

ABC transporters deal with non-proteinaceous substrate and a select few deal with small peptides, they will not be covered in detail here.[83] The nuclear envelope is continuous with and made from the ER membrane, yet the peripheral ER and nuclear envelope are distinct domains with generally different sets of proteins.[84] The nuclear envelope has a unique nuclear pore complex (NPC) which is involved in much more than protein transport.[85] Passage across the outer membrane of Gram-negative bacteria is usually achieved through bacterial secretion systems.[86,87] The membranes of the ER, mitochondria, chloroplasts, peroxisomes, and bacterial inner membrane contain translocation complexes and insertases for transport across and insertion into their membranes.[88]

3.1 Nuclear Pore Complex

The nuclear envelope consists of inner and outer nuclear membranes, which are separated by an internuclear membrane space of about 50 nm which is maintained by the linker of nucleoskeleton and cytoskeleton (LINC) complex that spans both membranes. The NPC not only spans both membranes, but also joins them together as the inner and outer nuclear membranes run along outer walls and are continuous with one another. This allows for the exchange of lipids and integral membrane proteins along the outside of the pores.[82] The NPC is a massive structure that weighs in at 120 MDa in humans, which is almost 35 times larger than ribosomes. Roughly 500 to 1,000 nucleoporin (Nup) subunit proteins, having approximately 30 different varieties, come together to form the NPC. The overall construction of the pore from the nuclear side to the cytoplasmic side consists of a nuclear basket, nuclear ring, inner pore ring, cytoplasmic ring, and filament-like disordered cytoplasmic domains. NPCs are much more than transport systems. They make contacts with chromatin, the cytoskeleton, and other complexes to influence their spatial organization. Amongst other roles, these contacts allow NPCs to act as important

regulators of transcription.[89] The pores are large enough to allow passive diffusion of molecules that are less than 40 kDa, while molecules up to 39 nm in size can pass through by a directed mechanism. Typically, snRNPs, histones, and transcription factors need to enter the nucleus from the cytoplasm while mRNA, tRNA, and ribosomal subunits travel from the nucleus to the cytoplasm. For the proteins, shuttling transport factors are responsible for recognition of either nuclear localization or export sequences (NLSs or NESs) and subsequently docking to the NPC for import or export. Other non-protein cargo also requires transport factors for directed passage through the NPCs. Of the Nups that make up the NPCs, FG Nups form a filamentous layer that seems to provide both a physical barrier for passage of molecules as well as providing a binding site for transport complexes. How the cargo passes through this filamentous barrier is currently a matter of debate.[90]

3.2 Bacterial Secretion Systems

Gram-negative bacteria have both an inner and an outer membrane that separates their cellular contents from the outside environment. The outer membrane presents another obstacle for the passage of proteins and as such Gram-negative bacteria have developed several unique and specialized secretion systems labeled type I-VI (T1-6SSs) (**Fig. 1.6**). Additionally, there is a so-called type

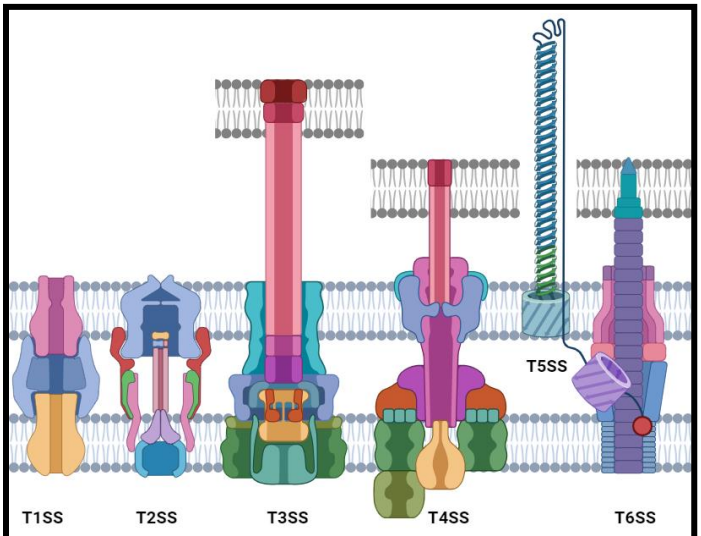

Figure 1.6: Bacterial secretion systems. The standard set of secretion systems includes types 1-6 which transport proteins across the two membranes (light blue) of Gram-negative bacteria. The T3SS, T4SS, and T6SS can also puncture the membranes of host cells (grey). While T2SS appears to be able to transport proteins across the inner bacterial membrane, both T2SS and T5SS substrates rely on Sec or TAT translocons to pass the inner bacterial membrane.

VII secretion system (T7SS) found only in Gram-positive bacteria, but whether it is a genuine secretion system is a matter of controversy. The controversy about what may or may not be considered a secretion system mostly revolves around proteins that become anchored to the cell surface, there may be up to eleven distinct secretion systems.[86,87] Passage through the inner membrane occurs through α-helical channels (like most eukaryotic protein conducting channels), while passage through the outer membrane occurs almost entirely through β-barrel channels.[87] While the passage of a proteins in an unfolded form generally requires smaller and less complex systems, some proteins must fold in the cytoplasm to acquire essential cofactors only available in the cytoplasm before export. Accordingly, they require larger more complex systems for their transport.[86,91] Typically, the proteins secreted by bacterial secretion systems are virulence factors that help the bacteria infect eukaryotic host cells.[86] The absence of these systems in eukaryotic cells as well as their role in infecting eukaryotic cells makes these good targets for antibacterial drugs. T1SSs span both inner and outer membranes and excrete a small number of unfolded proteins in a single step outside of the cell.[86] T1SSs are evolutionarily related to small molecule pumps.[87] T2SSs exports folded (or partially folded) proteins across the outer membrane after they previously passed across the inner membrane via either the Sec or TAT translocons, which will be discussed at a later point.[86] T2SSs are complex structures consisting of a dodecameric channel in the outer membrane, periplasmic pseudopilus, and an inner membrane platform. As hinted by the pseudopilus structure, these systems are evolutionarily related to the type IV pili assembly machinery.[87] T3SSs ("injectisomes") transport proteins in an unfolded state across the inner, outer, and most of the time, host cell membranes. In response to contact of the T3SS tip complex with a eukaryotic host cell, the T3SS translocon forms within the host cell membrane, allowing passage of proteins into the cell.[86,87] This system is evolutionarily related to the

specialized export system used by flagellum during their assembly which has been termed the Flagellar Type III Secretion System (fT3SS).[87,92] The T4SS can also span an additional host cell membrane, but it allows for passage of folded proteins or complexes and even DNA-protein complexes. They can also be used for the uptake of DNA.[86] The T4SS is unique in that the channel formed in the outer membrane is an α barrel consisting of amphipathic α-helices.[87] T5SSs pass the inner membrane as unfolded proteins through the Sec translocon and then insert a C-terminal β-barrel domain into the outer membrane, which allows for the passage of another domain of the same protein which is self-cleaved after transport (autotransporter) or a separate partner protein (two-partner or chaperone-usher, if an additional chaperone protein is needed).[86] While remarkably efficient, insertion of the β-barrel domain still requires assistance, which comes from the β-barrel assembly machinery (Bam)[87], which will be discussed momentarily. T6SSs have a needle-like extracellular component that can pierce the membrane of prokaryotic or eukaryotic cells and inject effector proteins into the target cell. Interestingly, the part that punctures the bacterial membrane shares a structural similarity to the machinery used by bacteriophages to puncture bacterial membranes. These are the well-recognized and accepted secretion systems, but more recently there are other systems that potentially expand the repertoire of known secretion systems and challenge the definition of secretion system.[86,87] Regardless of how these systems are ultimately named, they undoubtedly belong in this discussion of systems for transporting proteins across membranes.

Generally, secretion systems are defined as those that aid in the secretion of proteins across the bacterial cell outer membrane. Although mycobacteria are Gram-positive bacteria, they have a second membrane that is termed the mycomembrane. The T7SS was discovered in these bacteria and later in other Gram-positive bacteria that lack any sort of secondary

membrane. Whether T7SS aid passage across the mycomembrane or just the inner membrane and whether it should be considered a secretion system is a matter of debate. Another point of controversy is whether the T2SS related type IV pili assembly machinery, the T3SS related flagellar assembly machinery, and T5SS related the chaperone-usher system used by Type I pili should be considered secretion systems because the protein assemblies remain attached to the cell and are not secreted. Less controversial is the T8SS that is similar in concept yet structurally distinct to the T5SS chaperone-usher mechanism for the transport of subunits of curli filaments which pass into the extracellular space as soluble unfolded proteins, then fold and aggregate at the cell surface where they become attached. The T9SS has 2 proteins associated with the channel in the inner membrane and 12 proteins associated with the channel in the outer membrane. Its classification is controversial because it predominantly exports surface-attached proteins. Most controversial of all is the T10SS that allows for transport of an endopeptidase into the periplasm where it degrades peptidoglycan, which can cause outer membrane permeability and cell lysis resulting in the release of a chitinase. Later it was shown that chitinase could be released in the absence of cell lysis, which gave more credibility to this system as a true secretion system. A possible T11SS is a two-partner T5SS-like system responsible for transporting and anchoring lipoproteins to the extracellular face of the outer membrane. The transporter protein is structurally distinct from the T5SS transporter and contains a DUF560 domain, which is shared with other transporter proteins involved in transport of soluble proteins, such that DUF560 containing transporters may be classified as T11SSs.[87] One thing that almost all these secretion systems have in common is the need to insert a β-barrel channel into the outer membrane which itself requires a special machinery, as discussed next.

3.3 β-Barrel Insertases

As mentioned at the beginning of the discussion on bacterial secretion systems, the transmembrane domains of integral outer membrane proteins in Gram-negative bacteria are almost entirely β-strands, while the transmembrane domains of integral inner membrane proteins are almost entirely α-helixes. While transmembrane domains consisting of β-strands are rare in eukaryotes, they can be found in the outer membranes of mitochondria and chloroplasts, which is evidence of the evolutionary origin of these organelles (originating from endosymbiotic bacteria). The translocons of the outer membranes of mitochondria and chloroplasts (TOM and TOC, respectively) are examples of these types of proteins. Insertion of these types of proteins occurs through the Bam complex in prokaryotes, the TOB/SAM complex in mitochondria, and an unidentified complex in chloroplasts. The main subunits of the Bam and TOB/SAM complexes are β-barrel integral membrane proteins, Omp85/BamA and Tob55/Sam50, respectively. A homologous protein, Toc75-V/OEP80, has been identified in chloroplasts.[93] While all other signal sequences discussed in this dissertation are α-helical, the signal sequences of β-barrel proteins are β-strands.[94] The complexes of multiple subunits form large cylindrical structures with central cavities large enough to provide a protected environment for the formation of β-barrels with up to 22 β-strands within the membrane, yet complete details of the mechanism of insertion are yet to be elucidated. These large insertase complexes exclusively insert transmembrane proteins into membranes and are not involved in the passage of proteins through the membrane.[93]

3.4 Signal-Assembled Translocons

Translocons are protein complexes which are capable of both passing client proteins across and integrating client proteins into the membrane in which they reside. Passage across the membrane occurs through a central aqueous pore. Integration of transmembrane domains into the

membrane via a translocon occurs through the opening of a lateral gate in a clamshell like fashion. Proteins may flow in either direction through the channels and often chaperones or other proteins appear to aid proteins through the channel in the desired direction, although other mechanisms such as protein folding and membrane potential may also be at play in driving proteins through the channels. Chaperones and membrane potential along with the interaction of the complex with certain features in the substrate may also be necessary for correctly orienting transmembrane domains within the lipid layer.[91]

Signal-assembled translocons tend to have larger pore sizes than signal-gated translocons and can accept fully folded proteins or complexes.[91] Proteins that need to bind a cofactor only available in the cytoplasm, need to be folded and bind their respective cofactor(s) before transport to the next compartment. For signal-assembled translocons, a characteristic signal sequence targets these fully folded substrates to a specific receptor in the membrane, where the large translocon channel consisting of many multimers is then assembled in response. After transport of the substrate the channel is quickly disassembled to prevent membrane leakage. These α-helical translocons are found in peroxisomes (PEX),[95] bacteria (TAT), and chloroplast thylakoids (TAT/ΔpH).[96] By complexing with a protein which contains a signal sequence for these translocons, some proteins can gain passage without needing a signal sequence of their own.[91]

3.5 Mitochondrial Translocons

Mitochondria perform the crucial task of oxidative phosphorylation that results in the production of energy rich molecules ATP and NADH as well as the carbon rich pyruvate. Mitochondria are involved in many cellular functions such as signaling, quality control, and with energy and carbon sources readily available it is no wonder that the biosynthesis of many

molecules such as amino acids and lipids occurs in the mitochondria.[94] Mitochondria have their own DNA and produce their own mRNA which is by their own specialized ribosomes to make their own specialized proteins.[97] However, only about 1% of the proteins in the mitochondria (13 proteins in humans) are made from their own machinery. Currently there are five distinct transport pathways in mitochondria, each with a distinct signal sequence, to get the bulk of their proteins from the cytosol to their ultimate destination. There are four possible destinations: the inner compartment (the matrix), the inner membrane, the intermembrane space, or the outer membrane; however, the presequence pathway is capable of transporting proteins to different destinations based on more subtle variations of the signal sequence. The translocase of the outer membrane (TOM) channel complex is the point of entry for all, but one of these pathways. The complex consists of three receptors (Tom20/22/70), the central channel (Tom40), and three accessory proteins (Tom5/6/7). Interestingly, up to three Tom40 channels can group together into a single complex. Tom40 is a β-barrel protein consisting of 19 transmembrane β-strands and is large enough to contain separate paths for either hydrophobic or hydrophilic protein regions.[94]

Mitochondria have multiple different machineries in their two membranes and many distinct pathways for the biogenesis of mitochondrial proteins (**Fig. 1.7**). The presequence pathway is a versatile pathway which can be used to localize proteins to the matrix, the inner membrane, or alternatively the intermembrane space. The N-terminal signal sequence (presequence) folds into an aliphatic α-helix secondary structure[80] and the hydrophobic face is recognized by the Tom20 membrane receptor, which then passes the signal to the Tom22 central receptor that binds the positively charged face of helix.[98] Tom22 passes the presequence to Tom40, which is gated and allows for passage. Once the presequence emerges in the

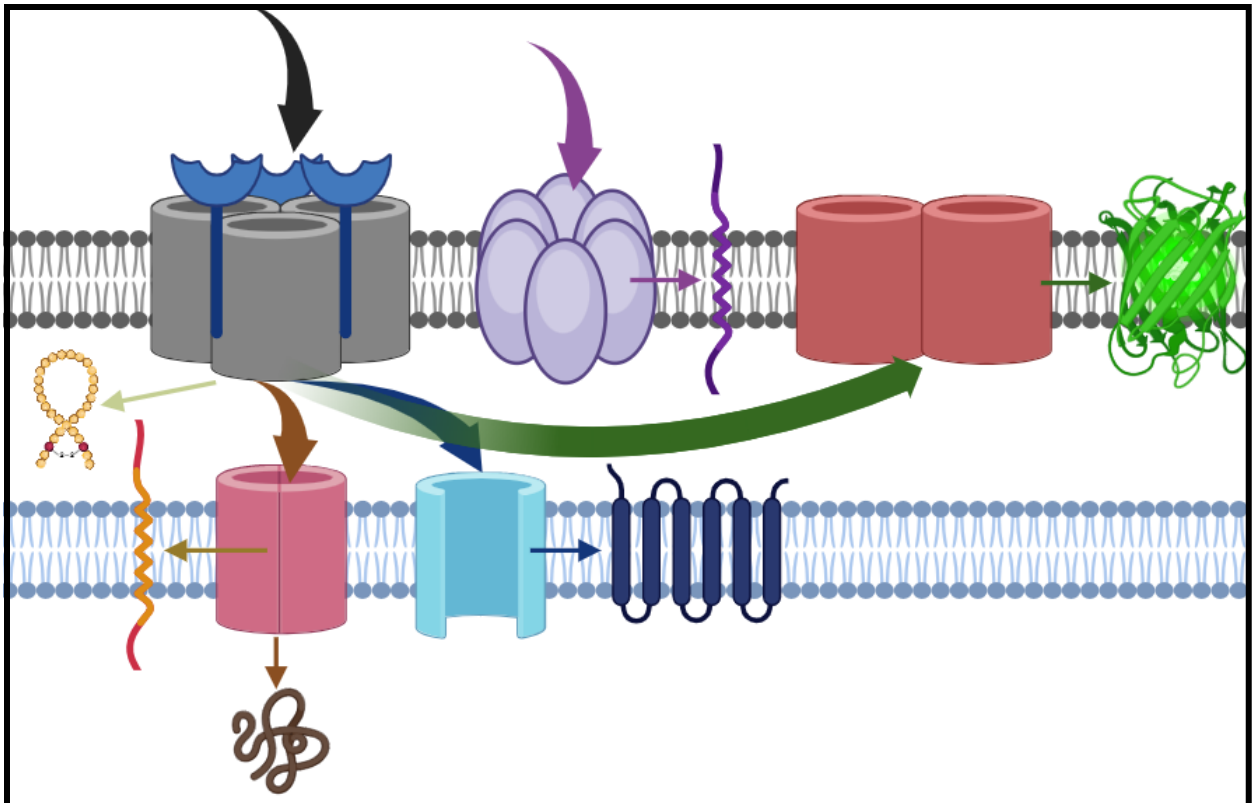

Figure 1.7: Mitochondrial translocons. The translocons of the mitochondria consist of the TOM complex (grey), MIM complex (light purple), and SAM complex (red) in the outer membrane (dark grey). The inner membrane (blue) contains the TIM23 complex (pink), and TIM22 complex (light blue). The MIM complex inserts α-helical outer membrane proteins (dark purple) into the membrane. Proteins with a presequences are initially targeted to the TOM complex and then take different paths from there. Proteins with cysteine motifs Cx3C or Cx9C (beige) form disulfide bonds are retained in the intermembrane space. The β-barrel proteins of the outer membrane (green) then pass into the SAM complex for assembly and insertion into the outer membrane. Multipass transmembrane metabolite carrier proteins (dark blue) pass through the TM22 complex for insertion into the inner membrane. Other inner membrane proteins (gold) are integrated into the inner membrane by TIM23 which can also pass soluble matrix proteins (brown) into the mitochondrial matrix.

intermembrane space the Tim50 subunit of the presequence translocase of the inner membrane (TIM23) channel complex along with the regulatory subunit Tim21 assist in inserting the presequence into the central channel formed by the Tim23 subunit. This couples the translocation of the client protein through both the TOM and TIM23 complexes simultaneously.[94] The inner membrane of mitochondria contains a membrane potential which is negative on the matrix side. This potential both activates the Tim23 channel as well as exerts a pulling force on the positively

charged presequence.[99] Proteins destined for the matrix need additional assistance from an ATPase, the presequence translocase-associated motor (PAM). The regulatory subunits Pam16-Pam18 also interact with the respiratory chain III-IV supercomplex although the reason for this interaction is not yet fully understood.[94] The membrane potential is sufficient for integral membrane proteins that exit through a lateral gate into the lipid environment of the membrane without the assistance of PAM,[99] but the Tim21 subunit links the TIM23 channel complex with the respiratory chain III-IV supercomplex. The respiratory chain III-IV supercomplex is a proton pump and presumably increases the local membrane potential, which increases the efficiency of the TIM23 channel complex. In a beautiful display of cooperation, the TIM23 channel complex is responsible for integration of respiratory chain subunits into the membrane and assist in the assembly of respiratory chain complexes. Insertion of transmembrane domains through the lateral gate of Tim23 is known as stop-transfer sorting.[94] Another strategy is for transmembrane domains to pass into the matrix through the central pore-like channel and then be recognized by the oxidase assembly (OXA) translocase, which inserts the transmembrane domains into the inner membrane. This is called conservative sorting. Some transmembrane proteins use a combination of these two different sorting strategies.[100] Oxa1 is the main component of the OXA translocase and is also used for co-translational insertion of proteins synthesized in the matrix by mitochondrial ribosomes.[101] Oxa1 is part of a family of insertases including ALBINO3 and YidC that promote insertion of substrates into chloroplast thylakoid and bacterial plasma membranes, respectively. More recently Oxa1 homologs have been found in the ER membrane as well.[102] Either during or after transport, the presequence is cleaved by the heterodimeric mitochondrial processing peptidase (MPP) and subsequently degraded by presequence protease (PreP). Typically, MPP is a soluble protein in the matrix, but in plants it is composed of two matrix

exposed subunits of the respiratory complex III. A second peptidase on the intermembrane side of the inner membrane, the inner-membrane peptidase (IMP), cleaves some preproteins a second time, which may result in their release into the intermembrane space as a soluble protein.[94]

The carrier pathway is used to insert a family of metabolite carrying proteins with six α-helical transmembrane proteins into the inner membrane. These proteins possess internal transmembrane domains (TMDs) as their targeting signals which are held in translocation competent, largely unfolded, states by chaperones in the cytosol before being passed to the Tom70 receptor followed by the central Tom22 receptor.[103] Carrier proteins are inserted into the Tom40 channel in a loop formation with both termini still in the cytosol and then translocated through the outer membrane. Chaperones associated with the N-terminus of Tom40 bind to the hydrophobic domains as they exit the channel. The chaperones then pass the carrier proteins off to the receptor-like protein Tim54 subunit of the carrier translocase of the inner membrane (TIM22) which integrates them into the inner membrane through the Tim22 channel forming subunit. Tim22 is evolutionarily related to Tim23 and similarly transmembrane domain insertion through a lateral gate is largely by membrane potential.[94]

Another pathway involves retention of proteins in the intermembrane space after transport through the TOM channel complex. Proteins with cysteine motifs Cx_3C or Cx_9C are recognized by the oxidoreductase Mia40 in the intermembrane space which catalyzes the formation of disulfide bonds, the electrons created in this process are then passed to the respiratory chain. The formation of disulfide bonds in client proteins is usually sufficient to promote folding and prevent further passage across membranes, but some proteins may continue to the matrix through TIM23 via the presequence pathway.[94]

The β-barrel proteins of the outer membrane have C-terminal β-hairpin signal sequences that target them to the TOM channel complex for passage into the intermembrane space where they are bound by chaperones. The C-terminal most β-strand of the β-hairpin then is all that is needed for the signal recognized by the previously discussed TOB/SAM complex which inserts β-barrel proteins into the outer membrane by a poorly understood mechanism.[104] The mitochondrial import (MIM) complex is another poorly understood complex. It is responsible for the insertion of N-terminal signal-anchored and polytopic α-helical integral membrane proteins into the outer membrane. For the insertion of tail anchored (C-terminal) integral membrane proteins a protein machinery has not been found, but lipid composition is known to be important for insertion. In addition, other routes into the outer membrane, such as through the lateral gate of the TOM channel complex are likely to be discovered in the future.[94]

3.6 Chloroplast Translocons

It is well understood that chloroplasts perform the essential task photosynthesis which converts CO_2 and water to glucose and oxygen using light energy. The details of its translocation machinery are not as well understood.[105] Like mitochondria chloroplasts evolved from endosymbiotic bacteria and most of the genome has been transferred to the nucleus over time, although they have retained a slightly larger genome with close to 100-200 genes.[106,107] Similar to mitochondria, chloroplasts have structurally distinct machinery for their outer (TOC) and inner (TIC) membranes.[91,108] TOC and TIC can also couple together through transient interactions so that a single protein can simultaneously pass through both membranes efficiently. Another parallel is the α-helical and β-barrel nature of TIC and TOM, respectively.[91,93,109,110] Complicating the translocation process for chloroplasts is that not only do they contain an outer and inner membrane, but the stroma (analogous to the mitochondrial matrix) also contains

thylakoids which are flattened membranes which are responsible for photosynthesis.[107] The classic pathway for import is to cross the outer membrane via the TOC channel complex and then the inner membrane via the TIC channel complex already mentioned previously. The signal sequence for this pathway is referred to as a transit peptide which is initially recognized by receptor and regulatory subunits Toc33/34 and Toc 159/132/120/90. These subunits have GTPase and can be phosphorylated which seems to aid in regulation, and additionally there are multiple subunits which may control substrate selectivity. After receptor binding the preprotein is passed to the Toc75 β-barrel channel forming subunit.[105,106] Similarly to the TOM channel complex, the TOC channel complex can consist of multiple Toc75 channel forming subunits (up to four subunits).[111] After the transit peptide exits the TOC channel complex it is then recognized and transported through the TIC channel complex. Currently there are two competing models about the constituents and function of this channel. It is not even clear if there may be multiple different complexes similar to the situation with TIM22/23 in mitochondria or a single genuine TIC complex.[105,112] Nonetheless it is clear that unlike TIM22/23 the TIC complex does not use membrane potential and is instead dependent on the action of an ATPase motor protein to drive the preprotein into the stroma, although the nature and identity of this motor protein is also a matter of debate.[105,106,112] Once in the stroma the transit peptide is removed by the stromal processing peptidase (SPP).[107]

An estimated 30% of imported proteins do not contain transit peptides.[113] Other routes into stroma may be through the transport of mRNA for translation in the stroma (mRNA transport to the mitochondrial matrix has also been demonstrated).[114] The insertion of β-barrel proteins into the chloroplast outer membrane is not well understood, but likely involves Toc75-V/OEP80. Additionally, transmembrane proteins of outer and inner membranes may be targeted

by a TMD which gets integrated into the membrane by stop-transfer sorting through lateral gate of either the TOC or TIC channel complexes, respectively,[107] and glycoproteins may first pass through the ER into the Golgi and be transferred by vesicles that fuse with the chloroplast membrane.[115] Lastly, yet to be discovered mechanisms also seem highly likely. Proteins that are retained in the intermembrane space likely pass through the TOC channel complex, but little is known about their retention or other possible routes.[116] One possible route passage from the stroma through a Sec-related translocon in the inner membrane, chloroplast SEC2 (cpSEC2).[107] In the stroma there are multiple pathways for insertion into the thylakoid membrane or lumen. Proteins that first pass through the TOC/TIC channels via recognition of a transit peptide may have the transit peptide cleaved by the inner envelope peptidase which exposes a new N-terminus with a secondary sorting signal which is recognized by one of the several thylakoid pathways. The TAT/ΔpH route for folded proteins which was already discussed earlier in the discussion on signal-assembled translocons is one such pathway. Another is through the Oxa1 related protein, ALBINO3, which can accept proteins from the stroma in a post-translational manner as well as co-translational translocation of proteins synthesized by chloroplast ribosomes. Another pathway is through the chloroplast Sec-related translocon, cpSEC1. The Sec-related Sec61 translocon will be discussed in great detail in the next section. Other pathways into thylakoids are vesicular trafficking and spontaneous insertion.[107,117]

3.7 Sec61: The Main ER Translocon

The ER, in terms of number of membranes and compartments, is much simpler than mitochondria and chloroplasts and as such has less diversity in its translocation machinery (**Fig. 1.8**). The main machinery is the Sec61 channel complex. Additionally, there are three Oxa1 insertase family members (GET1, EMC3, and TMCO1), which exclusively aid in insertion of

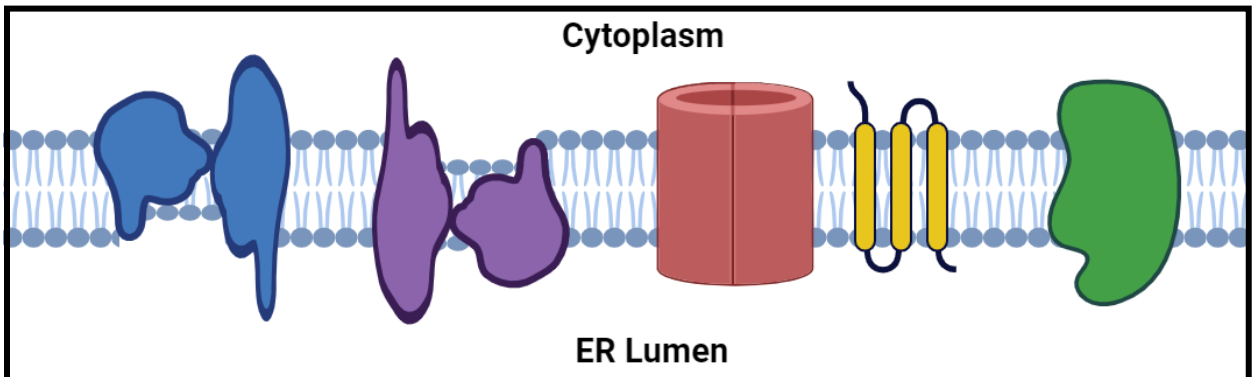

Figure 1.8: ER translocons. The translocons of the ER include the main Sec61 channel (red), Oxa1 insertase family members GET1 (purple), EMC (green), and TMCO1 (yellow), and the HRD1 retrotranslocon complex (blue).

transmembrane domains into the ER membrane. GET1 and EMC3 function in the post-translational insertion of tail-anchored (TA) proteins where EMC3 targets TMDs with lower hydrophobicity.[118,119] TMCO1 works in conjunction with Sec61 for the insertion of multipass membrane proteins that the Sec61 channel can't handle on its own.[120] There is also an unassisted mechanism for insertion into the ER membrane.[121] Lastly, the HRD1 complex constitutes a retrotranslocon that predominately exports misfolded proteins from the ER, which will be discussed at the end of this section.[122,123] The importance of the ER membrane protein transport system is undeniable. Not only for the function of the ER itself, but the ER is also responsible for the biogenesis and sorting of proteins destined for other locations. In fact, vesicular trafficking starting at the ER is the main mechanism of protein transport within and out of the eukaryotic cell.[124] This helps explain why ~7,000 of the ~20,000 human proteins produced in the cell are targeted to the ER.[125] Additionally, the ER lumen contains a large repertoire of chaperones and proteins for performing post-translational modifications, along with a complex and well developed quality control system to ensure proteins are properly folded and functional or degraded.[126] The best studied membrane transport channel system is that of SecYEG in bacterial inner membranes, and this is analogous to the Sec61 ER membrane channel in eukaryotes.[80] In addition to the high degree of similarity with SecYEG, it is likely that the importance of the ER

in protein biogenesis and transport has resulted in this system being intensely studied and better understood than the previously discussed systems. The Sec61 channel is also the site of action of CADA analogues, and hence of upmost importance to this dissertation. Accordingly, great care will be taken to review protein biogenesis at the ER in detail.

Localization to the ER, like all membranes, starts with recognition of a signal sequence. The classic signal sequence that targets proteins to the ER is known as a signal peptide (SP); however, there is some confusion in the literature about the use of this term. Some authors use the term SP in a more generic sense to include for example the mitochondrial presequences and chloroplasts transit peptides or even all signal sequences.[127] In this dissertation SP refers only to the N-terminal cleavable sequences that target proteins to the Sec61 channel (or SecYEG in bacteria). Additionally, many transmembrane proteins lack SPs, but are targeted to the ER by a TMD (generally the first TMD from the N-terminus of the protein).[125] As is typical of signal sequences, the SP lacks sequence conservation, but has conserved structural features. It is composed of a positively charged N-region, a hydrophobic α-helical H-region, and a polar C-region that ends with the cleavage site (**Fig. 1.9**). The amino acids downstream of the signal peptide are also important for the function of the signal peptides and need to have complementary features which are compatible with the signal peptide.[127]

The N-region is usually 1-5 residues long, but can be much longer. It is enriched in basic amino acids, which along with the N-terminal methionine (unformylated in eukaryotes) give it an

Figure 1.9: Conserved SP features. The N-region (red) is enriched for positively charged amino acids, the H-region (green) is hydrophobic and α-helical, the C-region is polar and contains the cleavage site which prefers small aliphatic amino acids at the -1 and -3 positions relative to the cut site. The protein N-terminus (black) is part of the flanking region that contributes to SP orientation.

overall positive charge.[80] The positive charge may interact with the negatively charged phosphate group of the lipid bilayer which improves translocation effeciency.[127] The "positive-inside rule" was first described in bacteria in reference to SecYEG complex located in the bacterial inner membrane. It describes the observation that TMDs with flanking positive charges would be oriented in the membrane such that the positive charges were on the inside of the cell.[128] For SPs, the flanking regions are those regions flanking the H-region: the N-region and on the other side a region including the C-region and a stretch of amino acids beyond (**Fig. 1.9**). The positively charged flanking region is held at the membrane surface on the cytoplasmic side by the membrane potential and interaction with negatively charged phosphate head groups of the phospholipids.[129,130] While a similar phenomenon is observed for eukaryotes, it is a much more dynamic situation where TMDs and SPs can re-orient within the channel after insertion.[131,132] It's the overall balance of charges across the flanking regions that is important.[127] Interactions between charged amino acids in the Sec61 channel and the positive charges in the flanking regions of the SP or TMD are responsible for achieving the correct orientation.[131] Thus, it is not simply the overall charge that is important, but also the locations of the charged residues in the flanking region that are important.[133]

Perhaps the most important region is the hydrophobic H-region. The hydrophobicity of the H-region plays a critical role in affecting translocation efficiency. Generally, the more hydrophobic the greater translocation efficiency, and leucine (a hydrophobic amino acid) is very common in the H-region of SPs.[127] Strongly hydrophobic H-regions may even eliminate the need for a positive charge in the N-region as demonstrated for E. coli SPs (which contain an N-formyl (non-charged) methionine at the N-terminus).[134] Yet if the signal peptide becomes too hydrophobic this may promote aggregation and be counterproductive to functional protein

expression.[127] While positively charged amino acids in the N-terminus and in the mature protein proximal to the cleavage site showed minor importance to the SP recognition by the SRP, the hydrophobicity of the H-region was shown to be the main determinate of SRP recognition and binding.[135] The hydrophobic amino acids also give the H-region a strong α-helical propensity. Importantly, the hydrophobicity and α-helical nature help signal peptides to insert between the α-helices of the Sec61 channel lateral gate and displace the Sec61 plug domain. This transitions the channel into an open state, a process known as gating, to allow for passage of the protein nascent chain through the channel.[127]

The C-region is important because it contains the cleavage site, which must be recognized and cleaved by the Sec61 associated signal peptidase (SPase) in order to release the mature chain from the membrane bound signal peptide. As such, signal peptide cleavage is essential for efficient translocation into the ER lumen.[127] The C-region is typically 3-7 amino acids long, where 4-5 amino acids optimally position the cut site in the SPase active site for cleavage.[127,136] The amino acid immediately before the cleavage site is referred to as the P1 or position -1 and the second amino acid before the cleavage site is referred to as P2, etc. Amino acids immediately after the cleavage site take to the naming system of P'1 or position +1 and so on.[127] The C-region typically contains to small aliphatic residues at positions -1 and -3, but exceptions are not uncommonly found, especially at the -3 position. The H-region often terminates with helix breaking residues glycine, proline, or serine (a much weaker helix breaker) and many C-regions have been predicted to have a β-turn structure.[136] When a signal peptide was modeled into the crystal structure of a bacterial signal peptidase, an extended β-strand conformation was required to give a favorable fit and for formation of hydrogen bonds with a conserved β-strand in the SPase.[137] This is in contrast to a crystal structure of the signal sequence

of OmpA in the lateral gate of the bacterial SecY channel which shows the entire signal sequence from N-region to C-region in an α-helical conformation. In this structure, the C-region forms an amphipathic α-helix with the side chains of polar residues at positions -2 and -5 occupying the inner cavity (in the space occupied the channel plug domain in the closed channel) and the nonpolar residues at positions -3 and -4 facing the lipid environment of the ER membrane. This amphipathic α-helix appears to be important for creating a seal in the lateral gate and preventing lipids from flowing into the channel. In this condensed α-helical conformation, the cleavage site appears too deep in the channel to be accessible for cleavage by SPase.[138] This highlights the fact that proteins are dynamic structures, and studies have shown the structure of signal peptides can vary from α-helix to β-strand to random coil depending on the environment.[139] The signal peptidase complex (SPC) transitions the C-region from an condensed α-helical conformation to an extended β-strand conformation during the cleavage process.[140] Cleavage typically occurs early in the biogenesis process, co-translationally, but in some cases it may occur late in the process, post-translationally. The timing is substrate specific, dependent on both the SP and part of the protein downstream of the cleavage site, and can affect proper folding, PTMs, and assembly. It was shown that the HIV-1 envelope glycoprotein gp160 is tethered to the ER membrane by its SP for at least 15 minutes after synthesis while the protein folds, forms disulfide bonds, becomes highly glycosylated, undergoes proline isomerization, and trimerizes. After all that, the signal peptide is cleaved and the protein is able to exit the ER. The H-region of the gp160 SP does not terminate with a helix breaking residue and the α-helix was predicted to extend into the cut site. Experimental insertion of a helix breaking residue near the cut site produced earlier co-translational cleavage, misfolding, and a poorly functioning protein.[141] This shows that C-region has a dynamic secondary structure that is an α-helix during gating of the

channel, but must extend into a β-strand for cleavage by the SPase. It warrants mentioning that the region upstream of the SP (N-terminal domain of the proprotein) was shown to affect the cleavage of the SP in the study of the SP of gp160,[141] it was also previously mentioned that positively charged amino acids in this upstream region have an effect on the orientation of the SP,[127] and this region (particularly positively charged residues) was also shown to be important to CADA susceptibility.[142] So while the upstream region is not a part of the SP per se, it certainly is important to the functioning of the SP.

The above description of SPs is that of the more common and more simple SPs which have a shorter average length and which exhibit the conserved functions of targeting to the ER membrane, as well as gating of the Sec61 channel. There are SPs with longer average lengths that often exhibit additional functionality and have less classical organization or features in terms of the N-region, H-region, and C-region, as described above. For example, there are some proteins that contain cryptic SPs which contain information for targeting to both the ER and mitochondrial membranes upstream of the signal peptidase cleavage site, giving way to a protein which may be targeted to either membrane. Alternatively, a traditional ER targeting SP may be followed by a traditional mitochondrial presequence that comes after the signal peptidase cleavage site. Despite mixing together of signal sequence for creating more complex protein localization patterns, longer SPs may persist after cleavage and have structures and functions that aren't related to protein sorting. While longer SPs are present in eukaryotes, longer SPs are not well studied in eukaryotic proteins and are hard to predict and therefore identify by programs such as SignalP which use shorter classically organized SPs in their training algorithms.[143] However, there are several examples in viral proteins have been studied in more detail. The 58 amino acid SP of the arenaviral glycoprotein C (GP-C) contains an extended N-region and two

H-regions; it associates with GP-C even after cleavage and assists in GP-C maturation and subsequent transport to the cell surface. A 98 amino acid SP found in mouse mammary tumor virus is highly functionalized. The SP is part of an alternatively spliced transcript that can produce either the Env or Rem protein. The Env SP becomes a type I membrane protein after cleavage, while the Rem SP becomes a soluble protein after cleavage, alternatively the Rem SP under certain conditions doesn't localize to the ER membrane and remains attached to Rem. The SP also contains both an NLS and NES and can help in export of viral transcripts containing introns from the nucleus as a regulatory factor for the production of alternatively spliced viral proteins.[144] Now that the SP has been described in detail, we can move on to description of the Sec61 translocation machinery starting with recognition of the SP by the SRP.

Before the SRP can gain access to the SP as it exits the ribosome, it interacts with the nascent polypeptide-associated complex (NAC). The NAC binds to the ribosome at a site overlapping with the SRP binding site and prevents binding of the SRP to a ribosome in the absence of a SP.[145] The NAC has been shown to be important in co-translational targeting of proteins to the mitochondria via their presequences,[146] but also has a flexible domain which interacts with the SRP and allows SRP scanning of the nascent chain. The emergence of a SP results in the release of NAC and binding of the SRP to the ribosome-nascent chain (RNC) complex.[145] The SRP structure is highly variable across species so the focus will be on the human SRP, which consists of the 7SL RNA consisting of an Alu domain and S domain. The 7SL RNA acts as a scaffold for the six protein subunits. SRP9 and SRP14 bind the Alu domain while SRP19, SRP54, SRP68, and SRP72 bind the S domain. SRP19 functions to stabilize the SRP complex in the correct structure.[147] The SP binds to SRP54 which causes the Alu domain (SRP9/14) to reach into the ribosome elongation factor binding site and arrest or retard nascent

protein elongation.[81,147] This gives SRP54 time to find and bind to the heterodimeric SRP receptor (SR). The exact role of SRP68 and SRP72 is not well understood, but they also seem to be involved in the targeting process. The binding of the RNC-SRP-SR complex to Sec61 will cause the dissociation of Sec62-Sec63 if it is present (involved in post-translational translocation, discussed later) from Sec61.[148] The SR consists of SRα and SRβ subunits, each with GTP-binding domains. SRP54 also contains a GTPase domain which associates with SRα. The SRP54 and SRα GTPases stimulate the GTPase activity of each other while the GTP-binding domain of SRβ lacks intrinsic GTPase activity, and requires a guanine nucleotide exchange factor (GEF). Both the activator and GEF of SRβ are currently unknown. Nonetheless, it is clear that hydrolysis of GTP plays a regulatory role in the process and drives targeting and handover in the right direction towards creation of a translocation complex which consists of the RNC complex bound to Sec61.[147] The SP is released by SRP54 and inserted into the Sec61 channel, the ribosome rotates 180º relative to Sec61 in the plane of the membrane, and the SRP and SR complexes dissociate from the Sec61-RNC complex.[148] A quality control mechanism known as Regulation of Aberrant Protein Production (RAPP) may be activity when SRP54 fails to properly recognize the SP. This is a poorly understood quality control mechanism, but it involves AGO (but not miRNA) and the end result is degradation of the mRNA associated with the RNC complex.[147] It is possible that this pathway could be activated for some targets of CADA analogues, but this is an interesting avenue of research that has yet to be investigated in detail.

The Sec61 channel is a heterotrimeric complex that forms a flexible pore that spans the ER membrane (**Fig. 1.10**). It is capable of allowing the passage of extended hydrophilic protein

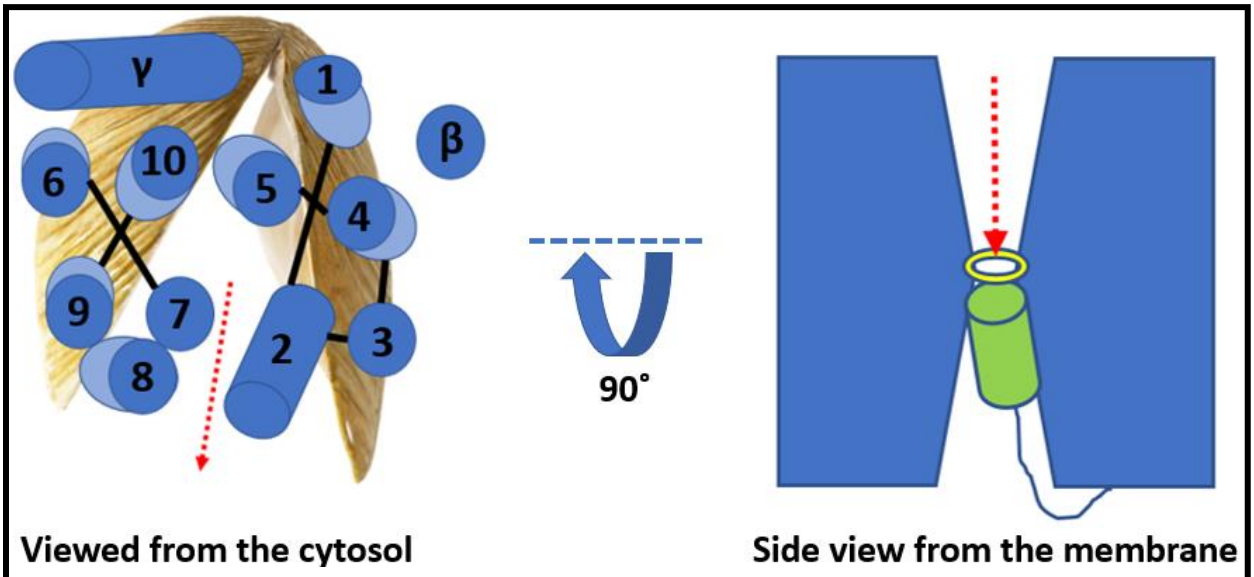

Figure 1.10: Structure of the Sec61 translocon channel. On the right side the channel is viewed from the cytosol. The ten TMDs of Sec61α are labeled from the N-terminus to C-terminus. TMDs of Sec61β and Sec61γ can also be seen on the backside of the channel. The opening for the lateral gate is indicated by the red dotted arrow. The image on the right shows the hour-glass shape of the channel when rotated 90˚ and viewed from the ER membrane. The pore-ring structure (yellow ring) forms a hydrophobic seal and the alpha-helical plug domain (orange cylinder) is shown blocking passage through the vertical gate (pathway shown by red dotted arrow).

segments vertically across the membrane into the aqueous lumen of the ER or the integration of hydrophobic α-helical segments laterally into the lipid environment of the ER membrane itself.[148–150] The Sec61 complex consists of the α subunit which forms the channel itself, and the peripherally bound β and γ subunits. The α subunit has 10 membrane spanning α-helical transmembrane segments numbered TMs 1-10 in order from the amino-terminus to carboxy-terminus. The channel TMs form an hourglass shape with the N- and C- terminal halves showing a pseudo-twofold symmetry. TMs 2, 5, 7, and 10 form the central pore-like structure which constricts approximately at the center of channel.[151,152] At the construction point, hydrophobic and mostly aliphatic amino acid side chains face towards each other in the cavity to form what is termed the pore ring (or vertical gate) via hydrophobic interactions. The pore ring is a hydrophobic seal that prevents leakage of ions and small molecules, but is flexible enough to expand around the extended peptide chain during translocation while still maintaining its

integrity as a barrier. Additionally, on the lumenal side of the pore a flexible α-helical plug domain between TMs 1 and 2 forms hydrophobic interactions with the pore ring and the lateral gate to further stabilize the seal when the channel is closed.[153] The two halves of pseudo-symmetric hourglass shaped channel come together to form a lateral gate capable of opening the channel laterally (like a clam-shell) towards the lipid environment of the ER membrane. This connection is formed between the TM helices 2 and 3 on one side and TM helices 7 and 8 on the other side. Interhelical interactions can seal the lateral gate shut preventing lipids leaking into the central cavity. Opposite of the lateral gate, a short loop between TMs 5 and 6 (loop 5/6) on the lumenal side along the γ subunit forms the hinge of the clam-shell, holding the structure together even as the lateral gate opens enough for hydrophobic α-helices to slide through. The γ subunit consists of an amphipathic α-helix that straddles the lipid/water interface on the cytosolic side of the membrane and a curved α-helical TM domain which roughly crosses backside of the channel at a 35º angle while contacting TMs 1, 5, 6, and 10.[151,152]

The Sec61 channel requires the help of other complexes to function properly and amongst others, the translocating chain-associated membrane protein 1 (TRAM1), the translocon-associated protein (TRAP) complex, and oligosaccharyl transferase complex (OST) are associated with the Sec61 complex *in vivo*.[148] TRAM1 has 8 TMDs with rather small cytosolic and lumenal domains, which make its visualization and identification in structural studies rather difficult. As such its positioning relative to Sec61 is not clear, but has been suggested as being on the backside hinge of the channel. It has been shown to be necessary for the biogenesis of a subset of Sec61 client proteins. This subset is poorly characterized, but may is enriched in proteins containing SPs with shorter N-regions and possibly shorter H-regions as

well. TRAM1 also has a poorly defined mechanism of action, but it may involve the its ability to influence phospholipid packing near the lateral gate.[154]

Different structures will be used to help understand conformations changes of the Sec61 channel during the process of co-translational translocation. Some are of isolated or detergent solubilized complexes and are not entirely representative of the actual conformations that occur in the native Sec61 channel complexes, yet are a useful conceptually for understanding channel gating. The first is a crystal structure of an isolated archaeal Sec61 channel complex consisting solely of the α, β, and γ subunits (PDB: 1RH5) which represents the closed or quiescent channel.[151] The second is a cryo-EM structure of a detergent solubilized mammalian (porcine) Sec61 channel bound to a non-translating ribosome (PDB: 3J7Q), which represents the ribosome primed channel.[152] During co-translational translocation, the ribosome is bound to Sec61 by interactions with cytosolic loops between TMs 6 and 7 (loop 6/7) and TMs 8 and 9 (loop 8/9) of the α subunit along with an interaction with the amphipathic helix of the γ-subunit.[152] At this point the exit tunnel of the ribosome is in line with the Sec61 channel through the ER membrane.[155] Comparing the closed channel with the primed channel, loop 6/7 is rotated 20-30º and while in the closed structure loop 8/9 is disordered and poorly resolved, loops 6/7 and 8/9 had some of the best resolution in the primed structure. This improved resolution is likely the effect of stabilization from binding to the ribosome. The change results in a strain that propagates to the weak link which is the lateral gate. TMs 2 and 3 of the lateral gate rotate from somewhat slanted to a more upright orientation disturbing the polar interactions between three amino acid side chains between TMs 2, 3, and 7 and creating a slight opening of the lateral gate between TMs 2 and 8 on the cytosolic side. This is a rather modest change, but it makes opening of the lateral gate easier.[151,152] Cryo-electron tomography (CET) of intact rough ER vesicles showed the

TRAP complex associated with almost all ribosome bound Sec61 complexes.[156] How the TRAP complex assists in gating is only recently coming to light.

The TRAP complex consists of α, β, γ, and δ subunits and is essential for the biogenesis of a subset of Sec61 clients with SPs that have low hydrophobicity or are rich in proline or glycine residues.[157] TRAPα is positioned such that it could contact the nascent protein as it leaves the Sec61 channel and in close proximity to the OST, which is consistent with studies that show the TRAP complex effects glycosylation.[158] Additionally, TRAP may be important for correctly orienting TMDs of a subset of proteins.[159] TRAPγ contains three purely cytosolic α-helices (A, D, and E), three purely intermembrane α-helices (B, C, and G), and one particularly long transmembrane α-helix that extends into the cytosol (F). TRAPγ seems to act as a scaffold as it interacts with the other subunits, the ribosome, Sec61α, and Sec61γ. The overall architecture of the Sec61/TRAP complex is "V" shaped with the ER membrane running laterally through the "V" such that the point of the "V" is in the lumen and the ends are sticking up into the cytosol where they make contacts with the ribosome. The point of the "V" is made up of the N-terminal domains of the TRAP α, β, and δ subunits which form a heterotrimeric complex consisting primarily of β-sheets in the ER lumen adjacent to the Sec61 channel. One arm of the "V" consists the TRAPγ which binds the ribosome in the cytosol, a bundle of TMDs from multiple TRAP subunits in the ER membrane, and the TRAP β and δ subunits in the ER lumen. The other arm of the "V" consists of TRAPα in the ER lumen and the Sec61 channel spanning the ER membrane and extending into the cytosol where it binds the ribosome.[158,160,161] In a structure bound to a non-translating ribosome, the four TMDs from the γ subunit forms a bundle of seven TMDs with the addition of one TMD from the C-terminus of each of the other subunits.[160] While in the structure bound to a translating ribosome, the TMD of TRAPα repositions towards

interaction with the both the lumenal (loop 5/6 of sec61α) and cytosolic (Sec61γ) components Sec61 lateral gate hinge.[158,161] Molecular dynamic simulations showed that in this structure the ribosome contacts at the two ends of the "V" squeeze together the two arms such that it creates a bulge in both the cytosolic and lumenal leaflets of the membrane with the convex surfaces pointing towards the cytosol. The bulge is more pronounced on the lumenal leaflet which causes a local thinning of the membrane. Deuterium labeling revealed the lipids of the both leaflets were less ordered with a more significant change observed for the lumenal leaflet. It was further speculated that the local composition of lipids may also be affected, but this requires further study. These changes may increase membrane fluidity.[161] A CET study of intact ER vesicles revealed the ribosome and TRAP bound Sec61 (PDB: 5A6U) had its lateral gate open even in the non-translocating state. While the lateral gate was open, the vertical gate remained occluded by the plug domain.[162] This shows that the interaction of the ribosome and TRAP with the Sec61 complexes helps to open the lateral gate and ease insertion of an SP or TMD into the ER membrane. The SP or TMD can then intercalate between the lateral gate helices and cause the displacement of the plug to open the vertical gate. This is how proteins engage the channel in a co-translational manner, yet a subset of proteins engages the Sec61 channel post-translationally, requiring a separate subset of ancillary proteins.

In humans the post-translational mode of translocation is mostly reserved for short polypeptides.[163] The channel requires the action of membrane proteins Sec62 and Sec63 for gating and the lumenal ATPase BiP to ratchet the peptide through the channel. Sec63 works first and opens the lateral gate by forming contacts with the Sec61 on both the cytosolic and lumenal sides of the channel and runs along a groove on along the backside hinge in between these contact sites. This provides a two-pronged mechanism to crack open the lateral gate.

Interestingly, like the TRAP complex Sec62 also forms a "V" shaped structure, but this may be somewhat coincidental as the placement and function are distinct. The "V" is positioned in front of the lateral gate of Sec61 and consist of both an N-terminal and C-terminal cytosolic domains, two TMDs (TM1 and TM2) which make the two arms of the "V", and a luminal loop that makes the point of the "V" (L1/2). Sec62 binds to the opened lateral gate of Sec61 and blocks lipids from entering the channel, and importantly destabilizes the plug domain causing opening of the vertical gate.[164] This is in contrast to the co-translational complex where the plug remains in place and must be displaced by the SP or a TMD.

A cryo-EM structure of a detergent solubilized mammalian (canine) Sec61 channel bound to a ribosome and engaged by a SP (PDB: 3JC2) revealed the structure of the channel opened by a SP.[165] The initial insertion of the SP may occur in a looped orientation with the N-terminus facing cytosol and the C-terminus into the lumen (N_{cyt}/C_{lum}) of the ER.[166] Given that the cleavage site is in the C-terminal region of the SP, this orientation is necessary for cleavage of the signal peptide by the lumenal SPase. On the other hand, it has been shown that the SP of hCD4 initially inserts head first and then undergo an inversion into the N_{cyt}/C_{lum} orientation.[132] How common this type of insertion is for SPs is unknown, but it has also been shown that C-terminal signal anchor (SA) TMDs of proteins that are targeted to the Sec61 channel post-translationally can insert in an initially head first orientation and then undergo an inversion in topology.[167] Regardless, of initial orientation, the SP intercalates into the lateral gate in between TMs 2 and 7 in a N_{cyt}/C_{lum} orientation that almost perfectly overlaps with the location of TM 2 in the closed structure.[151,165] This causes an approximately 22º rotation in TMs 1-5 and 10 compared with the primed structure, which results in an asymmetric opening (filled by the SP) of the lateral gate on the lumenal side of the channel.[152,165] As mentioned previously, TMs 2, 5, 7,

and 10 form the pore ring, and as TMs 2, 5, and 10 rotate away from TM 7, pore ring opens which additionally destabilized the plug domain which previously was in contact with the pore ring residues. This allows for opening of the vertical gate within the SP engaged channel.[165]

Once the vertical gate opens and the nascent chain passes into the ER lumen it is exposed to enzymes that process the protein in various different ways such as cleavage of the signal peptide or N-glycosylation. These are common examples of post-translational modifications (PTMs) and will be discussed in further detail, but there are many more. Greater than 10% of human proteins may undergo N-glycosylation, which is important for protein folding, trafficking, recognition, and signaling.[168] N-glycosylation occurs via the oligosaccharyltransferase (OST) complex, which recognizes an N-X-S/T motif (X is any amino acid other than proline). The OST transfers $(GlcNAc)_2Man_9Glc_3$ glycans from lipid-linked oligosaccharides (LLOs) onto the asparagine amide nitrogen.[169] In humans there is an OST-A complex that recognizes substrates co-translationally and an OST-B complex which recognizes substrates post-translationally. The complexes each contain ribophorin-I, ribophorin-II, OST48, TMEM258, DAD1, and OST4 subunits. While OST-A has an STT3A catalytic subunit and DC2 which binds to Sec61, OST-B has an STT3B catalytic subunit and either MAGT1 or TUSC3 that can reduce disulfide bonds to give access to N-glycosylation sites near disulfide bonds. Ribophorin-I has a region which contacts the translating ribosome in OST-A, but this region is disordered in OST-B and does not associate with the ribosome. As such OST-A make a super-complex with the Sec61, TRAP, and the ribosome so that it can perform N-glycosylation on client proteins as they leave the Sec61 channel prior to folding. The active site is too far away to reach motifs close to SPs or TMDs and these motifs are recognized post-translationally by OST-B, which explains the need for the

reducing subunits, as the client proteins may be partially folded and disulfide bonds may have already formed.[168]

The human SPC is responsible for recognition and cleavage of SPs from the N-terminus of proteins. The SPC only transiently associates with Sec61 and how the SP handover occurs is still unclear.[149] The complex consists of three accessory subunits SPC12, SPC22/23, and SPC25 and a catalytic subunit SEC11A/C.[170] The two paralogous catalytic subunits give rise to two distinct SPC complexes termed SPC-A and SPC-C. SEC11A/C subunits function via a catalytic Ser-His-Asp triad that sits within a hydrophobic β-strand lined groove. In the structure SEC11A/C and SPC22/23 form a lumenal domain made of β-sheets which connects to two transmembrane three-helix bundles (made from SPC25 and SEC11A/C and the other made from SPC12 and SPC22/23) that pass through the ER membrane and a small cytosolic domain consisting mainly of SPC12 and SPC25. Between the two transmembrane bundles is a gap that is termed the "TM window". The location of charged and hydrophobic residues facing the lipid-filled interior of the TM window work together to thin the membrane within this window and this thinning helps to ensure the selectivity of the complex for SPs opposed to TMDs, being as SPs containing a shorter hydrophobic α-helix. This is in conjunction with the preference for small aliphatic amino acids at positions -1 and -3 owing to the limited space within the active site groove which requires an extended β-strand conformation.[140] After cleavage, the SP is further degraded by the intramembrane enzyme signal peptide peptidase (SPP).[171]

After passage through the Sec61 channel in a largely unfolded state, proteins must then undergo the complex process of folding assisted by many different chaperones that are available in the ER. Post-translational modifications such as glycosylation, SP cleavage, and formation of disulfide bonds play key roles in regulation of protein folding. Under certain conditions such as

nutrient deprivation, or increased protein synthesis (as occurs in viral infections) the folding machinery may be ineffective and misfolded proteins accumulate in the ER. This will trigger the unfolded protein response (UPR) which consists of three branches: reduction in overall protein synthesis, increasing expression of genes which assist in proper protein folding, and activation of ER-associated degradation (ERAD). Activation of ERAD results in increased production of proteins involved in this pathway such as HRD1 which is an E3 ubiquitin ligase that acts as a retrotranslocon responsible for the export of misfolded protein substrate from the ER into the cytosol, where they are degraded. From N- to the C-terminus of HRD1 are a SP, six TMDs, a RING-finger domain, and a proline-rich cluster. The HRD1 complex includes SEL1L, Derlin (1, 2, or 3), Herp, and p97/VCP. SEL1L acts as a receptor for misfolded proteins, the Derlin family of proteins helps form a channel along with HRD1, Herp acts as a scaffold for holding the complex together and p97/VCP is an ATPase which provides the energy for retrotranslocation.[122] Two "half channels" are formed by Derlin and HRD1 which provides a pathway for passage of the substrate in a folded hairpin structure across a locally thinned membrane. Certain viral proteins and toxins may also use this channel for retrotranslocation into the cytosol while avoiding ubiquitination and degradation for their biogenesis.[123] The RING-finger domain of HRD1 is located in the cytosol and responsible for polyubiquitination of retrotranslocated substrates, marking them for degradation by the proteasome.[122] Certain viral proteins and toxins may also use this channel for retrotranslocation into the cytosol while avoiding ubiquitination and degradation for their biogenesis.[123] By activating ERAD and degrading the misfolded proteins in the ER lumen ER stress-induced apoptosis is avoided.[122]

Protein biogenesis is dependent on proper protein localization which often requires proteins to cross lipid membranes. Sequences in the protein are responsible for recognition and

aiding in the translocation process for different cellular compartments. The Sec61 channel is a complex protein processing channel in the ER membrane that is extremely important for translocation of a huge fraction of proteins within the cell. Proteins which pass through this channel contain SP or TMDs which are recognized by the translocation machinery for passage across or into the ER membrane. Traditional approaches to designing drugs has left room for the development of novel approaches such as translocation inhibition. CADA is a highly selective inhibitor of the Sec61 channel which depends on the unique SP sequence of its target proteins to down-modulate protein expression levels within cells. It is possible that CADA analogues can developed into a novel class of drugs with broad applicability.

Section 4 References

(1) Buccitelli, C.; Selbach, M. mRNAs, Proteins and the Emerging Principles of Gene Expression Control. *Nat Rev Genet* **2020**, *21* (10), 630–644. https://doi.org/10.1038/s41576-020-0258-4.

(2) Patrick, G. L. *An Introduction to Medicinal Chemistry*, Fifth edition.; Oxford University Press: Oxford, 2013.

(3) Oliphant, C. M.; Green, G. M. Quinolones: A Comprehensive Review. *Am Fam Physician* **2002**, *65* (3), 455–464.

(4) Mahmoud, S.; Hasabelnaby, S.; Hammad, S.; Sakr, T. Antiviral Nucleoside and Nucleotide Analogs: A Review. *Journal of Advanced Pharmacy Research* **2018**, *2* (2), 73–88. https://doi.org/10.21608/aprh.2018.5829.

(5) Van Meer, G.; Voelker, D. R.; Feigenson, G. W. Membrane Lipids: Where They Are and How They Behave. *Nat Rev Mol Cell Biol* **2008**, *9* (2), 112–124. https://doi.org/10.1038/nrm2330.

(6) Maclver, M. B.; Kendig, J. J. Anesthetic Effects on Resting Membrane Potential Are Voltage-Dependent and Agent-Specific. *Anesthesiology* **1991**, *74* (1), 83–88. https://doi.org/10.1097/00000542-199101000-00014.

(7) Ushioda, R.; Nagata, K. Redox-Mediated Regulatory Mechanisms of Endoplasmic Reticulum Homeostasis. *Cold Spring Harb Perspect Biol* **2019**, *11* (5), a033910. https://doi.org/10.1101/cshperspect.a033910.

(8) Flint, S. J.; Racaniello, V. R.; Rall, G. F.; Skalka, A. M.; Enquist, L. W. *Principles of Virology*, 4th edition.; ASM Press: Washington, DC, 2015.

(9) Nijampatnam, B.; Liotta, D. C. Recent Advances in the Development of HBV Capsid Assembly Modulators. *Current Opinion in Chemical Biology* **2019**, *50*, 73–79. https://doi.org/10.1016/j.cbpa.2019.02.009.

(10) Cole, A. G. Modulators of HBV Capsid Assembly as an Approach to Treating Hepatitis B Virus Infection. *Current Opinion in Pharmacology* **2016**, *30*, 131–137. https://doi.org/10.1016/j.coph.2016.08.004.

(11) Taverniti, V.; Ligat, G.; Debing, Y.; Kum, D. B.; Baumert, T. F.; Verrier, E. R. Capsid Assembly Modulators as Antiviral Agents against HBV: Molecular Mechanisms and Clinical Perspectives. *JCM* **2022**, *11* (5), 1349. https://doi.org/10.3390/jcm11051349.

(12) Lu, H.; Zhou, Q.; He, J.; Jiang, Z.; Peng, C.; Tong, R.; Shi, J. Recent Advances in the Development of Protein–Protein Interactions Modulators: Mechanisms and Clinical Trials. *Sig Transduct Target Ther* **2020**, *5* (1), 213. https://doi.org/10.1038/s41392-020-00315-3.

(13) Markossian, S.; Grossman, A.; Brimacombe, K. *Assay Guidance Manual*; Eli Lilly & Company and the National Center for Advancing Translational Sciences: Bethesda, MD, 2004.

(14) Raia, J. J.; Barone, J. A.; Byerly, W. G.; Lacy, C. R. Angiotensin-Converting Enzyme Inhibitors: A Comparative Review. *DICP* **1990**, *24* (5), 506–525. https://doi.org/10.1177/106002809002400512.

(15) R. Oladipupo, A. Toxin to Medicine and Bioisosterism in Drug Development: A Study of the Discovery and Development of ACE Inhibitors from Snake Venom. *Maced. Pharm. Bull.* **2020**, *66* (2), 15–33. https://doi.org/10.33320/maced.pharm.bull.2020.66.02.003.

(16) Schramm, V. L. Transition States, Analogues, and Drug Development. *ACS Chem. Biol.* **2013**, *8* (1), 71–81. https://doi.org/10.1021/cb300631k.

(17) De Béthune, M.-P. Non-Nucleoside Reverse Transcriptase Inhibitors (NNRTIs), Their Discovery, Development, and Use in the Treatment of HIV-1 Infection: A Review of the Last 20 Years (1989–2009). *Antiviral Research* **2010**, *85* (1), 75–90. https://doi.org/10.1016/j.antiviral.2009.09.008.

(18) Kohlstaedt, L. A.; Wang, J.; Friedman, J. M.; Rice, P. A.; Steitz, T. A. Crystal Structure at 3.5 Å Resolution of HIV-1 Reverse Transcriptase Complexed with an Inhibitor. *Science* **1992**, *256* (5065), 1783–1790. https://doi.org/10.1126/science.1377403.

(19) Rittinger, K.; Divita, G.; Goody, R. S. Human Immunodeficiency Virus Reverse Transcriptase Substrate-Induced Conformational Changes and the Mechanism of Inhibition by Nonnucleoside Inhibitors. *Proc. Natl. Acad. Sci. U.S.A.* **1995**, *92* (17), 8046–8049. https://doi.org/10.1073/pnas.92.17.8046.

(20) Spence, R. A.; Kati, W. M.; Anderson, K. S.; Johnson, K. A. Mechanism of Inhibition of HIV-1 Reverse Transcriptase by Nonnucleoside Inhibitors. *Science* **1995**, *267* (5200), 988–993. https://doi.org/10.1126/science.7532321.

(21) Xia, Q.; Radzio, J.; Anderson, K. S.; Sluis-Cremer, N. Probing Nonnucleoside Inhibitor-Induced Active-Site Distortion in HIV-1 Reverse Transcriptase by Transient Kinetic Analyses. *Protein Sci.* **2007**, *16* (8), 1728–1737. https://doi.org/10.1110/ps.072829007.

(22) Holdgate, G. A.; Meek, T. D.; Grimley, R. L. Mechanistic Enzymology in Drug Discovery: A Fresh Perspective. *Nat Rev Drug Discov* **2018**, *17* (2), 115–132. https://doi.org/10.1038/nrd.2017.219.

(23) Cornish-Bowden, A. Why Is Uncompetitive Inhibition so Rare?: A Possible Explanation, with Implications for the Design of Drugs and Pesticides. *FEBS Letters* **1986**, *203* (1), 3–6. https://doi.org/10.1016/0014-5793(86)81424-7.

(24) Menéndez-Arias, L.; Delgado, R. Update and Latest Advances in Antiretroviral Therapy. *Trends in Pharmacological Sciences* **2022**, *43* (1), 16–29. https://doi.org/10.1016/j.tips.2021.10.004.

(25) Nashed, N. T.; Aniana, A.; Ghirlando, R.; Chiliveri, S. C.; Louis, J. M. Modulation of the Monomer-Dimer Equilibrium and Catalytic Activity of SARS-CoV-2 Main Protease by a Transition-State Analog Inhibitor. *Commun Biol* **2022**, *5* (1), 160. https://doi.org/10.1038/s42003-022-03084-7.

(26) Gehringer, M.; Laufer, S. A. Emerging and Re-Emerging Warheads for Targeted Covalent Inhibitors: Applications in Medicinal Chemistry and Chemical Biology. *J. Med. Chem.* **2019**, *62* (12), 5673–5724. https://doi.org/10.1021/acs.jmedchem.8b01153.

(27) González-Bello, C. Designing Irreversible Inhibitors-Worth the Effort? *ChemMedChem* **2016**, *11* (1), 22–30. https://doi.org/10.1002/cmdc.201500469.

(28) Singh, J.; Petter, R. C.; Baillie, T. A.; Whitty, A. The Resurgence of Covalent Drugs. *Nat Rev Drug Discov* **2011**, *10* (4), 307–317. https://doi.org/10.1038/nrd3410.

(29) Anand, K.; Ziebuhr, J.; Wadhwani, P.; Mesters, J. R.; Hilgenfeld, R. Coronavirus Main Proteinase (3CL ^{pro}) Structure: Basis for Design of Anti-SARS Drugs. *Science* **2003**, *300* (5626), 1763–1767. https://doi.org/10.1126/science.1085658.

(30) Boike, L.; Henning, N. J.; Nomura, D. K. Advances in Covalent Drug Discovery. *Nat Rev Drug Discov* **2022**, *21* (12), 881–898. https://doi.org/10.1038/s41573-022-00542-z.

(31) Lucido, M. J.; Orlando, B. J.; Vecchio, A. J.; Malkowski, M. G. Crystal Structure of Aspirin-Acetylated Human Cyclooxygenase-2: Insight into the Formation of Products with Reversed Stereochemistry. *Biochemistry* **2016**, *55* (8), 1226–1238. https://doi.org/10.1021/acs.biochem.5b01378.

(32) Sutanto, F.; Konstantinidou, M.; Dömling, A. Covalent Inhibitors: A Rational Approach to Drug Discovery. *RSC Med. Chem.* **2020**, *11* (8), 876–884. https://doi.org/10.1039/D0MD00154F.

(33) Eto, M.; Kitazawa, T. Diversity and Plasticity in Signaling Pathways That Regulate Smooth Muscle Responsiveness: Paradigms and Paradoxes for the Myosin Phosphatase, the Master Regulator of Smooth Muscle Contraction. *J. Smooth Muscle Res.* **2017**, *53* (0), 1–19. https://doi.org/10.1540/jsmr.53.1.

(34) Kim, M.; Heo, G.; Kim, S.-Y. Neural Signalling of Gut Mechanosensation in Ingestive and Digestive Processes. *Nat Rev Neurosci* **2022**, *23* (3), 135–156. https://doi.org/10.1038/s41583-021-00544-7.

(35) Kiyokawa, H.; Morimoto, M. Notch Signaling in the Mammalian Respiratory System, Specifically the Trachea and Lungs, in Development, Homeostasis, Regeneration, and Disease. *Develop. Growth Differ* **2020**, *62* (1), 67–79. https://doi.org/10.1111/dgd.12628.
(36) Hollenberg, M. D. Growth Factors, Their Receptors and Development. *Am. J. Med. Genet.* **1989**, *34* (1), 35–42. https://doi.org/10.1002/ajmg.1320340109.
(37) Arnsten, A. F. T. Stress Signalling Pathways That Impair Prefrontal Cortex Structure and Function. *Nat Rev Neurosci* **2009**, *10* (6), 410–422. https://doi.org/10.1038/nrn2648.
(38) Gwinn, M. R.; Vallyathan, V. Respiratory Burst: Role in Signal Transduction in Alveolar Macrophages. *Journal of Toxicology and Environmental Health, Part B* **2006**, *9* (1), 27–39. https://doi.org/10.1080/15287390500196081.
(39) Stadler, M.; Monticelli, S.; Seidel, T.; Luger, D.; Salzer, I.; Boehm, S.; Holzer, W.; Schwarzer, C.; Urban, E.; Khom, S.; Langer, T.; Pace, V.; Hering, S. Design, Synthesis, and Pharmacological Evaluation of Novel B2/3 Subunit-Selective γ-Aminobutyric Acid Type A ($GABA_A$) Receptor Modulators. *J. Med. Chem.* **2019**, *62* (1), 317–341. https://doi.org/10.1021/acs.jmedchem.8b00859.
(40) Hauser, A. S.; Attwood, M. M.; Rask-Andersen, M.; Schiöth, H. B.; Gloriam, D. E. Trends in GPCR Drug Discovery: New Agents, Targets and Indications. *Nat Rev Drug Discov* **2017**, *16* (12), 829–842. https://doi.org/10.1038/nrd.2017.178.
(41) Zhang, Y.; Wang, K.; Yu, Z. Drug Development in Channelopathies: Allosteric Modulation of Ligand-Gated and Voltage-Gated Ion Channels. *J. Med. Chem.* **2020**, *63* (24), 15258–15278. https://doi.org/10.1021/acs.jmedchem.0c01304.
(42) Coe, J. W.; Brooks, P. R.; Vetelino, M. G.; Wirtz, M. C.; Arnold, E. P.; Huang, J.; Sands, S. B.; Davis, T. I.; Lebel, L. A.; Fox, C. B.; Shrikhande, A.; Heym, J. H.; Schaeffer, E.; Rollema, H.; Lu, Y.; Mansbach, R. S.; Chambers, L. K.; Rovetti, C. C.; Schulz, D. W.; Tingley, F. D.; O'Neill, B. T. Varenicline: An A4β2 Nicotinic Receptor Partial Agonist for Smoking Cessation. *J. Med. Chem.* **2005**, *48* (10), 3474–3477. https://doi.org/10.1021/jm050069n.
(43) Sriram, K.; Insel, P. A. G Protein-Coupled Receptors as Targets for Approved Drugs: How Many Targets and How Many Drugs? *Mol Pharmacol* **2018**, *93* (4), 251–258. https://doi.org/10.1124/mol.117.111062.
(44) Valentino, R. J.; Volkow, N. D. Untangling the Complexity of Opioid Receptor Function. *Neuropsychopharmacol* **2018**, *43* (13), 2514–2520. https://doi.org/10.1038/s41386-018-0225-3.
(45) Prommer, E. Levorphanol: Revisiting an Underutilized Analgesic. *Palliat Care* **2014**, *8*, PCRT.S13489. https://doi.org/10.4137/PCRT.S13489.
(46) Donkers, J. M.; Appelman, M. D.; Van De Graaf, S. F. J. Mechanistic Insights into the Inhibition of NTCP by Myrcludex B. *JHEP Reports* **2019**, *1* (4), 278–285. https://doi.org/10.1016/j.jhepr.2019.07.006.
(47) Shimura, S.; Watashi, K.; Fukano, K.; Peel, M.; Sluder, A.; Kawai, F.; Iwamoto, M.; Tsukuda, S.; Takeuchi, J. S.; Miyake, T.; Sugiyama, M.; Ogasawara, Y.; Park, S.-Y.; Tanaka, Y.; Kusuhara, H.; Mizokami, M.; Sureau, C.; Wakita, T. Cyclosporin Derivatives Inhibit Hepatitis B Virus Entry without Interfering with NTCP Transporter Activity. *Journal of Hepatology* **2017**, *66* (4), 685–692. https://doi.org/10.1016/j.jhep.2016.11.009.
(48) Rucktooa, P.; Haseler, C. A.; Van Elk, R.; Smit, A. B.; Gallagher, T.; Sixma, T. K. Structural Characterization of Binding Mode of Smoking Cessation Drugs to Nicotinic Acetylcholine Receptors through Study of Ligand Complexes with Acetylcholine-Binding Protein. *Journal of Biological Chemistry* **2012**, *287* (28), 23283–23293. https://doi.org/10.1074/jbc.M112.360347.
(49) Arias, H. R.; Feuerbach, D.; Targowska-Duda, K.; Kaczor, A. A.; Poso, A.; Jozwiak, K. Pharmacological and Molecular Studies on the Interaction of Varenicline with Different Nicotinic Acetylcholine Receptor Subtypes. Potential Mechanism Underlying Partial Agonism at Human

A4β2 and A3β4 Subtypes. *Biochimica et Biophysica Acta (BBA) - Biomembranes* **2015**, *1848* (2), 731–741. https://doi.org/10.1016/j.bbamem.2014.11.003.

(50) De Lera Ruiz, M.; Kraus, R. L. Voltage-Gated Sodium Channels: Structure, Function, Pharmacology, and Clinical Indications. *J. Med. Chem.* **2015**, *58* (18), 7093–7118. https://doi.org/10.1021/jm501981g.

(51) Kaczorowski, G. J.; McManus, O. B.; Priest, B. T.; Garcia, M. L. Ion Channels as Drug Targets: The Next GPCRs. *The Journal of General Physiology* **2008**, *131* (5), 399–405. https://doi.org/10.1085/jgp.200709946.

(52) Rask-Andersen, M.; Masuram, S.; Schiöth, H. B. The Druggable Genome: Evaluation of Drug Targets in Clinical Trials Suggests Major Shifts in Molecular Class and Indication. *Annu. Rev. Pharmacol. Toxicol.* **2014**, *54* (1), 9–26. https://doi.org/10.1146/annurev-pharmtox-011613-135943.

(53) Zhang, G.; Zhang, J.; Gao, Y.; Li, Y.; Li, Y. Strategies for Targeting Undruggable Targets. *Expert Opinion on Drug Discovery* **2022**, *17* (1), 55–69. https://doi.org/10.1080/17460441.2021.1969359.

(54) O'Brien Laramy, M. N.; Luthra, S.; Brown, M. F.; Bartlett, D. W. Delivering on the Promise of Protein Degraders. *Nat Rev Drug Discov* **2023**, *22* (5), 410–427. https://doi.org/10.1038/s41573-023-00652-2.

(55) Haggag, Y. A. Peptides as Drug Candidates: Limitations and Recent Development Perspectives. *BJSTR* **2018**, *8* (4). https://doi.org/10.26717/BJSTR.2018.08.001694.

(56) He, Y.; Khan, S.; Huo, Z.; Lv, D.; Zhang, X.; Liu, X.; Yuan, Y.; Hromas, R.; Xu, M.; Zheng, G.; Zhou, D. Proteolysis Targeting Chimeras (PROTACs) Are Emerging Therapeutics for Hematologic Malignancies. *J Hematol Oncol* **2020**, *13* (1), 103. https://doi.org/10.1186/s13045-020-00924-z.

(57) Sun, X.; Gao, H.; Yang, Y.; He, M.; Wu, Y.; Song, Y.; Tong, Y.; Rao, Y. PROTACs: Great Opportunities for Academia and Industry. *Sig Transduct Target Ther* **2019**, *4* (1), 64. https://doi.org/10.1038/s41392-019-0101-6.

(58) Kulkarni, J. A.; Witzigmann, D.; Thomson, S. B.; Chen, S.; Leavitt, B. R.; Cullis, P. R.; Van Der Meel, R. The Current Landscape of Nucleic Acid Therapeutics. *Nat. Nanotechnol.* **2021**, *16* (6), 630–643. https://doi.org/10.1038/s41565-021-00898-0.

(59) Chi, X.; Gatti, P.; Papoian, T. Safety of Antisense Oligonucleotide and siRNA-Based Therapeutics. *Drug Discovery Today* **2017**, *22* (5), 823–833. https://doi.org/10.1016/j.drudis.2017.01.013.

(60) Wang, A. Y. L. Modified mRNA-Based Vaccines Against Coronavirus Disease 2019. *Cell Transplant* **2022**, *31*, 096368972210902. https://doi.org/10.1177/09636897221090259.

(61) Ledford, H. Beyond CRISPR Babies: How Human Genome Editing Is Moving on after Scandal. *Nature* **2023**, d41586-023-00625-w. https://doi.org/10.1038/d41586-023-00625-w.

(62) Békés, M.; Langley, D. R.; Crews, C. M. PROTAC Targeted Protein Degraders: The Past Is Prologue. *Nat Rev Drug Discov* **2022**, *21* (3), 181–200. https://doi.org/10.1038/s41573-021-00371-6.

(63) Burke, M. R.; Smith, A. R.; Zheng, G. Overcoming Cancer Drug Resistance Utilizing PROTAC Technology. *Front. Cell Dev. Biol.* **2022**, *10*, 872729. https://doi.org/10.3389/fcell.2022.872729.

(64) Zheng, S.; Tan, Y.; Wang, Z.; Li, C.; Zhang, Z.; Sang, X.; Chen, H.; Yang, Y. Accelerated Rational PROTAC Design via Deep Learning and Molecular Simulations. *Nat Mach Intell* **2022**, *4* (9), 739–748. https://doi.org/10.1038/s42256-022-00527-y.

(65) Bondeson, D. P.; Smith, B. E.; Burslem, G. M.; Buhimschi, A. D.; Hines, J.; Jaime-Figueroa, S.; Wang, J.; Hamman, B. D.; Ishchenko, A.; Crews, C. M. Lessons in PROTAC Design from Selective Degradation with a Promiscuous Warhead. *Cell Chemical Biology* **2018**, *25* (1), 78-87.e5. https://doi.org/10.1016/j.chembiol.2017.09.010.

(66) Garber, K. The PROTAC Gold Rush. *Nat Biotechnol* **2022**, *40* (1), 12–16. https://doi.org/10.1038/s41587-021-01173-2.

(67) Schneider, M.; Radoux, C. J.; Hercules, A.; Ochoa, D.; Dunham, I.; Zalmas, L.-P.; Hessler, G.; Ruf, S.; Shanmugasundaram, V.; Hann, M. M.; Thomas, P. J.; Queisser, M. A.; Benowitz, A. B.; Brown, K.; Leach, A. R. The PROTACtable Genome. *Nat Rev Drug Discov* **2021**, *20* (10), 789–797. https://doi.org/10.1038/s41573-021-00245-x.

(68) Lin, J.; Zhou, D.; Steitz, T. A.; Polikanov, Y. S.; Gagnon, M. G. Ribosome-Targeting Antibiotics: Modes of Action, Mechanisms of Resistance, and Implications for Drug Design. *Annu. Rev. Biochem.* **2018**, *87* (1), 451–478. https://doi.org/10.1146/annurev-biochem-062917-011942.

(69) Lang, S.; Pfeffer, S.; Lee, P.-H.; Cavalié, A.; Helms, V.; Förster, F.; Zimmermann, R. An Update on Sec61 Channel Functions, Mechanisms, and Related Diseases. *Front. Physiol.* **2017**, *8*, 887. https://doi.org/10.3389/fphys.2017.00887.

(70) Lumangtad, L. A.; Bell, T. W. The Signal Peptide as a New Target for Drug Design. *Bioorganic & Medicinal Chemistry Letters* **2020**, *30* (10), 127115. https://doi.org/10.1016/j.bmcl.2020.127115.

(71) Pfeffer, S.; Dudek, J.; Schaffer, M.; Ng, B. G.; Albert, S.; Plitzko, J. M.; Baumeister, W.; Zimmermann, R.; Freeze, H. H.; Engel, B. D.; Förster, F. Dissecting the Molecular Organization of the Translocon-Associated Protein Complex. *Nat Commun* **2017**, *8* (1), 14516. https://doi.org/10.1038/ncomms14516.

(72) Simpson, L. M.; Glennie, L.; Brewer, A.; Zhao, J.-F.; Crooks, J.; Shpiro, N.; Sapkota, G. P. Target Protein Localization and Its Impact on PROTAC-Mediated Degradation. *Cell Chemical Biology* **2022**, *29* (10), 1482-1504.e7. https://doi.org/10.1016/j.chembiol.2022.08.004.

(73) Zhou, X.; Liao, W.-J.; Liao, J.-M.; Liao, P.; Lu, H. Ribosomal Proteins: Functions beyond the Ribosome. *Journal of Molecular Cell Biology* **2015**, *7* (2), 92–104. https://doi.org/10.1093/jmcb/mjv014.

(74) Warner, J. R.; Vilardell, J.; Sohn, J. H. Economics of Ribosome Biosynthesis. *Cold Spring Harbor Symposia on Quantitative Biology* **2001**, *66* (0), 567–574. https://doi.org/10.1101/sqb.2001.66.567.

(75) Hershey, J. W. B.; Sonenberg, N.; Mathews, M. B. Principles of Translational Control: An Overview. *Cold Spring Harbor Perspectives in Biology* **2012**, *4* (12), a011528–a011528. https://doi.org/10.1101/cshperspect.a011528.

(76) Jackson, R. J.; Hellen, C. U. T.; Pestova, T. V. The Mechanism of Eukaryotic Translation Initiation and Principles of Its Regulation. *Nat Rev Mol Cell Biol* **2010**, *11* (2), 113–127. https://doi.org/10.1038/nrm2838.

(77) Marshall, E.; Stansfield, I.; Romano, M. C. Ribosome Recycling Induces Optimal Translation Rate at Low Ribosomal Availability. *J. R. Soc. Interface.* **2014**, *11* (98), 20140589. https://doi.org/10.1098/rsif.2014.0589.

(78) Szaflarski, W.; Sowiński, M.; Leśniczak, M.; Ojha, S.; Aulas, A.; Dave, D.; Malla, S.; Anderson, P.; Ivanov, P.; Lyons, S. M. *A Novel Stress Response Pathway Regulates rRNA Biogenesis*; preprint; Biochemistry, 2020. https://doi.org/10.1101/2020.08.16.250183.

(79) Guerra-Moreno, A.; Isasa, M.; Bhanu, M. K.; Waterman, D. P.; Eapen, V. V.; Gygi, S. P.; Hanna, J. Proteomic Analysis Identifies Ribosome Reduction as an Effective Proteotoxic Stress Response. *Journal of Biological Chemistry* **2015**, *290* (50), 29695–29706. https://doi.org/10.1074/jbc.M115.684969.

(80) Chen, Y.; Shanmugam, S. K.; Dalbey, R. E. The Principles of Protein Targeting and Transport Across Cell Membranes. *Protein J* **2019**, *38* (3), 236–248. https://doi.org/10.1007/s10930-019-09847-2.

(81) Halic, M.; Becker, T.; Pool, M. R.; Spahn, C. M. T.; Grassucci, R. A.; Frank, J.; Beckmann, R. Structure of the Signal Recognition Particle Interacting with the Elongation-Arrested Ribosome. *Nature* **2004**, *427* (6977), 808–814. https://doi.org/10.1038/nature02342.

(82) Chang, Z.; Fu, X. Biogenesis of Secretory Proteins in Eukaryotic and Prokaryotic Cells. In *Encyclopedia of Cell Biology*; Elsevier, 2023; pp 689–702. https://doi.org/10.1016/B978-0-12-821618-7.00048-1.
(83) Alam, A.; Locher, K. P. Structure and Mechanism of Human ABC Transporters. *Annu Rev Biophys* **2023**, *52*, 275–300. https://doi.org/10.1146/annurev-biophys-111622-091232.
(84) English, A. R.; Voeltz, G. K. Endoplasmic Reticulum Structure and Interconnections with Other Organelles. *Cold Spring Harbor Perspectives in Biology* **2013**, *5* (4), a013227–a013227. https://doi.org/10.1101/cshperspect.a013227.
(85) Strambio-De-Castillia, C.; Niepel, M.; Rout, M. P. The Nuclear Pore Complex: Bridging Nuclear Transport and Gene Regulation. *Nat Rev Mol Cell Biol* **2010**, *11* (7), 490–501. https://doi.org/10.1038/nrm2928.
(86) Green, E. R.; Mecsas, J. Bacterial Secretion Systems: An Overview. *Microbiol Spectr* **2016**, *4* (1), 4.1.13. https://doi.org/10.1128/microbiolspec.VMBF-0012-2015.
(87) Filloux, A. Bacterial Protein Secretion Systems: Game of Types: This Article Is Part of the Bacterial Cell Envelopes Collection. *Microbiology* **2022**, *168* (5). https://doi.org/10.1099/mic.0.001193.
(88) Fewell, S.; Brodsky, J. *Entry into the Endoplasmic Reticulum: Protein Translocation, Folding and Quality Control*; Landes Bioscience: Austin, TX, 2000.
(89) Beck, M.; Hurt, E. The Nuclear Pore Complex: Understanding Its Function through Structural Insight. *Nat Rev Mol Cell Biol* **2017**, *18* (2), 73–89. https://doi.org/10.1038/nrm.2016.147.
(90) Suntharalingam, M.; Wente, S. R. Peering through the Pore. *Developmental Cell* **2003**, *4* (6), 775–789. https://doi.org/10.1016/S1534-5807(03)00162-X.
(91) Schnell, D. J.; Hebert, D. N. Protein Translocons. *Cell* **2003**, *112* (4), 491–505. https://doi.org/10.1016/S0092-8674(03)00110-7.
(92) Evans, L. D. B.; Bergen, P. M.; Bryant, O. J.; Fraser, G. M. Interactions of Flagellar Structural Subunits with the Membrane Export Machinery. In *The Bacterial Flagellum*; Minamino, T., Namba, K., Eds.; Methods in Molecular Biology; Springer New York: New York, NY, 2017; Vol. 1593, pp 17–35. https://doi.org/10.1007/978-1-4939-6927-2_2.
(93) Walther, D. M.; Rapaport, D.; Tommassen, J. Biogenesis of β-Barrel Membrane Proteins in Bacteria and Eukaryotes: Evolutionary Conservation and Divergence. *Cell. Mol. Life Sci.* **2009**, *66* (17), 2789–2804. https://doi.org/10.1007/s00018-009-0029-z.
(94) Wiedemann, N.; Pfanner, N. Mitochondrial Machineries for Protein Import and Assembly. *Annu. Rev. Biochem.* **2017**, *86* (1), 685–714. https://doi.org/10.1146/annurev-biochem-060815-014352.
(95) Gaussmann, S.; Gopalswamy, M.; Eberhardt, M.; Reuter, M.; Zou, P.; Schliebs, W.; Erdmann, R.; Sattler, M. Membrane Interactions of the Peroxisomal Proteins PEX5 and PEX14. *Front. Cell Dev. Biol.* **2021**, *9*, 651449. https://doi.org/10.3389/fcell.2021.651449.
(96) Rollauer, S. E.; Tarry, M. J.; Graham, J. E.; Jääskeläinen, M.; Jäger, F.; Johnson, S.; Krehenbrink, M.; Liu, S.-M.; Lukey, M. J.; Marcoux, J.; McDowell, M. A.; Rodriguez, F.; Roversi, P.; Stansfeld, P. J.; Robinson, C. V.; Sansom, M. S. P.; Palmer, T.; Högbom, M.; Berks, B. C.; Lea, S. M. Structure of the TatC Core of the Twin-Arginine Protein Transport System. *Nature* **2012**, *492* (7428), 210–214. https://doi.org/10.1038/nature11683.
(97) Greber, B. J.; Ban, N. Structure and Function of the Mitochondrial Ribosome. *Annu. Rev. Biochem.* **2016**, *85* (1), 103–132. https://doi.org/10.1146/annurev-biochem-060815-014343.
(98) Abe, Y.; Shodai, T.; Muto, T.; Mihara, K.; Torii, H.; Nishikawa, S.; Endo, T.; Kohda, D. Structural Basis of Presequence Recognition by the Mitochondrial Protein Import Receptor Tom20. *Cell* **2000**, *100* (5), 551–560. https://doi.org/10.1016/S0092-8674(00)80691-1.
(99) Van Der Laan, M.; Meinecke, M.; Dudek, J.; Hutu, D. P.; Lind, M.; Perschil, I.; Guiard, B.; Wagner, R.; Pfanner, N.; Rehling, P. Motor-Free Mitochondrial Presequence Translocase Drives Membrane

Integration of Preproteins. *Nat Cell Biol* **2007**, *9* (10), 1152–1159. https://doi.org/10.1038/ncb1635.

(100) Stiller, S. B.; Höpker, J.; Oeljeklaus, S.; Schütze, C.; Schrempp, S. G.; Vent-Schmidt, J.; Horvath, S. E.; Frazier, A. E.; Gebert, N.; van der Laan, M.; Bohnert, M.; Warscheid, B.; Pfanner, N.; Wiedemann, N. Mitochondrial OXA Translocase Plays a Major Role in Biogenesis of Inner-Membrane Proteins. *Cell Metabolism* **2016**, *23* (5), 901–908. https://doi.org/10.1016/j.cmet.2016.04.005.

(101) Pfeffer, S.; Woellhaf, M. W.; Herrmann, J. M.; Förster, F. Organization of the Mitochondrial Translation Machinery Studied in Situ by Cryoelectron Tomography. *Nat Commun* **2015**, *6* (1), 6019. https://doi.org/10.1038/ncomms7019.

(102) Chen, Y.; Dalbey, R. E. Oxa1 Superfamily: New Members Found in the ER. *Trends Biochem Sci* **2018**, *43* (3), 151–153. https://doi.org/10.1016/j.tibs.2017.12.005.

(103) Brix, J.; Rüdiger, S.; Bukau, B.; Schneider-Mergener, J.; Pfanner, N. Distribution of Binding Sequences for the Mitochondrial Import Receptors Tom20, Tom22, and Tom70 in a Presequence-Carrying Preprotein and a Non-Cleavable Preprotein. *Journal of Biological Chemistry* **1999**, *274* (23), 16522–16530. https://doi.org/10.1074/jbc.274.23.16522.

(104) Jores, T.; Klinger, A.; Groß, L. E.; Kawano, S.; Flinner, N.; Duchardt-Ferner, E.; Wöhnert, J.; Kalbacher, H.; Endo, T.; Schleiff, E.; Rapaport, D. Characterization of the Targeting Signal in Mitochondrial β-Barrel Proteins. *Nat Commun* **2016**, *7* (1), 12036. https://doi.org/10.1038/ncomms12036.

(105) Rochaix, J. Chloroplast Protein Import Machinery and Quality Control. *The FEBS Journal* **2022**, *289* (22), 6908–6918. https://doi.org/10.1111/febs.16464.

(106) Soll, J.; Schleiff, E. Protein Import into Chloroplasts. *Nat Rev Mol Cell Biol* **2004**, *5* (3), 198–208. https://doi.org/10.1038/nrm1333.

(107) Jarvis, P.; López-Juez, E. Biogenesis and Homeostasis of Chloroplasts and Other Plastids. *Nat Rev Mol Cell Biol* **2013**, *14* (12), 787–802. https://doi.org/10.1038/nrm3702.

(108) Zhou, S.; Ruan, M.; Li, Y.; Yang, J.; Bai, S.; Richter, C.; Schwalbe, H.; Xie, C.; Shen, B.; Wang, J. Solution Structure of the Voltage-Gated Tim23 Channel in Complex with a Mitochondrial Presequence Peptide. *Cell Res* **2021**, *31* (7), 821–824. https://doi.org/10.1038/s41422-020-00452-y.

(109) Jumper, J.; Evans, R.; Pritzel, A.; Green, T.; Figurnov, M.; Ronneberger, O.; Tunyasuvunakool, K.; Bates, R.; Žídek, A.; Potapenko, A.; Bridgland, A.; Meyer, C.; Kohl, S. A. A.; Ballard, A. J.; Cowie, A.; Romera-Paredes, B.; Nikolov, S.; Jain, R.; Adler, J.; Back, T.; Petersen, S.; Reiman, D.; Clancy, E.; Zielinski, M.; Steinegger, M.; Pacholska, M.; Berghammer, T.; Bodenstein, S.; Silver, D.; Vinyals, O.; Senior, A. W.; Kavukcuoglu, K.; Kohli, P.; Hassabis, D. Highly Accurate Protein Structure Prediction with AlphaFold. *Nature* **2021**, *596* (7873), 583–589. https://doi.org/10.1038/s41586-021-03819-2.

(110) Varadi, M.; Anyango, S.; Deshpande, M.; Nair, S.; Natassia, C.; Yordanova, G.; Yuan, D.; Stroe, O.; Wood, G.; Laydon, A.; Žídek, A.; Green, T.; Tunyasuvunakool, K.; Petersen, S.; Jumper, J.; Clancy, E.; Green, R.; Vora, A.; Lutfi, M.; Figurnov, M.; Cowie, A.; Hobbs, N.; Kohli, P.; Kleywegt, G.; Birney, E.; Hassabis, D.; Velankar, S. AlphaFold Protein Structure Database: Massively Expanding the Structural Coverage of Protein-Sequence Space with High-Accuracy Models. *Nucleic Acids Research* **2022**, *50* (D1), D439–D444. https://doi.org/10.1093/nar/gkab1061.

(111) Schleiff, E.; Soll, J.; Küchler, M.; Kühlbrandt, W.; Harrer, R. Characterization of the Translocon of the Outer Envelope of Chloroplasts. *The Journal of Cell Biology* **2003**, *160* (4), 541–551. https://doi.org/10.1083/jcb.200210060.

(112) Nakai, M. Reply: The Revised Model for Chloroplast Protein Import. *Plant Cell* **2020**, *32* (3), 543–546. https://doi.org/10.1105/tpc.19.00821.

(113) Armbruster, U.; Hertle, A.; Makarenko, E.; Zühlke, J.; Pribil, M.; Dietzmann, A.; Schliebner, I.; Aseeva, E.; Fenino, E.; Scharfenberg, M.; Voigt, C.; Leister, D. Chloroplast Proteins without Cleavable Transit Peptides: Rare Exceptions or a Major Constituent of the Chloroplast Proteome? *Molecular Plant* **2009**, *2* (6), 1325–1335. https://doi.org/10.1093/mp/ssp082.

(114) Weis, B. L.; Schleiff, E.; Zerges, W. Protein Targeting to Subcellular Organelles via mRNA Localization. *Biochimica et Biophysica Acta (BBA) - Molecular Cell Research* **2013**, *1833* (2), 260–273. https://doi.org/10.1016/j.bbamcr.2012.04.004.

(115) Villarejo, A.; Burén, S.; Larsson, S.; Déjardin, A.; Monné, M.; Rudhe, C.; Karlsson, J.; Jansson, S.; Lerouge, P.; Rolland, N.; Von Heijne, G.; Grebe, M.; Bako, L.; Samuelsson, G. Evidence for a Protein Transported through the Secretory Pathway En Route to the Higher Plant Chloroplast. *Nat Cell Biol* **2005**, *7* (12), 1224–1231. https://doi.org/10.1038/ncb1330.

(116) Chuang, M.; Chen, L.; Li, H. Chloroplast Import of an Intermembrane Space Protein Is Facilitated by Translocon Components Toc75 and Tic236. *Plant Direct* **2021**, *5* (11). https://doi.org/10.1002/pld3.356.

(117) Vothknecht, U. C.; Otters, S.; Hennig, R.; Schneider, D. Vipp1: A Very Important Protein in Plastids?! *Journal of Experimental Botany* **2012**, *63* (4), 1699–1712. https://doi.org/10.1093/jxb/err357.

(118) Wang, F.; Brown, E. C.; Mak, G.; Zhuang, J.; Denic, V. A Chaperone Cascade Sorts Proteins for Posttranslational Membrane Insertion into the Endoplasmic Reticulum. *Mol Cell* **2010**, *40* (1), 159–171. https://doi.org/10.1016/j.molcel.2010.08.038.

(119) Guna, A.; Volkmar, N.; Christianson, J. C.; Hegde, R. S. The ER Membrane Protein Complex Is a Transmembrane Domain Insertase. *Science* **2018**, *359* (6374), 470–473. https://doi.org/10.1126/science.aao3099.

(120) McGilvray, P. T.; Anghel, S. A.; Sundaram, A.; Zhong, F.; Trnka, M. J.; Fuller, J. R.; Hu, H.; Burlingame, A. L.; Keenan, R. J. An ER Translocon for Multi-Pass Membrane Protein Biogenesis. *Elife* **2020**, *9*, e56889. https://doi.org/10.7554/eLife.56889.

(121) Hegde, R. S.; Keenan, R. J. The Mechanisms of Integral Membrane Protein Biogenesis. *Nat Rev Mol Cell Biol* **2022**, *23* (2), 107–124. https://doi.org/10.1038/s41580-021-00413-2.

(122) Karamali, N.; Ebrahimnezhad, S.; Khaleghi Moghadam, R.; Daneshfar, N.; Rezaiemanesh, A. HRD1 in Human Malignant Neoplasms: Molecular Mechanisms and Novel Therapeutic Strategy for Cancer. *Life Sciences* **2022**, *301*, 120620. https://doi.org/10.1016/j.lfs.2022.120620.

(123) Wu, X.; Siggel, M.; Ovchinnikov, S.; Mi, W.; Svetlov, V.; Nudler, E.; Liao, M.; Hummer, G.; Rapoport, T. A. Structural Basis of ER-Associated Protein Degradation Mediated by the Hrd1 Ubiquitin Ligase Complex. *Science* **2020**, *368* (6489), eaaz2449. https://doi.org/10.1126/science.aaz2449.

(124) Kim, D. B.; Na, C.; Hwang, I.; Lee, D. W. Understanding Protein Translocation across Chloroplast Membranes: Translocons and Motor Proteins. *JIPB* **2023**, *65* (2), 408–416. https://doi.org/10.1111/jipb.13385.

(125) Hegde, R. S. Protein Maturation and Processing at the Endoplasmic Reticulum. In *The Liver: Biology and Pathobiology*; John Wiley & Sons Ltd., 2020; pp 108–121.

(126) Ellgaard, L.; McCaul, N.; Chatsisvili, A.; Braakman, I. Co- and Post-Translational Protein Folding in the ER: Co- and Post-Translational Protein Folding in the ER. *Traffic* **2016**, *17* (6), 615–638. https://doi.org/10.1111/tra.12392.

(127) Owji, H.; Nezafat, N.; Negahdaripour, M.; Hajiebrahimi, A.; Ghasemi, Y. A Comprehensive Review of Signal Peptides: Structure, Roles, and Applications. *European Journal of Cell Biology* **2018**, *97* (6), 422–441. https://doi.org/10.1016/j.ejcb.2018.06.003.

(128) Von Heijne, G. Membrane-Protein Topology. *Nat Rev Mol Cell Biol* **2006**, *7* (12), 909–918. https://doi.org/10.1038/nrm2063.

(129) Andersson, H.; von Heijne, G. Membrane Protein Topology: Effects of Delta Mu H+ on the Translocation of Charged Residues Explain the “positive inside” Rule. *EMBO J* **1994**, *13* (10), 2267–2272. https://doi.org/10.1002/j.1460-2075.1994.tb06508.x.

(130) van Klompenburg, W.; Nilsson, I.; von Heijne, G.; de Kruijff, B. Anionic Phospholipids Are Determinants of Membrane Protein Topology. *EMBO J* **1997**, *16* (14), 4261–4266. https://doi.org/10.1093/emboj/16.14.4261.

(131) Goder, V.; Junne, T.; Spiess, M. Sec61p Contributes to Signal Sequence Orientation According to the Positive-Inside Rule. *MBoC* **2004**, *15* (3), 1470–1478. https://doi.org/10.1091/mbc.e03-08-0599.

(132) Vermeire, K.; Bell, T. W.; Van Puyenbroeck, V.; Giraut, A.; Noppen, S.; Liekens, S.; Schols, D.; Hartmann, E.; Kalies, K.-U.; Marsh, M. Signal Peptide-Binding Drug as a Selective Inhibitor of Co-Translational Protein Translocation. *PLoS Biol* **2014**, *12* (12), e1002011. https://doi.org/10.1371/journal.pbio.1002011.

(133) Green, R.; Kramer, R. A.; Shields, D. Misplacement of the Amino-Terminal Positive Charge in the Prepro-Alpha-Factor Signal Peptide Disrupts Membrane Translocation in Vivo. *J Biol Chem* **1989**, *264* (5), 2963–2968.

(134) Hikita, C.; Mizushima, S. Effects of Total Hydrophobicity and Length of the Hydrophobic Domain of a Signal Peptide on in Vitro Translocation Efficiency. *J Biol Chem* **1992**, *267* (7), 4882–4888.

(135) Nilsson, I.; Lara, P.; Hessa, T.; Johnson, A. E.; Von Heijne, G.; Karamyshev, A. L. The Code for Directing Proteins for Translocation across ER Membrane: SRP Cotranslationally Recognizes Specific Features of a Signal Sequence. *Journal of Molecular Biology* **2015**, *427* (6), 1191–1201. https://doi.org/10.1016/j.jmb.2014.06.014.

(136) Nothwehr, S. F.; Gordon, J. I. Eukaryotic Signal Peptide Structure/Function Relationships. Identification of Conformational Features Which Influence the Site and Efficiency of Co-Translational Proteolytic Processing by Site-Directed Mutagenesis of Human Pre(Delta pro)Apolipoprotein A-II. *J Biol Chem* **1989**, *264* (7), 3979–3987.

(137) Paetzel, M.; Dalbey, R. E.; Strynadka, N. C. J. Crystal Structure of a Bacterial Signal Peptidase in Complex with a β-Lactam Inhibitor. *Nature* **1998**, *396* (6707), 186–190. https://doi.org/10.1038/24196.

(138) Li, L.; Park, E.; Ling, J.; Ingram, J.; Ploegh, H.; Rapoport, T. A. Crystal Structure of a Substrate-Engaged SecY Protein-Translocation Channel. *Nature* **2016**, *531* (7594), 395–399. https://doi.org/10.1038/nature17163.

(139) Izard, J. W.; Kendall, D. A. Signal Peptides: Exquisitely Designed Transport Promoters. *Mol Microbiol* **1994**, *13* (5), 765–773. https://doi.org/10.1111/j.1365-2958.1994.tb00469.x.

(140) Liaci, A. M.; Steigenberger, B.; Telles De Souza, P. C.; Tamara, S.; Gröllers-Mulderij, M.; Ogrissek, P.; Marrink, S. J.; Scheltema, R. A.; Förster, F. Structure of the Human Signal Peptidase Complex Reveals the Determinants for Signal Peptide Cleavage. *Molecular Cell* **2021**, *81* (19), 3934-3948.e11. https://doi.org/10.1016/j.molcel.2021.07.031.

(141) Snapp, E. L.; McCaul, N.; Quandte, M.; Cabartova, Z.; Bontjer, I.; Källgren, C.; Nilsson, I.; Land, A.; Von Heijne, G.; Sanders, R. W.; Braakman, I. Structure and Topology around the Cleavage Site Regulate Post-Translational Cleavage of the HIV-1 Gp160 Signal Peptide. *eLife* **2017**, *6*, e26067. https://doi.org/10.7554/eLife.26067.

(142) Van Puyenbroeck, V.; Pauwels, E.; Provinciael, B.; Bell, T. W.; Schols, D.; Kalies, K.; Hartmann, E.; Vermeire, K. Preprotein Signature for Full Susceptibility to the Co-translational Translocation Inhibitor Cyclotriazadisulfonamide. *Traffic* **2020**, *21* (2), 250–264. https://doi.org/10.1111/tra.12713.

(143) Hiss, J. A.; Schneider, G. Architecture, Function and Prediction of Long Signal Peptides. *Briefings in Bioinformatics* **2009**, *10* (5), 569–578. https://doi.org/10.1093/bib/bbp030.

(144) Kapp, K.; Schrempf, S.; Lemberg, M. K.; Dobberstein, B. Post-Targeting Functions of Signal Peptides. In *Madame Curie Bioscience Database*; Landes Bioscience: Austin, TX, 2009.
(145) Jomaa, A.; Gamerdinger, M.; Hsieh, H.-H.; Wallisch, A.; Chandrasekaran, V.; Ulusoy, Z.; Scaiola, A.; Hegde, R. S.; Shan, S.; Ban, N.; Deuerling, E. Mechanism of Signal Sequence Handover from NAC to SRP on Ribosomes during ER-Protein Targeting. *Science* **2022**, *375* (6583), 839–844. https://doi.org/10.1126/science.abl6459.
(146) George, R.; Walsh, P.; Beddoe, T.; Lithgow, T. The Nascent Polypeptide-Associated Complex (NAC) Promotes Interaction of Ribosomes with the Mitochondrial Surface in Vivo. *FEBS Letters* **2002**, *516* (1–3), 213–216. https://doi.org/10.1016/S0014-5793(02)02528-0.
(147) Kellogg, M. K.; Miller, S. C.; Tikhonova, E. B.; Karamyshev, A. L. SRPassing Co-Translational Targeting: The Role of the Signal Recognition Particle in Protein Targeting and mRNA Protection. *IJMS* **2021**, *22* (12), 6284. https://doi.org/10.3390/ijms22126284.
(148) Gemmer, M.; Förster, F. A Clearer Picture of the ER Translocon Complex. *Journal of Cell Science* **2020**, *133* (3), jcs231340. https://doi.org/10.1242/jcs.231340.
(149) Itskanov, S.; Park, E. Mechanism of Protein Translocation by the Sec61 Translocon Complex. *Cold Spring Harb Perspect Biol* **2023**, *15* (1), a041250. https://doi.org/10.1101/cshperspect.a041250.
(150) Rapoport, T. A.; Li, L.; Park, E. Structural and Mechanistic Insights into Protein Translocation. *Annu. Rev. Cell Dev. Biol.* **2017**, *33* (1), 369–390. https://doi.org/10.1146/annurev-cellbio-100616-060439.
(151) Berg, B. V. D.; Clemons, W. M.; Collinson, I.; Modis, Y.; Hartmann, E.; Harrison, S. C.; Rapoport, T. A. X-Ray Structure of a Protein-Conducting Channel. *Nature* **2004**, *427* (6969), 36–44. https://doi.org/10.1038/nature02218.
(152) Voorhees, R. M.; Fernández, I. S.; Scheres, S. H. W.; Hegde, R. S. Structure of the Mammalian Ribosome-Sec61 Complex to 3.4 Å Resolution. *Cell* **2014**, *157* (7), 1632–1643. https://doi.org/10.1016/j.cell.2014.05.024.
(153) Park, E.; Rapoport, T. A. Preserving the Membrane Barrier for Small Molecules during Bacterial Protein Translocation. *Nature* **2011**, *473* (7346), 239–242. https://doi.org/10.1038/nature10014.
(154) Klein, M.-C.; Lerner, M.; Nguyen, D.; Pfeffer, S.; Dudek, J.; Förster, F.; Helms, V.; Lang, S.; Zimmermann, R. TRAM1 Protein May Support ER Protein Import by Modulating the Phospholipid Bilayer near the Lateral Gate of the Sec61-Channel. *Channels* **2020**, *14* (1), 28–44. https://doi.org/10.1080/19336950.2020.1724759.
(155) Beckmann, R.; Bubeck, D.; Grassucci, R.; Penczek, P.; Verschoor, A.; Blobel, G.; Frank, J. Alignment of Conduits for the Nascent Polypeptide Chain in the Ribosome-Sec61 Complex. *Science* **1997**, *278* (5346), 2123–2126. https://doi.org/10.1126/science.278.5346.2123.
(156) Pfeffer, S.; Dudek, J.; Gogala, M.; Schorr, S.; Linxweiler, J.; Lang, S.; Becker, T.; Beckmann, R.; Zimmermann, R.; Förster, F. Structure of the Mammalian Oligosaccharyl-Transferase Complex in the Native ER Protein Translocon. *Nat Commun* **2014**, *5* (1), 3072. https://doi.org/10.1038/ncomms4072.
(157) Nguyen, D.; Stutz, R.; Schorr, S.; Lang, S.; Pfeffer, S.; Freeze, H. H.; Förster, F.; Helms, V.; Dudek, J.; Zimmermann, R. Proteomics Reveals Signal Peptide Features Determining the Client Specificity in Human TRAP-Dependent ER Protein Import. *Nat Commun* **2018**, *9* (1), 3765. https://doi.org/10.1038/s41467-018-06188-z.
(158) Jaskolowski, M.; Jomaa, A.; Gamerdinger, M.; Shrestha, S.; Leibundgut, M.; Deuerling, E.; Ban, N. Molecular Basis of the TRAP Complex Function in ER Protein Biogenesis. *Nat Struct Mol Biol* **2023**, *30* (6), 770–777. https://doi.org/10.1038/s41594-023-00990-0.
(159) Sommer, N.; Junne, T.; Kalies, K.-U.; Spiess, M.; Hartmann, E. TRAP Assists Membrane Protein Topogenesis at the Mammalian ER Membrane. *Biochimica et Biophysica Acta (BBA) - Molecular Cell Research* **2013**, *1833* (12), 3104–3111. https://doi.org/10.1016/j.bbamcr.2013.08.018.

(160) Pauwels, E.; Shewakramani, N. R.; De Wijngaert, B.; Camps, A.; Provinciael, B.; Stroobants, J.; Kalies, K.-U.; Hartmann, E.; Maes, P.; Vermeire, K.; Das, K. Structural Insights into TRAP Association with Ribosome-Sec61 Complex and Translocon Inhibition by a CADA Derivative. *Sci. Adv.* **2023**, *9* (9), eadf0797. https://doi.org/10.1126/sciadv.adf0797.

(161) Karki, S.; Javanainen, M.; Tranter, D.; Rehan, S.; Huiskonen, J. T.; Happonen, L.; Paavilainen, V. O. *Molecular View of ER Membrane Remodeling by the Sec61/TRAP Translocon*; preprint; Biochemistry, 2022. https://doi.org/10.1101/2022.09.30.510141.

(162) Pfeffer, S.; Burbaum, L.; Unverdorben, P.; Pech, M.; Chen, Y.; Zimmermann, R.; Beckmann, R.; Förster, F. Structure of the Native Sec61 Protein-Conducting Channel. *Nat Commun* **2015**, *6* (1), 8403. https://doi.org/10.1038/ncomms9403.

(163) Meyer, H.-A.; Grau, H.; Kraft, R.; Kostka, S.; Prehn, S.; Kalies, K.-U.; Hartmann, E. Mammalian Sec61 Is Associated with Sec62 and Sec63. *Journal of Biological Chemistry* **2000**, *275* (19), 14550–14557. https://doi.org/10.1074/jbc.275.19.14550.

(164) Itskanov, S.; Kuo, K. M.; Gumbart, J. C.; Park, E. Stepwise Gating of the Sec61 Protein-Conducting Channel by Sec63 and Sec62. *Nat Struct Mol Biol* **2021**, *28* (2), 162–172. https://doi.org/10.1038/s41594-020-00541-x.

(165) Voorhees, R. M.; Hegde, R. S. Structure of the Sec61 Channel Opened by a Signal Sequence. *Science* **2016**, *351* (6268), 88–91. https://doi.org/10.1126/science.aad4992.

(166) Shaw, A. S.; Rottier, P. J.; Rose, J. K. Evidence for the Loop Model of Signal-Sequence Insertion into the Endoplasmic Reticulum. *Proc. Natl. Acad. Sci. U.S.A.* **1988**, *85* (20), 7592–7596. https://doi.org/10.1073/pnas.85.20.7592.

(167) Devaraneni, P. K.; Conti, B.; Matsumura, Y.; Yang, Z.; Johnson, A. E.; Skach, W. R. Stepwise Insertion and Inversion of a Type II Signal Anchor Sequence in the Ribosome-Sec61 Translocon Complex. *Cell* **2011**, *146* (1), 134–147. https://doi.org/10.1016/j.cell.2011.06.004.

(168) Ramírez, A. S.; Kowal, J.; Locher, K. P. Cryo–Electron Microscopy Structures of Human Oligosaccharyltransferase Complexes OST-A and OST-B. *Science* **2019**, *366* (6471), 1372–1375. https://doi.org/10.1126/science.aaz3505.

(169) Kelleher, D. J.; Gilmore, R. An Evolving View of the Eukaryotic Oligosaccharyltransferase. *Glycobiology* **2006**, *16* (4), 47R-62R. https://doi.org/10.1093/glycob/cwj066.

(170) Evans, E. A.; Gilmore, R.; Blobel, G. Purification of Microsomal Signal Peptidase as a Complex. *Proc. Natl. Acad. Sci. U.S.A.* **1986**, *83* (3), 581–585. https://doi.org/10.1073/pnas.83.3.581.

(171) Voss, M.; Schröder, B.; Fluhrer, R. Mechanism, Specificity, and Physiology of Signal Peptide Peptidase (SPP) and SPP-like Proteases. *Biochimica et Biophysica Acta (BBA) - Biomembranes* **2013**, *1828* (12), 2828–2839. https://doi.org/10.1016/j.bbamem.2013.03.033.

Chapter 2: Synthesis and Pharmacokinetic Analysis

Note: Special thanks to the hard work and dedication of Dr. Amarawan Intasiri for the development of the pharmacokinetic methodology. Without her guidance and support this work would not have been possible.

Section 1: Introduction

In 1981 the AIDS epidemic started in the United States with a life expectancy of 6-12 months. In 1984 human immunodeficiency virus (HIV) was understood to be the cause of the disease. The height of the epidemic occurred in the 1990's, but improvements in therapy and testing helped bring a decline in infections and the severity of the disease. Today the life expectancy for those living with AIDS is close to normal but the HIV infection continues to be associated with fear and stigma.[1] CADA is a macrocyclic polyamine with three evenly spaced nitrogen atoms in a 12 membered ring. Two nitrogen atoms contain tosyl sidearms and the third a benzyl tail group, between the two side arms exists the head group with an alkene substituent (**Fig. 2.1**). It was discovered to inhibit both HIV as well as Human Herpes Virus 7 (HHV7) by down-modulation of the cell surface glycoprotein CD4, which is the receptor for entry of both viruses.[2] This inspired an initial round of synthesis of a series of analogues by changing the groups attached to the nitrogen atoms. A structure activity relationship study revealed a link between potency and steric bulk in the nitrogen-attached substituents, particularly for the tail group. The tail group giving greatest potency was found to be cyclohexylmethyl. Replacement of the head group alkene with groups bearing polar substituents was deleterious to activity. The electrostatic character of the sidearms were also

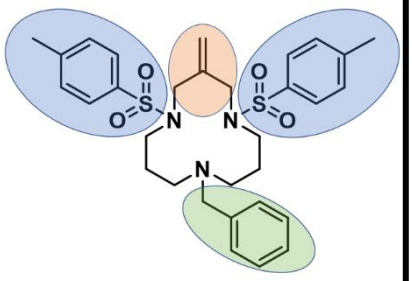

Figure 2.1: Structure of CADA. The sidearms are highlighted in blue, the head group is highlighted in red, and the tail group is highlighted in green.

shown to have an important effect on activity. In this early study a four-step synthesis of CADA gave an overall yield of 30%, but this scheme was limited to production of symmetrical analogues.[3] A breakthrough in the synthesis of CADA analogues came with the development of an alternative five-step approach which was capable of efficiently producing unsymmetrical analogues. Additionally, a method was developed for removing a 2-nitrobenzenesulfonyl sidearm by treatment with 2-mercaptoethanol which allowed for subsequent attachment of alternative sidearms. This gave the possibility for divergent synthesis in order to produce new analogues in an efficient manner from a single intermediate.[4] It was later shown that IC_{50} values correlated with increasing the size of the dipole moment across the benzene ring in the direction of the sulfur atom of the sidearms.[5]

The mechanism of CADA has been the subject of several studies and it represents an area of untapped potential in medicinal chemistry. At an early point it was shown that the down-modulatory activity on human CD4 was selective and not the result of reduced CD4 mRNA levels.[2] It was eventually shown that this activity was dependent on the structure of the CD4 SP and that CADA was acting at the Sec61 channel, blocking passage into the ER lumen and resulting in degradation of the protein. As a testament to the high level of specificity CADA was shown to have no effect on 14 other human T-cell receptors tested, as well as mouse CD4 (mCD4). Deletion of the cytosolic tail or replacement of the extracellular D1-D4 domains with CD8 (also CADA unsensitive) or mCD4 domains did not affect CADA sensitivity. Only the N-terminal SP and 7 residues of the mature protein. Surface plasmon resonance (SPR) experiments then revealed that CADA bound to human CD4 (hCD4), but not mCD4. By individually replacing the N-, H-, and C-regions of hCD4 with mCD4 sequences revealed an increase in the CC_{50} for the down-modulation of the chimeric hCD4 protein. The H-region had the strongest

affect while the N-region had a marginal affect. A cell-free translation system was used to further assess CADA's mechanism.[6] There are other known translocation inhibitors, but CADA is the most selective translocation inhibitor known to date which is thought to be related to its ability to directly interact with the SP of a nascent chain.[7]

A study using a cell-free translation and translocation system was able to give significant insight into the mechanism of CADA. Pancreatic reticulocyte membranes (RMs) originate from the ER and contain Sec61 channels. When RMs are added in a cell-free rabbit reticulocyte lysate, an SP can target the ribosome nascent-chain complex (RNC) to the Sec61 channels. The authors used an mRNA construct which coded for the SP plus an addition 7 residues of hCD4, fused to the first 80 residues of bovine pre-prolactin, and lacked a stopped codon. By using transcripts lacking a stop codon, translation of the protein proceeds to the end of the transcript and then stalls at the end, failing to terminate and release the nascent protein chain from the ribosome. A tight seal of the ribosome with the Sec61 protects the nascent-chain from degradation when treated with a protease (**Fig. 2.2**). Experiments using this set up showed that CADA treatment does affect the targeting of hCD4 SP to the Sec61 channel, as evidenced by a lack of protease degradation. Treatment with puromycin causes the release of nascent-chain from the ribosome and translocation into the RM lumen. The translocation proceeds with SP inversion and cleavage. Localization in the RM

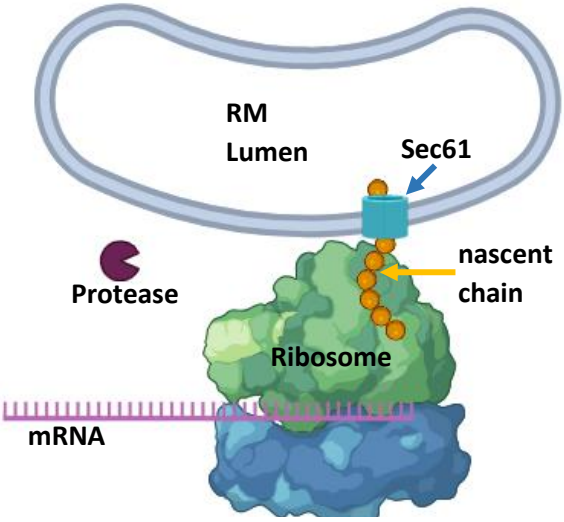

Figure 2.2: Cell-free translation system. In the cell-free translation system successful targeting of the nascent-chain (orange) to the Sec61 channel (teal) protects the protein from protease (purple) degradation.

protects the peptide from degradation upon protease treatment. CADA treatment produced an increase in the non-cleaved species which were sensitive to protease degradation. These two lines of evidence indicated CADA treatment interfered with translocation into the ER. In a cell, this translocation inhibition would cause degradation by ERAD in the cytosol. Furthermore, glycosylation occurs in the lumen of the ER and this can be used as an indication of lumenal exposure. Addition of 17 amino acids to the N-terminus of the SP with a N-linked-glycosylation site revealed that the SP of hCD4 inserts into Sec61 in a head-first topology as evidenced by glycosylation of the SP when translation was stalled at 75 amino acids (including 17 of the N-terminal extension an, 30 C-terminal amino acids are buried in the ribosome). CADA treatment did not significantly affect glycosylation for this construct. As the chain was extended by 4 residues to 79 amino acids CADA treatment produced a reduction in glycosylation compared to the same construct in the absence of CADA. At 88 amino acids glycosylation was still observed in the non-treated sample, but was completely abolished by CADA treatment. As the construct was extended to 97 amino acids glycosylation was reduced in the non-treated sample and disappeared at 105 amino acids. The loss in glycosylation in the absence of CADA is presumed to be the effect of the SP reorienting in the channel with the N-terminus flipping up and facing towards the cytosol. The results indicate that CADA doesn't interfere with the head-first insertion but seems to interfere at a later point during reorientation. This interference prevents proper gating of the channel and exposure of the C-region to the lumen. The authors speculated that CADA was trapping the SP in an intermediate conformation on the pathway to completion of the flip-turn.[6]

Another key paper that offered insight into the mechanism of action of CADA used an alanine scan of the hCD4 SP and the first seven amino acids of the mature protein to assess the

effect of every individual amino acid on the potency of CADA for down-modulation of the protein. This pinpointed Q15 as the single most important amino acid for CADA sensitivity in the SP of hCD4. Mutation of Q15 completely abolished the activity of CADA. This polar amino acid falls in the α-helical H-region and is thought to be mainly responsible for binding with CADA. Polar binding interactions are stronger in hydrophobic environments[8], possibly making a dipole-dipole interaction between Q15 and a sidearm of CADA particularly important. This is consistent with the finding that the strength of the dipole moment of the more polar sidearm correlated with CD4 down-modulation potency as mentioned previously. Other amino acids of importance were a positively charged arginine (R8) that may be important in helping to orient the N-terminus towards the cytosol and a helix-breaking proline (P20) which may be important in providing a hinge-point or generally adding flexibility to the more rigid α-helical region. In the mature protein region, the positively charged lysine residues K26, K27, and K32 all had a moderate contributions, suggesting an important effect of positive charges in this region relating to the orientation/reorientation of the SP.[9]

Some early attempts for determining the structure of CADA bound Sec61 complexed to a CD4 and SP nascent chain were not highly successful. Dr. Roland Beckman and Dr. Katharina Brauinger were able to obtain a Cryo-EM structure of the Sec61 complex with the CD4 SP in a horizontal position within the channel in the presence of CADA and presented this structure at the EMBO conference in 2017.[10] However, the Cryo-EM structures were no of high resolution and were never published. More recently the structures of the Sec61 channel bound to seven different translocation inhibitors (cotransin, decatransin, apratoxin, ipomoeassin, mycolactone, CADA, and eeyarestatin (**Fig. 2.3**)) were determined by Cryo-EM experiments. In previous experiments, the authors had noticed that they could get very high resolution for the yeast post-

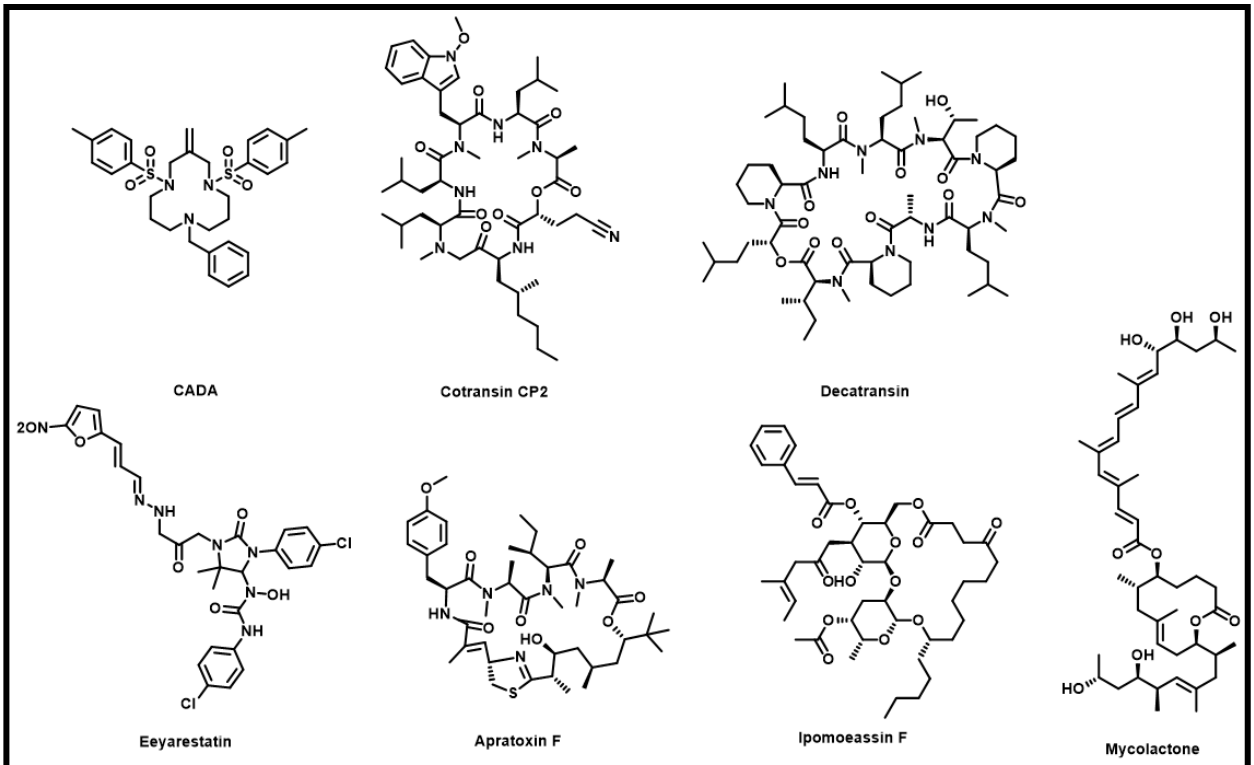

Figure 2.3: Sec61 inhibitors. Structures of seven inhibitors of the Sec61 channel.

translational structure with Sec62-63 and Sec71-72 bound to Sec61. This inspired the authors to make a chimeric human Sec61 channel capable of binding to the fungal specific non-essential Sec71-72 complex. They were able to isolate the chimeric Sec61 complexed with the human Sec62-63 and yeast Sec71-72 in the presence of inhibitors and get high resolution structures via Cryo-EM. This study showed the Sec61 channel in a partially opened state consistent with the post-translation complex, and that all inhibitors were bound in a lipid exposed pocket adjacent to the lateral gate and just above the plug domain on the cytosolic side of the channel. The partially opened state is consistent with that expected as an intermediate along the opening of the channel during co-translation translocation. This binding was hypothesized to hold the vertical gate of the channel shut and prevent movement of the translocating protein through channel. Unfortunately, the complex did not contain a bound SP to show the possibility of interactions between inhibitors and the SP. While interactions with the SP could not be observed, the authors noted hydrophobic

interactions between the Q127 and N300 of the Sec61 channel and all the inhibitors.[11] It is interesting to note that interactions with glutamine within hydrophobic regions apparently occur both between CADA and the Sec61 channel and between CADA and the hCD4 SP.

The compounds were bound in a location consistent with previous studies which produced resistance mutations of Sec61 for inhibition for these compounds. By and large, the mutations were located in the plug and lateral gate region of Sec61 in locations nearby the binding sites of the compounds and often inferred cross resistance to multiple inhibitors. Some resistance mutations occur in the upper portion of the channel opening towards the cytosolic side, but mutations in this region tend to not affect inhibition by these compounds as strongly. Interestingly, the residues Q127 and N300 (or analogous residues when tested in non-human Sec61 channels) were rarely detected in the previous mutagenesis studies surveyed, only two studies identified Q127 as important for binding mycolactone and none identified N300.[12–19] This may have to do with the functional significance of these residues which are part of a conserved polar cluster in the channel which form contacts with each other in the closed channel.[11] The other contacts with the compounds were with non-polar residues, while mutagenesis studies tended to identify and focus on polar residues.[11–19] A study which identified mutations associated with resistance to the CADA analogue CK147, identified mutations D60G, R66G, P83H, and Q127K as conferring resistance to CK147 induced inhibition.[19] In the Cryo-EM study, CADA was shown to contact non-polar plug residues F62, M65, I68, and L69, but not R66. In fact, all these mutations are proximal to the site of binding, but only Q127 appears to interact with CADA.[11] The true binding site is still a matter of debate with different Cryo-EM studies revealing different binding sites for various inhibitors. The cotransin analogue KZR-8445 was shown to bind in the SP-binding site.[20] In another study, mycolactone was shown to bind

towards the top of the cytosolic side of the channel opening.[18] In a TRAP-Sec61-CK147 complex the CADA analogue was shown to bind on the lumenal side of the plug.[19] These three studies did not use the chimeric human Sec61 channel in a post-translational state as discussed above, and it may be argued that the chimeric post-translational channel created an artificial binding site that was favorable to binding by non-polar contacts with the inhibitors. For now, further studies are needed to clear up the true binding sites of the Sec61 inhibitor in the Sec61 channel.

If correct, the structure did provide insight into differences in the specificity of some of these inhibitors. Of the seven inhibitors, only cotransin and CADA are considered selective while the others broadly inhibit the channel. Mycolactone and eeyarestatin have long extensions that protrude into the channel interior likely blocking a larger area of the channel and making it more difficult for SPs to displace their binding interaction with the channel likely contributing to their non-selective nature. Additionally, the lateral gate of the channel was observed to be in a range of states in terms of being more open in the case of cotransin and CADA to all the way closed in the case of ipomoeassin. This also is a likely contributor to specificity. Interestingly, CADA was observed to have the hydrophobic tail group facing into the lipid environment and one of its sidearms facing into the channel interior where it could possibly interact with specific residues on SPs as they pass over the plug on the way towards the lateral gate.[11] It is possible that this interaction could help hold the SP back and prevent integration into the lateral gate, effectively preventing the SP from gating the channel. In the case where there is no interaction with the SP, the growing nascent chain may be able to push the SP past CADA and into the lateral gate where the SP could gate the channel disturbing the plug and pore region which would disrupt the interactions of CADA with the channel and allow for nascent chain passage. This

may be a partial explanation for the specificity of CADA analogues, but further experiments with the SP bound complex are necessary for further insights. This may also explain why it was previously observed that the N-terminal glycosylation tag extension on hCD4 SP was able to pass into the ER lumen in the presence of CADA for shorter hCD4 peptide lengths, but when the peptide chain was extended to a length sufficiently long enough to allow for the interaction of Q15 of the SP to interact with CADA, exposure to the lumen was blocked.

The specificity of CADA was noted early in the study of CADA analogues, but the search for off-target proteins was limited in scope and originally only 14 other cell surface T-cell glycoprotein receptors were examined for down-modulation.[2,6] Later a much larger panel of proteins (444) were individually identified and quantified human $CD4^+$ T lymphocytes using a PowerBlot Western Array with a panel of 1,000 different monoclonal antibodies. The identified 54 antibody signals were differentially regulated (28 down-modulated) in response to treatment by CADA. They selected 9 of the differentially regulated proteins (those with the highest confidence level) for validation by individual immunoblots and of these, only retinoblastoma-like protein 2 (pRb2) was confirmed to be up-modulated. They then investigated hCD4-related proteins Lck and c-Jun and were able to confirm that c-Jun was down-modulated by 1.9-fold (compared with CD4 at 8.2-fold). Both pRb2 and c-Jun are involved in cell cycle progression, but they found CADA had no effect on cell cycle progression. They found that the only down-modulated protein predicted to contain an SP or signal anchor was sortilin. Using cotransfected HEK293T cells expressing wild-type hCD4 and a sortilin-GFP construct, they could detect CADA induced reductions of both proteins, but hCD4 was reduced by about 50% more. Cell-free translation studies confirmed that down-modulatory activity was dependent on the SP sequence of sortilin.[21] Later a mass spectrometry approach analyzed the membrane fraction of T-

cells and was able to quantify 3,007 integral membrane proteins. In addition to hCD4 and sortilin they identified and validated 3 more CADA targets that were down-modulated in an SP-dependent manner (ERLEC1, PTK7, and DNAJC3). CD4 remained the most strongly affected of these proteins. The SPs of all the substrates showed considerable variation, all contained polar amino acids in the hydrophobic region and all also contained Gln and Pro (or the other helix breaker Gly) residues in the SP or N-terminus of the mature chain (**Fig. 2.4**). This confirms that CADA is the most specific translocation known thus far.[22]

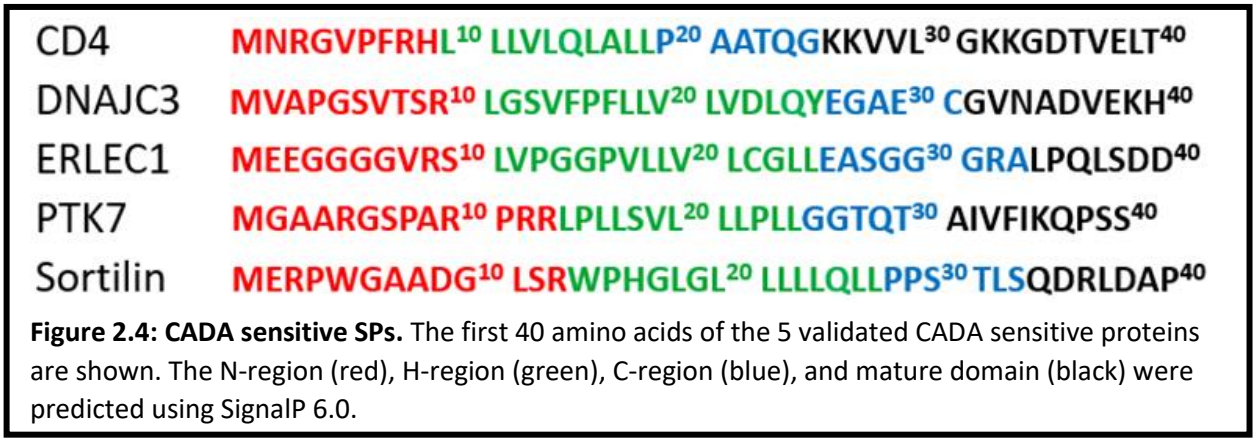

Figure 2.4: CADA sensitive SPs. The first 40 amino acids of the 5 validated CADA sensitive proteins are shown. The N-region (red), H-region (green), C-region (blue), and mature domain (black) were predicted using SignalP 6.0.

While development of therapeutics for AIDS has hit a point where CADA is unlikely to be developed into a medication for this disease, there are many other diseases for which CADA and its analogues have shown promise for development of novel therapeutic strategies. These include many other viruses such as HBV, RSV, SARS-CoV-2, chikungunya, and dengue. Additional disease targets include breast cancer, preterm labor, Grave's disease, and opioid addiction. This indicates a wealth of untapped potential for highly specific protein down-modulating drugs that interact with the Sec61 channel and target protein SPs. It has been exciting to be a part of this research and it will be interesting to see what comes in the future.

Section 2: Results and Discussion

2.1 Synthesis

A previous study of CADA analogues revealed a correlation between the size of the dipole moment in the plane of the benzene ring of the more polar side-arm of CADA analogues and potency for CD4 down-modulation.[5] Electron donating groups (EDGs) in the meta and para positions or electron withdrawing groups (EWGs) in the ortho position are capable of increasing the dipole moment in the direction towards the sulfur atom (**Fig. 2.5**). As such it was determined to use benzenesulfonyl chlorides with these types of substituents in order to try to synthesize highly potent analogues. In total nine new macrocyclic CADA analogues were synthesized (**Fig. 2.6**). Compounds RK002 and RK008 both have the strong electron withdrawing nitro group in the ortho position which would give a strong dipole moment. RK008 also has a meta methoxy group which would further increase the strength of this dipole moment; placement of the methoxy and nitro groups on opposite sides of the ring yields a strong effect due to resonance between the two groups. The para nitrogen atoms in RK006 and RK007 have lone pair electrons which can donate to the aromatic ring in resonance. The azide in RK007 is a powerful electron donating group and it could also be used in photo-crosslinking experiments. RK009 has three electron donating methoxy groups on the opposite side of the ring to the sulfur

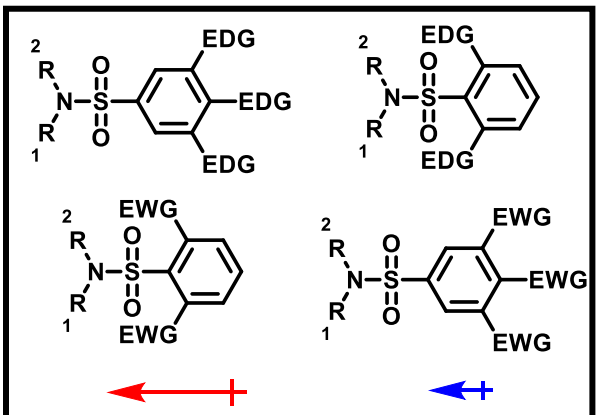

Figure 2.5: Dipole moments of aryl sulfonamides. Putting electron donating or withdrawing groups on the right side of the benzene ring can increase (red arrow) or decrease (blue arrow) the size of the dipole moment in the plane of the benzene ring.

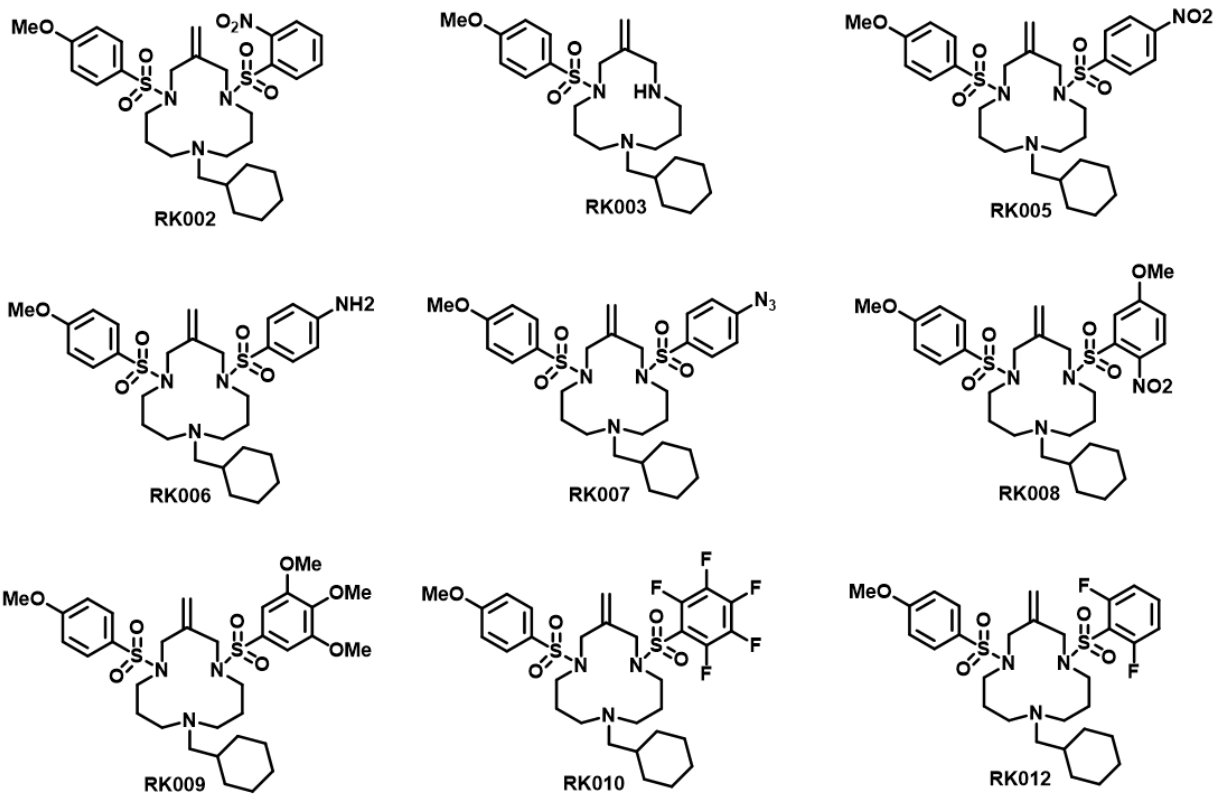

Figure 2.6: Nine new macrocyclic CADA analogues.

atom which gives this analogue a large dipole moment. RK010 and RK012 both have fluorine atoms on the benzene ring which are electron withdrawing due to the electronegativity of fluorine, but fluorine can also donate electron density through resonance making it an interesting addition. In RK012 two fluorine atoms are added in each ortho position giving the potential for a strong dipole moment towards the sulfur atom. In RK010 the benzene ring is completely filled with fluorine atoms making for a highly polarizable ring. RK005 has the powerful electron withdrawing nitro group in the para position which would produce a compound with a weak dipole moment which provides a counter example to help test the importance of the dipole moment. RK003 contains only one sidearm and was mainly synthesized as a common intermediate for new analogues, but basic nitrogen could become charged and make a salt bridge with acidic amino acids in SPs.

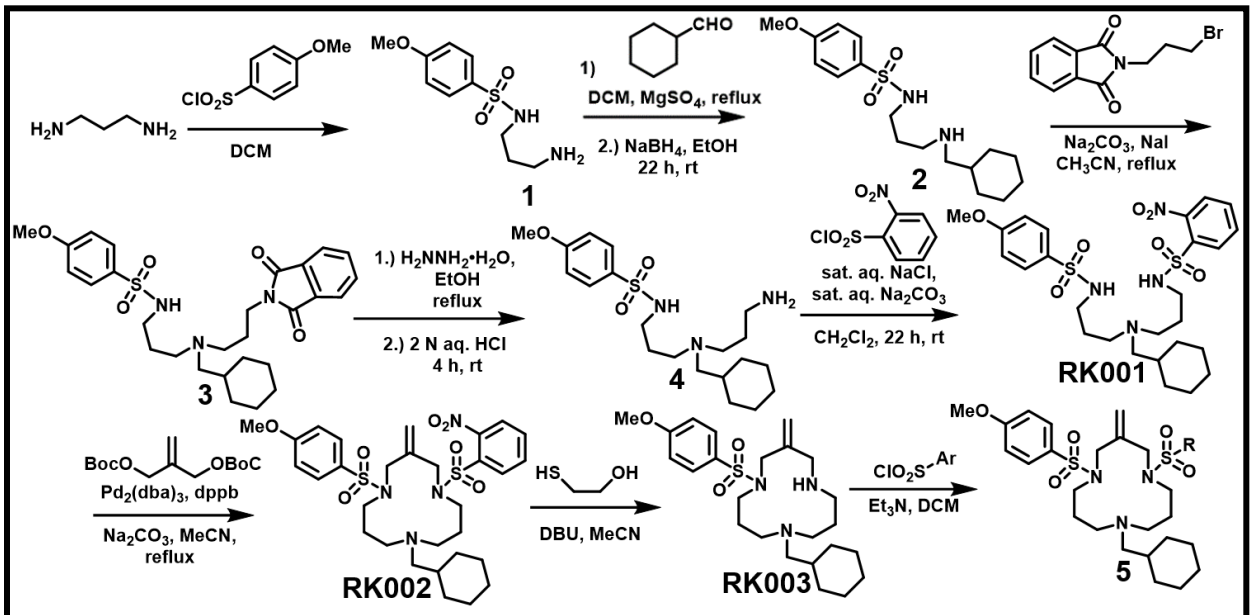

Scheme 2.1: Synthetic route for the formation of new CADA analogues.

To synthesize new CADA analogues a divergent synthesis scheme was adapted from previously published work (**scheme 2.1**).[5] This route required 7 steps to the divergent intermediate RK003 and gave an average overall yield of 7.8%. In the first step, the starting material 1,3-diaminopropane was converted to compound **1** by sulfonation with 4-methoxy-benzensulfonyl chloride in 57% yield. Reductive alkylation of compound **1** with cyclohexane carboxaldehyde gave compound **2** in 74% yield. Chain elongation by was accomplished by N-alkylation using N-(3-bromopropyl)phthalimide and a catalytic amount of NaI to give compound **3** in 91% yield. Compound **4** was produced by deprotection with hydrazine monohydrate in 98% yield. In the next step, RK001 was produced by sulfonation under Schotten-Baumann conditions with 2-nitrobenzenesulfonyl chloride in 73% yield. Compound **4** was also used as a divergent intermediate in the production of some additional analogues which will be discussed later. Macrocyclization was achieved by a palladium catalyzed reaction with 2-methylene-1,3-propanebis(tert-butylcarbonate), which produced RK002 in 50% yield. Treatment with 2-mercaptoethanol and DBU produced the one-armed compound, RK003, in 73% yield.

RK003 was sulfonated with four different arylsulfonyl chlorides under basic conditions to produce new compounds RK008 (68%), RK009 (67%), RK010 (55%), and RK012 (63%). While the fluorinated sulfonyl chlorides where commercially available, the other two sulfonyl chlorides were synthesized in-house. The 3,4,5-trimethoxybenzene-1-sulfonyl chloride was synthesized by following a previously published synthesis except SO_2 gas was generated *in situ* opposed to bubbled into the system (**Scheme 2.2**).[23] A Sandmeyer reaction converted 3,4,5-trimethoxyaniline to a diazonium salt intermediate using HNO_2 generated *in situ*. The intermediate was sulfonated with SO_2 gas generated *in situ* followed by chlorination with CuCl to give compound **6** in 33% yield. The 5-methoxy-2-nitrobenzenesulfonyl chloride was also synthesized by following a patented procedure (**Scheme 2.3**). The starting material 3-fluoro-4-nitroanisole was first converted to the sulfonic acid by an aromatic substitution reaction which replaced the fluorine atom to give compound **7** in 95% yield. Compound **7** was then chlorinated by $SOCl_2$ with catalytic amount of DMF to give compound **8** in 97% yield.

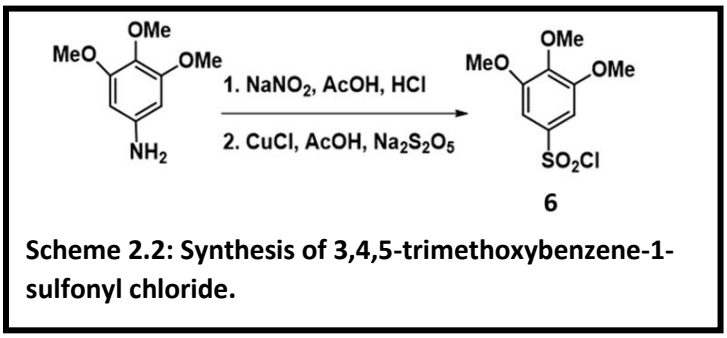

Scheme 2.2: Synthesis of 3,4,5-trimethoxybenzene-1-sulfonyl chloride.

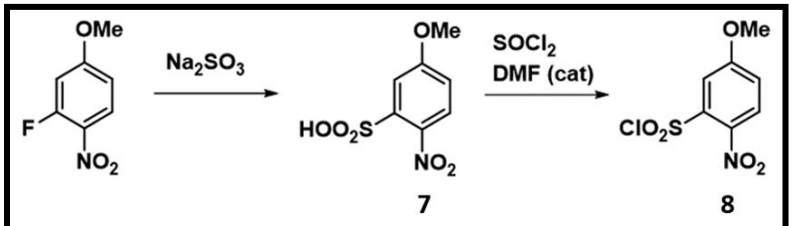

Scheme 2.3: Synthesis of 5-methoxy-2-nitrobenzene-1-sulfonyl chloride.

TL020 (**Fig. 2.7**) was previously determined to be a potent anti-HBV compound as part of an

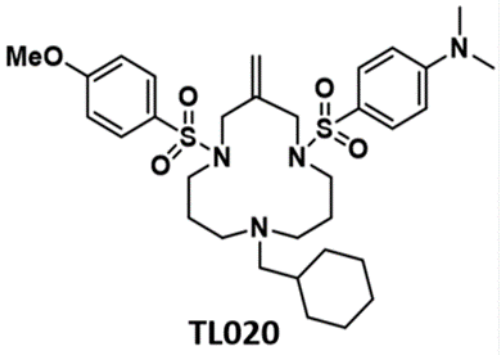

Figure 2.7: Structure of TL020.

unpublished screening program conducted in the laboratory of Dr. Brent Korba. Investigation of the biological activity will be covered in chapter 3, but before further testing could be conducted it was necessary to synthesize enough compound to complete this biological testing. The 4-(dimethylamino)benzenesulfonyl chloride side-arm was synthesized in three steps (**Scheme 2.4**) starting with the synthesis of bis(trimethylsilyl)sulfate by stirring chlorotrimethylsilane and H_2SO_4 under reflux in cyclohexane to give the compound **9** in 58% yield. This was used to sulfonate N,N-dimethylaniline which gave compound **10** in 95% yield. The sulfonic acid was chlorinated with PCl_5 to give compound **11** in 38% yield. Starting with compound 4 the previously synthesized TL020 was resynthesized for further biological testing. A 4-(dimethylamino)benzenesulfonyl chloride was attached using the same Schotten-Baumann conditions used previously to give TL016 with a yield of 98.0%. Alternatively, the Schotten-Baumann conditions with 4-nitrobenzenesulfonyl chloride produced RK004 with a yield of 83%. TL016 and RK004 were each cyclized using the same palladium catalyzed macrocyclization reaction described previously to give TL020 (50%) and RK005 (20%), respectively.

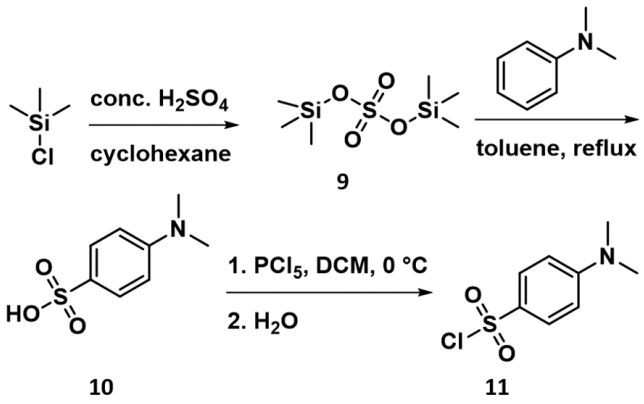

9 10 11

Scheme 2.4: Synthesis of 4-(dimethylamino)benzenesulfonyl chloride.

In order to further study the location of CADA binding to the Sec61 channel it was determined to use an aryl azide to photo-crosslink a CADA analogue to the channel and subsequently use LC-MS/MS to determine the site of crosslinking. RK005 was the starting compound for the synthesis of this CADA analogue (**Scheme 2.5**). $NaBH_4$ was used to reduce the nitro group of RK005 to a primary amine producing RK006 in a yield of 92%. This primary

amine was converted to an azide through formation of a diazonium salt intermediate which was the reacted with NaN_3 to give RK007 in 65% yield.[24]

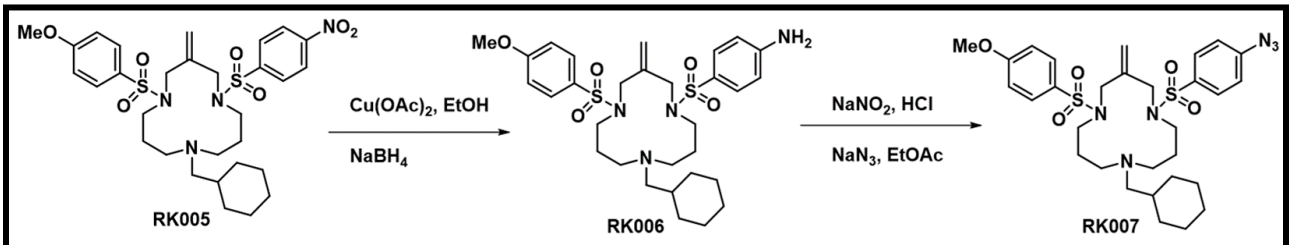

Scheme 2.5: Synthetic route for the formation of photo-crosslinking aryl azide CADA analogue.

2.2 Pharmacokinetics

Along with some previously synthesized TL and DJ series of compounds, the new macrocyclic compounds synthesized were tested for the pharmacokinetic properties. The pharmacokinetic properties of kinetic solubility and membrane permeability are important for the development of new drug compounds. These are important parameters which determine how the drugs will be absorbed and where they end up in the body.[25] Additionally, these are important parameters for CADA analogues as they act intracellularly in a channel embedded in the ER membrane. It is possible that they access their binding site above the plug in the Sec61 channel through absorption into the ER membrane and passage through the lateral gate. Accordingly, a delicate balance between solubility and membrane absorption may be required for development of CADA analogues into medicines. To assist measuring the concentrations of the compounds and determine their kinetic solubility and membrane permeability, it was decided to first record their UV absorption spectra so that the maximum absorption wavelengths and molar absorptivities could be used for detection. Additionally, the ε values in MeOH were determined at this time for use in estimating their ε values in water.

Thermodynamic solubility determines the equilibrium that is achieved when a crystalline solid sample is mixed with a solvent. This is a lower throughput process that requires a larger

amount of sample material. Kinetic solubility measures the concentration at which compounds in concentrated solutions begin to precipitate when diluted with water.[26] For our testing we determined the kinetic solubility of our compounds in PBS containing 1% DMSO. Multiple analytical methods were explored to determine the kinetic solubility of the newly synthesized compounds. The first method that was explored was using nephelometry. Nephelometry measures light scattering to determine the turbidity of suspensions. Because precipitation causes the solution to become turbid, the use of nephelometry is a convenient method for determination of kinetic solubility.[27] We found that many CADA analogues, including those in the RK series of compounds, produce large amorphous precipitates that scatter the light in unpredictable and non-reproducible ways. This resulted in data with very low R^2 values and a lack of consistency from one trial to the next. To check the results from nephelometry, a manual method was implemented where a large volume of solvent was used in clear glass vials so that a series of compound dilutions could be checked by eye for turbidity or formation of precipitates. The results from these two methods were inconsistent. For this reason, UV-visible spectroscopy was then explored which produced much more reproducible and accurate results in a high throughput manner. Two methods, similar in concept, but using slightly different ways of calculating the result were tested. These methods required the preparation of a slightly different solutions. Conceptually, a solution of the compound in DMSO would be spiked into a solution of PBS and DMSO such that final percentage of DMSO would be 1%. The compound is added in at a concentration above its kinetic solubility so a precipitate would form. The precipitate is pelleted by high-speed centrifugation and the supernatant containing the soluble compound is removed. This concentration of the solute in the supernatant is measured by UV-visible absorption spectroscopy to determine the kinetic solubility. Because of the low solubility of the compounds,

the standard addition technique was used to give improved accuracy and ensure that measurements were performed within the linear range of detection for the instrument. The multiple point standard addition uses a standard curve for calculating the concentration of the supernatant containing the soluble compound. The standard curve consists of five different concentrations of the compound and a blank which are mixed with the soluble sample and MeOH. The MeOH was added to ensures that the compound does not precipitate. Care was taken to ensure that the final composition of the solvent was consistent across all solutions measured by adding an appropriate amount of DMSO to each solution. A standard curve was made from these samples and used to calculate the concentration of the soluble sample. In the single point standard addition method, the concentration was determined by comparing the absorbance of the sample with the absorbance of the sample with a known quantity of compound spiked into it. Before addition of the spike MeOH was added to both samples such that the spiked in compound would not precipitate. Additionally, care was taken to ensure the final composition of the solvent was consistent across all solutions measured. Both methods produced reliable results for determination of the kinetic solubility in most cases. The exceptions being when the λ_{max} of the compound was too close to 230 nm due to high background absorption from the DMSO. Because the single point standard addition method was quicker to perform this method was selected for the kinetic determination of all RK macrocyclic compounds.

The λ_{max} and extinction coefficient in MeOH, and the kinetic solubility was determined for CADA, TL020, and RK compounds (**Table 2.1**). Comparing the structures of the compounds reported, the results can be rationalized. CADA has two tosyl side-arms and has the lowest reported kinetic solubility. The methyl groups on these side arms are hydrophobic and only weakly contribute to the polarity of the benzene ring so this low solubility is not surprising. It is

Table 2.1: UV-visible absorption, ClogP, and kinetic solubility results for CADA, TL020, & RK compounds. The reported solubility was determined using the UV detection with single point standard addition. ClogP calculated using molinspiration software.

Compound	λ_{max}	ε ($mol^{-1}cm^{-1}$) in MeOH	ClogP	Solubility in PBS w/ 1% DMSO (µM)	SD (µM)
CADA	230	25,500	5.19	1.0	0.3
TL020	283	29,900	5.34	5.3	0.7
RK002	242	23,800	5.15	6.8	0.1
RK003	243	19,200	1.07	81.2	3.6
RK005	243	20,500	5.20	6.3	0.5
RK006	269	20,700	4.31	6.3	0.1
RK007	263	25,100	6.29	4.6	0.2
RK008	241	26,800	5.18	8.7	1.0
RK009	245	27,400	4.87	7.9	1.3
RK010	241	19,500	5.77	8.0	0.4
RK012	241	20,000	5.47	4.8	0.2

also the only compound to have benzyl tail rather than the cyclohexylmethyl tail group, which should improve solubility, but it appears that this was not sufficient to overcome the effect from the two side-arms. On the other end of the spectrum is RK003 which contains only one side-arm and in the place of the other is a secondary amine which can be protonated and contain a positive charge in PBS, pH 7.4. This charge and the lack of the side-arm produced a highly soluble compound compared with all the others. The rest ranged from 4.6 µM to 8.7 µM such that they were all fairly similar. However, compound RK008 was the most soluble of this group which contained three powerful electron-donating methoxy substituents located in the meta and para positions of the benzene ring. Additionally, these methoxy substituents are hydrogen bond acceptors and capable of interacting with water molecules. As such it is not surprising that RK008 has the highest solubility in this group. Lastly, TL020 is on the low end of the spectrum for solubility of this series of compounds which indicates that the RK compounds may have stronger dipole moments than TL020 which was one goal in their synthesis. The ClogP values, which indicate the degree of hydrophobicity, of compounds and lower values should correlate with higher solubility in a largely aqueous media such as that used in the kinetic solubility

experiments. Other than RK003 which stood out as having by far the lowest ClogP and highest solubility values, the ClogP values correlated poorly with experimental solubilities. This could be an indication of error in both the experimental and calculated values making it hard to distinguish between the compounds which all clustered closely together in terms of both values. It is however interesting to note that a series of TL compounds were also tested for solubility and these compounds generally exhibit higher solubilities **(Table 2.2)**. This may because in varying from the structure of TL020, the RK series of compounds kept the methoxy containing side arm constant and replaced the dimethylamino containing side-arms in all the subsequent analogues. In the TL series of compounds, the dimethylamino containing side-arm was kept constant and the methoxy containing side arm was varied. It appears that the dimethylamino group is capable of producing compounds with improved solubility over the methoxy side arm.

Table 2.2: Kinetic solubility results for TL compounds. The reported solubility was determined using the UV detection with single point standard addition method.

	λ_{max}	Solubility in PBS w/ 1% DMSO (µM)	SD (µM)
TL022	281	12.4	0.8
TL027	283	39.0	2.2
TL032	283	7.9	0.8
TL033	283	8.7	0.2
TL037	283	3.1	0.1
TL038	283	15.9	0.3
TL039	285	1.7	0.3
TL042	284	12.3	2.1
TL043	283	20.7	1.6
TL045	237	9.4	0.1

Oral administration is the preferred route for drug administration because it can be comfortably self-administered at home and has a high rate of patient compliance with the dosing schedule. Orally administered drugs are absorbed almost entirely in the gastrointestinal tract (GIT). The plasma membrane of cells that line the GIT forms a barrier for diffusion of small molecules from the GIT into the circulatory system. It is critical that orally administered drugs can pass this barrier by either active transport or passive diffusion. Additionally, the ability to

Table 2.3. Permeability results. Shown is a compilation of the apparent permeability (P_e) results for both GIT and BBB PAMPA experiments.

GIT-PAMPA		BBB-PAMPA	
Compound	P_e ($\times 10^{-6}$ cm/s)	Compound	P_e ($\times 10^{-6}$ cm/s)
CADA	0	CADA	0
DJ013	0	RK003	13.4 ± 2.7
RK002	0	RK007	0
RK003	0	RK008	0
RK007	0	TK016	9.7 ± 6.7
RK009	0	TL020	0
TK010	13.0 ± 8.6	TL023	0
TL020	10.3 ± 4.3	TL027	0
TL022	0	VGD071	0
TL023	0		
TL027	15.0 ± 3.4		
TL032	0		
TL039	0		
TL042	0		
TL045	0		
nilotinib	19.2 ± 0.1		

pass across the blood brain barrier (BBB) can be another important aspect for drug compounds. Either the compound needs access to the get to its site of action in the brain, or if the desired site of action is elsewhere in the body it would be preferred the compound not be able to cross the BBB and cause unwanted side effects. A parallel artificial membrane assay (PAMPA) uses an artificial membrane with similar passive permeability properties to either the cellular GIT or BBB barrier and is a common method for predicting *in vivo* permeability of drug compounds[28,29]. Compounds were selected for characterization of their passive permeability to GIT or BBB membranes via PAMPA (**Table 2.3**). These results indicate the overall permeability of the tested CADA compounds tend to be very low. Most were not permeable and of all the compounds tested nilotinib which is not a CADA analogue had the highest value. Of note TL020 had a P_e of 10.3 X 10^{-6} cm/s for GIT and was zero when tested for BBB. This is a bonus given that passage across the BBB would not be desirable for an HBV drug candidate. While the permeability is

currently low, formulation would likely be able to overcome this deficiency and improve the absorption in the gut. With the general lack of permeability for the compounds tested it is hard to determine structural features that lead to improved permeability, but all three CADA compounds with non-zero values for GIT had a 4-dimethylamino sidearm so this group appears to be beneficial to permeability. However, given the overall low solubility of CADA analogues and the known mechanism of action it seems highly likely that the compounds are accumulating within membranes. Accumulation in the ER membrane gives the drugs access to their Sec61 binding site through the lateral gate of the channel, so it may be that low solubility and a tendency to accumulate in membranes is a positive trait for the activity of CADA analogues. Furthermore, this property is important to understand for cell-based assays, as the number of cells and the volume of treatment media will affect the overall concentration of the drug within cellular membranes and effect the result of the assay. For this reason, it is important to keep these parameters in mind and not just the concentration of the compound in the treatment media when interpreting data from cell-based assays. The effect of cell density on drug sensitivity was indeed observed in my experience with the many cell-based assays performed.

Section 3: Experimental

3.1 General Methods

All reactions were performed under using N_2 atmosphere. Glassware was dried in a 120 ºC oven before use. All reaction solvents were HPLC grade purchased from ThermoFisher. Acetonitrile was dried by distillation from CaH_2. All reagents were ACS reagent grade or better and stored under dry conditions at temperatures recommended by the supplier. Reagents were purchased from Aldrich Chemical Company, Acros Organics, AmBeed, Chemimpex, or Fisher Scientific. Reagents were used without further purification unless noted. Trituration was performed by sonication for 15 minutes in15 mL of anhydrous diethyl ether three times. Overnight incubations ranged from 16-24 h. Drying *in vacuo* was done with a minimum of 0.1 mm of pressure at room temperature for 24 h. Column chromatography used Sorbent Technologies neutral alumina (50-200 mm) or standard grade silica (32-63 mm) unless noted otherwise. Melting points were measured on a Mel-Temp apparatus and were left uncorrected. ^{1}H NMR (400 MHz or 500 MHz) and ^{13}C NMR (100 MHz or 125 MHz) spectra were measured using either a Varian 400 or a Varian Unity+ 500 spectrometer. Chemical shifts (δ) are reported as ppm units relative to solvent: ^{1}H, $CDCl_3$/TMS = 0.00 or 7.26 ($CDCl_3$); ^{13}C, $CDCl_3$ = 77.16 ppm. Infrared spectra (IR) were measured using a neat sample on a Nicolet 6700 FTIR spectrometer. Mass spectra (MS) were measured using a Waters Micromass ZQ electrospray ionization quadrupole mass spectrometer with positive ion detection (capillary voltage = 3.5 kV). Samples for combustion microanalysis were dried at 78 °C (0.1 mm) for 2 d. Dried samples were sent to NuMega Resonance Labs, Inc for microanalysis determination. Samples were at least 96% pure, as shown by combustion microanalysis, before making stock solutions for pharmacokinetic or biological testing. Stock solutions were made by weighing out no less than 10 mg on an analytical balance

and dissolving in enough MeOH or DCM to make the concentration close to 10 or 20 µM, respectively. Microanalysis results were used to determine the mw for calculation of actual concentrations.

3.2 Synthesis of Sidearms & Reagents

Synthesis of bis(trimethylsilyl) sulfate[30]

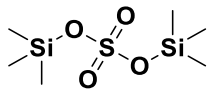

To a 1 L round bottom flask equipped with a condenser, 110 mL (0.86 mol) of chlorotrimethylsilane and 250 mL of cyclohexane were added and stirred. Then 23 mL (0.43 mol) of conc. H_2SO_4 was slowly added. The solution was stirred and heated under reflux for 45 minutes until the solution stopped bubbling. The solution was concentrated by rotary evaporation. The residue was purified by vacuum distillation (1 mm) heating the flask in an oil bath at 170 °C. This yielded 61.3 g (0.25 mol, 58.1%) of bis(trimethylsilyl) sulfate as a white crystallin solid.

Synthesis of 4-(dimethylamino)benzenesulfonic acid[30]

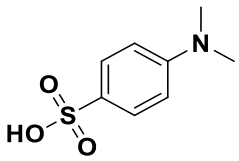

In a 2 L round bottom flask equipped with a condenser, 12.4g (50 mmol) of bis(trimethylsilyl)sulfate, 6.06 g (50 mmol) of N,N-dimethylaniline and 100 mL of anhydrous toluene were added and stirred. The mixture was heated under reflux for 2 h. The mixture was cooled to r.t. and vacuum filtered. The residue was washed with diethyl ether (3 x 150 mL) and

dried *in vacuo*. This yielded 9.51 g (47.3 mmol, 94.6%) of 4-(dimethylamino)benzenesulfonic acid as a pale-greenish solid.

Synthesis of 4-(dimethylamino)benzenesulfonyl chloride[30]

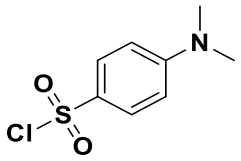

To a 1 L round bottom flask, 10.47 g (51 mmol) of PCl_5 and 500 mL of DCM were stirred at 0° C. Then 9.28 g (45.4 mmol) of 4-dimethylaminobenzenesulfonic acid was added in portions. The mixture was stirred at 0 °C for 4 h. Then 200 mL of H_2O was added slowly and stirred at 0 °C, until no further bubbling occurred. A separatory funnel was used to collect the organic layer and then extract the compound from the aqueous layer with DCM (3 x 100 mL). The combined organic layers were dried with Na_2SO_4 and filtered. The filtrate was concentrated by rotary evaporation and dried *in vacuo*, giving the crude product as a yellowish solid. This was further purified by heating at reflux with 130 mL of hexanes for 1 h. The mixture was cooled to r.t. The supernatant was decanted into a beaker and then cooled to 0 °C in ice bath for recrystallization. After 30 minutes the yellowish crystals collected by vacuum filtration. The mother liquor was boiled to reduce the volume and then cooled to 0 °C in ice bath to get a second crop of purified crystals. The crystals were combined and dried *in vacuo* to get 3.81 g (17.3 mmol, 38.1%) 4-(dimethylamino)benzenesulfonyl chloride as yellow crystals.

Synthesis of 3,4,5-trimethoxybenzenesulfonyl chloride[23]

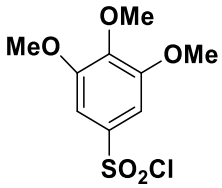

Into a 125 mL round bottom flask equipped with a reflux condenser, a solution of 2.25 g (15 mmol) of 3,4,5-trimethoxyaniline in 10 mL of MeCN, 10 mL of conc. aq. HCl, and 2 mL of glacial acetic acid were stirred and heated at 50 °C for 20 minutes. The mixture was then cooled to 0 °C on an ice bath. Then a solution of 1.15 g (16.5 mmol) of $NaNO_2$ in 2 mL of H_2O was added dropwise. The resulting solution was stirred for 45 min at -10 °C on a NaCl ice bath to form the diazonium salt. Meanwhile in a 250 mL round bottom flask a mixture of 8.55 g (45 mmol) of $Na_2S_2O_5$, 0.37 g (3.75 mmol) of CuCl, and 25 mL of glacial acetic acid was stirred under N_2 gas for 45 min until it turned blue-green. The mixture was then cooled to 0 °C on an ice bath and the diazonium salt was added dropwise, keeping the mixture below 30 °C, then it was stirred for 1 h at r.t. under N_2 gas. Then 100 mL of ether/H_2O (1:1, v/v) was added and the mixture was transferred to a separatory funnel. The layers were separated and the aq. layer was extracted with ether (3 x 50 mL). The combined organic layers were washed with 150 mL of sat. aq. $NaHCO_3$. The organic phase was dried over Na_2SO_4, vacuum filtered, concentrated by rotary evaporation, and dried *in vacuo*, giving 1.71 g of yellowish solid. The crude product was dissolved in minimal amount of DCM and adsorbed to the top of a silica flash column, which was eluted with hexane/EtOAc (17:3, v/v). The desired fraction was collected, concentrated by rotary evaporation, and dried *in vacuo*. This yielded 1.06 g (3.97 mmol, 26.5%) of 3,4,5-trimethoxybenzenesulfonyl chloride as pure white solid.

Synthesis of 5-methoxy-2-nitrobenzenesulfonic acid[31]

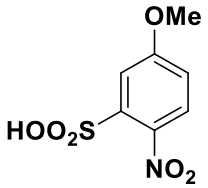

In a 125 mL round bottom flask equipped with a reflux condenser, a mixture of 2.0 g (12 mmol) of 3-fluoro-4-nitroanisole, 3.34 g (26.5 mmol) Na_2SO_3, and 24 mL of EtOH was stirred under N_2 and heated in a 70 °C oil bath. Then a solution of 3.34 g (26.5 mmol) of Na_2SO_3 in 72 mL of EtOH/H2O (4:5, v/v) was added to the flask. The reaction mixture was stirred at 70 °C for 16 h, cooled to room temperature, and 2 mL of conc. aq. HCl was added to bring the pH to 2. The solution was concentrated by rotary evaporation and dried *in vacuo*. Then 12 mL of saturated aq. NaCl solution was added to the residue and the mixture was boiled under reflux for 2 h. The solution was then cooled to 0 °C on an ice bath to precipitate the product, which was collected by vacuum filtration and rinsed with 25 mL of ice-cold saturate aq. NaCl solution. The residue was collected and dried *in vacuo*. A mixture of the residue in hot EtOH was vacuum filtered, concentrated by rotary evaporation, and dried *in vacuo*. This yielded 2.58 g (11.1 mmol, 94.9%) of 5-methoxy-2-nitrobenzenesulfonic acid as white powder.

Synthesis of 5-methoxy-2-nitrobenzenesulfonyl chloride[31]

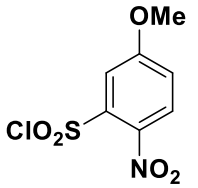

In a 125 mL round bottom flask equipped with a reflux condenser and gas inlet, 2.58 g (11.1 mmol) of 5-methoxy-2-nitrobenzenesulfonic acid, 5.14 g (43.2 mmol) of $SOCl_2$, and 0.27 mL DMF (cat.) were heated to 90 °C in an oil bath and stirred under N_2 gas for 3 h. The flask

was cooled to room temperature and the contents were concentrated by rotary evaporation, then dried *in vacuo*. The residue was shaken with 50 mL H_2O and 50 mL chloroform, the layers were separated and the aq. layer was extracted with chloroform (3 x 50 mL). The combined organic layers were washed with 100 mL $NaHCO_3$, dried over Na_2SO_4, vacuum filtered, concentrated by rotary evaporation, and the residue was dried *in vacuo*, giving 1.28 g (5.09 mmol, 45.9%) of 5-methoxy-2-nitrobenzenesulfonyl chloride as a viscous orange liquid.

Synthesis of 2-methylene-1,3-propane bis(*tert*-butylcarbonate)[4]

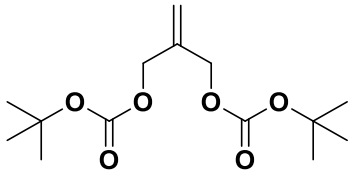

In a 1 L round bottom flask equipped with a gas inlet, 9.64 g (107 mmol) of 2-methylene-1,3-propanediol and 57.7 g (264 mmol) di-*tert*-butyl dicarbonate were stirred with 230 mL of Et_2O under N_2. Then 4.07 g (33.3 mmol) of DMAP was added, the reaction mixture stirred for 24 h, then washed with sat. aq. $CuSO_4$ (3 x 20 mL), sat. aq. $NaHCO_3$ (3 x 35 mL), and sat. aq. NaCl (35 mL). The organic layer was collected, dried over Na_2SO_4, vacuum filtered, concentrated by rotary evaporation, and the residue was dried *in vacuo.* This yielded 30.0 g (104. mmol, 97.3%) 2-methylene-1,3- propane bis(*tert*-butylcarbonate) as a yellowish liquid.

3.3 Synthesis of CADA analogues

Synthesis of N-(3-aminopropyl)-4-methoxybenzenesulfonamide[4]

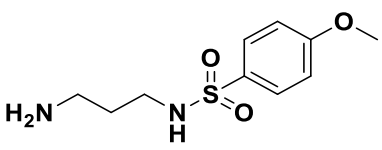

In a 1 L round bottom flask equipped with an addition funnel and nitrogen inlet, 39.5 g (534 mmol) of 1,3-diaminopropane was added, cooled to 0 °C, and stirred under nitrogen. Then a solution of 11.03 g (53.4 mmol) of 4-methoxybenzenesulfonyl chloride in 150 mL of DCM was placed in the addition funnel and slowly added to the reaction flask dropwise over a period of 4 h. The solution was stirred under N_2 for 30 min at 0 °C, then stirred under nitrogen at r.t. overnight. The reaction mixture was concentrated by rotary evaporation and the residue was dried *in vacuo*. A mixture of the residue in 50 mL of water, was gently boiled, and stirred for 30 minutes. The solution was vacuum filtered, and the filtrate was stored at -20 °C for 18 h to crystallize the product. The mixture was warmed to r.t. to thaw the H_2O, and the residue was collected by vacuum filtration. The filtrate reduced by boiling and was recrystallized at -20 °C. The mixture was warmed to r.t. to thaw the H_2O, and the residue was collected by vacuum filtration. Both crystalline residues were combined and dried *in vacuo*. This yielded 7.47 g (30.6 mmol, 40.2-57.3%) of N-(3-aminopropyl)-4-methoxybenzenesulfonamide as a white solid.

Synthesis of N-(3-((cyclohexylmethyl)aminopropyl)-4-methoxybenzenesulfonamide[4]

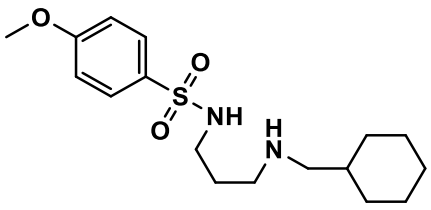

In a 1 L round bottom flask equipped with a condenser and nitrogen inlet, a solution of 17.17 g (70.27 mmol) of N-(3-aminopropyl)-4-methoxybenzenesulfonamide and 190 mL of DCM were stirred under N_2. Then a mixture of 8.67 g (77.3 mmol) of cyclohexane carboxaldehyde and 25.38 g (210.8 mmol) of anhydrous $MgSO_4$ was added to the flask. The reaction mixture was boiled under reflux and N_2 gas overnight. The mixture was cooled to r.t.,

vacuum filtered, concentrated by rotary evaporation and the residue was dried *in vacuo*. Then a mixture of 2.91 g (76.9 mmol) of sodium borohydride and 70 mL of absolute EtOH was added and the mixture stirred overnight. The product was collected by vacuum filtration, and extracted with 50 mL of EtOH. The product in the filtrate was concentrated by rotary evaporation and mixed with 150 mL of H_2O and 70 mL of DCM. The mixture was added to a separatory funnel, the layers were separated and the aqueous layer was extracted with DCM (3 x 70 mL). The combined organic layers were dried with Na_2SO_4, vacuum filtered, concentrated by rotary evaporation, and the residue was dried *in vacuo*. This produced a clear oil as a crude product which was dissolved in a minimal amount of DCM and adsorbed to the top of a silica column which was eluted with EtOAc/Et_3N (100:1, v/v). The desired fraction was collected, concentrated by rotary evaporation and dried *in vacuo*. This yielded 17.70 g (51.99 mmol, 74.0%) of compound N-(3-((cyclohexylmethyl)aminopropyl)-4-methoxy-benzenesulfonamide as a clear oil.

Synthesis of N-(3-((cyclohexylmethyl)(3-(1,3-dioxoisoindolin-2-yl)propyl)amino)propyl)-4-methoxybenzenesulfonamide[4]

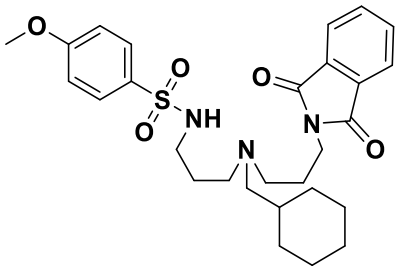

To a 1 L round bottom flask equipped with a condenser and gas inlet, a mixture of 28.67 g (84.20 mmol) of N-(3-((cyclohexylmethyl)aminopropyl)-4-methoxybenzenesulfonamide, 58.04 g (216.6 mmol) of N-(3-bromopropyl)phthalimide, 11.69 g (110.3 mmol) of Na_2CO_3, 2.73 g (20.4

mmol) of NaI, and 370 mL of acetonitrile was heated and stirred under reflux for 18 h. The mixture was cooled to r.t., the residue collected by vacuum filtration, and the product extracted with 300 mL of acetonitrile. The product in the filtrate was concentrated by rotary evaporation and the residue dried *in vacuo*, yielding 78.23 g of crude product as a yellow oil. The crude product was dissolved in a minimal amount of DCM and adsorbed to the top of a flash silica column which was eluted with hexanes/EtOAc (5:2, v/v). After removal of the impurities, the desired compound was eluted with ethanol, concentrated by rotary evaporation, and dried *in vacuo*. This yielded 40.47 g (76.69 mmol, 75.3-91.1%) of N-(3-((cyclohexylmethyl)(3-(1,3-dioxoisoindolin-2- yl)propyl)amino)propyl)-4-methoxy-benzenesulfonamide as a yellow viscous oil.

Synthesis of N-(3-aminopropyl)-N-(3-*p*-methoxybenzenesulfonamidopropyl)cyclohexylmethylamine[4]

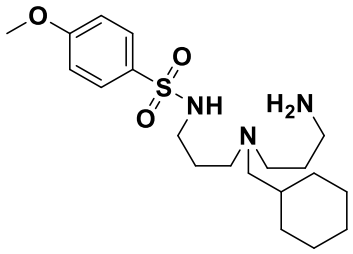

To a 1 L round bottom flask equipped with a condenser and gas inlet, a mixture of 40.47 g (76.69 mmol) of N-(3-((cyclohexylmethyl)(3-(1,3-dioxoisoindolin-2-yl)propyl)amino)propyl)-4-methoxybenzenesulfonamide, 91.0 mL (1.88 mol) of hydrazine monohydrate, and 630 mL of EtOH was stirred and heated under reflux and N_2 gas for 3 h. The reaction mixture was cooled to r.t., concentrated by rotary evaporation, and dried *in vacuo*. Then 2 N aq. HCl was slowly added and the mixture was stirred at r.t. until the white fumes no longer formed. Then 6 N aq. NaOH was added to bring the pH to 10 and 50 mL of DCM was added. The mixture was transferred to a separatory funnel. The layers were separated the aqueous layer was extracted with DCM (4 x 50

mL). The combined organic layers were dried over Na_2SO_4, vacuum filtered, concentrated by rotary evaporation and dried *in vacuo*. This yielded 29.88 g (75.15 mmol, 90.3-98.0%) of N-(3-((3- aminopropyl)(cyclohexylmethyl)amino)propyl)-4-methoxybenzenesulfonamide as a viscous yellow oil.

Synthesis of N'-(*p*-dimethylaminobenzenesulfonyl)-N"-(*p*-methoxybenzenesulfonyl)-[N, N-bis(3-aminopropyl)cyclohexylmethylamine] (TL016)[32]

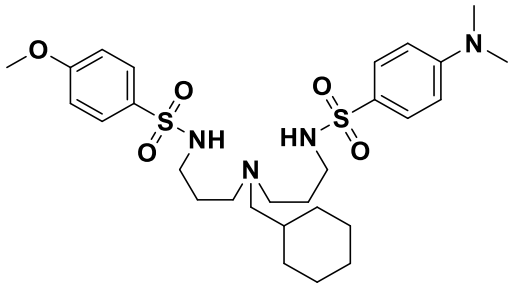

To a 1 L round bottom flask equipped with a gas inlet, a mixture of 4.95 g (12.4 mmol) of N-(3-aminopropyl)-N-(3-*p*-methoxybenzenesulfonamidopropyl)cyclohexylmethylamine, 2.73 g (12.4 mmol) of 4-(dimethylamino)-benzenesulfonyl chloride, 75 mL of sat. aq. NaCl solution, 75 mL of sat. aq. Na_2CO_3 solution, and 75 mL of DCM was stirred stirred under N_2 gas at r.t. for 18 h. The mixture was transferred to a separatory funnel, the layers were separated and the aqueous layer was extracted with DCM (4 x 50 mL). The combined organic layers were dried over Na_2SO_4, vacuum filtered, concentrated by rotary evaporation, and dried *in vacuo*, yielding 7.12 g of crude as yellow oil. The crude product was dissolved in a minimal amount of DCM and adsorbed to the top of a silica column which was eluted with hexanes/EtOAc (1:3, v/v). The desired fraction was collected, concentrated by rotary evaporation, and dried *in vacuo*. This produced 5.09 g (70%) of N'-(*p*-dimethylaminobenzenesulfonyl)-N"-(*p*-

methoxybenzenesulfonyl)-[N, N-bis(3-aminopropyl)cyclohexylmethylamine] as a yellow oil. ^{1}H NMR (400 MHz, $CDCl_3$) matched with expected literature value.

Synthesis of N'-(*p*-methoxybenzenesulfonyl)- N"-(*o*-nitrobenzenesulfonyl)- [N, N-bis(3-aminopropyl)cyclohexylmethylamine] (RK001)[4]

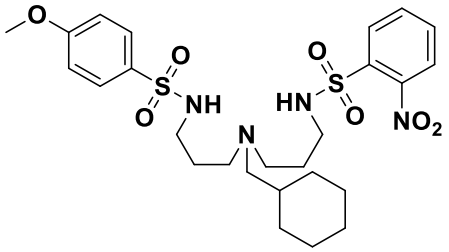

To a 2 L round bottom flask equipped with a gas inlet, a mixture of 25.45 g (64.00 mmol) of N-(3-aminopropyl)-N-(3-*p*-methoxybenzenesulfonamidopropyl)cyclohexylmethylamine, 14.18 g (64.00 mmol) of 2-nitrobenzenesulfonyl chloride, 385 mL of sat. aq. NaCl solution, 385 mL of sat. aq. Na_2CO_3 solution, and 385 mL of DCM was stirred under N_2 gas at r.t. for 18 h. A separatory funnel was used to remove the organic layer. The mixture was transferred to a separatory funnel, the layers were separated and the aqueous layer was extracted with DCM (4 x 250 mL). The combined organic layers were dried over Na_2SO_4, vacuum filtered, concentrated by rotary evaporation, and dried *in vacuo*, yielding 36.84 g of crude product as a yellow oil. The crude product was dissolved in a minimal amount of DCM and adsorbed to the top of a flash silica column which was eluted with hexanes/EtOAc/Et_3N (60:40:1, v/v). The desired fraction was collected, concentrated by rotary evaporation, and dried *in vacuo*. This produced 27.08 g (46.47 mmol, 72.6%) of N'-(*p*-methoxybenzenesulfonyl)- N"-(*o*-nitrobenzenesulfonyl)- [N, N-bis(3-aminopropyl)cyclohexylmethylamine] as a viscous yellow liquid. ^{1}H NMR (400 MHz, $CDCl_3$) δ 8.13 (d, 7 Hz, 1H, 3-ArNO_2), 7.83 (d, 6 Hz, 1H, 6-ArNO_2), 7.76 (m, 4H, 4,5-ArNO_2, *o*-ArOCH_3), 6.97 (d, 9 Hz, 2H, *m*-ArOCH_3), 5.94 (bs, 2H, NH), 3.87 (m, 3H, OCH_3), 3.15 (t, 6 Hz,

2H, CH_2NSO_2), 2.98 (t, 6 Hz, 2H, CH_2NSO_2), 2.39 (m, 4H, C*H*$_2$NCH$_2$Cy), 2.07 (d, 7 Hz, 2H, CH_2Cy), 1.64 (m, 10H, CCH_2C, Cy), 1.36 (m, 1H, CH), 1.14 (m, 2H, Cy), 0.78 (m, 2H, Cy). ^{13}C NMR (100 MHz, $CDCl_3$) δ 162.8, 148.1, 133.7, 133.5, 132.7, 131.6, 131.0, 129.2, 125.2, 114.2, 61.8, 55.6, 53.4, 52.3, 42.7, 35.5, 31.9, 26.6, 26.3, 26.0, 25.6. A portion was stirred with 2 M HCl in MeOH/H_2O for 4 h. The resulting salt was concentrated by rotary evaporation, triturated with ether, and dried *in vacuo* to give the HCl salt as a white solid. IR (neat, cm^{-1}) 3064 (w, br), 2931 (w), 2852 (w), 2603 (w, br), 1596 (w),1540 (m), 1498 (w), 1442 (w), 1327 (m), 1259 (m), 1152 (s), 1094 (m), 1023 (w), 946 (w), 852 (m), 635 (m), 783 (w), 803 (w), 730 (m), 654 (m), 628 (w), 585 (m), 560 (s), 533 (m). MS (ESI$^+$) *m/z* 450.28 (MH$^+$). Anal. Calcd. for $C_{26}H_{38}N_4O_7S_2 \cdot HCl \cdot H_2O$: C, 49.01; H, 6.49; N, 8.79. Found: C, 49.09; H,6.18; N, 8.95.

Synthesis of 9-cyclohexylmethyl-1-(4-dimethylaminobenzenesulfonyl)-3-methylene-5-(*p*-methoxybenzenesulfonyl)-1,5,9-triazacyclododecane (TL020)[32]

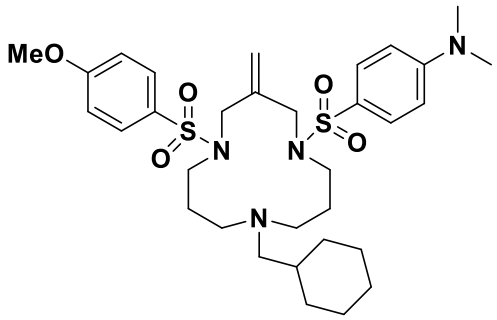

Prior to proceeding all glassware and the stir bar was dried either *in vacuo* or in the oven. To a 500 mL round bottom flask equipped with a condenser and gas inlet a mixture of 3.41 g (5.86 mmol) of N'-(*p*-dimethylaminobenzenesulfonyl)-N"-(*p*-methoxybenzenesulfonyl)-[N,N-bis(3-aminopropyl)cyclohexylmethylamine], 4.22 g (14.7 mmol) 2-methylene-1,3- propanebis(tert-butylcarbonate), 0.62 g (5.9 mmol) Na_2CO_3, 0.32 g (0.35 mmol) $Pd_2(dba)_3$, 0.33 g (0.76 mmol) of dppb, and 650 mL of dry acetonitrile was stirred under N_2 gas and boiled under reflux for 18

h. The mixture was cooled to r.t. and concentrated by rotary evaporation. The residue was dissolved in 100 mL of DCM and vacuum filtered, the filtrate was transferred to a separatory funnel and washed with sat. aq. $NaHCO_3$ (3 x 50 mL) and sat. aq. NaCl (50 mL). The organic layer was dried over Na_2SO_4, vacuum filtered, concentrated by rotary evaporation, and dried *in vacuo,* yielding 3.10 g of crude product as an amber oil. The crude product was dissolved in a minimal amount of DCM and adsorbed to the top of a silica column which was eluted with hexanes/EtOAc (1:4, v/v) for 3 minutes then increased to hexanes/EtOAc (2:3, v/v) over 25 minutes. The desired fraction was collected, concentrated by rotary evaporation, and dried *in vacuo*. This produced 1.86 g (2.95 mmol, 50.4%) of 9-cyclohexylmethyl-1-(4-dimethylaminobenzenesulfonyl)-3-methylene-5-(*p*-methoxysulfonyl)-1,5,9-triazacyclododecane as a white glassy solid. A mixture of the product and 20 mL of 2 N HCl in MeOH were stirred at r.t. for 6 h. The solution was concentrated by rotary evaporation and dried *in vacuo*. The residue was washed with diethyl ether (3 x 25 mL) and dried *in vacuo*. This yielded 1.85 g (2.76 mmol, 47.1%) of 9-cyclohexylmethyl-1-(4-dimethylaminobenzenesulfonyl)-3-methylene-5-(*p*-methoxysulfonyl)-1,5,9-triazacyclododecane as a white powder. MS (ESI^+) *m/z* 583.23 (MH^+). Anal. Calcd. for $C_{32}H_{48}N_4O_5S_2 \cdot HCl$: C, 57.42; H, 7.38; N, 8.37. Found: C, 57.12; H, 7.37; N, 8.12. ^1H NMR (400 MHz, $CDCl_3$) matched with expected literature value.

Synthesis of 9-cyclohexylmethyl-5-(*p*-methoxybenzenesulfonyl)-3-methylene-1-(*o*-nitrobenzenesulfonyl)-1,5,9-triazacyclododecane (RK002)[4]

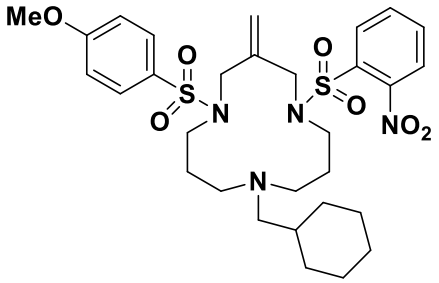

Procedure #1: Using 2-methylene-1,3-propane bis(*tert*-methoxycarbonate)

Prior to proceeding all the glassware and the stir bar was dried either *in vacuo* or in the oven. To a 250 mL round bottom flask equipped with a condenser and gas inlet a mixture of 3.72 g (6.38 mmol) of N'-(*p*-methoxybenzenesulfonyl)- N"-(*o*-nitrobenzenesulfonyl)- [N,N-bis(3-aminopropyl)cyclohexylmethylamine], 3.26 g (16.0 mmol) 2-methylene-1,3-propanebis(methoxycarbonate), 0.34 g (3.2 mmol) Na_2CO_3, 0.35 g (0.38 mmol) $Pd_2(dba)_3$, 0.35 g (0.83 mmol) of dppb, and 110 mL of dry acetonitrile was stirred under N_2 gas and boiled under reflux for 18 h. The mixture was cooled to r.t. and concentrated by rotary evaporation. The residue was dissolved in 90 mL of DCM and vacuum filtered, the filtrate was transferred to a separatory funnel and washed with sat. aq. $NaHCO_3$ (3 x 45 mL) and sat. aq. NaCl (45 mL). The organic layer was dried over Na_2SO_4, vacuum filtered, concentrated by rotary evaporation, and dried *in vacuo*, yielding 3.24 g of crude product as an amber oil. The crude product dissolved in a minimal amount of DCM and adsorbed to the top of a silica column which was eluted with hexanes/EtOAc (3:7, v/v) over 25 minutes. The desired fraction was collected, concentrated by rotary evaporation, and dried *in vacuo*. A mixture of the product and 25 mL of 2 N HCl in MeOH were stirred at r.t. for 6 h. The solution was concentrated by rotary evaporation and dried *in vacuo*. The residue was washed with diethyl ether (3 x 25 mL) and dried *in vacuo*. This yielded 0.81 g (1.3 mmol, 20.4%) of 9-cyclohexylmethyl-5-(p-methoxybenzenesulfonyl)-3-methylene-1-(o-nitrobenzenesulfonyl)-1,5,9-triazacyclododecane as a white powder.

Procedure #2: Using 2-methylene-1,3-propane bis(*tert*-butylcarbonate)

Prior to proceeding all glassware and the stir bar was dried either in vacuo or in the oven. To a 250 mL round-bottom flask equipped with a condenser and gas inlet 4.02 g (6.90 mmol) of N'-(*p*-methoxybenzenesulfonyl)- N"-(*o*-nitrobenzenesulfonyl)- [N,N-bis(3-aminopropyl)cyclohexylmethylamine], 4.97 g (17.3 mmol) 2-methylene-1,3-propane bis(*tert*-butylcarbonate), 0.37 g (3.5 mmol) Na_2CO_3, 0.38 g (0.41 mmol) $Pd_2(dba)_3$, and 0.38 g (0.90 mmol) of dppb, and 120 mL of dry acetonitrile was stirred under N_2 and boiled under reflux for 18 h. The mixture was cooled to r.t. and concentrated by rotary evaporation. The residue was dissolved in 95 mL of DCM and vacuum filtered, the filtrate was transferred to a separatory funnel and washed with sat. aq. $NaHCO_3$ (3 x 50 mL) and sat. aq. NaCl (50 mL). The organic layer was dried over Na_2SO_4, vacuum filtered, concentrated by rotary evaporation, and dried *in vacuo*, yielding 3.56 g of crude product as an amber oil. The crude product dissolved in a minimal amount of DCM and adsorbed to the top of a silica column which was eluted with hexanes/EtOAc (3:7, v/v) over 25 minutes. The desired fraction was collected, concentrated by rotary evaporation, and dried *in vacuo*. This produced 0.91 g (1.4 mmol, 20.3%) 9-cyclohexylmethyl-5-(p-methoxybenzenesulfonyl)-3-methylene-1-(o-nitrobenzenesulfonyl)-1,5,9-triazacyclododecane as a white powder. ^{1}H NMR (400 MHz, $CDCl_3$) δ 8.01 (m, 1 H, *o*-$ArNO_2$), 7.68 (m, 5 H, *m*,*p*-$ArNO_2$, *o*-$ArOCH_3$), 7.01 (d, 9 Hz, 2 H, *m*-$ArOCH_3$), 5.17 (s, 1 H, C=CH_2), 5.11 (s, 1 H, C=CH_2), 4.17 (s, 2 H, H4), 3.88 (s, 3 H, OCH_3), 3.59 (s, 2 H, H2), 3.51 (t, 8 Hz, 2 H, H6), 2.93 (t, 6 Hz, 2 H, H12), 2.39 (t, 5 Hz, 2 H, H8), 2.25 (t, 6 Hz, 2 H, 2.08, H10), 1.99 (d, 7 Hz, 2 H, CH_2Cy), 1.82 (t, 6 Hz 2 H, H7), 1.63 (m, 7 H, H11, Cy), 1.17 (m, 4H, CH, Cy), 0.71 (m, 2 H, Cy).^{13}C NMR (100 MHz, $CDCl_3$) *δ* 163.1, 148.0, 137.7, 133.7, 133.4, 131.7, 130.5, 129.6, 128.4, 124.1, 116.5, 114.4, 62.2, 55.7, 54.7, 51.3, 49.5, 47.6, 45.7, 42.8, 35.9, 32.0, 26.8,

26.2, 26.0, 23.8. A mixture of the product and 25 mL of 2 N HCl MeOH/H_2O was stirred at r.t. for 6 h. The solution was concentrated by rotary evaporation and dried *in vacuo*. The residue was washed with diethyl ether (3 x 25 mL) and dried *in vacuo*. This yielded 0.96 g (1.4 mmol, 20.3%) 9-cyclohexylmethyl-5-(*p*-methoxybenzenesulfonyl)-3-methylene-1-(*o*-nitrobenzenesulfonyl)-1,5,9-triazacyclododecane as a white powder. MP 135.4 – 137.9 ˚C (decom). IR (neat, cm^{-1}) 2928 (w), 2853 (w), 2501 (w, br), 1595 (w), 1541 (m), 1498 (w), 1452 (w), 1337 (m), 1308 (w), 1262 (m), 1155 (s), 1094 (m), 1018 (w), 933 (w), 852 (w), 834 (w), 806 (m), 773 (w), 729 (w), 709 (w), 683 (w), 653 (w), 559 (m), 506 (s). MS (ESI^+) *m/z* 635.26 (MH^+). Anal. Calcd. for $C_{30}H_{42}N_4O_7S_2 \cdot HCl$: C, 53.68; H, 6.46; N, 8.35. Found: C, 53.67; H, 6.22; N, 8.24.

Synthesis of 9-cyclohexylmethyl-1-(*p*-methoxybenzenesulfonyl)-3-methylene-1,5,9-triazacyclododecane (RK003)[4]

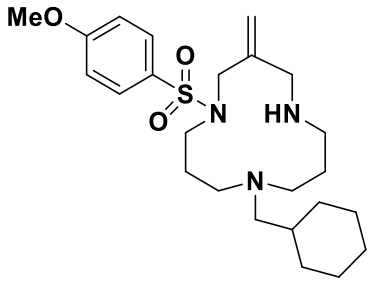

In 500 mL two-neck round bottom flask equipped with a condenser and gas inlet a mixture of 4.62 g (7.27 mmol) 9-cyclohexylmethyl-5-(*p*-methoxybenzenesulfonyl)-3-methylene-1-(*o*-nitrobenzenesulfonyl)-1,5,9-triazacyclododecane, 3.43 mL (22.5 mmol) DBU, and 150 mL dry acetonitrile was stirred under N_2 gas at r.t. for 15 min before addition of 0.61 mL (8.72 mmol) 2-mercaptoethanol. The outlet on the condenser was bubbled through a bleach bath. The reaction stirred under N_2 gas at r.t. for 18 h. The reaction mixture was filtered over an alumina flash

column, washed with acetonitrile, and the filtrate concentrated concentrated by rotary evaporation. A mixture of the residue, 9.23 g of $NaHCO_3$, 250 mL of H_2O, and 250 mL of 2-propanol was stirred at r.t. for 18 h. Then 300 mL of sat. aq. NaCl and and the amount required of 2 N aq. NaOH was added to bring the pH to 14. The mixture was transferred to a separatory funnel, the layers were separated and the aqueous layer was extracted with DCM (4 x 300 mL). The combined organic layers were dried over Na_2SO_4, vacuum filtered, concentrated by rotary evaporation. This produced 6.13 g of crude product as a yellow oil which was dissolved in a minimal amount of DCM and adsorbed to the top of a silica column which was eluted with EtOAc for 10 minutes then increased to EtOAc/MeOH (49:1, v/v) over 30 minutes. The desired fraction was collected, concentrated by rotary evaporation, and dried *in vacuo*. This produced 2.39 g (5.32 mmol, 73.1%) 9-cyclohexylmethyl-1-(*p*-methoxybenzenesulfonyl)-3-methylene-1,5,9-triazacyclododecane as a white glassy solid. ^{1}H NMR (400 MHz, $CDCl_3$) δ 7.76 (d, 9 Hz, 2H o-$ArOCH_3$), 6.94 (d, 9 Hz, 2H *m*-$ArOCH_3$), 5.08 (m, 2H, $C=CH_2$), 3.93 (s, 2H, H2), 3.86 (s, 3H, OCH_3), 3.39 – 3.30 (m, 2H, H12), 3.15 (s, 2H, H4), 2.59 (bs, 2H, H6), 2.30 (bs, 2H, H8/H10), 2.19 (bs, 2H, H8/H10), 1.96 (d, 7 Hz, 2H, CH_2Cy), 1.65 (m, 6H, Cy), 1.47 (m, 4H, H7, H11), 1.31 (m, 1H, NH), 1.22 – 1.07 (m, 3H, Cy), 0.73 (q, 11 Hz, 2H, Cy). ^{13}C NMR (100 MHz, $CDCl_3$) δ 163.7, 135.9, 129.8, 126.9, 122.7, 114.7, 61.2, 55.8, 54.8, 48.1, 47.3, 44.2, 42.6, 33.6, 31.5, 25.7, 25.4. A sample of the free base was dissolved in 2 M HCl MeOH/H_2O and stirred. The solution was then concentrated by rotary evaporation and the residue dried *in vacuo*. The solid was washed anhydrous diethyl ether (3 x 25 mL) and dried *in vacuo* to give the HCl salt as a white solid. MP 168.8 – 173.4 ˚C (decom). IR (neat, cm^{-1}) 3383 (w, br), 2924 (w), 2849 (w), 2599 (w, br), 1594 (m), 1497 (w), 1450 (w), 1339 (m), 1310 (w), 1264 (m), 1180 (w), 1153 (s), 1114 (w), 1092 (m), 1023 (w), 987 (w), 943 (w), 886 (w), 839 (w), 806 (m), 778 (w), 749 (w),

719 (w), 696 (m), 655 (w), 628 (w), 596 (m), 556 (s), 518 (w), 505 (s). MS (ESI^+) *m/z* 450.28 (MH^+). Anal. Calcd. for $C_{24}H_{39}N_3O_3S \cdot 2HCl \cdot 1.5H_2O$: C, 52.45; H, 8.07; N, 7.65. Found: C, 52.22; H, 7.88; N, 7.65.

Synthesis of N'-(*p*-methoxybenzenesulfonyl)- N"-(*p*-nitrobenzenesulfonyl)- [N, N-bis(3-aminopropyl)cyclohexylmethylamine] (RK004)[4]

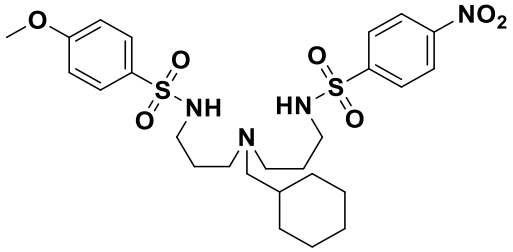

To a 2 L round bottom flask equipped with a gas inlet, a mixture of 17.20 g (43.25 mmol) of N-(3-aminopropyl)-N-(3-*p*-methoxybenzenesulfonamidopropyl)cyclohexylmethylamine, 9.58 g (43.3 mmol) of 2-nitrobenzenesulfonyl chloride, 260 mL of sat. aq. NaCl solution, 260 mL of sat. aq. Na_2CO_3 solution, and 260 mL of DCM was stirred under N_2 gas at r.t. for 18 h. A separatory funnel was used to remove the organic layer. The mixture was transferred to a separatory funnel, the layers were separated and the aqueous layer was extracted with DCM (4 x 175 mL). The combined organic layers were dried over Na_2SO_4, vacuum filtered, concentrated by rotary evaporation, and dried *in vacuo*, yielding 25.31 g of crude product as a yellow oil. The crude product was dissolved in a minimal amount of DCM and adsorbed to the top of an alumina column which was eluted with hexanes/EtOAc (1:9, v/v). The desired fraction was collected, concentrated by rotary evaporation, and dried *in vacuo*. This produced 21.07 g (36.16 mmol, 83.6%) of N'-(*p*-methoxybenzenesulfonyl)- N"-(*p*-nitrobenzenesulfonyl)- [N, N-bis(3-aminopropyl)cyclohexylmethylamine] as a viscous yellow liquid. ^1H NMR (400 MHz, $CDCl_3$) δ 8.35 (d, 8 Hz, 2H, *m*-$ArNO_2$), 8.05 (d, 8 Hz, 2H, *o*-$ArNO_2$), 7.78 (d, 9 Hz, 2H, *o*-$ArOCH_3$), 6.98 (d, 9 Hz, 2H, *m*-$ArOCH_3$), 3.88 (s, 3H, OCH_3), 3.09 (t, 6 Hz, 2H, CH_2NSO_2), 2.98 (t, 6 Hz, 2H,

CH_2NSO_2), 2.42 (m, 4H, C*H*$_2$NCH$_2$Cy), 2.08 (d, 7 Hz, 2H, CH$_2$Cy), 1.67 (m, 10H, CCH$_2$C, Cy), 1.37 (m, 1H, CH), 1.14 (m, 2H, Cy), 0.80 (m, Hz, 2H, Cy). ^{13}C NMR (100 MHz, $CDCl_3$) δ 162.9, 149.9, 146.2, 131.3, 129.2, 128.3, 124.3, 114.3, 62.1, 55.6, 53.2, 53.1, 42.8, 42.6, 35.6, 32.0, 26.5, 26.0, 25.8. A sample of the free base was dissolved in 2 M HCl MeOH/H_2O and stirred. The solution was then concentrated by rotary evaporation and the residue dried *in vacuo*. The solid was washed with anhydrous diethyl ether (3 x 25 mL) and dried *in vacuo* to give the HCl salt as a white solid. IR (neat, cm^{-1}) 3064 (w, br), 2930 (w), 2852 (w), 2603 (w, br), 1597 (w), 1528 (m), 1499 (w), 1448 (w), 1349 (m), 1309 (m), 1259 (m), 1153 (s), 1093 (s), 1023 (w), 946 (w), 835 (w), 804 (w), 737 (m), 686 (w), 609 (m), 560 (s), 522 (w), 507 (s). MS (ESI$^+$) *m/z* 583.23 (MH$^+$). Anal. Calcd. for $C_{26}H_{38}N_4O_7S_2 \cdot HCl \cdot 1.25H_2O$: C, 48.84; H, 6.50; N, 8.76. Found: C, 48.47; H, 6.09; N, 8.81.

Synthesis of 9-cyclohexylmethyl-5-(*p*-methoxybenzenesulfonyl)-3-methylene-1-(*p*-nitrobenzenesulfonyl)-1,5,9-triazacyclododecane (RK005)[5]

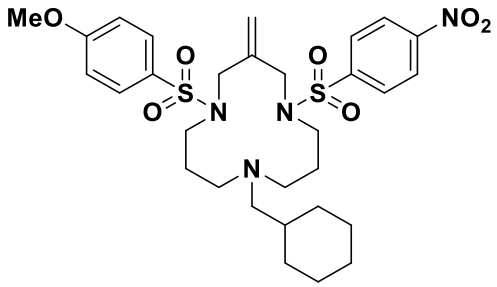

Prior to proceeding all glassware and the stir bar was dried in the oven. To a 1 L round bottom flask equipped with a condenser and gas inlet 13.48 g (23.13 mmol) of N'-(*p*-methoxybenzenesulfonyl)- N"-(*p*-nitrobenzenesulfonyl)- [N,N-bis(3-aminopropyl)cyclohexylmethylamine], 16.67 g (57.83 mmol) 2-methylene-1,3- propanebis(*tert*-

butylcarbonate), 1.23 g (11.6 mmol) Na_2CO_3, 1.28 g (3.01 mmol) of dppb, 1.27 g (1.39 mmol) of $Pd_2(dba)_3$, and 120 mL of dry acetonitrile were stirred under N_2 gas and boiled under reflux for 24 h. The mixture was cooled to r.t. and concentrated by rotary evaporation. The residue was dissolved in 300 mL of DCM and vacuum filtered, the filtrate was transferred to a separatory funnel and washed with sat. aq. $NaHCO_3$ (3 x 150 mL) and sat. aq. NaCl (150 mL). The organic layer was dried over Na_2SO_4, vacuum filtered, concentrated by rotary evaporation, and dried *in vacuo*. The crude product was dissolved in a minimal amount of DCM and adsorbed to the top of a silica column which was eluted with hexanes/EtOAc/Et_3N (70:30:1, v/v). The desired fraction was collected, concentrated by rotary evaporation, and dried *in vacuo*. This produced 2.90 g (4.57 mmol, 19.8%) of 9-cyclohexylmethyl-1-(*p*-methoxysulfonyl)-3-methylene-5-(*o*-nitrobenzenesulfonyl)-1,5,9-triazacyclododecane as a yellow solid. ^{1}H NMR (400 MHz, $CDCl_3$) δ 8.38 (d, 8 Hz, 2H, *m*-$ArNO_2$), 8.01 (d, 8 Hz, 2H, *o*-$ArNO_2$), 7.70 (d, 9 Hz, 2H, *o*-$ArOCH_3$), 7.01 (d, 9 Hz, 2H, *m*-$ArOCH_3$), 5.17 (d, 5 Hz, 2H, C=CH_2), 4.01 (s, 2 H, C*H*$_2$C=CH_2), 3.89 (s, 3H, OCH_3), 3.67 (s, 2H, C*H*$_2$C=CH_2), 3.38 (t, 7 Hz, 2H, CH_2NSO_2), 3.00 (t, 7 Hz, 2H, CH_2NSO_2), 2.33 (t, 6 Hz, 2H, C*H*$_2$NCH_2Cy), 2.24 (t, 6 Hz, 2H, 2.08, C*H*$_2$NCH_2Cy), 1.99 (d, 6 Hz, 2H, CH_2Cy), 1.73 (m, 2H, CCH_2C), 1.63 (m, 5H, CCH_2C, Cy), 1.52 (m, 3H, Cy), 1.13 (m, 3H, CH, Cy), 0.70 (m, Hz, 2H, Cy). ^{13}C NMR (100 MHz, $CDCl_3$) *δ* 163.1, 150.0, 145.8, 137.6, 129.5, 129.0, 128.3, 124.5, 116.6, 114.4, 62.1, 55.7, 53.3, 50.8, 49.6, 48.6, 45.4, 43.3, 35.9, 32.0, 26.8, 26.0, 25.6, 23.8. The product was dissolved in 30 mL 2 N HCl in MeOH/H_2O and stirred for 4 h. The resulting salt was concentrated by rotary evaporation, wash with anhydrous diethyl ether (3 x 25 mL), and dried *in vacuo*. This produced 2.90 g (4.32 mmol, 18.7%) of 9-cyclohexylmethyl-1-(*p*-methoxysulfonyl)-3-methylene-5-(*o*-nitrobenzenesulfonyl)-1,5,9-triazacyclododecane (RK005) as a yellow solid. MP 147.3 – 151.2 ˚C (decom). IR (neat, cm^{-1})

2928 (w), 2853 (w), 2444 (w, br), 1595 (w), 1529 (m), 1498 (w), 1449 (w), 1348 (m), 1308 (m), 1260 (m), 1155 (s), 1091 (m), 1019 (w), 900 (w), 855 (w), 837 (w), 806 (w), 740 (m), 689 (w), 628 (w), 604 (m), 584 (m), 558 (s), 523 (w), 508 (m). MS (ESI^+) *m/z* 635.26 (MH^+). Anal. Calcd. for $C_{30}H_{42}N_4O_7S_2 \cdot HCl \cdot H_2O$: C, 56.76; H, 6.67; N, 8.83. Found: C, 52.51; H, 6.32; N, 8.16.

Synthesis of 9-cyclohexylmethyl-1-(*p*-aminobenzensulfonyl)-3-methylene-5-(*p*-methoxybenzensulfonyl)-1,5,9-triazacyclododecane (RK006)[24]

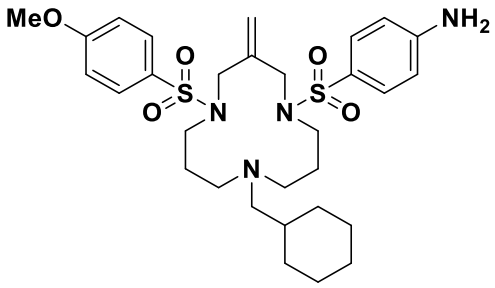

To a 500 mL round-bottom flask equipped with a condenser and gas inlet, a mixture of 1.19 g (1.87 mmol) of 9-cyclohexylmethyl-1-(*p*-methoxysulfonyl)-3-methylene-5-(*p*-nitrobenzenesulfonyl)-1,5,9-triazacyclododecane, 43 mL sat. aq. $Cu(OAc)_2$, and 170 mL EtOH was stirred under N_2 gas at r.t. for 40 minutes. Then 2.28 g (61.71 mmol) of $NaBH_4$ was slowly added over 30 minutes and the reaction was stirred under N_2 gas at r.t. for 18 h. The solution was vacuum filtered and concentrated by rotary evaporation. A mixture of the residue, 70 mL of sat. aq. $NaHCO_3$, and 70 mL of DCM was transferred to a separatory funnel. The layers were separated and the aq. layer was extracted with DCM (3 x 70 mL). The combined organic layers were washed with 150 mL of sat. aq. $NaHCO_3$. The organic phase was dried over Na_2SO_4, vacuum filtered, concentrated by rotary evaporation, and dried *in vacuo*. The crude product was dissolved in a minimal amount of DCM and adsorbed to the top of a silica column which was eluted with hexanes/EtOAc/Et_3N (50:50:1, v/v). The desired fraction was collected, concentrated

by rotary evaporation, and dried *in vacuo*. This produced 1.04 g (1.72 mmol, 92.0%) of 9-cyclohexylmethyl-1-(*p*-aminobenzensulfonyl)-3-methylene-5-(*p*-methoxybenzensulfonyl)-1,5,9-triazacyclododecane (RK006) as an off-white powder. ^{1}H NMR (400 MHz, $CDCl_3$) δ 7.73 (d, 9 Hz, 2 H, *o*-$ArOCH_3$), 7.55 (d, 9 Hz, 2 H, *o*-$ArNH_2$) 6.99 (d, 9 Hz, 2 H, *m*-$ArOCH_3$), 6.70 (d, 9 Hz, 2 H, *m*-$ArNH_2$), 5.17 (s, 2 H, $C=CH_2$), 4.12 (s, 2 H, H2), 3.88 (s, 3 H, OCH_3), 3.82 (s, 2 H, NH_2), 3.73 (s, 2 H, H4), 3.19 (t, 7 Hz, 2 H, H12), 3.08 (t, 7 Hz, 2 H, H6), 2.26 (m, 4 H, H10,H8), 1.96 (d, 7 Hz, 2 H, CH_2Cy), 1.61 (m, 10 H, H7, H11, Cy), 1.13 (m, 3 H, CH, Cy), 0.69 (m, 2 H, Cy). ^{13}C NMR (100 MHz, $CDCl_3$) *δ* 162.82, 150.44, 138.19, 130.65, 129.40, 129.31, 126.61, 116.43, 114.30, 114.15, 62.18, 55.61, 51.54, 50.55, 50.25, 44.35, 43.83, 35.92, 31.96, 26.80, 26.06, 24.68, 24.15. The product was dissolved in 15 mL 2 N HCl in MeOH/H_2O and stirred for 4 h. The resulting salt was concentrated by rotary evaporation, washed with anhydrous diethyl ether (3 x 25 mL), and dried *in vacuo*. This produced 1.10 g (1.72 mmol, 92.0%) of 9-cyclohexylmethyl-1-(*p*-aminobenzensulfonyl)-3-methylene-5-(*p*-methoxybenzensulfonyl)-1,5,9-triazacyclododecane (RK006) as an off-white powder. MP 129.0 – 130.9 ˚C (decom). IR (neat, cm^{-1}) 2927 (w), 2850 (w), 2565 (w, br), 2145 (w), 1959 (w), 1630 (w), 1595 (m), 1497 (m), 1440 (w), 1311 (m), 1260 (m), 1152 (s), 1091 (m), 1019 (m), 901 (w), 835 (m), 807 (m), 780 (w), 691 (m), 660 (m). MS (ESI^+) *m/z* 605.28 (MH^+). Anal. Calcd. for $C_{30}H_{44}N_4O_5S_2$•HCl: C, 56.19; H, 7.07; N, 8.74. Found: C, 56.18; H,7.02; N, 8.88.

9-cyclohexylmethyl-1-(*p*-azidobenzenesulfonyl)-3-methylene-5-(*p*-methoxybenzenesulfonyl)-1,5,9-triazacyclododecane (RK007)[24]

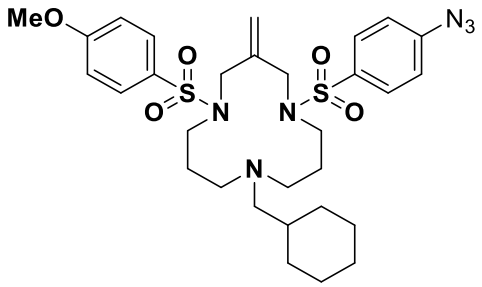

To a 250 mL round-bottom flask equipped with a gas inlet, a mixture of 0.51 g (0.85 mmol) of 9-cyclohexylmethyl-1-(*p*-aminobenzensulfonyl)-3-methylene-5-(*p*-methoxybenzenesulfonyl)-1,5,9-triazacyclododecane (RK006) and 4.0 mL of EtOAc was stirred under N_2 gas at 0 °C. Then 0.34 mL of conc. aq. HCl was added dropwise followed by dropwise addition of a mixture of 0.07 g (1.0 mmol) of $NaNO_2$ and 1.2 mL of H_2O. The reaction mixture was stirred under N_2 gas at 0 °C for 1 h. Then a mixture of 0.067 g (1.0 mmol) of NaN_3 and 5.9 mL of H_2O was added and the reaction was stirred under N_2 gas at r.t. for 18 h. Then 30 mL of 1 N aq. NaOH was added to the solution and the mixture was transferred to a separatory funnel. The layers were separated and the aq. layer was extracted with EtOAc (3 x 50 mL). The combined organic layers were dried over Na_2SO_4, vacuum filtered, concentrated by rotary evaporation. The crude product was dissolved in a minimal amount of DCM and adsorbed to the top of an alumina column which was eluted with hexanes/EtOAc (7:3, v/v). The desired fraction was collected, concentrated by rotary evaporation, and dried *in vacuo*. This produced 0.35 g (0.55 mmol, 65% of 9-cyclohexylmethyl-1-(*p*-azidobenzenesulfonyl)-3-methylene-5-(*p*-methoxybenzenesulfonyl)-1,5,9-triazacyclododecane as a foamy off-white solid. ^{1}H NMR (400 MHz, $CDCl_3$) δ 7.79 (d, 9 Hz, 2 H, *o*-ArN_3), 7.72 (d, 9 Hz, 2 H, *o*-$ArOCH_3$), 7.15 (d, 8 Hz, 2 H, *m*-ArN_3), 7.00 (d, 9 Hz, 2 H, *m*-$ArOCH_3$), 5.18 (d, 5 Hz, 2 H, C=CH_2), 3.89 (s, 3 H, OCH_3), 3.86 (s, 2 H, H4), 3.74 (s, 2 H, H2), 3.23 (t, 7 Hz, 2 H, H12), 3.09 (t, 7 Hz, 2 H, H6), 2.29 (t, 6 Hz, 2 H, H10), 2.26 (t, 6 Hz, 2 H, H8), 1.99 (d, 6 Hz, 2 H, CH_2Cy), 1.60 (m, 10 H, H7, H11, Cy), 1.12 (m, 3 H, Cy), 0.71 (m, 2 H,

Cy). ^{13}C NMR (100 MHz, $CDCl_3$) δ 162.9, 144.7, 137.9, 135.3, 129.8, 129.4, 129.1, 119.5, 116.6, 114.3, 62.2, 55.6, 51.8, 50.5, 50.1, 44.6, 43.8, 35.9, 32.0, 29.7, 26.8, 26.0, 24.9, 24.1. The product was dissolved in 10 mL of 2 N HCl MeOH/H_2O and stirred for 2 h, then concentrated by rotary evaporation and dried *in vacuo*. The compound was washed with anhydrous diethyl ether (3 X 20 mL) and dried *in vacuo*. This produced 0.33 g (0.49 mmol, 58%) of 9-cyclohexylmethyl-1-(*p*-azidobenzenesulfonyl)-3-methylene-5-(*p*-methoxybenzenesulfonyl)-1,5,9-triazacyclododecane (RK007) as an of white powder. MP 118.6 – 119.2 ˚C (decom). IR (neat, cm^{-1}) 2924 (w), 2853 (w), 2409 (w, br), 2127 (m), 2100 (m), 1588 (m), 1493(m), 1493 (m), 1452 (w), 1376 (w), 1334 (m), 1304 (m), 1284 (m), 1258 (m), 1155 (s), 1127 (m), 1091 (m), 1018 (m), 997 (m), 945 (w), 921 (w), 879 (w), 835 (m), 805 (m), 767 (m), 727 (m), 704 (m), 677 (m), 649 (m), 614 (m), 583 (m), 556 (s), 545 (m), 529 (m). MS (ESI^+) *m/z* 631.27 (MH^+). Anal. Calcd. for $C_{30}H_{42}N_6O_5S_2$•HCl•$2H_2O$: C, 51.23; H, 6.74; N, 11.95. Found: C, 51.45; H,6.74; N, 12.08.

Synthesis of 9-cyclohexylmethyl-5-(*p*-methoxybenzenesulfonyl)-3-methylene-1-(5-methoxy-2-nitrobenzenesulfonyl)-1,5,9-triazacyclododecane (RK008)[4]

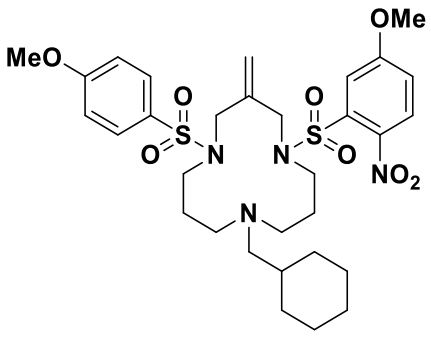

To a 1 L round-bottom flask equipped with a gas inlet, a mixture of 600 mg (1.33 mmol) of 9-cyclohexylmethyl-1-(p-methoxybenzenesulfonyl)-3-methylene-1,5,9-triazacyclododecane (RK003), 403 mg (1.60 mmol) of 5-methoxy-2-nitrobenzenesulfonyl chloride, 202 mg (2.00

mmol) of Et_3N, and 66.5 mL of DCM were stirred under N_2 gas at r.t. for 18 h. Then a solution of 50 mL of sat. aq. NaCl and 50 mL of sat. aq. $NaHCO_3$ was added to the reaction mixture, and the mixture was transferred to a separatory funnel. The layers were separated and the aq. layer was extracted with DCM (3 x 50 mL). The combined organic layers were dried over Na_2SO_4, vacuum filtered, concentrated by rotary evaporation, and dried *in vacuo*. This produced 0.99 g of crude product as a yellow glassy solid which was dissolved in a minimal amount of DCM and adsorbed to the top of an alumina column which was eluted hexanes/EtOAc (7:3, v/v). The desired fraction was collected, concentrated by rotary evaporation, and dried *in vacuo*. This produced 0.60 g (0.90 mmol, 68%) of 9-cyclohexylmethyl-5-(*p*-methoxybenzenesulfonyl)-3-methylene-1-(5-methoxy-2-nitrobenzenesulfonyl)-1,5,9-triazacyclododecane as white glassy solid. ^{1}H NMR (400 MHz, $CDCl_3$) δ 7.72 (m, 3 H, 3-$ArNO_2$/OCH_3, *o*-$ArOCH_3$), 7.52 (d, 3 Hz, 1 H, 6-$ArNO_2$/OCH_3), 7.09 (dd, 6 Hz, 3 Hz, 1 H, 4-$ArNO_2$/OCH_3), 7.01 (d, 9 Hz, 2 H, *m*-$ArOCH_3$), 5.20 (s, 1 H, C=CH_2), 5.12 (s, 1 H, C=CH_2), 4.19 (s, 2 H, H2), 3.95 (s, 3 H, $ArNO_2$/OCH_3), 3.88 (s, 3 H, ArOCH_3), 3.59 (s, 2 H, H4), 3.53 (t, 7 Hz, 2 H, H12), 2.93 (t, 6 Hz, 2 H, H6), 2.40 (m, 2 H, H10), 2.26 (t, 5 Hz, 2 H, H8), 2.00 (d, 7 Hz, 2 H, CH_2Cy), 1.83 (m, 2 H, H11), 1.64 (m, 8 H, H7, Cy), 1.15 (m, 3 H, Cy), 0.73 (m, 2 H, Cy). ^{13}C NMR (100 MHz, $CDCl_3$) δ 163.1, 161.7, 141.2, 137.8, 136.2, 129.6, 128.4, 126.9, 117.3, 116.6, 116.4, 114.3, 62.2, 56.4, 55.6, 54.8, 51.4, 49.5, 47.6, 45.7, 42.9, 35.9, 32.0, 26.8, 26.3, 26.0, 23.9. The product was stirred with 10 mL of 2 N HCl in MeOH/H_2O for 4 h. The resulting salt was concentrated by rotary evaporation, washed with anhydrous diethyl ether (3 x 25 mL), and dried *in vacuo* to give the HCl salt as a white solid. This produced 0.63 g (0.90 mmol, 68%) of 9-cyclohexylmethyl-5-(*p*-methoxybenzenesulfonyl)-3-methylene-1-(5-methoxy-2-nitrobenzenesulfonyl)-1,5,9-triazacyclododecane (RK008) as white powder. MP 138.8 – 139.9 ˚C (decom). IR (neat, cm^{-1})

2924 (w), 2850 (w), 2493 (w, br), 1594 (w), 1534 (w), 1498 (w), 1451 (w), 1335 (m), 1261 (m), 1153 (s), 1093 (w), 1020 (w), 881 (w), 832 (w), 807 (w), 737 (w), 692 (w), 579 (m), 559 (s), 522 (w), 507 (w). MS (ESI^+) *m/z* 665.27 (MH^+). Anal. Calcd. for $C_{36}H_{44}N_4O_8S_2 \cdot 0.5\ HCl \cdot 1\ H_2O$: C, 53.11; H, 6.69; N, 7.99. Found: C, 52.71; H, 7.10; N, 7.79.

Synthesis of 9-cyclohexylmethyl-5-(*p*-methoxybenzenesulfonyl)-3-methylene-1-(3,4,5-trimethoxybenzenesulfonyl)-1,5,9-triazacyclododecane (RK009)[4]

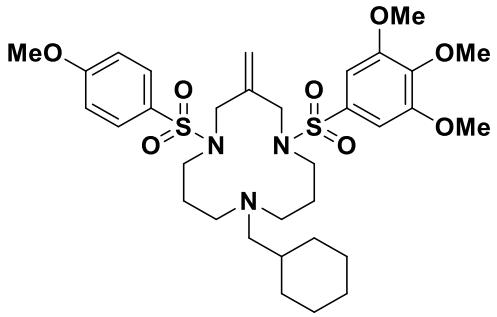

To a 500 mL round-bottom flask equipped with a gas inlet, a mixture of 400 mg (0.89 mmol) of 9-cyclohexylmethyl-1-(*p*-methoxybenzenesulfonyl)-3-methylene-1,5,9-triazacyclododecane (RK003), 243 mg (1.07 mmol) of 3,4,5-trimethoxyzbenzenesulfonyl chloride, 136 mg (1.34 mmol) of Et_3N, and 44.5 mL of DCM was stirred under N_2 gas at r.t. for 18 h. Then a solution of 50 mL of sat. aq. NaCl and 50 mL of sat. aq. $NaHCO_3$ was added to the reaction mixture, and the mixture was transferred to a separatory funnel. The layers were separated and the aq. layer was extracted with DCM (3 x 50 mL). The combined organic layers were dried over Na_2SO_4, vacuum filtered, concentrated by rotary evaporation, and dried *in vacuo*. This produced 0.63 g of crude product as a yellow glassy solid which was dissolved in a minimal amount of DCM and adsorbed to the top of an alumina column which was eluted hexanes/EtOAc (4:1, v/v). The desired fraction was collected, concentrated by rotary evaporation, and dried *in vacuo*. This produced 0.41 g (0.60 mmol 67%) of 9-cyclohexylmethyl-5-(*p*-methoxybenzenesulfonyl)-3-methylene-1-

(3,4,5-trimethoxybenzenesulfonyl)-1,5,9-triazacyclododecane as a white glassy solid. ^{1}H NMR (400 MHz, $CDCl_3$) δ 7.72 (d, 9 Hz, 2 H, *o*-$ArOCH_3$), 7.01 (m, 4 H, *m*-$ArOCH_3$, *m*-$Ar(OCH_3)_3$), 5.19 (s, 2 H, C=CH_2), 3.92 (s, 9 H, $Ar(OCH_3)_3$), 3.89 (s, 5 H, $ArOCH_3$, H2), 3.78 (s, 2 H, H4), 3.24 (t, 7 Hz, 2 H, H12), 3.12 (t, 7 Hz, 2 H, H6), 2.28 (m, 4 H, H10, H8), 1.98 (d, 6 Hz, 2 H, CH_2Cy), 1.64 (m, 10 H, H7, H11, Cy), 1.14 (m, 3 H, Cy), 0.70 (m, 2 H, Cy). ^{13}C NMR (100 MHz, $CDCl_3$) δ 162.9, 153.4, 141.6, 138.1, 133.7, 130.1, 129.4, 116.4, 114.3, 104.5, 62.2, 61.0, 56.5, 55.6, 51.4, 50.4, 50.1, 44.5, 44.0, 35.9, 32.0, 26.8, 26.1, 24.7, 24.3. The product was stirred with 6 mL of 2 N HCl in MeOH/H_2O for 4 h. The resulting salt was concentrated by rotary evaporation, washed with anhydrous diethyl ether (3 x 25 mL), and dried *in vacuo* to give the HCl salt as a white solid. This produced 0.42 g (0.59 mmol 66%) of 9-cyclohexylmethyl-5-(*p*-methoxybenzenesulfonyl)-3-methylene-1-(3,4,5-trimethoxybenzenesulfonyl)-1,5,9-triazacyclododecane (RK009) as white powder. MP 132.8 – 137.3 ˚C (decom). IR (neat, cm^{-1}) 2930 (w), 2853 (w), 2455 (w, br), 1593 (w), 1498 (w), 1454 (w), 1409 (w), 1333 (m), 1311 (m), 1260 (m), 1151 (s), 1123 (s), 1019 (w), 901 (w), 837 (w), 807 (w), 777 (w), 725 (w), 686 (w), 662 (w), 629 (w), 599 (m), 559 (s), 523 (w), 515 (w), 507 (w). MS (ESI+) m/z 680.30 (MH+). Anal. Calcd. for $C_{33}H_{49}N_3O_8S_2$·1 HCl·0.25 H_2O: C, 54.30; H, 7.01; N, 5.76. Found: C, 54.45; H, 6.56; N, 5.86.

Synthesis of 9-cyclohexylmethyl-1-(2,3,4,5,6-pentafluorobenzenesulfonyl)-5-(*p*-methoxybenzenesulfonyl)-3-methylene-1,5,9-triazacyclododecane (RK010)[4]

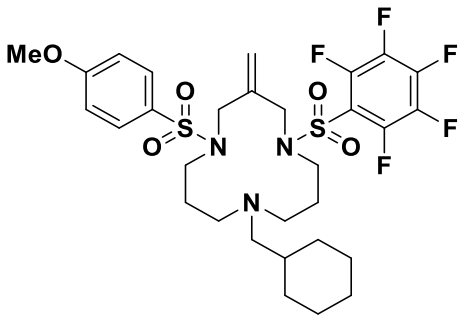

To a 250 mL round-bottom flask equipped with a gas inlet, a mixture of 0.20 g (0.44 mmol) of 9-cyclohexylmethyl-1-(*p*-methoxybenzenesulfonyl)-3-methylene-1,5,9-triazacyclododecane (RK003), 0.14 g (0.53 mmol) of 2,3,4,5,6-pentafluorobenzenesulfonyl chloride, 67 mg (0.66 mmol) of Et_3N, and 22.0 mL of DCM were stirred under N_2 gas at r.t. for 18 h. Then a solution of 25 mL of sat. aq. NaCl and 25 mL of sat. aq. $NaHCO_3$ was added to the reaction mixture, and the mixture was transferred to a separatory funnel. The layers were separated and the aq. layer was extracted with DCM (3 x 50 mL). The combined organic layers were dried over Na_2SO_4, vacuum filtered, concentrated by rotary evaporation, and dried *in vacuo*. This produced 0.41 g of crude product as a yellow glassy solid which was dissolved in a minimal amount of DCM and adsorbed to the top of a silica column which was eluted hexanes/EtOAc (97:3, v/v) for 3 minutes then the solution was brought to hexanes/EtOAc (13:7, v/v) over 30 minutes. The desired fraction was collected, concentrated by rotary evaporation, and dried *in vacuo*. This produced 0.16 g (0.24 mmol, 55%) 9-cyclohexylmethyl-1-(2,3,4,5,6-pentafluorobenzenesulfonyl)-5-(*p*-methoxybenzenesulfonyl)-3-methylene-1,5,9-triazacyclododecane (RK010) as a white glassy solid. MP 70.6 – 71.2 ˚C (decom). ^{1}H NMR (400 MHz, $CDCl_3$) δ 7.71 (d, 9 Hz, 2 H, *o*-ArOCH_3), 7.01 (d, 9 Hz, 2 H, *m*-ArOCH_3), 5.19 (s, 2 H, C=CH_2), 4.15 (s, 2 H, H2), 3.89 (s, 3 H, ArOCH_3), 3.65 (s, 2 H, H4), 3.53 (t, 7 Hz, 2 H, H12), 2.98 (t, 6 Hz, 2 H, H6), 2.38 (t, 6 Hz, 2 H, H10) 2.27 (t, 6 Hz, 2 H, H8), 2.00 (d, 7 Hz, 2 H, CH_2Cy), 1.78 (t, 6 Hz, 2 H, H11), 1.64 (m, 8 H, H7, Cy), 1.15 (m, 3 H, Cy), 0.73 (m, 2 H, Cy). ^{13}C NMR (100 MHz, $CDCl_3$) δ 163.1, 145.9,

143.3, 137.7, 129.6, 128.7, 116.6, 114.4, 62.1, 55.7, 53.8, 50.8, 49.5, 48.0, 45.6, 43.4, 35.8, 32.0, 29.7, 27.8, 26.7, 26.0, 23.4. IR (neat, cm^{-1}) 2923 (w), 2850 (w), 2804 (w), 1644 (w), 1596 (w), 1579 (w), 1521 (m), 1494 (s), 1464 (w), 1355 (m), 1337 (m), 1299 (w), 1259 (m), 1157 (s), 1096 (s), 1026 (m), 990 (s), 938 (w), 910 (w), 880 (w), 855 (m), 834 (m), 807 (w), 791 (w), 775 (w), 744 (w), 729 (w), 689 (m), 664 (w), 642 (w), 629 (w), 600 (m), 577 (m), 559 (s), 522 (m), 515 (w), 507 (m). MS (ESI+) m/z 680.22 (MH+). Anal. Calcd. for $C_{31}H_{38}F_5N_3O_5S_2$: C, 53.82; H, 5.54; N, 6.07. Found: C, 54.04; H, 5.44; N, 6.05.

Synthesis of 9-cyclohexylmethyl-1-(2,6-difluorobenzenesulfonyl)-5-(*p*-methoxybenzenesulfonyl)-3-methylene-1,5,9-triazacyclododecane (RK012)[4]

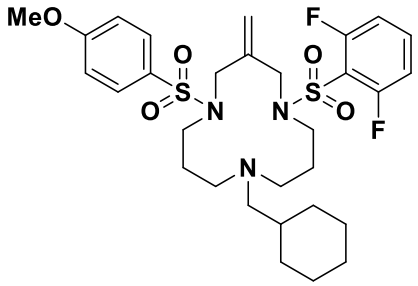

To a 250 mL round-bottom flask equipped with a gas inlet, a mixture of 200 mg (0.44 mmol) of 9-cyclohexylmethyl-1-(*p*-methoxybenzenesulfonyl)-3-methylene-1,5,9-triazacyclododecane (RK003), 121 mg (0.57 mmol) of 2,6-difluorobenzenesulfonyl chloride, 111 mg (1.10 mmol) of Et_3N, and 22.0 mL of DCM was stirred under N_2 gas at r.t. for 18 h. Then a solution of 25 mL of sat. aq. NaCl and 25 mL of sat. aq. $NaHCO_3$ was added to the reaction mixture, and the mixture was transferred to a separatory funnel. The layers were separated and the aq. layer was extracted with DCM (3 x 50 mL). The combined organic layers were dried over Na_2SO_4, vacuum filtered, concentrated by rotary evaporation, and dried *in vacuo*. This produced 0.60 g of crude product as a yellow glassy solid which was dissolved in a minimal amount of DCM and adsorbed to the top

of a silica column which was eluted hexanes/EtOAc (97:3, v/v) for 3 minutes then the solution was brought to hexanes/EtOAc (13:7, v/v) over 30 minutes and continued to elute with this solvent for 20 minutes. The desired fraction was collected, concentrated by rotary evaporation, and dried *in vacuo*. This produced 172 mg (0.28 mmol, 62.5%) 9-cyclohexylmethyl-1-(2,6-difluorobenzenesulfonyl)-5-(*p*-methoxybenzenesulfonyl)-3-methylene-1,5,9-triazacyclododecane (RK012) as a white glassy solid. MP 68.9 – 70.3 ˚C (decom). ^{1}H NMR (400 MHz, $CDCl_3$) δ 7.71 (d, 9 Hz, 2 H, *o*-$ArOCH_3$), 7.50 (m, 1 H, *p*-ArF_2), 7.02 (m, 4 H, *m*-$ArOCH_3$, *m*-ArF_2), 5.23 (s, 1 H, C=CH_2), 5.18 (s, 1 H, C=CH_2), 4.10 (s, 2 H, H2), 3.89 (s, 3 H, ArOCH_3), 3.70 (s, 2 H, H4), 3.46 (t, 7 Hz, 2 H, H12), 3.04 (t, 7 Hz, 2 H, H6), 2.35 (t, 6 Hz, 4 H, H8), 2.25 (t, 6 Hz, 2 H, H10) 1.99 (d, 6 Hz, 2 H, CH_2Cy), 1.74 (t, 5 Hz, 2 H, H7), 1.64 (m, 8 H, H11, Cy), 1.15 (m, 3 H, Cy), 0.72 (m, 2 H, Cy). ^{13}C NMR (100 MHz, $CDCl_3$) δ 163.0, 161.0, 158.4, 138.0, 134.3, 129.5, 129.3, 116.5, 114.3, 113.3, 113.1, 62.2, 55.6, 52.9, 50.7, 49.8, 48.9, 45.0, 43.5, 35.9, 31.9, 29.7, 26.8, 26.0, 25.4, 23.6. IR (neat, cm^{-1}) 2922 (w), 2850 (w), 2803 (w), 1611 (w), 1596 (w), 1498 (w), 1466 (m), 1337 (m), 1307 (w), 1282 (w), 1259 (m), 1236 (w), 1156 (s), 1107 (w), 1094 (w), 1072 (w), 1027 (w), 1002 (m), 964 (w), 938 (w), 910 (w), 879 (w), 835 (w), 793 (m), 744 (w), 728 (w), 663 (w), 629 (w), 578 (m), 559 (s), 533 (s), 512 (s), 501 (s). MS (ESI+) m/z 626.25 (MH+). Anal. Calcd. for $C_{31}H_{41}F_2N_3O_5S_2$: C, 58.38; H, 6.48; N, 6.59. Found: C, 58.68; H, 6.22; N, 6.33.

3.4 Pharmacokinetics

Determination of λ_{max} and Extinction Coefficient

Materials & Reagents
~10 mM compound stock solution in HPLC grade MeOH
2 quartz 1 cm pathlength cuvettes from Fisher Scientific
20 µL micropipette with tips
5 mL glass volumetric flasks with stopper
ACS grade MeOH
Beaker
Compressed air
Cotton
Glass pasteur pipettes and bulb
UV-2550 UV-VIS Spectrophotometer

Procedure

A volumetric flask was filled with ACS grade MeOH just below fill line. First, 8 µL of stock compound solution was added to the flask via micropipette. A Pasteur pipette was used to add MeOH to bring the bottom of the meniscus to the fill line. The flask was capped with stopper and inverted to mix thoroughly. The instrument was autozeroed with no cuvettes in either chamber; then a baseline spectrum from 400 to 200 nm was recorded with ACS grade MeOH in the cuvettes in both chambers. The MeOH was removed from the cuvette in the sample chamber and dried with compressed air blown through a pipette with cotton filter. The diluted compound from the volumetric flask was added to this cuvette which was then returned to the sample chamber. The spectrum was recorded from 400 to 200 nm. The lambda max was noted, and four more dilutions were made to cover a range of absorbances at the lambda max from approximately 0.1 to 1.0. The points were plotted on a graph with concentration on the x-axis and absorbance on the y-axis with a minimum acceptable R^2 value of 0.999. The slope of the line * 10^6 gave the extinction coefficient in $M^{-1}cm^{-1}$.

Determination of Kinetic Solubility

Method 1: Nephelometry

Materials & Reagents
~20 mM compound stock solution in HPLC grade DMSO
300 µL multichannel micropipette
96-well flat bottom, clear, PS, plates
Glass vials with screw cap lids
HPLC grade DMSO
Micropipettes with tips
Nepheloskan Ascent from Thermo Labsystems
PBS (pH 7.4) from Gibco
Vortex

Procedure

Six glass vials were loaded with 871.2 µL of PBS and each received either 0, 2.2, 2.6, 3.0, 3.6, or 4.0 µL of DMSO. To the vial that did not receive any DMSO 8.8 µL of stock solution was added and the vial was immediately vortexed. After 5 minutes, 6.6 µL of stock solution was added to the vial that received 2.2 µL of DMSO and the vial was immediately vortexed. After 5 minutes, 6.2, 5.8, 5.2, and 4.8 µL of stock solution was added successively to the vials that received 2.6, 3.0, 3.6 and 4.0 µL, respectively. Then all these vials were vortexed. The time was noted, then the first vial (no DMSO, 8.8 µL stock) was vortexed a second time and 200 µL from the was added to triplicate wells with pipetting up and down three times to mix in between additions. With a multichannel pipette set at 100 µL this solution was mixed 5 times by pipetting up and down and then 100 µL was removed and mixed in an adjacent well that was pre-loaded with 100 µL of PBS containing 1% DMSO. This was mixed 5 times by pipetting up and down before removing 100 µL and mixing with another adjacent well that was pre-loaded with 100 µL of PBS containing 1% DMSO. This was repeated to create a 2X dilution series of 8 total concentrations in triplicate. From the last set of wells in the series 100 µL of the mixed solution was removed and discarded to ensure the final volume of all wells was 100 µL. Once 5 minutes had passed after the first vial was vortexed for the second time, the second vial (2.2 µL DMSO, 6.6 µL stock) was vortexed a second time and 200 µL from the was added to triplicate wells with

pipetting up and down three times to mix in between additions. As before a multichannel pipette was used to create a 2X dilution series of 8 total concentrations in triplicate. Once 5 minutes had passed after the second vial was vortexed for the second time, each remaining vial in order of preparation was vortexed and 100 µL of solution added to the plate in triplicate with mixing 5 times by pipetting up and down between each addition. The instrument was programmed to shake for 2 minutes, then incubate for 30 minutes at 37 °C. This was followed by 3 minutes of shaking before reading using the nephelometer with PMT voltage of 500 and lamp voltage of 10.0 using an integration time of 1,000 ms. The solubility was determined as the point at which a large increase in counts was observed by fitting two separate lines to the points that were either flat or began increasing in counts and determining the intersection of these two lines.

Method 2: Visual

Materials & Reagents
~20 mM compound stock solution in HPLC grade DMSO
300 µL multichannel micropipette
Glass vials with screw cap lids
HPLC grade DMSO
Micropipettes with tips
Oven set at 37° C
PBS (pH 7.4) from Gibco
Vortex

Procedure

To individual glass vials 871.2 µL of PBS was added. From 0 to 8.6 µL of DMSO was added next, followed by corresponding amount of stock solution so that the total of DMSO and stock solution added to each vial would add up to 8.8 µL. After addition of the stock solution the vial was vortexed and observed for a couple of minutes before placing in 37° C incubator for 30 minutes. The presence of precipitates before and after incubation were recorded and the lowest

concentration that had precipitates before incubation, but that disappeared after incubation was determined to be the concentration of solubility.

Method 3: UV with multiple point standard addition

Materials & Reagents
~20 mM compound stock solution in HPLC grade DMSO
2 mL MCT tubes from Fisher Scientific
96-well, UV, flat bottom plates
HPLC grade DMSO and MeOH
International Equipment Co. Clinical Centrifuge
Micropipettes with tips
PBS (pH 7.4) from Gibco
Synergy HTX Multi-Mode Microplate Reader from BioTek
Vortex

Procedure

To a 2 mL snap cap tube 1386 µL of PBS was mixed with 14 µL of 20 mM compound stock solution in DMSO. The tube was vortexed and incubated at 37° C for 30 minutes. After incubation, the tube was vortexed and centrifuged for 5 minutes to pellet precipitate. The supernatant was removed by pipette and transferred to a fresh tube. A blank control tube was made by adding 600 µL of MeOH and 200 µL of PBS containing 1% DMSO. Six tubes were prepared by mixing 0, 0.8, 1.6, 2.4, 3.2, or 4.0 µL of ~10 mM compound stock solution in MeOH with 200 µL of supernatant prepared earlier and the appropriate amount of MeOH necessary to bring the final volume to 800 µL. Each tube was vortexed and 200 µL was added to wells in a 96-well plate in triplicate. Absorbance was measured at the lambda max of the compound. The average of blank control was subtracted from average values for all other samples before calculating solubility as per formula below.

Calculation

Graph the absorbance (y-axis) against the volume of 10 mM compound stock spiked into supernatant solution (x-axis).

$$Kinetic\ Solubility = -\frac{x - intercept * concentration\ of\ stock\ solution\ in\ MeOH}{volume\ of\ supernatant\ added}$$

Method 4: UV with single point standard addition

Materials & Reagents
~20 mM compound stock solution in HPLC grade DMSO
2 mL MCT tubes from Fisher Scientific
96-well, UV, flat bottom plates
HPLC grade DMSO and MeOH
International Equipment Co. Clinical Centrifuge
Micropipettes with tips
PBS (pH 7.4) from Gibco
Synergy HTX Multi-Mode Microplate Reader from BioTek
Vortex

Procedure:

To check the solubility of the spiking solution, 400 µL transport solvent (TS) (PBS pH 7.4 containing 1% DMSO), 399.6 µL of MeOH, 0.4 µL of 20 mM stock solution in DMSO were added to a 2 mL Denville tube and vortexed to mix. After 5 min incubation at rt the tube was vortexed again and the solution was aspirated into glass Pasteur pipette to check for presence of precipitates. If there were precipitates, the volumes could be adjusted to give a higher percentage of MeOH. To make 1400 µL of a 100 µM sample in PBS containing 1% DMSO, 1386 µL of PBS with 7 µL of DMSO and 7 µL of 20 mM stock solution in DMSO were added to a 2 mL Denville tube and vortexed to mix. After 5 min incubation at rt the tube was vortexed again and then centrifuged for 5 min at max speed to pellet the precipitates. Then 880 µL of the supernatant was removed with a micropipette and added to a fresh 2 mL tube. To prepare the blank solution, 400 µL of TS, 399.6 µL of MeOH, and 0.4 µL of DMSO were added to a 2 mL tube and vortexed to mix. To prepare the sample solution, 400 µL of supernatant, 399.6 µL of MeOH, and 0.4 µL of DMSO were added to a 2 mL tube and vortexed to mix. To prepare the sample plus

spike solution, 400 µL of supernatant, 399.6 µL of MeOH, and 0.4 µL of 20 mM compound stock in DMSO were added to a 2 mL tube and vortexed to mix. All four solutions (spiking, blank, sample, sample plus spike solutions), were added to 96-well UV plate (200 µL in triplicate) and the absorbance was read at the compounds λ_{max}. The average and standard deviation of the triplicates were calculated, and the absorbance of the blank solution subtracted from the absorbances for all other solutions' averages. Equation 1 was then used to determine the concentration of the supernatant which was representative of the kinetic solubility of the compound in PBS with 1% DMSO.

Calculation

$$C_{supernatant} = \frac{Abs_{sample\ solution} * C_{stock} * V_{stock}}{V_{supernatant} * (Abs_{sample\ plus\ spike\ solution} - Abs_{sample\ solution})}$$

C represents the concentration in µM, Abs represents the absorbance, and V represents the volume in µL (V_{stock} is the volume of 20 mM stock added in the sample plus spike solutions, ie: 0.4 µL; $V_{supernatant}$ is the volume of supernatant added in the sample and sample plus spike solutions, ie: 400 µL). Note that the spiking solution was not used in the equation but was used to ensure that absorbances for were in expected ranges and to check for precipitation. For each compound at least 3 total trials were performed. Averages and standard deviations were then calculated for the concentration of the supernatant and recorded as kinetic solubility in µM.

Solutions Table (all volumes in µL)

	PBS	1% DMSO in PBS	Supernatant	MeOH	DMSO	Stock
Supernatant	1386	0	0	0	7	7
Spiking soln	0	400	0	399.6	0	0.4
Sample	0	0	400	399.6	0.4	0
Sample + Spike	0	0	400	399.6	0	0.4
Blank	0	400	0	399.6	0.4	0

Determination of Permeability Using PAMPA

Materials & Reagents
~20 mM compound stock solution in HPLC grade DMSO
0.2 mL plastic tubes
0.6 mL plastic tubes
1.5 mL plastic tubes
2.0 mL plastic tubes
5 mL glass vials
96-well plates with 0.45 µm hydrophobic high protein binding IP membrane
96-well polystyrene multiscreen reciever plates
Agilent Eclipse XDR-C18 5 µm 2.1 X 150 mm HPLC column
Agilent Technologies 1220 Infinity II LC
Analytical grade scale
Dodecane
Filtered and degassed phosphate buffer (pH 3.0)
Glass HPLC vial with cap
HPLC grade Acetonitrile
HPLC grade DMSO
HPLC vial inserts
Lecithin
PBS (pH 7.4) from Gibco
PBS containing 1% DMSO
Plate sealer tape
Plate shaker

Procedure

Each compound was dissolved in DMSO to a concentration of 20 mM in 1.5 mL plastic tubes and this stock solution was used to make a 2 mM working solution in DMSO in 0.2 mL plastic tubes, as well as a 200 µM working solution in acetonitrile containing 1% DMSO. The 2 mM working solution was used to prepare 1,800 µL of experimental compound solutions for each compound in PBS containing 1% DMSO and between 3 to 20 µM final concentration of the compound (depending on solubility) in 5 mL glass vials. For example, to prepare a 10 µM solution, 9.0 µL of the 2 mM working solution and 9.0 µL of DMSO were mixed with 1782 µL of PBS and vortexed. For GIT-PAMPA, a membrane solution of 5% lecithin in dodecane was

prepared by dissolving 0.028 g of lecithin in 560 µL of dodecane in a 1.5 mL plastic tube. For BBB-PAMPA, a membrane solution of 2% lecithin in dodecane was prepared by dissolving 0.010 g of porcine polar brain lipid (PBL) in 500 µL of dodecane in a 1.5 mL plastic tube. The membrane solution was vortexed, then 5 µL was added on to the bottom side of the PAMPA filter being careful not to touch the filter with the pipette tip. The membrane was allowed to dry for 25 minutes. The bottom plate was used as the donor plate and 300 µL of the experimental compound solution in PBS containing 1% DMSO (prepared above) or just PBS containing 1% DMSO as the experimental blank solution were added to each well. Experimental compound solutions were tested in quadruplicate while the experimental blank solution was tested only once. The top plate was used as the receiver plate, which was placed into the bottom plate. Then 300 µL of PBS containing 1% DMSO was added into each well. The plate was shaken at 300 rpm for 18 hours. After incubation at r.t., 270 µL was removed from each donor and receiver well and placed into 0.6 mL plastic tubes. For each compound 1400 µL of working spiking solution was prepared in acetonitrile containing 1% DMSO and between 3 to 9 µM final concentration of the compound (depending on the starting concentration of compound added to donor well). For example, to prepare a 6 µM solution, 4.2 µL of the 2 mM working solution and 9.8 µL of DMSO were mixed with 1386 µL of PBS and vortexed. A 5-point standard curve was prepared for HPLC analysis. For each of the five concentrations, 300 µL solutions in 0.6 mL plastic tubes were prepared by adding 200 µL of PBS containing 1% DMSO, and the appropriate amounts of acetonitrile containing 1% DMSO as well as the 200 µM working solution in acetonitrile containing 1% DMSO such that the desired final concentration of compound was achieved in a 300 µL final volume. For example, a 4 µM solution was prepared by mixing 200 µL of PBS containing 1% DMSO, 94.0 µL of acetonitrile containing 1% DMSO, and 6 µL of

200 µM working solution in acetonitrile containing 1% DMSO. Solutions A-E were made according to the solutions table below. To make 300 µL of the HPLC A solution, blank of the blank, 200 µL of PBS containing 1% DMSO and 100 µL of acetonitrile containing 1% DMSO were added to a 0.6 mL plastic tube. To make 300 µL of the HPLC B solution, spiking sample (SS), 200 µL of PBS containing 1% DMSO and 100 µL of 200 µM working spiking solution in acetonitrile containing 1% DMSO were added to a 0.6 mL plastic tube. To make 300 µL of the HPLC C solution, blank, 200 µL of the experimental blank solution from each of the donor and acceptor wells (now in 0.6 mL plastic tubes as described above) and 100 µL of acetonitrile containing 1% DMSO were added to 0.6 mL plastic tubes. To make 300 µL of the HPLC D solution, compound control (C_0), 200 µL of the experimental compound solution in PBS containing 1% DMSO (from the remaining solution that was added to the donor wells) and 100 µL of acetonitrile containing 1% DMSO were added to a 0.6 mL plastic tube. To make 300 µL of the HPLC E solution, compound plus spiking control sample (SSC_0), 200 µL of the experimental compound solution in PBS containing 1% DMSO (from the starting solution that was added to the donor wells) and 100 µL of the working spiking solution in acetonitrile containing 1% DMSO were added to a 0.6 mL plastic tube. To make 300 µL of the HPLC F solution, compound test samples (SSm), 200 µL of the experimental compound solution in PBS containing 1% DMSO (pulled from each of the donor and acceptor wells) and 100 µL of the 200 µM working spiking solution in acetonitrile containing 1% DMSO were added to a 0.6 mL plastic tube. All the above described 300 µL solutions were vortexed and 120 µL was added to HPLC vials with plastic inserts. For each HPLC sample, 30 µL was injected onto the HPLC column in triplicate. Each compound was eluted in a mixture of phosphate buffer and acetonitrile and detected by observing absorbance at the previously determined λ_{max}.

Solutions Table (all volumes in µL)

Solution	PBS + 1% DMSO	MeCN + 1% DMSO	200 µM working solution (MeCN + 1% DMSO)	Elemental Blank (PBS + 1% DMSO)	C_0 (PBS + 1% DMSO)
A	200	100	0	0	0
B	200	0	100	0	0
C	0	100	0	200	0
D	0	100	0	0	200
E	0	0	100	0	200

Section 4: References

(1) Fauci, A. S.; Lane, H. C. Four Decades of HIV/AIDS — Much Accomplished, Much to Do. *N Engl J Med* **2020**, *383* (1), 1–4. https://doi.org/10.1056/NEJMp1916753.

(2) Vermeire, K.; Zhang, Y.; Princen, K.; Hatse, S.; Samala, M. F.; Dey, K.; Choi, H.-J.; Ahn, Y.; Sodoma, A.; Snoeck, R.; Andrei, G.; De Clercq, E.; Bell, T. W.; Schols, D. CADA Inhibits Human Immunodeficiency Virus and Human Herpesvirus 7 Replication by Down-Modulation of the Cellular CD4 Receptor. *Virology* **2002**, *302* (2), 342–353. https://doi.org/10.1006/viro.2002.1624.

(3) Bell, T. W.; Anugu, S.; Bailey, P.; Catalano, V. J.; Dey, K.; Drew, M. G. B.; Duffy, N. H.; Jin, Q.; Samala, M. F.; Sodoma, A.; Welch, W. H.; Schols, D.; Vermeire, K. Synthesis and Structure−Activity Relationship Studies of CD4 Down-Modulating Cyclotriazadisulfonamide (CADA) Analogues. *J. Med. Chem.* **2006**, *49* (4), 1291–1312. https://doi.org/10.1021/jm0582524.

(4) Demillo, V. G.; Goulinet-Mateo, F.; Kim, J.; Schols, D.; Vermeire, K.; Bell, T. W. Unsymmetrical Cyclotriazadisulfonamide (CADA) Compounds as Human CD4 Receptor Down-Modulating Agents. *J. Med. Chem.* **2011**, *54* (16), 5712–5721. https://doi.org/10.1021/jm2002603.

(5) Chawla, R.; Van Puyenbroeck, V.; Pflug, N. C.; Sama, A.; Ali, R.; Schols, D.; Vermeire, K.; Bell, T. W. Tuning Side Arm Electronics in Unsymmetrical Cyclotriazadisulfonamide (CADA) Endoplasmic Reticulum (ER) Translocation Inhibitors to Improve Their Human Cluster of Differentiation 4 (CD4) Receptor Down-Modulating Potencies. *J. Med. Chem.* **2016**, *59* (6), 2633–2647. https://doi.org/10.1021/acs.jmedchem.5b01832.

(6) Vermeire, K.; Bell, T. W.; Van Puyenbroeck, V.; Giraut, A.; Noppen, S.; Liekens, S.; Schols, D.; Hartmann, E.; Kalies, K.-U.; Marsh, M. Signal Peptide-Binding Drug as a Selective Inhibitor of Co-Translational Protein Translocation. *PLoS Biol* **2014**, *12* (12), e1002011. https://doi.org/10.1371/journal.pbio.1002011.

(7) Lumangtad, L. A.; Bell, T. W. The Signal Peptide as a New Target for Drug Design. *Bioorganic & Medicinal Chemistry Letters* **2020**, *30* (10), 127115. https://doi.org/10.1016/j.bmcl.2020.127115.

(8) Hassan, S.; Adam, F.; Abu Bakar, M. R.; Abdul Mudalip, S. K. Evaluation of Solvents' Effect on Solubility, Intermolecular Interaction Energies and Habit of Ascorbic Acid Crystals. *Journal of Saudi Chemical Society* **2019**, *23* (2), 239–248. https://doi.org/10.1016/j.jscs.2018.07.002.

(9) Van Puyenbroeck, V.; Pauwels, E.; Provinciael, B.; Bell, T. W.; Schols, D.; Kalies, K.; Hartmann, E.; Vermeire, K. Preprotein Signature for Full Susceptibility to the Co-translational Translocation Inhibitor Cyclotriazadisulfonamide. *Traffic* **2020**, *21* (2), 250–264. https://doi.org/10.1111/tra.12713.

(10) Brauinger, K. Cryo-EM of Sec61 with CADA, 2017.

(11) Itskanov, S.; Wang, L.; Junne, T.; Sherriff, R.; Xiao, L.; Blanchard, N.; Shi, W. Q.; Forsyth, C.; Hoepfner, D.; Spiess, M.; Park, E. A Common Mechanism of Sec61 Translocon Inhibition by Small Molecules. *Nat Chem Biol* **2023**, *19* (9), 1063–1071. https://doi.org/10.1038/s41589-023-01337-y.

(12) MacKinnon, A. L.; Paavilainen, V. O.; Sharma, A.; Hegde, R. S.; Taunton, J. An Allosteric Sec61 Inhibitor Traps Nascent Transmembrane Helices at the Lateral Gate. *eLife* **2014**, *3*, e01483. https://doi.org/10.7554/eLife.01483.

(13) Junne, T.; Wong, J.; Studer, C.; Aust, T.; Bauer, B. W.; Beibel, M.; Bhullar, B.; Bruccoleri, R.; Eichenberger, J.; Estoppey, D.; Hartmann, N.; Knapp, B.; Krastel, P.; Melin, N.; Oakeley, E. J.; Oberer, L.; Riedl, R.; Roma, G.; Schuierer, S.; Petersen, F.; Tallarico, J. A.; Rapoport, T. A.; Spiess, M.; Hoepfner, D. Decatransin, a New Natural Product Inhibiting Protein Translocation at the Sec61/SecYEG Translocon. *J Cell Sci* **2015**, *128* (6), 1217–1229. https://doi.org/10.1242/jcs.165746.

(14) Paatero, A. O.; Kellosalo, J.; Dunyak, B. M.; Almaliti, J.; Gestwicki, J. E.; Gerwick, W. H.; Taunton, J.; Paavilainen, V. O. Apratoxin Kills Cells by Direct Blockade of the Sec61 Protein Translocation Channel. *Cell Chem Biol* **2016**, *23* (5), 561–566. https://doi.org/10.1016/j.chembiol.2016.04.008.

(15) Baron, L.; Paatero, A. O.; Morel, J.-D.; Impens, F.; Guenin-Macé, L.; Saint-Auret, S.; Blanchard, N.; Dillmann, R.; Niang, F.; Pellegrini, S.; Taunton, J.; Paavilainen, V. O.; Demangel, C. Mycolactone Subverts Immunity by Selectively Blocking the Sec61 Translocon. *J Exp Med* **2016**, *213* (13), 2885–2896. https://doi.org/10.1084/jem.20160662.

(16) Zong, G.; Hu, Z.; O'Keefe, S.; Tranter, D.; Iannotti, M. J.; Baron, L.; Hall, B.; Corfield, K.; Paatero, A. O.; Henderson, M. J.; Roboti, P.; Zhou, J.; Sun, X.; Govindarajan, M.; Rohde, J. M.; Blanchard, N.; Simmonds, R.; Inglese, J.; Du, Y.; Demangel, C.; High, S.; Paavilainen, V. O.; Shi, W. Q. Ipomoeassin F Binds Sec61α to Inhibit Protein Translocation. *J. Am. Chem. Soc.* **2019**, *141* (21), 8450–8461. https://doi.org/10.1021/jacs.8b13506.

(17) Tranter, D.; Paatero, A. O.; Kawaguchi, S.; Kazemi, S.; Serrill, J. D.; Kellosalo, J.; Vogel, W. K.; Richter, U.; Mattos, D. R.; Wan, X.; Thornburg, C. C.; Oishi, S.; McPhail, K. L.; Ishmael, J. E.; Paavilainen, V. O. Coibamide A Targets Sec61 to Prevent Biogenesis of Secretory and Membrane Proteins. *ACS Chem. Biol.* **2020**, *15* (8), 2125–2136. https://doi.org/10.1021/acschembio.0c00325.

(18) Gérard, S. F.; Hall, B. S.; Zaki, A. M.; Corfield, K. A.; Mayerhofer, P. U.; Costa, C.; Whelligan, D. K.; Biggin, P. C.; Simmonds, R. E.; Higgins, M. K. Structure of the Inhibited State of the Sec Translocon. *Molecular Cell* **2020**, *79* (3), 406-415.e7. https://doi.org/10.1016/j.molcel.2020.06.013.

(19) Pauwels, E.; Shewakramani, N. R.; De Wijngaert, B.; Camps, A.; Provinciael, B.; Stroobants, J.; Kalies, K.-U.; Hartmann, E.; Maes, P.; Vermeire, K.; Das, K. Structural Insights into TRAP Association with Ribosome-Sec61 Complex and Translocon Inhibition by a CADA Derivative. *Sci. Adv.* **2023**, *9* (9), eadf0797. https://doi.org/10.1126/sciadv.adf0797.

(20) Rehan, S.; Tranter, D.; Sharp, P. P.; Craven, G. B.; Lowe, E.; Anderl, J. L.; Muchamuel, T.; Abrishami, V.; Kuivanen, S.; Wenzell, N. A.; Jennings, A.; Kalyanaraman, C.; Strandin, T.; Javanainen, M.; Vapalahti, O.; Jacobson, M. P.; McMinn, D.; Kirk, C. J.; Huiskonen, J. T.; Taunton, J.; Paavilainen, V. O. Signal Peptide Mimicry Primes Sec61 for Client-Selective Inhibition. *Nat Chem Biol* **2023**, *19* (9), 1054–1062. https://doi.org/10.1038/s41589-023-01326-1.

(21) Van Puyenbroeck, V.; Claeys, E.; Schols, D.; Bell, T. W.; Vermeire, K. A Proteomic Survey Indicates Sortilin as a Secondary Substrate of the ER Translocation Inhibitor Cyclotriazadisulfonamide (CADA). *Mol Cell Proteomics* **2017**, *16* (2), 157–167. https://doi.org/10.1074/mcp.M116.061051.

(22) Pauwels, E.; Rutz, C.; Provinciael, B.; Stroobants, J.; Schols, D.; Hartmann, E.; Krause, E.; Stephanowitz, H.; Schülein, R.; Vermeire, K. A Proteomic Study on the Membrane

Protein Fraction of T Cells Confirms High Substrate Selectivity for the ER Translocation Inhibitor Cyclotriazadisulfonamide. *Molecular & Cellular Proteomics* **2021**, *20*, 100144. https://doi.org/10.1016/j.mcpro.2021.100144.

(23) Ji, Y.-Z.; Li, H.-J.; Zhang, J.-Y.; Wu, Y.-C. Switchable Regioselection of C–H Thiolation of Indoles Using Different TMS Counterions. *Chem. Commun.* **2019**, *55* (79), 11864–11867. https://doi.org/10.1039/C9CC05652A.

(24) Ali, R. Synthesis and CD4 Down-Modulation Potencies of CADA Head Analogs, 2015.

(25) Pleuvry, B. J. Factors Affecting Drug Absorption and Distribution. *Anaesthesia & Intensive Care Medicine* **2005**, *6* (4), 135–138. https://doi.org/10.1383/anes.6.4.135.63632.

(26) Di, L.; Kerns, E. H. Profiling Drug-like Properties in Discovery Research. *Current Opinion in Chemical Biology* **2003**, *7* (3), 402–408. https://doi.org/10.1016/S1367-5931(03)00055-3.

(27) Dehring, K. A.; Workman, H. L.; Miller, K. D.; Mandagere, A.; Poole, S. K. Automated Robotic Liquid Handling/Laser-Based Nephelometry System for High Throughput Measurement of Kinetic Aqueous Solubility. *Journal of Pharmaceutical and Biomedical Analysis* **2004**, *36* (3), 447–456. https://doi.org/10.1016/j.jpba.2004.07.022.

(28) Rácz, A.; Vincze, A.; Volk, B.; Balogh, G. T. Extending the Limitations in the Prediction of PAMPA Permeability with Machine Learning Algorithms. *European Journal of Pharmaceutical Sciences* **2023**, *188*, 106514. https://doi.org/10.1016/j.ejps.2023.106514.

(29) Volpe, D. A. Application of Method Suitability for Drug Permeability Classification. *AAPS J* **2010**, *12* (4), 670–678. https://doi.org/10.1208/s12248-010-9227-8.

(30) Binisti, C.; Assogba, L.; Touboul, E.; Mounier, C.; Huet, J.; Ombetta, J. E.; Dong, C. Z.; Redeuilh, C.; Heymans, F.; Godfroid, J. J. Structure-Activity Relationships in Platelet-Activating Factor (PAF). 11-From PAF-Antagonism to Phospholipase A(2) Inhibition: Syntheses and Structure-Activity Relationships in 1-Arylsulfamido-2-Alkylpiperazines. *Eur J Med Chem* **2001**, *36* (10), 809–828. https://doi.org/10.1016/s0223-5234(01)01274-0.

(31) Buhr, W. Novel Sulfonaminoquinoline Hepcidin Antagonists, 2012.

(32) Le, T. Synthesis of Sulfonamides Towards Down-Modulation of CD4, Gp160, and TSHR, 2019.

Chapter 3: Determining TL020 anti-HBV Target Protein

Section 1: Introduction

In 2019 the World Health Organization (WHO) reported that an estimated 296 million people were living with chronic hepatitis B virus (HBV) infection. They further estimated that this would result in 820,000 deaths per year mainly due to liver cirrhosis and hepatocellular carcinoma (HCC). In the US and elsewhere, several stigmas exist for people chronically infected with HBV partly because it is spread by sex and injection drug use. However; it can also be spread by saliva and is often spread amongst infants in a child care setting or amongst households by normal and mundane contact. Additionally, perinatal transmission (from mother to baby) accounts for 13-26% of the global chronically infected population. Exposure to HBV can result in either an acute or chronic, and age is a strong risk factor in the development of chronic infection. A chronic infection will occur 90% of the time for newborns, 25-50% of the time for children ages 1-5, and just 5-10% of the time in teenagers and adults.[1] There is an effective vaccine against HBV and globally its implementation has reduced chronic infection from 4.7% to 1.3% in children under 5 years old. While the global vaccination coverage was estimated to be 84% in 2016, this does not relieve the burden for those 296 million already chronically infected people.[2]

The current FDA approved therapeutics for treatment of HBV are pegylated interferon alpha (PEG-IFN α) and nucleos(t)ide analogues (NAs). The mechanism of PEG-IFN α is complex; it relies on stimulation of the immune system to degrade viral mRNA, inhibit protein synthesis and HBV replication, and prevent infection of new cells. It may also stimulate clearance of infected cells. The mechanism of NAs is much more straightforward; they work by competitive inhibition of HBV polymerase (pol) which prevents synthesis of viral DNA. A

benefit of PEG-IFN α over NAs is increased rates of HBeAg and HBsAg seroconversion (disappearance of the antigen and appearance of antigen specific antibodies in serum) leading to immune-mediated clearance and a finite course of treatment. Unfortunately, the use of PEG-IFN α has been limited due to severe side effects, contraindications for pregnant or decompensated cirrhosis patients, and low adherence due to the drug delivery method (subcutaneous injection). NAs have gone through several generations of development, and the newer generation are very effective, have mild side effects, can be administered orally, and have a high barrier to resistance. While they are preferred over PEG-IFN α, the rates of seroconversion are low and the course of treatment is indefinite. Due to the general failure of NAs to lead to a sustained response there are currently many new HBV drugs in the development. These include viral entry inhibitors, RNAi, HBsAg release inhibitors, immunotherapy approaches, capsid assembly modulators, cccDNA inhibitors, and vaccines.[3] It is clear that a new approach is needed and that understanding the viral life cycle will be useful for discovering a new approaches for treatment.

The HBV genome is a partially double stranded relaxed circular DNA (rcDNA) molecule that is very efficiently organized due to its diminutive size of just 3.2 kB which is on the extreme low end in terms of the size of viral genomes. The genome contains only 4 genes producing 5 unique RNA transcripts and 7 different proteins. The pregenomic RNA (pgRNA) is a full length transcript of the viral genome and drives synthesis of both the core protein (Cp) and pol.[4] While the pgRNA 5' UTR directs the synthesis of multiple copies of Cp, an alternative AUG start codon can be recognized by either leaky scanning or backward scanning to direct the synthesis of a single pol which will remain covalently attached to the pgRNA after synthesis.[5,6] The pgRNA also has an encapsidating signal (epsilon), which along with the covalently bound pol directs packaging of a single pgRNA-pol complex into a viral icosahedral capsid consisting of 90 (T=3)

or more typically 120 (T=4) Cp homodimers.[7] Pol contains a terminal protein (TP) domain (which serves as the primer for negative-strand DNA synthesis), a spacer domain, a reverse transcriptase (RT) domain (capable of both RNA and DNA dependent DNA polymerization), and an RNase H domain (which degrades the pgRNA after negative-strand DNA synthesis). The RT enzyme becomes active only after packaging into the capsid and uses the pgRNA as a template for negative-strand DNA synthesis. The negative-strand then becomes a template for the partial synthesis of the positive-strand DNA, creating the rcDNA viral genome.[4]

Capsids containing rcDNA can be transported from the cytosol to the nucleus where the rcDNA is converted to covalently closed circular DNA (cccDNA), which functions like a minichromosome and is structurally similar to euchromatin (transcriptionally active chromosomal DNA). It is packed with the same cellular proteins that constitute euchromatin in cellular DNA along with the viral X (HBx) and Cp proteins. This long lived and stable cccDNA is largely the reason current antivirals fail to clear the virus from cells during chronic HBV infection.[8] Additionally, viral DNA in the nucleus may be integrated into the host cell genome by processes mediated by cellular proteins. About 10% of the time during formation of rcDNA, an error in the standard process leads to the creation of double stranded linear DNA (dslDNA). This is the form of viral DNA which most commonly gets integrated into the host genome.[5] Integration is a rather rare occurrence at the cellular level and only 0.1-0.01% of hepatocytes show evidence of integration during transient transfections. However, during the course of a chronic infection it becomes more or less a guarantee and can drive progression to hepatocellular carcinoma (HCC).[5] While eradication of integrated viral DNA is not currently a feasible option, it is fortunate that the integrated DNA does not remain fully functional and is typically only capable of expressing HBV surface (HBs or S) proteins.[4]

Alternatively, capsids containing rcDNA can become enveloped by a membrane rich in HBs and be exported from the cell as infectious particles (Dane particles).[4] There is a nested set of three different HBs are distinguished by length, all sharing a common C-terminal S domain. The small S protein (SHBs) consists solely of the S domain. The medium S protein (MHBs) has an additional pre-S2 domain. The large S protein (LHBs) contains the S, pre-S2, and an additional pre-S1 domain.[9] The proteins are integrated into the ER membrane as integral transmembrane proteins and help envelope the viral capsid, and are involved in the export of viral particles from the cell. The pre-S1 domain of LHB is also responsible for interaction with the viral entry receptor, sodium taurocholate cotransporting polypeptide (NTCP).[10] Additionally, HBs proteins can form empty membranous vesicles called subviral particles (SVPs) which are excreted from the cell in excess of 10,000- to 100,000-fold above the infectious Dane particles. The S protein constitutes the HBV surface antigen (HBsAg) that is recognized by human immune system antibodies for neutralization and destruction. This high rate of SVP secretion serves as a decoy for the infectious Dane particles, helping them avoid immune detection as well as leading to a state known as immune exhaustion. This state of immune exhaustion, is characterized by poor functioning of antigen specific T-cells and HBsAg-specific memory B cells which no longer produce antibodies.[9] This is characteristic of a chronic HBV infection and a functional cure is defined by a HBsAg negative phase with persistently low levels of HBV DNA. A functional cure is distinct from a complete sterilizing cure which would include complete eradication viral DNA, including the cccDNA and any integrated HBV DNA. Elimination of integrated HBV DNA is not currently feasible; therefore, a partial cure has been defined as detectable HBsAg (expressed from integrated HBV DNA) with persistently undetectable serum levels of HBV DNA after stopping treatment.[11]

The only HBV protein not yet discussed is the pre-core protein. The pre-core RNA is identical with the pgRNA except that it includes a short 5' extension. The pre-core protein and Cp share the majority of their sequence, except for a short 30 amino acid N-terminal extension in the pre-core protein which includes a SP, 19 amino acids in length. The SP directs passage of pre-core into the ER via the Sec61 channel, and is then removed by the cellular SPase. The pre-core protein is further processed by cleavage at the C-terminus before being secreted from the cell as the hepatitis B e antigen (HBeAg).[8] It was found that the pre-core protein lacking a signal peptide localized to the cytoplasm and formed hybrid viral capsids with Cp that were devoid of pgRNA. This had a strong inhibitory effect on viral replication by sequestering Cp into inactive hybrid capsids.[12] It is feasible that a CADA compound could prevents translocation of the pre-core protein, routing it to the cytosol where it could form hybrid viral capsids that reduce viral replication. Because the nucleotides encoding the pre-core N-terminus overlap with the pgRNA packaging signal, the N-terminal region is highly conserved amongst the *Hepadnaviradae* family of viruses which causes similar disease across a variety of host organisms.[13] Targeting the pre-core SP by a CADA analogue would be a strong and novel strategy, effective against all HBV genotypes, that minimizes the chance of viral escape due to mutation.

While so far the discussion has focused on viral proteins, this is a great oversimplification as the virus relies on a large number of host proteins for completion of its life cycle. Entry of the virus requires interaction with cell surface proteins heparan sulfate proteoglycan (HSPG), glypican-5 (GPC5), and the already mentioned NTCP. Entry typically occurs via clathrin-dependent endocytosis, followed by Rab5/7 dependent transport along to the late endosomal compartment where de-envelopment occurs, likely involving caveolin-1. The capsid contains a NLS which is recognized by soluble factors and triggers transport along tubulin microtubules to

the nucleus where importin α and β transport the capsid through the nuclear pore complex (NPC). Once in the nucleus the capsid disassembles and the rcDNA is released. The rcDNA is converted to cccDNA by a complex and not fully understood, which is process mediated by host cell proteins. The conversion cccDNA involves removal of the covalently attached pol by tyrosyl-DNA-phosphodiesterases (deproteination), removal of a short terminal redundant sequence and an RNA primer by endonucleases, filling of gaps in both the plus and minus HBV DNA strands by DNA polymerase κ, ligation by DNA ligase 1 or 3, and supercoiling by topoisomerase 1 or 2. Additionally, dslDNA can be converted to cccDNA in a process involving other proteins such as Ku80, ligase 4, and components of the NHEJ DNA repair pathway. The NHEJ DNA repair pathway can also result in integration of dslDNA into the host chromosome. The cccDNA is complexed with cellular histone and non-histone proteins and viral Cp and X proteins to make a minichromosome. Epigenetic modifications, transcription factors, and RNA pol II mediate synthesis of the viral transcripts which can be alternatively spliced leading to further complexity of viral products that are not well understood, characterized, or even known. The transcripts are then exported to the cytosol for translation which occurs via the ribosomes along with all the other accessories proteins involved.[6]

The C-terminal domain of Cp is regulated by a series of phosphorylation and dephosphorylation events to promote pgRNA encapsidation, capsid maturation, envelopment, and egress. The mechanistic steps are not fully understood, but several kinases such as PKC-α and SRPK1 are known to be involved. The chaperone Hsp90 helps to stabilize the capsid while Hsp40 destabilizes the capsid. Together these proteins help regulate proper capsid assembly. Hsp90 and other cofactors assists in the folding of pol. Reverse transcription of pgRNA in the capsid is assisted by several host proteins including eIF4E, DDX3, and APOBEC3G. The three

HBs and the pre-core proteins are expressed at the ER membrane, pass through the Sec61 channel, and are processed and folded by multiple ER lumenal proteins.[6] The pre-core protein SP is cleaved by SPase, leaving a 10 amino acid N-terminal extension compared to Cp. The protein is sent for export through the secretory pathway, andd the C-terminus has multiple cleavage sites that can be recognized by endopeptidases such as furin to create a variety of different products although the functional significance of these alternative processing events is not well understood.[14] The HBs proteins all share a common N-glycosylation site and the MHBs has an additional N-glycosylation site as well as an O-glycosylation site. The glycans are further processed by processing enzymes and folding is assisted by chaperones such as Hsp70, BiP and calnexin. Protein disulfide isomerase (PDI) is important for correct formation of disulfide linkages important for assembly of the viral envelope. Maturation and egress rely on host proteins involved in many different cellular processes, such as the multi vesicular body (MVB) machinery (DN ESCRT III, Vps4A/B, λ-2 adaptin, and NEDD4). Autophagy is induced by HBs and X proteins and autophagy proteins LC3 and Rab7 have been shown to be required for HBV replication. Lastly, HMG CoA reductase influences production of the lipids and sterols that are necessary for secretion.[6] While the host cell uses all these proteins and process for its own purposes, the host cell is able to compensate for loss of function due to its large genome which contains some built in redundancy and alternative pathways. It is therefore possible to target some of these host proteins which will have serious consequences for the viral life cycle while producing less severe consequence in the host cell. While the consequences to the cell and overall the person are a major concern for this approach, an advantage is that it limits the possibility of viral escape mutants. Furthermore, if a sustained response can be achieved these negative consequences will be temporary. Various strategies for targeting host cell proteins are

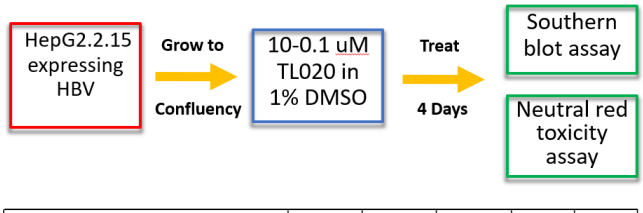

Assay (μM)	EC_{50}	EC_{90}	CC_{50}	SI_{50}	SI_{90}
Primary, DNA (virion)	0.49	1.2	38	78	32
Secondary, DNA (virion)	0.63	1.6	53	84	33
Secondary, DNA (cellular)	1.2	5.9	53	44	9.0

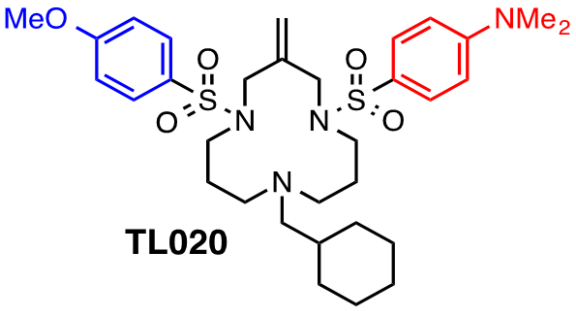

Figure 3.1: Anti-HBV activity of TL020. The assay outline is shown in the upper left portion with the results reported below. The primary assay only screened for the excretion of HBV virions in the media, while the secondary assay retested the excretion of HBV virions and additionally tested for the presence of intracellular HBV DNA. The structure of TL020 is shown on the right side.

common and may prove to be vital for achieving a sustained response to treatment that is thus far lacking.[6,15]

The CADA analogue, TL020, was tested for activity against HBV in the laboratory of Dr. Brent Korba as part of an NIH funded screening program for the discovery of therapeutics for the treatment of HBV (**Fig. 3.1**). The assay implemented HepG2.2.15 cells which have two fully functional HBV dslDNA fragments integrated into the X chromosome of the HepG2 parental cell line.[16] To quantify and compare the activity of compounds medicinal chemist often use EC_{50}s, which are determined experimentally by testing the activity of a compound at multiple concentrations and producing a dose response curve. A non-linear regression can be used to calculate the effective concentration that produces 50% of the desired effect. A relative EC_{50} corresponds to the inflection point in the graph (the point half-way between the two plateaus or half of the maximal observed effect). An absolute EC_{50} corresponds the to the point that represents 50% of the control (**Fig. 3.2**). Similarly, the concentration that kills 50% of the cells is called the CC_{50}.[17] By determining the absolute EC_{50} and CC_{50} values, TL020 was identified as a potent anti-HBV compound with a CC_{50} observed at a concentration two orders of magnitude lower the EC_{50}. The average EC_{50} for reduction of secreted virion in HepG2.2.15 cells was 0.56

µM (n=2), while the average CC_{50} for reduction of cellular viability was 46 µM (n=2). Interestingly, TL020 less potently reduced intracellular HBV DNA with a CC_{50} of 1.2 µM (n=1). The parental HepG2 cell line does not express the NTCP entry receptor. As such HepG2.2.15 cells serve as a model for monitoring HBV replication, but not for cellular entry and infection.[10] Because HBV DNA replication occurs independently of envelopment and secretion, and the assay detected a strong reduction in intracellular levels of HBV DNA, it is clear that the inhibitory affect is occurring at the steps in the HBV life-cycle between mRNA transcription and rcDNA synthesis. Owing to the mechanism of action of TL020, it is likely that the reduction in intracellular HBV DNA is not related to processes that occur in the nucleus (transcription, or mRNA processing and export), and it is more likely related to processes that occur at or proximal to the ER membrane. While it is possible that the activity of TL020 may be due to a direct interaction with a viral protein and in particular the SP containing Pre-core protein, strictly looking at the numbers of host proteins needing during replication indicates that disturbance of host cell proteins may be a more likely explanation for the inhibition of HBV replication.

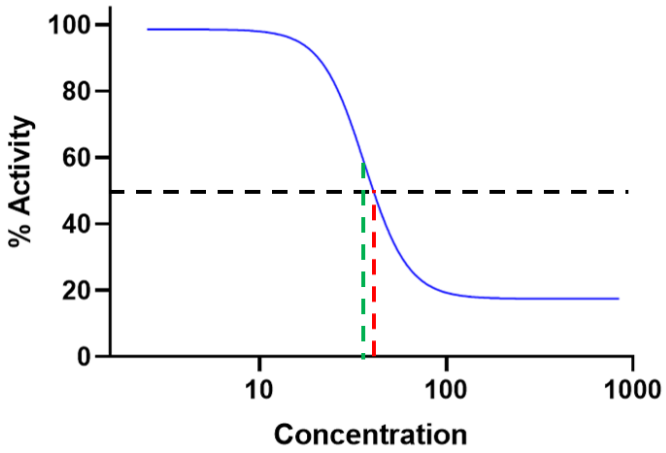

Figure 3.2: Absolute and relative CC_{50}s. An example dose response curve (blue line) is shown to demonstrate the difference between the absolute (red dotted lines) CC_{50} which is determined by where the dose response curve crosses the line for 50% acitivity (black dotted line) and relative (green dotted lines) CC_{50} which is determined by the inflection point in the dose response curve.

Section 2: Results and Discussion

2.1 Effects on Protein Levels

Determining the effect of TL020 on the expression of HepG2 host cell proteins could provide valuable information for finding a possible mechanism for inhibition of HBV replication as well as for understanding the specificity and cellular consequences of TL020 treatment. It was determined to use LC-MS/MS to compare protein expression patterns of TL020 treated cells with non-treated cells. Before beginning the LC-MS/MS experiments we wanted to look at the effect of TL020 treatment on HepG2 cell viability. This also gave a better understanding of which assay parameters, such as cell seeding density, dosage, and treatment time, to use in the LC-MS/MS experiment. Because the eventual goal was proteomics analysis, serum-free media was used during treatment to reduce the introduction of non-cellular proteins making for more reliable analysis.

The effect on cellular viability of TL020 treatment was determined at various timepoints using CellQuanti-Blue reagent. CellQuanti-Blue reagent is a non-fluorescent dye that when reduced by metabolically active cells is converted to a fluorescent product. Cells were grown in 96-well plates and incubated for either 24, 48, or 72 hours with increasing concentrations of TL020 in serum-free media containing 1% DMSO. The negative control wells were treated with serum-free media containing 1% DMSO or serum-free media without DMSO. Before addition of the CellQuanti-Blue reagent the cell density was observed under an inverted brightfield microscope to estimate cell density. The fluorescent results were consistent with brightfield observations in that the wells which were observed to have a higher density produced higher fluorescent intensities. Cell viability was affected at high TL020 concentrations and this was more severe with longer treatment periods. These results largely match with those from previous

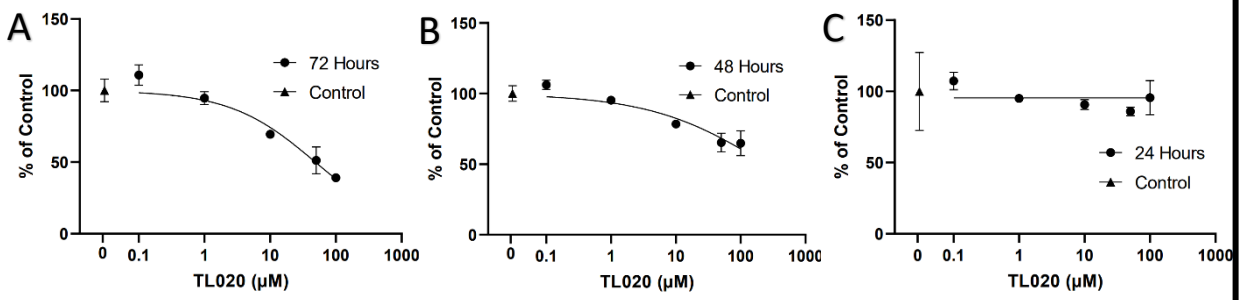

Figure 3.3: Dose response for TL020 on HepG2 cells. Cells were treated for 72 h (A), 48 h (B), or 24 h (C) with varying concentrations of TL020. Fluorescence was measured using an excitation of 544 nm and an emission of 590 nm. The average signal from wells without cells (background) was subtracted from all other wells. The data was normalized to wells with cells treated with serum-free media containing 1% DMSO. The data was fit to nonlinear regression four parameter curve. Error bars show the standard deviation.

experiments. For a 72-hour treatment period a CC_{50} of 48.6 µM (35.1-69.7 µM with 95% confidence) was calculated from these results (**Fig. 3.3**). The results from Dr. Korba's lab using a 96-hour treatment period gave a CC_{50} ranging from 38-53 µM. A seeding density of $1.25*10^4$ cells per well in a 96-well plate ($3.91*10^4$ cells/cm^2) produced ~80% confluent cultures as determined by microscopy after 72 hours (a 24-hour incubation with media supplemented with 10% fetal bovine serum (FBS) after seeding followed by a 48-hour incubation with serum-free media containing 1% DMSO). Increasing the serum-free media incubation to 72 hours produced fully confluent yet still metabolically healthy cultures.

Another check before doing the LC-MS/MS experiment, was to determine whether the conditions used would produce notable changes in protein expression levels after treatment by using SDS-PAGE. Based on the CC_{50} of 48.6 µM an EC_{50} of 0.56 µM of it was determined to use a 20 µM TL020 concentration to keep cells healthy yet insure a strong effect on protein expression levels. Cells were plated in 12-well plates at $2.50*10^5$ cells per well ($7.14*10^4$ cells/cm^2) incubated with the 20 µM TL020 for 72 hours before collecting both the media and lysate fractions. The protein concentration was determined by using a bicinchoninic acid (BCA) assay and then 5 µg samples were loaded into a 10% polyacrylamide, non-reducing gel for SDS-

PAGE analysis. The gel revealed two distinct bands greater than 250 kDa in size that were no longer detected in the media and significantly reduced in the lysates upon treatment with TL020 (**Fig. 3.4**). This gave us confidence that the treatment conditions were sufficient to produce significant effects on protein expression levels in HepG2 cells. However, there was some concern that the treatment period may be too long, because the cultures were fully confluent. Additionally, a literature review revealed that HepG2 cells protein secretion peaked after 16 h in serum-free media, at which point the secreted proteins began to degrade.[18] For the production of samples for LC-MS/MS, the treatment period was reduced to 48 hours for collection of cell lysates and to 16 hours for collection of proteins secreted into the media. Prior to submission of samples to UNR proteomics center, the 16-hour media samples were checked for changes in protein production via SDS-PAGE once more (**Fig. 3.5**). This confirmed the loss of a large protein band greater than 250 kDa in size upon TL020 treatment after just 16 hours.

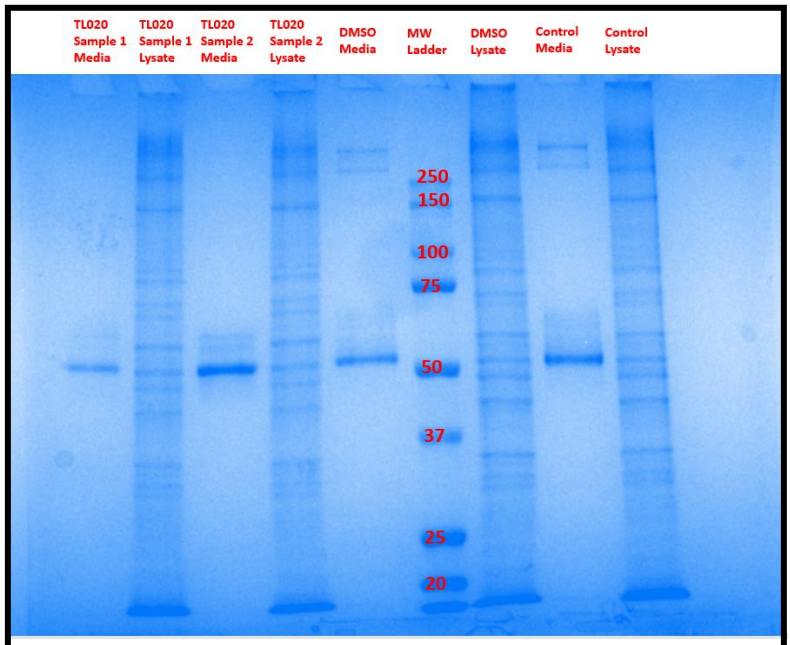

Figure 3.4: SDS gel for HepG2 cell treatment. Lysate samples were loaded at 5 µg per well. Media samples could not be quantified before loading. Labels on ladder indicate approximate size in kDa.

The analysis of the LC-MS/MS results was done by the UNR bioinformatics center, using the first two principal components to determine differential protein expression. Using a threshold of 0.6-fold change and a p-value of 0.01, revealed 132 differentially expressed proteins in the

media samples. Of these differentially expressed proteins 120 (90.9%) showed reduced levels. This strong preference for reduced protein levels over increased protein levels is consistent with the down-modulatory mechanism of CADA analogues. Of these proteins with reduced expressions levels, 35 (29.2%) had SPs. Being as only about 10% of the human proteome is predicted to contain SPs this shows a strong enrichment for reduction of proteins containing SPs which is also consistent with an SP-dependent mechanism of down-regulation being at play.[19]

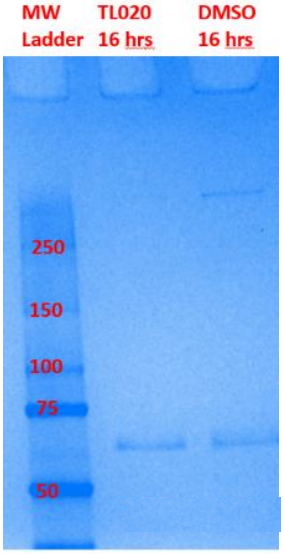

Figure 3.5: SDS gel for shortened treatment. Media samples after 16 h. treatment time. Labels on ladder indicate approximate size in kDa.

While analysis of the media sample showed some interesting results, many of proteins detected as differentially expressed where likely false positives. For example, two proteins involved in glycosaminoglycan biosynthesis of HSPG and two proteins involved in autophagy had reduced levels after TL020 treatment. Down-regulation of these proteins would have negative effects on viral attachment to the cell surface and HBV DNA replication, respectively.[6,20] The problem is that these proteins do not have SPs and are not known to be secreted according to the UniProt database. Furthermore, these were not shown to be significantly differentially expressed in the cell lysate samples. As such the list was further reduced to those which were annotated as being secreted in UniProt. Two proteins with functions consistent with secretion and one protein which didn't have an annotation for subcellular location were also included in the list. This reduced the list of potential TL020 targeted proteins found in the media samples to 26 (**Table 3.1**). While it is not highly likely that secreted proteins could affect intracellular HBV DNA replication in

Table 3.1: Down-modulated secreted proteins. 26 proteins with SPs and predicted to be secreted were down-modulated using threshold of 0.6-fold change and a p-value of 0.01.

Protein Name	UniProt ID	% Difference
Hyaluronidase-1	Q12794	-98.69
Ectonucleotide pyrophosphatase/phosphodiesterase family member 2	Q13822	-97.61
Tissue factor pathway inhibitor	P10646	-97.37
von Willebrand factor A domain-containing protein 1	Q6PCB0	-96.94
Prothrombin	P00734	-94.39
Vitamin K-dependent protein C	P04070	-94.39
Carboxypeptidase E	P16870	-94.08
Serine protease inhibitor Kazal-type 1	P00995	-93.76
Coagulation factor X	P00742	-93.73
Matrilin-3	O15232	-92.49
Transforming growth factor-beta-induced protein ig-h3	Q15582	-89.90
Palmitoleoyl-protein carboxylesterase NOTUM	Q6P988	-89.06
Neuropilin-1	O14786	-88.92
Apolipoprotein C-III	P02656	-87.99
APOC1	P02654	-87.91
Reelin	P78509	-87.03
Collagen alpha-1(VII) chain	Q02388	-85.85
Biotinidase	P43251	-85.42
Gelsolin	P06396	-83.49
Cadherin-1	P12830	-79.98
Transthyretin	P02766	-78.95
Gastricsin	P20142	-78.47
Coagulation factor V	P12259	-75.80
Syndecan-1	P18827	-66.72
Carboxypeptidase B2	Q96IY4	-65.03
Oxidoreductase NAD-binding domain-containing protein 1	Q96HP4	-64.31

HepG2.2.15 cells, reviewing this list revealed some interesting targets. Cadherin-1 (also called E-cadherin) is involved in glycosylation of NTCP and has been shown to effect viral entry.[21] Additionally, syndecan-1 is a glycoprotein which bears heparan sulfate and could aid in cell surface attachment of the virus.[22] As mentioned previously, HepG2.2.15 cells don't express the

NTCP entry receptor or allow for viral reinfection; however, these could be valuable targets that increases the *in vitro* effectiveness of TL020.

Being as the reduction of intracellular HBV DNA levels would be expected to be the result of changes in intracellular and not excreted proteins, further analysis was restricted to the lysate samples. Looking at the cell lysate sample revealed a large set of 385 differentially expressed proteins with greater than 0.6-fold change and a p-value less than 0.01. Using Kyoto Encyclopedia of Genes and Genomes (KEGG) pathway analysis revealed the two most disturbed pathways were ECM-receptor interaction and protein processing in the ER. This is not at

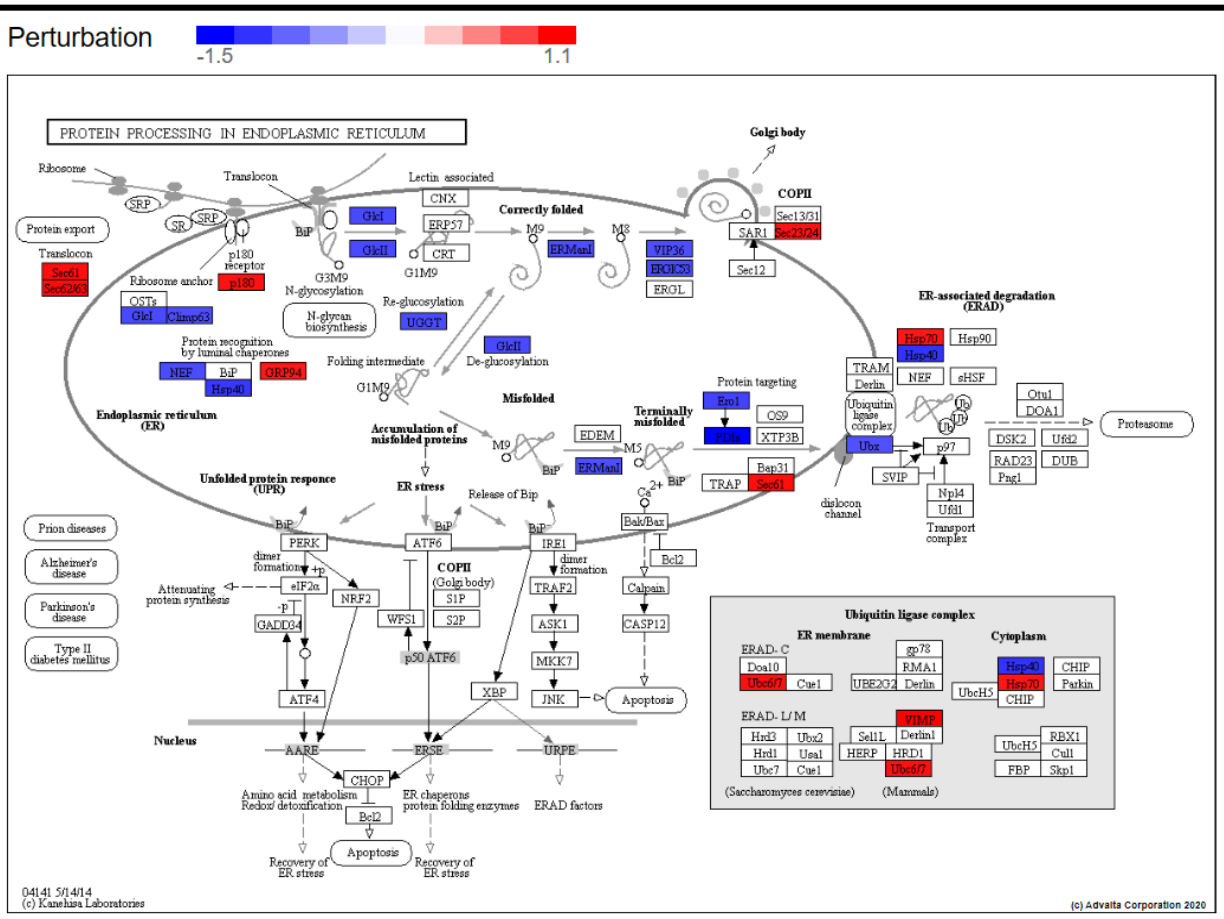

Figure 3.6: Differentially expressed in the ER. 29 proteins (often part of the same complex as shown in the image) involved in protein processing in the ER were differentially expressed using threshold of 0.6-fold change and a p-value of 0.01. Red indicates a positive fold-change (FC) and blue indicates a negative FC.

surprising based on the fact that CADA analogues have previously been shown to disrupt expression of several cell-surface receptors and the site of action is the Sec61 channel in the ER membrane. A total of 29 proteins involved in protein processing in the ER were differentially regulated; 10 of which had increased expression levels and 19 of which had reduced expression levels (**Fig. 3.6**).

Of the proteins with increased expression levels (**Table 3.2**) were Sec61α and Sec63, likely an indication of channel malfunctioning. Three proteins involved in the ERAD pathway were also upregulated, VIMP, Ube2j1, and the Hsp90 family chaperone GRP94. VIMP helps to transfer misfolded proteins from the ER to the cytosol.[23] Ube2j1 attaches ubiquitin to misfolded proteins, marking them for degradation.[24] GRP94 appears to play a regulatory role in assembly of protein complexes involved in ERAD.[25] The ER membrane receptor, p180 (also upregulated), has been shown to bind poly(A) tails of particular mRNAs in order to localize them to the ER in an SP and translation independent mechanism. Upregulation of p180 may be the result of mRNAs destined to the ER membrane accumulating in the cytosol due to a blockage of the Sec61 channel.[26] Three Hsp70 family chaperones Hsp70-1, Hsp70-1t, and Hsp70-6 were found to be upregulated; Hsp70-1 and Hsp70-6 are stress-inducible so this to be expected with CADA analogues. Furthermore, Hsp70-2 differs from Hsp70-1 by only 2 amino acids and it is likely that

Table 3.2: Up-modulated in the ER. 10 proteins involved in protein processing in the ER were up-modulated using threshold of 0.6-fold change and a p-value of 0.01.

Protein Name	Alternative Name	Uniprot ID	% Difference	P-Value
Selenoprotein S	VIMP	Q9BQE4	412.25	3.62E-03
Translocation protein SEC63 homolog	Sec63	Q9UGP8	222.08	7.71E-03
Protein transport protein Sec61 subunit alpha isoform 1	Sec61α	P61619	207.10	7.40E-05
Ribosome-binding protein 1	p180	Q9P2E9	127.57	1.58E-03
Protein transport protein Sec24D	Sec24D	O94855	97.90	3.59E-03
Ubiquitin-conjugating enzyme E2 J1	Ube2j1	Q9Y385	97.45	6.93E-03
Heat shock 70 kDa protein 1A	Hsp70-2	P0DMV8	57.98	4.81E-04
Heat shock 70 kDa protein 6	Hsp70-6	P17066	34.30	9.69E-03
Heat shock 70 kDa protein 1-like	Hsp70-1t	P34931	33.42	2.60E-03
Endoplasmin	GRP94	P14625	24.40	8.12E-03

Hsp70-2 which is also stress-inducible was upregulated as well, but reliable distinction of these almost identical proteins requires a more sophisticated approach. Typically, these two proteins are simply called Hsp70 and not distinguished as separate proteins.[27] It was mentioned previously that Hsp70 is implicated in proper folding of viral HBs proteins. Additionally, Hsp70 and Hsp90 synergistically function to aid the assembly of viral Cp into capsids.[28] The upregulation of Hsp70 would be beneficial to HBV replication in the absence of other negative perturbations. While these Hsp70s are stress-inducible, an initially surprising observation is the lack of upregulated proteins involved in both ER stress and the UPR. However, these pathways are initiated within the ER lumen, and TL020 blocks protein translocation into the ER lumen so it is reasonable that TL020 avoids activation of these pathways. Eight proteins involved in the apoptosis pathway were differentially expressed, but five of the eight were actually down-modulated indicating that apoptosis had not been induced to any major extent across the population of cells.

Of greatest interest was the discovery that the protein transport protein Sec24D was upregulated. This protein is part of the coat protein complex II (COPII) which forms protein transport vesicles which bud out from the ER and proceeds to the Golgi complex.[29] Importantly, it appears that upregulation of Sec24D could be at least partially responsible for the anti-HBV activity of TL020. Previous research showed enhanced Sec24D expression significantly reduced HBV DNA and that siRNA knockout had the opposite effect. The authors speculated that this was linked to increasing amounts of saturated fatty acids, which was shown to inhibit viral replication.[30,31]

Looking at the down-modulated proteins there were many proteins that could have an effect on the HBV life cycle (**Table 3.3**). Quite interesting are the four DnaJ/Hsp40 chaperones (DnaJC3, DnaJC10, DnaJB11, and DnaJB12) that were downregulated. There are 41 DnaJ proteins in humans that use their J domain to bind to Hsp70 chaperones, stimulate Hsp70 ATPase activity, and stabilize the interaction between Hsp70s and their substrates.[32] DnaJC3, DnaJC10, and DnaJB11 are all co-chaperones for the ER lumenal chaperone BiP.[32,33] Furthermore Bap, the nucleotide exchange factor necessary for the activity of BiP, was downregulated.[34] DnaJC3 is normally upregulated during ER stress and works to restart translation at the end of a period of ER stress by interaction with the translation inhibitor PERK.[35] Of greater interest is the fact that DnaJC3 is known to target proteins for degradation in a co-translational manner during ER stress.[35] A previous proteomics study using T-lymphoid SUP-T1 cells found DnaJC3 to be down-modulated by CADA.[36] A follow-up study to this found it was likely that DnaJC3 was helping to remove proteins stalled in Sec61 by the action of

Table 3.3: Down-modulated in the ER. 19 proteins involved in protein processing in the ER were down-modulated using threshold of 0.6-fold change and a p-value of 0.01.

Protein Name	Alternative Name	Uniprot ID	% Difference	P-Value
DnaJ homolog subfamily C member 3	DnaJC3 or ERdj6	Q13217	-90.05	2.09E-04
DnaJ homolog subfamily B member 12	DnaJB12	Q9NXW2	-88.17	7.82E-03
ERO1-like protein beta	ERO1-Lα	Q86YB8	-74.95	8.27E-03
ERO1-like protein alpha	ERO1-Lβ	Q96HE7	-71.74	2.86E-03
Neutral alpha-glucosidase AB	α-glucosidase II	Q14697	-65.09	1.64E-04
Mannosyl-oligosaccharide glucosidase	α-glucosidase I	Q13724	-62.04	4.49E-04
Protein disulfide-isomerase	PDI	P07237	-60.34	4.19E-03
Glucosidase 2 subunit beta	β-glucosidase II	P14314	-58.90	2.35E-03
UDP-glucose:glycoprotein glucosyltransferase 1	UGT1	Q9NYU2	-52.19	1.04E-03
DnaJ homolog subfamily C member 10	DnaJC10 or ERdj5	Q8IXB1	-51.68	1.33E-03
Protein ERGIC-53	ERGIC53	P49257	-51.44	2.29E-03
Protein disulfide-isomerase A4	ERp70	P13667	-46.09	4.87E-03
Nucleotide exchange factor SIL1	Bap	Q9H173	-45.52	3.12E-03
DnaJ homolog subfamily B member 11	DnaJB11 or ERdj3	Q9UBS4	-42.84	6.05E-03
Thioredoxin domain-containing protein 5	ERp46	Q8NBS9	-41.54	6.08E-03
Vesicular integral-membrane protein VIP36	VIP36	Q12907	-40.67	2.54E-03
Cytoskeleton-associated protein 4	CKAP4 or ERGIC63	Q07065	-38.65	7.98E-04
Mannosyl-oligosaccharide 1,2-alpha-mannosidase IA	1,2-α-mannosidase IA	P33908	-38.06	2.28E-03
NSFL1 cofactor p47	p47	Q9UNZ2	-19.86	1.68E-04

CADA. The authors showed that the reduced DnaJC3 levels in the presence of CADA was able to rescue some of the stalled substrates and speculated that this could be because giving the SPs more time in the Sec61 channel gave the SPs a higher chance to disrupt the CADA mediated blockade and successfully gate the channel for passage.[37] DnaJC10 is a disulfide isomerase, and as part of the ERAD response can reduce disulfide bonds of misfolded proteins to aid in their retrotranslocation through the ubiquitin gated Hrd1 retrotranslocon channel from the ER lumen to the cytosol for degradation by the proteasome.[35,38] DnaJC10 also interacts with ERAD-enhancing α-mannosidase-like protein (EDEM) which is involved in ERAD for glycosylated proteins which are not properly folded.[38,39] DnaJB11 is a type II transmembrane protein that is stress-induced and also involved in ERAD of misfolded proteins; however, it may also function in aiding in the normal folding of proteins not destined for degradation.[35,40] DnaJB12, also a type II transmembrane protein, which recruits a cytosolic Hsp70-8 (Hsc70) chaperone to the ER membrane is involved in ERAD for misfolded membrane proteins.[41] DnaJB12 was recently determined to be target of a novel class of antiviral drug for HBV, nucleic acid polymers (NAPs), which inhibit SVP assembly and secretion.[42] However, NAPs have no effect on other parts of the viral lifecycle including production of viral DNA or the infections Dane particles.[43]

Analysis of the proteins with reduced expression levels revealed a surprisingly large list of proteins, like DnaJB12, known to be or potentially involved with HBs processing and HBs mediated egress of viral particles. This indicates TL020 is potentially a highly potent and multimodal HBV inhibitor. Although these proteins cannot account for the reduced levels of intracellular HBV DNA seen in HepG2.2.15 cells, in many cases they may account for the greater potency of TL020 for reduction of secreted over the intracellular HBV DNA. Three glucosidase proteins, α-glucosidase I & II and β-glucosidase II were all downregulated. After the

OST complex adds $(GlcNAc)_2Man_9Glc_3$ to an asparagine amide nitrogen (N-glycosylation), the glycan chain can be further processed. Glucosidase I is responsible for the removal of the terminal glucose (Glc) unit and glucosidase II removes the penultimate glucose units.[44,45] The glycoprotein then undergoes chaperone assisted folding followed by removal of the ultimate terminal glucose removed by glucosidase II to give $(GlcNAc)_2Man_9$.[45] This processing is important for HBs maturation and glucosidase inhibitors were shown to be a promising HBV antiviral strategy that reduced HBV virion and SVP secretion in HepG2.2.15 cells.[44,46] TL020 also downregulated UGT1, which is a quality control enzyme that recognizes misfolded $(GlcNAc)_2Man_9$ glycoproteins and can add back a single glucose unit to N-glycans, preventing export from the ER and sending them back for another round of chaperone assisted re-folding and de-glycosylation by glucosidase II. Proteins that repeatedly fail to pass the quality control check are eventually degraded by the ERAD pathway.[47] Two studies revealed HBV infected HCC tissue had decreased levels of UGT1 revealing a possible a link between reduced UGT1 levels and HCC, which would be concerning for TL020 treatment and something that would warrant further investigation and consideration with TL020 treatment.[48,49] Next in line and also downregulated was 1,2-α-mannosidase IA, which can remove the terminal mannose (Man) unit from $(GlcNAc)_2Man_9$. HBV was shown to upregulate 1,2-α-mannosidase IA along with other similar mannosidase enzymes via the PPARα signalling pathway.[50]

Four members of the disulfide isomerase family were all down-modulated: DnaJC10 (already discussed above), PDI, ERp46, and ERp70. As previously mentioned, PDI is known to be aid in folding of HBs, and it is possible that that ERp46 and ERp70 are also involved.[6] Additionally, both ERO1-Lα and β which are ER resident proteins involved in recharging various disulfide isomerase including PDI and ERp70 were down-modulated.[51,52] After capsid

envelopment, ERGIC53 (also reduced by TL020 treatment) binds to the N146-linked glycan of HBs in the viral envelope to aid in egress.[53] Another down-regulated protein with a similar role in binding HBs-type glycans during transport and sorting is VIP36, which has been suggested as being possibly involved in HBV trafficking.[44] Another down-modulated protein was ERGIC63, which is involved in anchoring the ER membrane to cytoskeleton and also associated with poor prognosis for HCC.[54]

Of interest is the fact that p47, a p97/VCP cofactor, was slightly down-regulated. P97 stimulates NF-κB activity, and HBx was shown to interact with p97 to enhance its NF-κB stimulatory activity.[55,56] Meanwhile, the viral pol protein inhibits NF-κB, indicating that the timing of NF- κB activation or repression is critical to the different stages of the viral lifecycle.[57] Being as HBx affects viral transcription, it has also been suggested that P97 should effect viral transcription.[55] Additionally, the different branches that lead to ERAD converge at p97 as it is central the process of retrotranslocation and handover to the proteasome.[35] It has been shown that this process is involved in HBs degradation and antigen presentation by MHC I.[58] Lastly, p97 was shown to be have a positive effect on the life cycles of the *Flaviviridae*, *Picornaviridae*, and *Herpesviridae* virus families.[55] Although TL020 down-modulation of p47 was modest (20%), p47 represents an interesting broad-spectrum antiviral target and it's down-modulation would most likely have negative consequences for HBV replication.

The analysis of differentially regulated proteins involved in protein processing in the ER revealed specific proteins involved in the ERAD pathway were strategically up- or down-modulated in what appeared to be an attempt to overcome the effects of Sec61 blockade. A surprisingly large number of proteins involved the processing of the HBs glycoproteins were down-modulated which is highly likely to have a strong therapeutic value for HBV treatment.

Despite the great amount of promise in down-modulation of these proteins for HBV treatment, they don't explain the ability of TL020 to reduce intracellular HBV DNA in HepG2.2.15 cells. However, the discovery of the upregulation of Sec24D revealed a strong candidate for explaining this intracellular reduction of HBV DNA and warrants further investigation in future studies.

It is worth questioning how many of the down-modulated proteins discussed are down-modulated through the SP-dependent mechanism that has been thoroughly demonstrated for CADA compounds or whether another regulatory mechanism such as transcriptional regulation is at play. Because so many of the down-modulated proteins had very similar functions and many of the functions seemed to be consistent with relief of the effects of Sec61 blockade, it is likely that only a portion of these proteins was down-modulated by TL020 blocking their passage through Sec61. The remainder could be affected by cellular regulatory mechanisms. This would be consistent with the previous studies which showed CADA compounds to be highly selective.[59]

The list of differentially expressed proteins was further narrowed to 91 proteins by using a Bonferroni adjusted p-value of less than 0.05. This gave a higher confidence in the proteins to be truly differentially expressed. Of these proteins, 58 (63.7%) showed reduced levels. Of these proteins with reduced expressions levels, 30 (51.7%) had SPs, which is an even stronger enrichment for SP-containing proteins than seen in the media sample and is consistent with the expected down-modulatory mechanism of CADA analogues. A signature of this mechanism is a reduction of protein levels without reducing levels of the respective mRNA. To check the levels of mRNA of these respective proteins a qRT-PCR approach was implemented.

2.2 Effects on mRNA Levels

To investigate mRNA levels, HepG2 cells were treated in a similar fashion to the proteomics experiments and total RNA was extracted from cells either treated with 20 µM TL020 or a DMSO control. The RNA from 3 replicate treatments with either TL020 or DMSO was pooled and purified over spin columns. RNA integrity number was determined via an Agilent TapeStation instrument to confirm samples were of high quality (**Fig. 3.7**). RNA was subsequently converted to cDNA via reverse transcription. Primers were designed for specific amplification of each target gene from table 1 and used to amplify cDNA from each sample type to get relative quantification of mRNA levels in response to TL020 treatment. Primer design was done with the aid of either NCBI primer design tool or Harvard's PrimerBank. Primers for reference genes (TUBB2A, TBP, and CYC1) were selected from previously validated HepG2 reference genes by.[60] Primers were checked for specificity using MFEprimer[3.1] and checked for primer dimer formation using Integrated DNA Technologies' Primer Dimer Tool. The initial round of testing was used to validate the method used to normalize and calculate the fold change in mRNA levels when comparing TL020 treatment with the DMSO control. The results of this initial testing revealed that the reference genes were replicated with high efficiency and that they only had minor changes in expression between control and treatment (**Table 3.4**). Because similar results were obtained for all methods (even when low efficiency was observed), and the FC calculated using the pffafl method (see methods) followed by averaging across all reference genes does not require the use of a relative

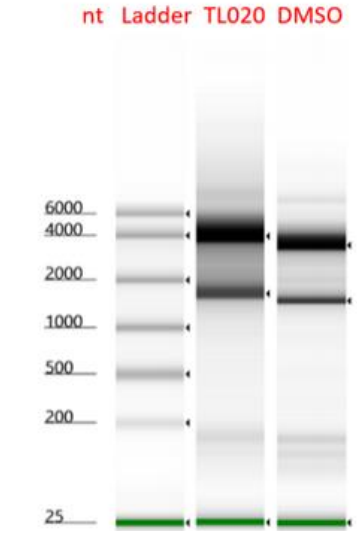

Figure 3.7: RNA integrity number. Analysis by TapeStation revealed RNA for TL020 treated sample was 9.3 and for DMSO control was 10.0.

Table 3.4: Optimization and determination of suitable FC calculation method. TUBB2a, TBP, and CYC1 were used as reference genes. The % difference and all FC calculations were done by comparing Cq's between (-) and (+) for 50 ng samples. The FC #1 was calculated via the ΔΔCT method using the reference gene closest to each gene in terms of efficiency. The FC #2 was calculated using the pffafl method with each reference gene and averaging. The FC #3 was calculated by using the geometric mean method. (-) denotes cDNA from 1% DMSO control HepG2 cells, while (+) denotes cDNA from 20 µM TL020 in 1% DMSO treated HepG2 cells. An "X" means the value could not be calculated.

Gene	E	R2	Cq for 100 ng (-)	Cq for 50 ng (-)	Cq for 20 ng (-)	Cq for 5 ng (-)	Cq for 0.5 ng (-)	Cq for 50 ng (+)	NTC	% Dif	FC #1	FC #2	FC #3
TUBB2a	1.926	0.9973	21.07	21.88	23.09	25.36	29.05	22.27	X	-22.77%	X	X	0.8746
TBP	1.996	0.9975	24.03	24.80	26.17	28.50	31.52	24.72	X	5.27%	X	X	1.1922
CYC1	1.895	0.995	21.24	22.21	23.38	25.42	29.55	22.47	X	-15.33%	X	X	0.9590
JPT1	1.886	0.9977	20.72	21.50	23.01	25.07	29.00	22.32	X	-40.22%	0.6826	0.6827	0.6771
SCD	1.873	0.996	18.20	19.15	20.28	22.59	26.60	20.83	X	-65.31%	0.3719	0.3961	0.3928
ICAM1	1.939	0.9997	24.09	25.05	26.42	28.48	32.07	26.84	X	-69.37%	0.3811	0.3498	0.3470
APOC3	1.847	0.9944	20.14	21.15	22.53	24.44	28.84	19.93	X	110.86%	2.7828	2.4079	2.3881
BCAM	1.896	0.9939	21.43	22.09	23.44	25.53	29.60	23.82	X	-67.02%	0.3602	0.3766	0.3735
PTPRF	1.612	0.9976	27.44	29.30	31.36	34.11	38.71	29.51	X	-9.70%	1.0327	1.0312	1.0227
PLOD3	1.845	0.9982	22.70	24.16	25.55	27.93	31.45	24.38	X	-12.77%	1.0261	0.9961	0.9880
ENPP2	1.84	0.9916	24.24	25.21	26.66	28.43	33.01	26.65	X	-58.62%	0.4394	0.4725	0.4687
CDH2	1.827	0.9979	22.55	23.48	25.13	27.15	31.33	X	X	-100.00%	X	X	X

standard curve, it was determined that this method would be used for screening the remaining genes. The following testing for the mRNA of all 30 proteins revealed that 14 had similar or increased levels of mRNA indicating that the down-modulation was not the result of transcriptional or other forms of regulation upstream of protein synthesis (**Table 3.5**). However, this does not mean mechanisms other than Sec61 blockade are not at play. The KEGG analysis revealed a strong disturbance in key chaperones and protein processing machinery in the ER which could easily lead to perturbations in protein levels not related to the SP-dependent mechanism of CADA analogues. As a result, further testing such as cell free translation/translocation experiments would be necessary to confirm these as true targets of TL020. A few of these targets were tested in such experiments performed by Dr. Bell and Dr. Intasiri which confirmed them to be new targets of TL020.

Table 3.5: Relative difference in protein and mRNA transcript abundance. TUBB2a, TBP, and CYC1 were used as reference genes. 50 ng of cDNA template was used in each reaction. The mRNA FC was calculated using the pffafl method with each reference gene and averaging.

Protein Name	Uniprot ID	Gene ID	Protein % Change	mRNA FC	$\Delta\Delta G_{app}$
Basal cell adhesion molecule	P50895	BCAM	-93.57%	0.37	7.47
Receptor-type tyrosine-protein phosphatase F	P10586	PTPRF	-90.54%	1.02	4.45
Agrin	O00468	AGRN	-90.28%	N/A	5.25
Laminin subunit beta-1	P07942	LAMB1	-90.17%	0.42	3.97
DnaJ homolog subfamily C member 3	Q13217	DNAJC3	-90.05%	2.68	0.01
Procollagen-lysine,2-oxoglutarate 5-dioxygenase 2	O00469	PLOD2	-89.50%	0.32	1.76
Integrin alpha-1	P56199	ITGA1	-88.31%	0.53	5.05
Inactive tyrosine-protein kinase 7	Q13308	PTK7	-83.94%	0.78	6.07
Multifunctional procollagen lysine hydroxylase and glycosyltransferase LH3	O60568	PLOD3	-83.90%	0.99	5.40
Laminin subunit alpha-5	O15230	LAMA5	-83.22%	0.64	1.48
Sortilin	Q99523	SORT1	-82.00%	0.61	3.44
Lysosomal alpha-mannosidase	O00754	MAN2B1	-81.21%	1.67	6.06
Peptidyl-prolyl cis-trans isomerase FKBP9	O95302	FKBP9	-81.20%	0.97	4.07
Legumain	Q99538	LGMN	-79.19%	0.59	0.64
Phospholipase A2 group XV	Q8NCC3	PLA2G15	-78.89%	0.63	4.02
Apolipoprotein B-100	P04114	APOB	-77.86%	1.22	-1.55
General transcription factor 3C polypeptide 3	Q9Y5Q9	C3	-72.51%	1.49	1.52
Protein canopy homolog 2	Q9Y2B0	CNPY2	-71.51%	1.47	2.14
Oxytocin-neurophysin 1	P01178	NEU1	-68.10%	1.91	4.43
Intercellular adhesion molecule 1	P05362	ICAM1	-67.37%	0.35	2.49
Alpha-1-antichymotrypsin	P01011	SERPINA3	-67.36%	0.15	4.52
Cadherin-2	P19022	CDH2	-66.38%	N/A	-0.49
Procollagen galactosyltransferase 1	Q8NBJ5	COLGALT1	-66.09%	0.48	4.55
Neutral alpha-glucosidase AB	Q14697	GANAB	-65.09%	1.17	-0.02
Protein disulfide-isomerase A5	Q14554	PDIA5	-60.02%	2.10	1.58
Out at first protein homolog	Q86UD1	OAF	-59.33%	1.32	-0.19
Malectin	Q14165	MLEC	-58.68%	2.33	2.78
ER membrane protein complex subunit 1	Q8N766	EMC1	-58.22%	0.86	0.15
Cation-independent mannose-6-phosphate receptor	P11717	IGF2R	-57.43%	1.64	11.07
Gamma-glutamyl hydrolase	Q92820	GGH	-50.55%	1.68	-0.28

2.3 Luciferase Screening Assay

It was determined that a new screening platform could help to identify other CADA analogues that have therapeutic potential. Five targets were selected for the initial development of a luciferase screening assay (CD4, sortilin, endoplasmic reticulum lectin 1, DnaJC3, and inactive tyrosine-protein kinase 7). CD4 is not expressed in HepG2 cells, but the other four were all detected as down-modulated in the LC-MS/MS experiment. CD4 was included due to it being the first identified target and most well studied target of CADA analogues. A collaborator, Dr. Massimo D'Agostino was able to develop a novel platform for screening CADA analogues that involves the use a dual luciferase assay. Dr. D'Agostino's lab sent us five different pIRES

expression plasmids with the SP of each protein cloned onto the N-terminus of the firefly luciferase. The firefly luciferase gene was followed by an internal ribosome entry site (IRES) and in frame Renilla luciferase protein. Experiments in their laboratory revealed an interesting phenomenon with the CD4 construct. When they tested it they found that in the absence of treatment the SP directed the firefly luciferase into the ER lumen where it was inactive after cell lysis and addition of the luciferase substrate. Treatment with CADA or the highly active analogue, CK147, blocked passage into the ER and salvaged the activity of the luciferase. This was surprising because CADA treatment normally leads to degradation of target proteins, but the firefly luciferase apparently avoids degradation and is stable in the cytosol. A great advantage of this assay is that the increase is signal occurs relatively rapidly after treatment allowing for short treatment times.

The plasmids were received on filter paper, extracted with Milli-Q water, and the concentrations and purities were checked by Nano-Drop (**Table 3.6**). The results indicated the plasmids were of low purity after extraction, but this wasn't a major concern, because they needed to be amplified prior to use. Chemically competent *E. coli* cells were transformed with the plasmids and the cells were grown on LB agar plates with ampicillin for selection of transformed cells. After overnight incubation at 37 °C individual colonies were selected for liquid cultures grown at 37 °C in a shaking incubator overnight in LB media with ampicillin. The next day, a portion of the culture was used to make a glycerol stock while the remainder was lysed and the plasmids extracted and purified using a

Table 3.6: Plasmids initial purity and concentration. Plasmids were extracted in Milli-Q water from filter paper and absorbance was read on a Nano-Drop.

Plasmid SP	A_{260}	A_{260}/A_{280}	Concentration (ng/µL)
SORT1	0.534	1.35	26.7
CD4	0.755	1.34	37.8
ERLEC1	0.484	1.29	24.2
DNAJC3	0.567	1.32	28.4
PTK7	0.449	1.25	22.5

MiniPrep kit from Qiagen. The plasmids were eluted from the spin columns in 50 µL of AE buffer and the purity and concentration were checked by Nano-Drop (**Table 3.7**). This gave the plasmids in high purity and good yields. The plasmids were verified by doing digestion with NheI and XhoI restriction enzymes which was predicted to produce fragments 3.7 Kb and 4.2 Kb in size by using SnapGene software. After digestion the fragments were ran on a 1% agarose gel and visualized by using ethidium bromide fluorescence (**Fig. 3.8**). This revealed 3 fragments were produced; one was close to 3.7 Kb, while the other two were around 3.2 Kb and 1.0 Kb. This indicated that there was an off-target cleavage event in the larger 4.2 Kb fragment which produced the two smaller fragments. Regardless, this confirmed the *E. coli* cultures were amplifying the desired plasmids. A larger quantity of plasmid was desired in order to make a single stock to complete all the desired and future testing. As such, the glycerol stocks were used to inoculate 500 mL LB medium containing ampicillin. For these larger cultures the plasmids were extracted and purified by separation in a CsCl gradient via ultracentrifugation. The plasmids obtained from this method were resuspended in 400 µL of Tris-EDTA (TE) buffer and the concentrations and purities were checked by Nano-Drop (**Table 3.8**).

Table 3.7: Plasmids purity and concentration after MiniPrep. Plasmids were amplified in E. coli and purified with a Qiagen MiniPrep kit. Absorbance was read on a Nano-Drop.

Plasmid SP	A_{260}	A_{260}/A_{280}	Concentration (ng/µL)
SORT1	7.614	1.85	380.7
CD4	8.285	1.85	414.3
ERLEC1	7.692	1.85	384.6
DNAJC3	8.637	1.85	431.9
PTK7	7.528	1.85	376.4

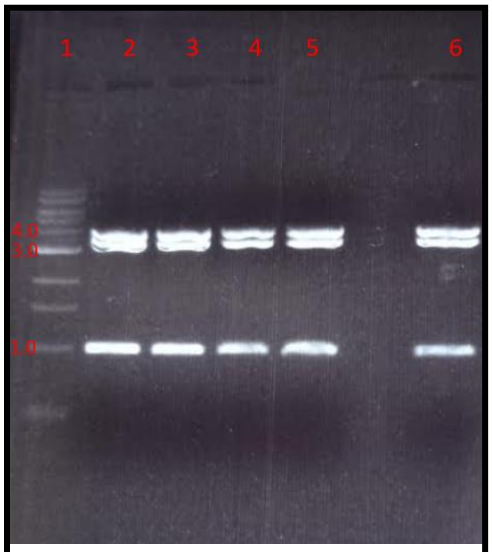

Figure 3.8: Agarose gel of restriction digest. The purified plasmids were incubated with NheI and XhoI restriction enzymes. Lane 1 is the DNA ladder, lanes 2-6 are the plasmids with the SP insert of SORT1, CD4, ERLEC1, DNAJC3, and PTK7, respectively.

Table 3.8: Plasmids purity and concentration after separation in a CsCl gradient. Plasmids were amplified in E. coli and purified by separation in a CsCl gradient via ultracentrifugation. Absorbance was read on a Nano-Drop.

Plasmid SP	A_{260}	A_{260}/A_{280}	Concentration (ng/µL)
SORT1	21.131	1.91	1056.5
CD4	21.936	1.89	1096.8
ERLEC1	23.045	1.92	1152.2
DNAJC3	17.244	1.90	862.2
PTK7	49.668	1.50	2483.4

The purity for SORT1, CD4, ERLEC1, and DNAJC3 SP containing plasmids showed that there could be some residual RNA, but was good enough to move forward with transfection experiments. The PTK7 SP containing plasmid on the other hand had very poor purity as indicated by a low A_{260}/A_{280} ratio. For this reason, a second purification was performed for this plasmid once again using a CsCl gradient. This produced concentration and purity values on par with the other plasmid preps (A_{260} = 23.493, A_{260}/A_{280} = 1.87, concentration = 1,174.7 ng/µL). An initial transfection experiment using Hek293 cells and the CD4 SP plasmid was performed using a commercially available dual luciferase detection kit. Cells were plated in 12-well plates at 1.0 X 10^5 cells/well and grown overnight before transfecting with the plasmid. Transfected cells were incubated for 5 hours before they were washed and detached by incubation with 0.05% trypsin-EDTA for 1 minute. The trypsin was neutralized by mixing with 12 times the volume of media supplemented with 10% FBS. The cell suspension was plated into a 96-well plate and the cells were grown overnight. The next day the cells were incubated in media containing 20 µM CK147 with 1% DMSO for 6 h. CK147 was previously shown to have strong activity in the dual luciferase assay using the CD4 SP plasmid. The experiment revealed that incubation with CK147 increased the ratio of firefly luciferase to Renilla luciferase from 0.69 with DMSO alone to 1.10 with CK147 treatment. This strong increase in the relative firefly luciferase signal was consistent with the previous experiments and indicated that the plasmid could be used to detect the activity of CADA analogues for inhibition of translocation of firefly luciferase with the N-terminally attached CD4 SP. Due to the high cost of the commercial

reagent and the availability of a published recipe for firefly and Renilla detection reagents, in-house detection reagents were made and tested.[61] Using the at home reagent showed that the incubation with CK147 increased the ratio of firefly luciferase to Renilla luciferase from 1.52 +/- 0.36 with DMSO alone to 4.60 +/- 2.65 with CK147. While the assay requires further optimization to improve on the accuracy and consistency it is clear that the in-house reagent can be successfully used for drug screening purposes. Parameters that should be targeted for improvement in the future are the volume of lysate and reagents used for detection, the cell plating concentration, and treatment time. The 10 µL volumes for the lysate and subsequently both detection reagents, are not sufficient to make an even layer of liquid in the bottom of the plate and it is likely that the addition of a slightly higher volume would produce a more consistent output. The standard recommended volume for substrate solutions are 100 µL, but an initial attempt to use this volume produced very little signal. This is suspected to be due to the small amount of corresponding enzyme in the 10 µL of lysate. Perhaps an increase in lysate volume to match the increased volume of the reagents would create a more stable signal that doesn't rapidly decay with time; in the proof of concept assay multiple readings a few seconds apart showed that the signal produced a rapid flash that dissipated in a matter of seconds making consistency in the reading very difficult. Furthermore, it would be worth optimizing the detection solutions. The substrates for both firefly and Renilla luciferase give the solutions a yellow color, and visual inspection reveals that the substrates are at a much higher concentration in the commercial reagents as compared to the in-house reagents. The ideal amount of substrate would be that which saturates the luciferase enzymes and keeps them saturated for at least 10 seconds to give ample time for adding, mixing, and reading.

Section 3: Experimental

Note: Special thanks to Dr. Robert Ryan and Dr. Subhash Verma for their guidance and support as well as for allowing me to work in their laboratories and use their reagents and equipment. Special thanks to Dr. Massimo D'Agostino and his laboratory for cloning and providing the SP-Luc pIRES plasmids. Special thanks to Irina Romenskaia and Kabita Adhikari for their patience, guidance, and help with growing cells. Special thanks to Timsy Uppal for her advice and support with doing the plasmid preparations. Without the help of these individuals I would not have been able to do this work.

3.1 General Methods

HepG2 originally from ATCC were donated from the cells maintained by Irina Romenskaia in Dr. Robert Ryan's laboratory. HEK293 cells originally from ATCC were donated from the cells maintained by Kabita Adhikari in Dr. Subhash Verma's laboratory. HepG2 and HEK293 cells were worked with under biosafety level II (BSLII) conditions taking all appropriate precautions. All work involving the growth of HepG2 or HEK293 cells was performed under strict aseptic conditions working in a class II biosafety cabinet (BSC) and wearing appropriate personal protection equipment (PPE) including gloves, lab coat, and safety glasses. All surfaces were cleaned before and after work with 70% ethanol. All materials in contact with the cells or culture media were purchased as sterile equipment or sterilized via autoclave. After use, all materials in contact with the cells or culture media were decontaminated by treatment with freshly prepared 20% bleach for a minimum of 15 minutes or sterilized in an autoclave. Unless otherwise noted, HepG2 cells were grown in a complete media that was prepared by mixing 450 mL of Eagles Minimum Essential Medium (EMEM), 50 mL of fetal bovine serum (FBS), 5 mL of 100X GlutaMax, 5 mL of 100X non-essential amino acids

(NEAA), 5 mL of 100X sodium pyruvate, and 2.5 mL of 200X penicillin-streptomycin (PEST). Serum-free media was prepared by mixing 492.5 mL of EMEM, 5 mL of 100X GlutaMax, and 2.5 mL of 200X PEST. All media components were purchased from Gibco except PEST was purchased from SigmaAldrich. HepG2 cells were maintained in sterile, treated 100 mm petri dishes incubated in a 37 ºC incubator with a 5% CO_2 atmosphere and split every three days by removal of the media, washing with 10 mL of PBS (pH 7.4), and addition of 2 mL of 0.05% Trypsin-EDTA. The cells were incubated with the trypsin solution for 5-8 minutes at 37 ºC. During this incubation time the cells were periodically removed from the incubator and checked for detachment using an inverted microscope. Once detached 8 mL of fresh media was added and the cells were mixed by pipetting the entire solution through a 200 µL micropipette tip fitted on the end of a serological pipette 3-5 times. The cell suspension was then split at ratios of 1:4, 1:6, or 1:8 as desired. Cell counting was performed by removing 100 µL of the cell suspension and thoroughly mixing with 400 µL of media, then pipetting 17 µL onto a hemocytometer. A total of 10 squares were counted and the cell/mL was determined by dividing the total number of cells by the number of squares counted (10) then multiplying by the dilution factor (5X) and lastly multiply by 10^4. HEK293 cells were grown in a complete media that was prepared by mixing 440 mL of Dulbecco's Modified Eagle Medium (DMEM), with 50 mL of FBS, 5 mL of 100X NEAA, and 5 mL of 200X PEST. HEK293 cells were grown in treated T75 flasks incubated in a 37 ºC incubator with a 5% CO_2 atmosphere and split every two days by decanting the media, washing with 5 mL of PBS (pH 7.4), and additing of 2 mL of 0.05% Trypsin-EDTA. The cells were incubated with the trypsin solution for 1-2 minutes at r.t., watching for detachment with an inverted microscope. Once cells detached 8 mL of fresh media was added to the flask and the suspension was transferred to a sterile 15 mL conical tube which was centrifuged at 100 rcf for 5

min. The supernatant was decanted and the pellet was resuspended in 2 mL of fresh media. The cells were seeded back into a T75 flask by adding 200 µL of the cell suspension and 10 mL of fresh media. To perform a cell count, 20 µL of the cell suspension was removed and mixed with 60 µL of PBS. A 10 µL aliquot of this was mixed with 10 µL of trypan blue and 15 µL was added to a cell counting slide. The cells were counted on a Nexcelom Cellometer Auto T4 selecting a dilution factor of eight and selecting HEK293 under cell type.

3.2 Effects on Protein Levels

Changes in Viability of HepG2 Cells After TL020 Exposure

Materials and Reagents

Table 3.9: Materials and reagents for viability of HepG2 cells.

20 mM TL020 in DMSO	Gibco NEAA
Black 96-well plate	Hemocytometer
CellQuanti-Blue™ Cell Viability Assay Kit	HepG2 cells
Class II BSC	Inverted microscope
CO_2 incubator	Micropipettes
Fluorescent plate reader	Sigma Aldrich 200X Penicillin-Streptomycin
Gibco 0.05% Trypsin-EDTA	Sterile, treated 100 X 20 mm petri dish
Gibco 100X sodium pyruvate	Sterile 2 mL snap cap tubes
Gibco EMEM	Sterile PBS (pH 7.4)
Gibco FBS	Sterile pipette tips
Gibco GlutaMax	Sterile serological pipettes
	Sterile, treated 96-well plate

Procedure

HepG2 cells were plated at 1.25 x 10^4 cells/well in 100 µL of media, in three 96-well cell culture plates, and incubated for 24 h at 37 °C with 5% CO_2. The test compound, TL020, was diluted into serum-free media containing 1% DMSO. For a 100 µM concentration, 9.5 µL DMSO was mixed with 1,881 µL of serum-free media and warmed to 37 °C then 9.5 µL of TL020 (20 mM in DMSO) was added and vortexed. In a similar way, dilutions of 50, 10, 1, and

0.1 μM were also prepared. With the exception being that 1 and 0.1 μM dilution were made from TL020 stock at 10 mM concentration in DMSO. Additionally, a solution of serum-free media containing 1% DMSO was prepared as a control. The complete media was aspirated from the wells and 100 μL of serum-free media containing compound at the various dilutions described above was added to wells in sets of four. As controls serum-free media containing 1% DMSO, or serum-free media by itself were tested in sets of eight by aspirating complete media from the wells and adding 100 μL of solution per well. Additionally, a set of four wells that were previously left without cells received 100 μL of serum-free media and was used as a background control during analysis. Each plate was treated in this same way and then returned to the incubator for either 24, 48, or 72 h incubations before proceeding to the next step. After incubation, 10 μL of CellQuanti-Blue™ reagent was warmed to r.t. and added to each well with the lights in the BSC turned off. The plate was gently agitated and then returned to incubator for 2 h. The solutions were then transferred to black 96-well plates and fluorescent intensity was read with an excitation of 544 nm and an emission of 590 nm.

Calculations

$$\%\, Viability\ (relative\ to\ cell\ only\ control) = \left\{\frac{(\text{fluorescence for test well} - \text{average fluorescence for no cell control})}{(\text{average fluorescence for cell only control} - \text{average fluorescence for no cell control})}\right\} \times 100$$

Changes in Protein Expression of HepG2 Cells After TL020 Exposure

Treating HepG2 Cells with TL020

Materials and Reagents

Table 3.10: Materials and reagents for TL020 treatment of HepG2 cells.	
1 mL syringe	Micropipettes
100 mL graduated cylinder	MilliQ water
20 mM TL020 in DMSO	NaCl
21 1/2 gauge need	pH probe
250 mL beaker	SDS
Class II BSC	Sigma Aldrich 200X Penicillin-Streptomycin
CO_2 incubator	sodium deoxycholate
EDTA	Sorvall Biofuge Pico
Gibco 0.05% Trypsin-EDTA	Sterile 2 mL snap cap tubes
Gibco 100X sodium pyruvate	Sterile PBS (pH 7.4)
Gibco EMEM	Sterile pipette tips
Gibco FBS	Sterile serological pipettes
Gibco GlutaMax	Sterile, treated 100 X 20 mm petri dish
Gibco NEAA	Sterile, treated 12-well plate
Hemocytometer	Tris-HCl
HepG2 cells	Triton X-100
Inverted microscope	Vortexer

Preparation of Essential Solutions

100 mL of **1 M Tris-HCl pH 8.0** was prepared by dissolving 15.759 g of Tris-HCl in a beaker with 80 mL of MilliQ water. The solution was added to a graduated cylinder and brought up to 100 mL with MilliQ water. The pH was checked and didn't need adjusting.

100 mL of **RIPA lysis buffer** was prepared by dissolving 2.5 mL of Tris-HCl pH 8.0, 0.877 g of NaCl, 0.146 g of EDTA, 1 mL of Triton X-100 (added w/ a syringe), 1 g of a sodium deoxycholate, and 0.1 g of SDS in 80 mL of MilliQ water in a beaker. The solution was added to a graduated cylinder and brought up to 100 mL with MilliQ water.

Procedure

HepG2 cells were plated at 2.5 x 10^5 cells/well in 1 mL of complete media, in a 12-well cell culture plate, and incubated for 24 h at 37 °C with 5% CO_2. The test compound, TL020, was diluted into serum-free media containing 1% DMSO. For a 20 μM concentration, 135 μL DMSO was mixed with 14.85 mL of serum-free media and warmed to 37 °C then 15 μL of 20 mM

TL020 in DMSO was added and the solution wasvortexed. Additionally, a solution of serum-free media containing 1% DMSO was prepared as a control. The complete media was aspirated from the wells and 1 mL of serum-free media containing 20 μM TL020 and 1% DMSO was added to replicate wells. As controls serum-free media containing 1% DMSO, or serum-free media by itself were tested in replicate wells by aspirating off the complete media and adding 1 mL of the desired solution per well. The plate was incubated for 72 h at 37 °C with 5% CO_2. After incubation, the media was collected into 1.5 mL tubes and centrifuged at 5,000 rpm at 0 °C for 5 minutes. The supernatant was collected and stored at -20 °C (later samples were used for SDS-PAGE or precipitated and sent to proteomics center for MS analysis). The cells that remained attached to the bottom of the wells were rinsed with 1 mL of ice-cold PBS. Then 100 μL of RIPA buffer was pipetted onto the cells and the plate was placed on ice and rocked for 20 minutes. The wells were scraped, and the lysates were collected by aspiration. The wells were washed with an additional 100 μL of PBS which was added to the lysate. The lysates were passed through a 21 ½ gauge needle 5 times to shear DNA. Lysates were then centrifuged at 13,000 rpm at 0 °C for 20 minutes. The supernatant was collected sent directly to proteomics center for MS analysis or stored at -20 °C and later used for SDS-PAGE.

BCA Protein Assay and SDS-PAGE

Materials and Reagents

Table 3.11: Materials and reagents for BCA assay and SDS-PAGE.

4X Laemmli Sample Buffer	Pierce BCA protein assay kit
96-well plate	Plastic container
Absorbance plate reader	Precision Plus Protein dual color standards
Bio-Rad 10% precast gel	Protein samples
Bio-Rad gel apparatus	Sterile 2 mL snap cap tubes
Bio-Rad Gel Doc imager	Sterile PBS (pH 7.4)
Heating bead bath	Sterile pipette tips
LabSafe GEL Blue	Sterile serological pipettes

Procedure

Samples were thawed on ice and protein concentrations were determined using BCA assay following the manufacturer's instructions. Bovine serum albumin (BSA) standards were prepared by diluting the BSA stock in the provided diluent making eight concentrations ranging from 25 µg/mL to 2,000 µg/mL. Reagent A was mixed with Reagent B in a 50:1 ratio to making the working reagent (WR). Next, 25 µL of the standards and samples were added to the wells of a 96-well plate and 200 µL of the WR was added to each well. The plate was placed on a plate shaker to mix for 30 seconds, then covered and incubated at 37 ºC for 30 minutes. The absorbance was read at 562 nm. A plot of the standards was used to make a standard curve and the linear fit to these points was used to back calculate the concentration of the protein samples. The SDS-PAGE apparatus was set up with a 10% gel and running buffer. Samples were diluted with PBS and 4x laemmli sample buffer then heated at 80 °C for 15 minutes. Because the media samples had too low of a protein concentration to accurately determine they were not diluted prior to mixing with 4x laemmli sample buffer (37.5 µL sample and 12.5 µL of laemmli). The results from the BCA assay were used to dilute lysate samples with PBS to get final protein concentration of 0.25 µg/µL after addition of laemmli. The gel was loaded with 20 µL for the lysate samples, 25 µL for the media samples, and 3 µL for the Precision Plus Protein™ Dual Color Standards. The gel was run at 200 V for 32 minutes, removed from the cassette, washed 3 times for 5 min each with diH_2O, then submersed in LabSafe GEL Blue, and rocked for 1.5 h. The gel was rinsed with diH_20 multiple times to clear up background staining then imaged on Bio-Rad Molecular Imager®.

Media Protein Precipitation

Materials and Reagents

Table 3.12: Materials and reagents for precipitation.

-20 °C Freezer	Media samples	Serological pipettes
2 mL snap cap tubes	Methanol	Sorvall Biofuge Pico
Chloroform	PBS (pH 7.4)	Vortexer
diH_20	Pipette tips	

Procedure

For 600 µL of thawed media sample, 300 µL of ice-cold methanol, 75 µL of ice-cold chloroform, and 225 µL of ice-cold H_2O were added. This mixture was vortexed vigorously and centrifuged at 13,000 rpm for 10 minutes. The top layer of methanol/H_2O was removed being careful not to disturb the interface. An additional 100 µL of ice-cold methanol was added to the solution which was then vortexed vigorously and centrifuged at 13,000 rpm for 10 minutes. The supernatant was removed and another 100 µL of ice-cold methanol was added to the solution which was then vortexed vigorously and centrifuged at 13,000 rpm for 10 minutes. The supernatant was removed, and pellet was air dried before suspension in 100 µL of ice-cold PBS. Samples were then frozen at -20 °C and sent to the proteomics center for MS analysis.

3.2 Effects on mRNA Levels

Changes in mRNA Expression of HepG2 Cells After TL020 Exposure

Treating HepG2 Cells with TL020

Materials and Reagents

Table 3.13: Materials and reagents for treating HepG2 cells.		
20 mM TL020 in DMSO	Gibco FBS	Sigma Aldrich 200X Penicillin-Streptomycin
200 proof ethanol	Gibco GlutaMax	Sterile PBS (pH 7.4)
Class II BSC	Gibco NEAA	Sterile pipette tips
CO_2 incubator	Hemocytometer	Sterile serological pipettes
Eppendorf Centrifuge 5424	HepG2 cells	Sterile, treated 100 X 20 mm petri dish
Gibco 0.05% Trypsin-EDTA	Inverted microscope	Sterile, treated 6-well plate
Gibco 100X sodium pyruvate	NanoDrop	Vortexer
Gibco EMEM	Rnase free 1.5 mL tubes	Zymo Quick-RNA MiniPrep Kit

Procedure

HepG2 cells were plated at 5.0 x 10^5 cells/well in 2 mL of complete media, in a 6-well cell culture plate, and incubated for 24 h at 37 °C with 5% CO_2. The test compound, TL020, was diluted into serum-free media containing 1% DMSO. For a 20 μM concentration, 63 μL DMSO was mixed with 6.93 mL of serum-free media and warmed to 37 °C then 7 μL of 20 mM TL020 in DMSO was added and the solution was vortexed. Additionally, a solution serum-free media containing 1% DMSO was prepared as a no compound control. The complete media was aspirated from the wells and 1 mL of serum-free media containing 20 μM TL020 and 1% DMSO or serum-free media containing 1% DMSO was added to replicate wells. The plate was incubated for 72 h at 37 °C with 5% CO_2. After incubation, RNA was isolated using Zymo Research® *Quick*-RNA™ MiniPrep kit. All materials and reagents were RNase free and care was taken to avoid contamination of samples with RNase. Media was removed by aspiration and each well received 300 μL of RNA Lysis Buffer. The three TL020 treated wells and separately the three 1% DMSO only wells were combined and transferred to 1.5 mL tubes then centrifuged at 16,000 rcf for 30 sec. The supernatant was transferred to Spin-Away™ Filters in collection tubes and centrifuged at 16,000 rcf for 30 sec. An equivalent volume of 100% ethanol was added to the flow-through and mixed. This solution was transferred to Zymo-Spin™ IIICG Columns in collection tubes and centrifuged at 16,000 rcf for 30 sec. Next 400 μL of RNA Wash Buffer was

added to the column which was centrifuged at 16,000 rcf for 30 sec. A mixture of 5 µL DNase I with 75 µL of DNA Digestion Buffer was added to the column and incubated at r.t. for 15 minutes. Next 400 µL of RNA Prep Buffer was added to the column which was centrifuged at 16,000 rcf for 30 sec. This was followed by 700 µL RNA Wash Buffer centrifugation at 16,000 rcf for 30 sec. Another 400 µL RNA Wash Buffer was added followed by centrifugation at 16,000 rcf for 2 minutes. The column was transferred to new collection tube and the RNA was eluted by adding 100 µL DNase/RNase-free water to the column and centrifugating at 16,000 rcf for 30 sec. The RNA was stored at -20 °C temporarily for 1 week before moving to -70 °C. The RNA concentration and purity was checked by NanoDrop. The TL020 treated sample gave values of 495.9 ng/µL (49.59 µg) $A_{260/280}$ = 2.06, $A_{260/230}$ = 2.07. The 1% DMSO only sample gave values of 587.4 ng/µL (58.74 µg) $A_{260/280}$ = 2.05, $A_{260/230}$ = 2.18.

Reverse Transcription for Creating cDNA from RNA

Materials and Reagents

Table 3.14: Materials and reagents for reverse transcription reaction.

DEPC treated water	Micropipettes	Sterile pipette tips with filter
High-Capacity cDNA Reverse Transcription Kit	Rnase free 1.5 mL tubes	Thermal cycler
Microcentrifuge	Rnase free PCR tubes	Vortexer

Procedure

The cDNA was made using Thermo Fisher Scientific® High-Capacity cDNA Reverse Transcription Kit following the manufacturer's instructions. All components were thawed on ice. A master mix was prepared for running ten reactions for each sample by making a master mix that consisted of 21 µL of 10X RT Buffer, 8.4 µL of 25X dNTP Mix, 21 µL of 10X RT Random Primers, 10.5 µL of MultiScribe™ Reverse Transcriptase, and 44.1 µL of nuclease-free H_2O. Both RNA samples were diluted to 0.2 µg/µL in nuclease-free H_2O. Each reaction was prepared by mixing 10 µL of the master mix with 10 µL of the diluted 0.2 µg/µL RNA sample. The tubes

were briefly centrifuged to eliminate bubbles, then placed in the thermocycler which was run using the following steps: 25 °C for 25 min, 37 °C for 120 min, 85 °C for 5 minutes. The cDNA was stored at -20 °C.

Designing primers for use with SYBR Green detection

Procedure

The desired gene to be amplified was first searched using the National Center for Biotechnology Information (NCBI) Gene website (https://www.ncbi.nlm.nih.gov/gene). Upon reviewing the annotated transcripts from the GRCh38 genome assembly, the shortest transcript was selected. The RefSeq ID for this gene was then entered into the "PCR Template" box in the NCBI Primer-BLAST tool (https://www.ncbi.nlm.nih.gov/tools/primer-blast/). For the first attempt, the parameters of the search were either left as default or changed accordingly: PCR minimum product size = 45, PCR maximum product size = 210, # of primers to return = 20, minimum Tm = 58, max Tm difference = 2, primer must span an exon-exon junction, primer must be separated by at least one intron on the corresponding genomic DNA with intron minimum length = 80, exclude predicted RefSeq transcripts, exclude uncultured/environmental sample sequences, primer must have at least 6 total mismatches to unintended targets, ignore targets that have 9 or more mismatches to the primer, maximum target size = 3000, allow primer to amplify mRNA splice variants, show results in a new window, maximum primer pairs to screen = 2000, PCR product minimum Tm = 65, minimum primer size = 18, optimum primer size = 23, maximum primer size = 30, minimum GC content = 35, maximum GC content = 65, maximum poly-X = 3, maximum self-complementarity of any = 6, maximum self-complementarity of 3' = 2, maximum pair-complementarity of any = 6, maximum pair-complementarity of any = 2, concentration of divalent cations =3, concentration of dNTPs = 0.8,

annealing oligo concentration = 200, salt correction formula = Owczarzy et. 2004. The results were reviewed to find primer pairs predicted to amplify all annotated RefSeq transcripts for the gene of interest and that were not predicted to amplify any RefSeq transcripts from other genes. If none of the primer pairs were predicted to amplify all annotated RefSeq transcripts for the gene of interest, then the search was repeated after setting the forward primer "from" position and the reverse primer "to" position to span a region of the transcript shared by all transcripts. If all the primer pairs were predicted to amplify off-target genes, then the search was repeated by relaxing the requirement for either spanning exon junctions or spanning an intron, focusing the search to smaller regions shared by all transcripts, or lastly reducing the stringency of primer pair specificity by returning parameters to the default settings. When the search returned results with multiple primer pairs predicted to amplify all annotated RefSeq transcripts for the gene of interest and that were not predicted to amplify any RefSeq transcripts from other genes, then the primer pairs were prioritized based on the principles of avoiding repeats of Gs or Cs longer than 3 bases, with Gs or Cs on the ends of the primers, GC content preferably between 50-60%, and low self-complementarity numbers. The most promising primer pair was then selected for further validation using IDT's OligoAnalyzer tool (https://www.idtdna.com/calc/analyzer). Parameter sets were changed to qPCR and each primer sequence was checked for formation of hairpins, self-dimers, and hetero-dimers to the other primer in the pair. If any of these queries returned structures with ΔG values less than -7 then these primer pairs were not used, and another primer pair was selected and checked by the OligoAnalyzer tool.

qPCR for Relative Quantification of Gene Expression

Materials and Equipment

Table 3.15: Materials and reagents for qPCR.	
96-well plate microcentrifuge	Sterile pipette tips with filter
Rnase free 1.5 mL tubes	Micropipettes
96-well PCR plate	PowerTrack SYBR green master mix
Adhesive plate sealer	cDNA samples
RT-PCR thermocycler	DEPC treated water

Procedure

All reagents were thawed on ice. Primers were diluted to 3 μM concentrations with H_2O then forward and reverse primer pairs were mixed 1:1 to create primer working solutions. The DMSO control cDNA was diluted to 100 ng/μL, 50 ng/μL, 20 ng/μL, 5 ng/μL, and 0.5 ng/μL with H_2O. The TL020 treated cDNA was diluted of 50 ng/μL. The PowerTrack SYBR Green Master Mix, 40X Yellow Sample Buffer, and H_2O were premixed in a 20:1:9.2 ratio. Each reaction was set up by pipetting 7.55 μL of this premixed PowerTrack SYBR Green Master Mix and 40X Yellow Sample Buffer solution per well in the clear well PCR plates followed by 1.6 μL of the appropriate premixed (1:1) forward and reverse primer, and 1 μL of the appropriate cDNA dilution. Seven reactions in total were set up for each gene, which differed in the cDNA template they received. These were the five dilutions for the DMSO control cDNA, the one dilution of TL020 treated cDNA, and no template control (1 μL H_2O added instead of cDNA). The plate was covered with optical adhesive, and briefly centrifuged before being placed in the RT-PCR thermocycler. Using the integrated software, the instrument was set up to monitor both ROX and SYBR green dyes. The cycling conditions were set to 1) 95 °C for 2 min, 2) 95 °C for 5 sec, 3) 55°C for 30 sec, 4) 60 °C for 30 sec, 5) go to step 2 (39X), 6) 1.6 °C/sec to 95 °C hold for 15 sec, 7) 1.6 °C to 60 °C hold for 1 min, 8) 0.1 °C/sec to 95 °C hold for 15 sec, 9) 65 °C for 5 sec, 10) 95 °C in 0.5 °C increments. The lid temperature was set to 105 °C. The instrument was set to

monitor the reactions for steps 1-5 and 9-10. The software automatically calculated Cq values. TUBB2a, TBP, and CYC1 were used as reference genes in the analysis.

Calculations

Relative Standard Curve:

The relative standard curve is generated by graphing the log of the starting amount of template DNA (in ng) on the x-axis with the resulting C_q value on the y-axis and creating a best fit line through those points. The relative amount in each sample is calculated by plugging in the C_q value for y, solving for x, and taking the anti-log of this value.

Percent difference

$$\%\, dif = \frac{relative\ amount\ in\ treated\ sample - relative\ amount\ in\ untreated\ sample}{relative\ amount\ in\ untreated\ sample}$$

FC using ΔΔCT method

$$\Delta\mathrm{CTE} = Cq\ for\ GOI\ with\ treatment\ cDNA - Cq\ for\ ref\ gene\ with\ treatment\ cDNA$$

$$\Delta CTC = Cq\ for\ GOI\ with\ control\ cDNA - Cq\ for\ ref\ gene\ with\ control\ cDNA$$

$$\Delta\Delta CT = \Delta CTE - \Delta CTC$$

$$FC = 2^{-\Delta\Delta CT}$$

FC using pffafl method

$$E = 10^{\frac{-1}{slope\ of\ relative\ standard\ curve}}$$

$$\mathrm{FC} = \frac{E_{GOI}^{Cq\ for\ GOI\ with\ control\ cDNA - Cq\ for\ GOI\ with\ treatment\ cDNA}}{E_{ref}^{Cq\ for\ ref\ gene\ with\ control\ cDNA - Cq\ for\ ref\ gene\ with\ treatment\ cDNA}}$$

Determine using each reference gene individually and take the average FC.

FC using geometric mean method

$$E = 10^{\frac{-1}{slope\ of\ relative\ standard\ curve}}$$

$$\mathrm{RQ} = E_{ref}^{Cq\ for\ ref\ gene\ with\ control\ cDNA - Cq\ for\ ref\ gene\ with\ treatment\ cDNA}$$

Determine RQ for each reference gene individually and take the geometric mean (using GEOMEAN function in excel) of all three to use as denominator in bellow equation.

$$\mathrm{FC} = \frac{E_{GOI}^{Cq\ for\ GOI\ with\ control\ cDNA - Cq\ for\ GOI\ with\ treatment\ cDNA}}{GEOMEAN(RQ's_{all\ ref\ genes})}$$

3.4 Luciferase Screening Assay

Establishing a Dual Luciferase Assay for Compound Screening

Plasmid Extraction and Amplification

Materials and Reagents

Table 3.16: Materials and reagents for plasmid extraction and amplification.

100 mg/mL ampicillin stock	Nano-Drop
100 X 15 mm petri dishes	One Shot Stble3 chemically competent *E. coli*
37 ˚C incubator	Qiagen MiniPrep Kit
37 ˚C shaking incubator	S.O.C medium
40% glycerol in water	Scissors
70% EtOH	Sorvall Legend X1R centrifuge
Agar	Sterile 1.5 mL snap cap tubes
Autoclave	Sterile cell culture tubes
Bunsen burner & striker	Sterile Milli-Q water
Filter paper with plasmid sample	Sterile silica beads
Kim-wipe	Tryptone
NaCl	Yeast extract

Preparation of essential solutions

Prepare **500 mL of sterile LB medium + ampicillin** by adding 5 g of tryptone, 2.5 g of yeast extract, 5 g of NaCl, and 400 mL of Milli-Q water to a 1 L beaker. Transfer solution to a graduated cylinder and fill to 500 mL with MilliQ water and stir with magnetic stir bar to dissolve. Add to a 1 L Erlenmeyer flask and cover with foil. Autoclave to sterilize. Allow to cool, then working under the flame of a Bunsen burner add 250 µL of 100 mg/mL stock of ampicillin.

Prepare **500 mL of sterile LB agar + ampicillin** by adding 10 g of agar, 5 g of tryptone, 2.5 g of yeast extract, 5 g of NaCl, and 400 mL of Milli-Q water to a 1 L beaker. Transfer solution to a graduated cylinder and fill to 500 mL with MilliQ water and stir with magnetic stir bar to dissolve. Add to a 1 L Erlenmeyer flask and cover with foil. Autoclave to sterilize. Allow to cool to around 50 ºC, then working under the flame of a Bunsen burner, add 250 µL of 100 mg/mL stock of ampicillin pour into petri dishes and cover petri dish. Allow to harden and store petri dishes upside down at 4 ºC.

Procedure

Extract plasmids from filter paper by cutting the filter paper into small pieces using scissors cleaned with water and 70% EtOH and place filter paper into 1.5 mL centrifuge tubes. Add 100 µL of Milli-Q H_2O and push down paper with the pipette tip so that the pieces of filter paper are fully submerged. Incubate for 10 min in a 37 °C water bath then centrifuge at 3,000 rcf for 5 min. Use a pipette tip to compress paper as much as possible to squeeze out the water while aspirating up the water and dispense into a new 1.5 mL tube. Check the concentration on Nano-Drop by first cleaning Nano-Drop with autoclaved Milli-Q H_2O and kim-wipe. On the Nano-Drop interface select “dsDNA”. Pipette 1 µL of autoclaved Milli-Q H_2O to the sensor and close the lid. On the Nano-Drop interface select “Blank”. Clean the sensor with a kim-wipe and confirm the blank reading by repeating. Clean the sensor with a kim-wipe and pipette 1 µL of sample (plasmid extracted from filter paper above) onto the sensor. Close the lid and select “read”. Record A_{260}, $A_{260/280}$, and concentration. Transfect One Shot™ Stble3™ chemically competent cells by warming 1.4 mL of S.O.C medium to room temperature. Warm LB agar + ampicillin plates to 37 °C. Thaw 5 vials (~10 µL/vial) of One Shot™ Stble3™ chemically competent cells on ice. Add 4 µL of each plasmid to a separate vial of One Shot™ Stble3™ chemically competent cells, mix gently by inversion. Incubate 30 min on ice. Heat-shock cells by

placing the vials in a 37 °C water bath for 45 sec. Place the vials back on ice for 2 min, then add 250 µL of room temperature S.O.C. medium to each vial. Tape the vials horizontally in the shaking incubator and set to 220 rpm at 37 °C for 1 h. Working in the sterile field created by a Bunsen burner, pipette the cells from each vial onto an LB agar + ampicillin plate and add about 10 sterile silica plating beads to the plate. Place the lid on the plate and shake in a horizontal direction on the bench top so the silica beads spread the cells around the plate. Remove the lid, invert the plate and gently tamp the beads loose onto a paper towel. Put the lid back on. Place the plates upside-down in a 37 °C incubator overnight. The next day, working under the sterile field created by a Bunsen burner, select four isolated colonies on each plate and grow the colonies in 2.5 mL of LB media containing ampicillin. To select the colony, lightly touch with a 10 µL pipette tip then eject the tip into a Sterile Falcon™ cell culture tube containing 2.5 mL of LB media containing ampicillin. Incubate in a shaking incubator at 37 °C overnight. The next day, working under the sterile field created by a Bunsen burner, pipette 500 µL of the cell suspension into an autoclaved 1.5 mL centrifuge tube containing 500 µL of 40% glycerol in water. Mix and store at -80 °C as a glycerol stock. Use the remaining cell suspension for the MiniPrep. Extract the plasmids from the One Shot™ Stble3™ chemically competent cells by decanting half of the remaining cell suspension into an autoclaved 1.5 mL centrifuge tube and pellet by centrifugation at 11,000 rcf. Discard the supernatant and decant the remaining cell suspension into the same tube. Pellet by centrifugation at 11,000 rcf. Discard the supernatant. Thoroughly resuspend the pellet in 250 µL of ice-cold Buffer A1 by pipetting up and down. Pipette 250 µL of Buffer A2 into the tube and gently mix by inversion. Incubate at room temperature for 5 min. Pipette 300 µL of Buffer A3 into the tube and gently mix by inversion until no blue color from Buffer A2 is observed. Clarify the lysate by centrifuging at 11,000 rcf for 5 min. Pipette supernatant into a

new autoclaved 1.5 mL tube, trying to avoid the white precipitate as much as possible, and centrifuging at 11,000 rcf for 5 min. Pipette 750 µL of the supernatant into a NucleoSpin® Plasmid Column and place the column into one of the 2 mL collection tubes provided by the kit. Centrifuge at 11,000 rcf for 1 min. Discard the flow-through and add the remainder of the supernatant. Centrifuge at 11,000 rcf for 1 min. Discard the flow-through. Wash the silica membrane by pipetting 500 µL of Buffer AW onto the column and centrifuging for 1 min at 11,000 rcf. Discard the flow-through. Pipette 600 µL of Buffer A4 onto the column and centrifuge at 11,000 rcf for 1 min. Discard the flow-through. Centrifuge at 11,000 rcf for 2 min. Place the column into an autoclaved 1.5 mL centrifuge tube. Pipette 50 µL of Buffer AE onto the column and incubate 1 min at room temperature. Centrifuge at 11,000 rcf for 1 min. Discard the column and save the flow-through in the centrifuge tube. Store at -20 °C.

Plasmid Agarose Gel Quality Check

Materials and Reagents

Table 3.17: Materials and reagents for plasmid extraction and amplification.

1 Kb DNA ladder (NEB #3232)	Agarose	GelDock imager
10 mg/mL ethidium bromide	BioLabs CutSmart Buffer	NheI restriction enzyme
6X DNA loading dye	DNA gel apparatus	Tris-acetate-EDTA (TAE)
8-well gel cassette	DNA gel mold	XhoI restriction enzyme

Procedure

Plasmids were thawed on ice and the concentrations checked by Nano-Drop as described previously. To get around 0.5 µg of plasmid, 2 µL of plasmid was used for each digestion reaction. For each plasmid 14 µL Milli-Q H_2O, 2 µL CutSmart® Buffer, 1 µL NheI restriction enzyme, 1 µL of XhoI restriction enzyme, and 2 µL of plasmid were added into a 1.5 mL centrifuge tube. The tubes were briefly vortexed to mix and then spun down in a microcentrifuge. The reactions were incubated for 2 h in a 37 °C water bath. During the incubation, a 1% agarose gel with 0.3 µg/mL ethidium bromide was prepared by dissolving 1.0 g

agarose in 100 mL of TAE buffer which required heating to a boil in a microwave and swirling until the agarose was fully dissolved. The solution was cooled to roughly 40 °C, then 3 µL of ethidium bromide (10 mg/ml) was added. This was then poured into a gel mold with an 8-well cassette and allow to solidify. The gel was transfered to the running apparatus and the apparatus filled with TAE buffer. Then the 8-well cassette was removed. Once plasmid restriction enzyme digestion reaction was complete, the reaction was removed from the water bath and 2 µL of 6X loading dye was added to the reaction. The first lane of the gel received 5 µL of 1 kb DNA ladder. The second through seventh lane, received 15 µL of each one of the reactions. The gel was run at 80 V for 1 h then imaged with a GelDock™ imager.

CsCl Gradient Plasmid Purification

Materials and Reagents

Table 3.18: Materials and reagents for CsCl gradient purification.

1 L beaker	F14S-6X250Y rotor
1 L erlenmeyer flask	Magnetic stir bar
1 L graduated cylinder	MilliQ water
1% ethidium bromide solution	NaCl
100 mg/mL ampicillin stock	NaOAc
15 mL conical tube	NaOH
200 proof ethanol	NH_4OAc
3 mL syringe	SDS
3,500 MWCO dialysis tubing	Soldering iron
70% ethanol	Sorvall 250 mL centrifuge tubes
Aluminum foil	Sorvall Legend X1R centrifuge
Autoclave	Sorvall mX 120 Micro-UltraCentrifuge
Bunsen burner & striker	Sorvall RC 6+ centrifuge
Butanol saturated with water	Stir plate
Clone-Top centrifuge tube metal sealing cap	Syringe needle
Clone-Top Polyallomer 11 X 32 mm centrifuge tubes	Tris-Base
CsCl	Tris-EDTA buffer (TE)
D sucrose	Tryptone
Dialysis tubing clips	Yeast extract
EDTA	

Preparation of essential solutions

Prepare **500 mL of LB medium** by adding 5 g of tryptone, 2.5 g of yeast extract, and 5 g of NaCl to a 1 L graduated cylinder. Fill to 500 mL with MilliQ water and stir with magnetic stir bar to dissolve. Pour 250 mL into two separate 1 L Erlenmeyer flasks. Cover with aluminum foil and autoclave using liquids setting on autoclave. Allow to cool to room temperature before use.

Prepare **1 L of 50X TE Buffer** by adding 60.5 g of Tris-Base, and 18.5 g of EDTA to a 1 L beaker filled with 800 mL of Milli-Q H_2O and stir until dissolved. Pour into 1 L graduated cylinder and fill to 1L with Milli-Q H_2O. Bring to pH 7.5 with HCl.

Prepare **1 L of sucrose solution (5 M sucrose, 50 mM Tris-HCl, 10 mM EMA, pH 8.0)** by adding 1712 g of sucrose, 50 mL of 1 M Tris-HCl pH 8.0, and 20 mL of 0.5 M EMA pH 8.0 to a 1 L volumetric flask and fill to just below neck of flask with MilliQ water. Swirl until dissolved then fill to line with MilliQ water and invert to mix.

Prepare **250 mL of 2% SDS (w/v), 0.2 M NaOH solution** by adding 5.0 g SDS and 2.0 g NaOH to a 250 mL volumetric flask and fill to just below neck of flask with MilliQ water. Swirl until dissolved then fill to line with MilliQ water and invert to mix.

Prepare **100 mL of 7.5 M NH_4OAc** by adding 57.8 g NH_4OAc to a 100 mL volumetric flask and fill to just below neck of flask with MilliQ water. Swirl until dissolved then fill to line with MilliQ water and invert to mix.

Prepare **saturated solution of CsCl in TE buffer** by adding 10g CsCl and 10 mL TE buffer to a 50 mL conical tube. Place on shaker until CsCl is fully dissolved.

Procedure

Culture transformed E. coli cells by working under flame and using aseptic technique. To a sterile 1 L Erlenmeyer flasks with 500 mL of sterile LB medium add 500 µL of 100 mg/mL ampicillin stock. Thaw the glycerol stock of transformed *E. coli* cells on ice and pipette 200 µL

of the stock into a separate flask to inoculate. Place the flask into a shaking 37 °C incubator overnight. Add half of the overnight culture to a Sorvall 250 mL centrifuge bottle and centrifuge in Sorvall RC 6+ Centrifuge at 4,500 rpm (3,100 rcf) for 7 min. Decant off supernatant, add the remaining overnight culture to the bottle, and centrifuge at 4,500 rpm for 7 min. Add 10 mL of sucrose solution and resuspend bacterial pellet by vortexing. Leave for 10 min. at r.t. then vortex. Add 20 mL of 2% SDS (w/v), 0.2 M NaOH solution and invert bottle 8-10 times. Place the bottle on ice and incubate 10 min. Add 15 mL of ice-cold 7.5 M NH_4OAc and incubate for 10 min on ice. Invert bottle until chunks are broken. Centrifuge in Sorvall RC 6+ Centrifuge at 4,500 rpm (3,100 rcf) for 7 min. Gravity filter supernatant through 2 Kimwipes placed in a funnel as the filter into a new Sorvall 250 mL centrifuge bottle. Add 25 mL of isopropanol and invert to mix. Incubate at 4 °C overnight. Centrifuge in Sorvall RC 6+ Centrifuge at 4,500 rpm (3,100 rcf) for 7 min. Decant off supernatant. Let residual isopropanol dry by placing the bottle upside down over a Kimwipe. Add 3 mL (or 2.2 mL) of 1X TE and pipette up and down to resuspend pellet. Incubate at 55 °C in a water bath to help resuspend if necessary. Add 3.2 g of CsCl and vortex to dissolve. Add 30 µL of 1% EtdBr solution. Vortex to mix. Use a 3 mL syringe with needle to add equal volumes of solution into 2 Clone-Top centrifuge tubes (don't fill past the neck of the tube). Place metal sealing cap on Clone-Top centrifuge tubes. Turn on Bunsen burner and heat the tip of the soldering iron. Once soldering iron is hot press evenly on the metal caps until plastic softens. Use metal sealing piece to apply even pressure to the caps and gently push down to seal. Check to ensure the tube is completely sealed before centrifugation. If necessary, repeat until sealed. Centrifuge at 120,000 rpm at 4 °C for 3.5 h in Sorvall mX 120 Micro-UltraCentrifuge. Using a syringe needle, poke 2 holes in lid of each of the Clone-Top centrifuge tubes. Push the needle through one of the holes and use the syringe to remove the pink DNA

band. Combine the bands from the 2 tubes into a single new Clone-Top centrifuge tube and fill to the neck with saturated solution of CsCl in TE buffer. Seal the top as described previously. Centrifuge at 120,000 rpm at 4 °C for 3.5 h in Sorvall mX 120 Micro-UltraCentrifuge. Remove the pink DNA band with a syringe as described previously, but this time dispense into a 15 mL conical tube and don't add saturated CsCl in TE buffer. To remove EtdBr, add an equivalent volume of butanol saturated with water. Pipette up and down to mix then pipette off the upper layer (repeat up to 3X until solution is clear when checked against a white background). Fold dialysis bag over itself 3 times and seal using the dialysis clip. Pipette lower aqueous layer from previous step into the dialysis bag and seal other end similarly by folding 3 times and securing with the dialysis clip. Place bag in beaker with 1 L of TE buffer per bag, stir, and incubate overnight. Transfer from dialysis bag to a new 15 mL conical tube. Add $1/10^{th}$ the volume of 3 M NaOAc and 2.5 volumes of 100% EtOH. Place at -20 °C to precipitate for 2 h. Centrifuge at 4,000 rpm (3,005 rcf) at 4 °C in Sorvall Legend X1R centrifuge for 10 min. Decant supernatant. Add 3 mL of 70% EtOH. Centrifuge at 4,000 rpm (3,005 rcf) at 4 °C in Sorvall Legend X1R centrifuge for 10 min. Decant supernatant. Let residual EtOH dry by placing tube upside down over a Kimwipe. Resuspend in 400 µL TE buffer. Check the concentration via Nano-Drop by first cleaning the Nano-Drop with autoclaved Milli-Q H_2O and kim-wipe. On the Nano-Drop interface select "dsDNA". Pipette 1 µL of autoclaved Milli-Q H_2O to the sensor and close the lid. On the Nano-Drop interface select "Blank". Clean the sensor with a kim-wipe and confirm the blank reading by repeating. Clean the sensor with a kim-wipe and pipette 1 µL of sample (plasmid extracted from filter paper above) onto the sensor. Close the lid and select "read". Record A_{260}, $A_{260/280}$, and concentration.

CD4 SP Dual Luciferase Proof of Concept Assay

Materials and Reagent

Table 3.19: Materials and reagents for dual luciferase proof of concept assay.

0.5 mL plastic tube	Gibco DMEM	Sterile 4 mL glass vials w/ lids
20 mM Stock solutions	Gibco FBS	Sterile 50 mL plastic tube
37 ˚C bead bath	HPLC grade DMSO	Sterile 96-well tissue culture plate
96-well white luminescence plate	Inverted Microscope	Sterile glass pasteur pipette
Cell counter	Micropipettes	Sterile PBS (pH 7.4)
Cell counting slides	Multichannel Pipette	Sterile pipette bulb
Centrifuge	Plate reader	Sterile pipette tips
Class II BSC	Sigma Aldrich 200X Penicillin-Streptomycin	Sterile reagent reservoirs
CO_2 Incubator	SP-Luc pIRES vector	Sterile T75 Flask
Dual Luciferase Reporter System	Sterile 0.2 µM PTFE filter	Trypan blue solution
Gibco 0.25% Trypsin (no EDTA)	Sterile 15 mL plastic tube	X-tremeGENE HP DNA
Gibco 100X NEAA	Sterile 20 mL syringe	

Preparation of essential solutions

Prepare **sterile complete media** under strict aseptic conditions by mixing 440 mL of DMEM, 50 mL of FBS, 5 mL of Pen/Strep, and 5 mL MEM NEAA in a sterile 500 mL bottle. Invert gently to mix.

In a sterile 4 mL glass vial, prepare 3.6 mL of **sterile complete media containing 1% DMSO**. Pipette 36 mL of sterile DMSO into a sterile 4 mL glass vial containing 3,564 mL of sterile complete media.

In a sterile 4 mL glass vial, prepare 3.6 mL of **sterile complete media containing 20 µM compound in 1% DMSO**. Pipette 32.4 mL of sterile DMSO followed by 3.6 µL of 20 mM compound stock into a sterile 4 mL glass vial containing 3,564 mL of sterile complete media.

Procedure

Plate 1.0 X 10^5 cells/well in 1.0 mL of media into 3 wells of a sterile 12-well cell culture plate and cultivate for 24 hours. Warm OPTIMEM, plasmid, & X-Treme reagent to room temperature. Prepare a mock transfection solution in a sterile 2 mL plastic tube by adding 110 µL of OPTIMEM and 1.21 µL of TE buffer. Pipette 100 µL up and down 5 times to mix. Mix the stock X-Treme reagent by inverting the stock bottle, then add 3.3 µL of X-Treme reagent to the

mock transfection solution. Prepare the transfection solution in a sterile 2 mL plastic tube by pipetting 210 µL of OPTIMEM, followed by 2.31 µL of plasmid. Pipette 100 µL up and down 5 times to mix. Mix the stock X-Treme reagent by inverting the stock bottle, then add 6.3 µL of X-Treme reagent to the transfection solution. Incubate both solutions for 30 minutes at r.t. Add 100 µL mock transfection solution into one of the wells with cells. Add 100 µL transfection mix into two of the wells with cells. Incubate for 5 h. Wash the wells with 1.0 mL of 37 °C sterile PBS, then add 100 µL of 37 °C sterile 0.05% Trypsin-EDTA solution and wait approximately 1 min. Monitor the wells the entire time, gently tap the side of the plate about every 15 seconds and as soon as the cells detach add 1,200 µL of 37 °C sterile complete media to each well. Transfer mock transfected well to a sterile 15 mL plastic tube and the CD4sp transfected wells to another sterile 15 mL plastic tube. Gently mix mock transfected cell suspension and add 100 µL/well to 8 wells of a sterile 96-well cell culture plate. Gently mix CD4sp transfected cell suspension and add 100 µL/well to 16 wells of the same sterile 96-well cell culture plate. Incubate the cells overnight. Wash the cells with 200 µL of PBS. First remove the PBS from the control treatment wells, then add 100 mL of 37 ^{o}C sterile complete media containing 1.0% DMSO to the control treatment wells. Then remove the PBS from the CK147 treatment wells, and add 100 mL of 37 ^{o}C sterile complete media containing 20 µM CK147 and 1.0% DMSO to the CK147 treatment wells. Place the plate in a 37 ^{o}C humidity-controlled 5% CO_2 incubator for 6 hours. Remove the media from all wells and wash with 100 µL of ice-cold sterile PBS. Add 35 µL of ice-cold passive lysis buffer and incubate 30 minutes on ice. Pipette 10 µL up and down 7 times each to mix then transfer 10 µL of the lysate from each well to two separate wells of a white 96-well plate. Add 10 µL of LARII and detect immediately using a luminescence plate reader. Add 10

µL of stop and glow solution (mix buffer with substrate in a 50:1 ratio immediately prior to use) and detect immediately using a luminescence plate reader.

CD4 SP Dual Luciferase Assay with DIY Detection Reagents

Materials and Reagent

Table 3.20: Materials and reagents for testing DIY detection reagents.

0.5 mL plastic tube	Luciferin
20 mM Stock solutions	$MgSO_4$
37 ˚C bead bath	Micropipettes
96-well white luminescence plate	Multichannel Pipette
ATP	Na_2EDTA
Cell counter	NaN_3
Cell counting slides	Plate reader
Centrifuge	Promega passive lysis buffer (PLB)
Class II BSC	Sigma Aldrich 200X Penicillin-Streptomycin
CO_2 Incubator	SP-Luc pIRES vector
CoA	Sterile 0.2 µM PTFE filter
Coelenterazine	Sterile 15 mL plastic tube
DTT	Sterile 20 mL syringe
Dual Luciferase Reporter System	Sterile 4 mL glass vials w/ lids
EGTA	Sterile 50 mL plastic tube
Gibco 0.25% Trypsin (no EDTA)	Sterile 96-well tissue culture plate
Gibco 100X NEAA	Sterile glass pasteur pipette
Gibco DMEM	Sterile PBS (pH 7.4)
Gibco FBS	Sterile pipette bulb
Glycylglycine	Sterile pipette tips
HPLC grade DMSO	Sterile reagent reservoirs
Inverted Microscope	Sterile T75 Flask
K_2HPO_4	Trypan blue solution
KH_2PO_4	X-tremeGENE HP DNA

Preparation of essential solutions

Using strict aseptic technique prepare **sterile complete media** by mixing 440 mL of DMEM, 50 mL of FBS, 5 mL of Pen/Strep, and 5 mL MEM NEAA in a sterile 500 mL bottle. Invert gently to mix.

In a sterile 4 mL glass vial, using strict aseptic technique prepare 3.6 mL of **sterile complete media containing 1% DMSO**. Pipette 36 µL of sterile DMSO into a sterile 4 mL glass vial containing 3,564 µL of sterile complete media.

In a sterile 4 mL glass vial, using strict aseptic technique prepare 3.6 mL of **sterile complete media containing 20 µM compound in 1% DMSO**. Pipette 32.4 µL of sterile DMSO followed by 3.6 µL of 20 mM compound stock into a sterile 4 mL glass vial containing 3,564 µL of sterile complete media.

In a 100 mL volumetric flask, prepare 100 mL of **15 mM KH_2PO_4 solution**. Add 0.2041 g KH_2PO_4 and fill to 100 mL with distilled water.

In a 100 mL volumetric flask, prepare 100 mL of **15 mM K_2HPO_4 solution**. Add 0.2613 g K_2HPO_4 and fill to 100 mL with distilled water.

In a 250 mL beaker, prepare **phosphate buffer pH 8.0**. Add 100 mL of K_2HPO_4 and a magnetic stir bar. Stir and place pH probe in liquid. Bring to pH 8.0 by adding KH_2PO_4 dropwise.

In a 50 mL volumetric flask, prepare 50 mL of **10X firefly reagent solution**. Add 0.0771 g of DTT, 0.0384 g of CoA, and 0.0105 g of luciferin and fill to 50 mL with Phosphate buffer pH 8.0. Store at -80 ºC.

In a 25 mL volumetric flask, prepare 25 mL of **firefly assay buffer**. Add 0.0826 g of glycylglycine, 0.0380 g of EGTA, 0.0276 g of ATP, 0.0924 g of $MgSO_4$, and 2.5 mL of 10X firefly reagent solution. Fill to 25 mL with phosphate buffer pH 8.0. Store at -80 ºC.

In a 100 mL volumetric flask, prepare 100 mL of **220 mM KH_2PO_4**. Add 2.994 g KH_2PO_4 and fill to 100 mL with distilled water.

In a 25 mL volumetric flask, prepare 25 mL of **220 mM K_2HPO_4**. Add 2.994 g KH_2PO_4 and fill to 25 mL with distilled water.

Add the solution to a 100 mL beaker with a stir bar and stir. Place pH probe in liquid and add conc. Phosphoric acid to bring pH to 5.1.

In a 5 mL volumetric flask, prepare 5 mL of **10X NaN_3 solution**. Add 0.0211 g of NaN3 to a 5 mL volumetric flask and fill with phosphate buffer pH 5.1.

In a 25 mL volumetric flask, prepare 25 mL of **Renilla assay buffer (no substrate)**. Add 1.6071 g of NaCl, 0.0205 g of Na_2EDTA dihydrate, 0.0110 g of BSA, 2.5 mL of 10X NaN_3 solution, and fill to 25 mL w/ Phosphate buffer pH 5.1. Store at -80 ºC.

In a 5 mL volumetric flask, prepare 5 mL of **472.3 µM coelentrerazine solution**. Add 1 mL of phosphate buffer pH 5.1 to the new vial of coelenterazine from AmBeed (lot: A544127-001). Allow to dissolve then transfer to 5 mL volumetric flask and fill to 5 mL with phosphate buffer pH 5.1. Store at -80 ºC.

Procedure

Plate 1.0 X 10^5 cells/well in 1.0 mL of media into 3 wells of a sterile 12-well cell culture plate and cultivate for 24 hours. Warm OPTIMEM, plasmid, & X-Treme reagent to room temperature. Prepare a mock transfection solution in a sterile 2 mL plastic tube by adding 110 µL of OPTIMEM and 1.21 µL of TE buffer. Pipette 100 µL up and down 5 times to mix. Mix the stock X-Treme reagent by inverting the stock bottle, then add 3.3 µL of X-Treme reagent to the mock transfection solution. Prepare the transfection solution in a sterile 2 mL plastic tube by pipetting 210 µL of OPTIMEM, followed by 2.31 µL of plasmid. Pipette 100 µL up and down 5 times to mix. Mix the stock X-Treme reagent by inverting the stock bottle, then add 6.3 µL of X-Treme reagent to the transfection solution. Incubate both solutions for 30 minutes at r.t. Add 100 µL mock transfection solution into one of the wells with cells. Add 100 µL transfection mix into two of the wells with cells. Incubate for 5 h. Wash the wells with 1.0 mL of 37 °C sterile PBS,

then add 100 µL of 37 °C sterile 0.05% Trypsin-EDTA solution and wait approximately 1 min. Monitor the wells the entire time, gently tap the side of the plate about every 15 seconds and as soon as the cells detach add 1,200 µL of 37 °C sterile complete media to each well. Transfer mock transfected well to a sterile 15 mL plastic tube and the CD4sp transfected wells to another sterile 15 mL plastic tube. Gently mix mock transfected cell suspension and add 100 µL/well to 8 wells of a sterile 96-well cell culture plate. Gently mix CD4sp transfected cell suspension and add 100 µL/well to 16 wells of the same sterile 96-well cell culture plate. Incubate the cells overnight. Wash the cells with 200 µL of PBS. First remove the PBS from the control treatment wells, then add 100 mL of 37 ºC sterile complete media containing 1.0% DMSO to the control treatment wells. Then remove the PBS from the CK147 treatment wells, and add 100 mL of 37 ºC sterile complete media containing 20 µM CK147 and 1.0% DMSO to the CK147 treatment wells. Place the plate in a 37 ºC humidity-controlled 5% CO_2 incubator for 6 hours. Remove the media from all wells and wash with 100 µL of ice-cold sterile PBS. Add 35 µL of ice-cold passive lysis buffer and incubate 30 minutes on ice. Allow detection reagents to warm to r.t., then mix 12.1 µL of 472.3 µM coelenterazine with 3.989 mL of Renilla assay buffer. Mix 8 µL SAG substrate with 400 µL SAG buffer. After the 30-minute incubation, pipette 10 µL of the lysate up and down 7 times to mix and transfer 10 µL of the lysate from each well to two separate wells of a white 96-well plate. Add 10 µL of LARII, pipette up and down 3 times. Immediately detect luminescence using plate reader, reading from the top with 0.3 sec. integration time. Add 10 µL of stop and glow solution, pipette up and down 3 times. Immediately detect luminescence using plate reader, reading from the top with 0.3 sec. integration time. Alternatively, add 10 µL of firefly assay buffer, pipette up and down 3 times. Immediately detect luminescence using plate reader, reading from the top with 0.3 sec.

integration time. Add 10 µL of Renilla assay buffer, pipette up and down 3 times. Immediately detect luminescence using plate reader, reading from the top with 0.3 sec. integration time.

Section 4: References

(1) Abdel-Hady, M.; Kelly, D. Chronic Hepatitis B in Children and Adolescents: Epidemiology and Management. *Pediatr Drugs* **2013**, *15* (4), 311–317. https://doi.org/10.1007/s40272-013-0010-z.

(2) Seto, W.-K.; Lo, Y.-R.; Pawlotsky, J.-M.; Yuen, M.-F. Chronic Hepatitis B Virus Infection. *The Lancet* **2018**, *392* (10161), 2313–2324. https://doi.org/10.1016/S0140-6736(18)31865-8.

(3) Tsai, E. Review of Current and Potential Treatments for Chronic Hepatitis B Virus Infection. *Gastroenterol Hepatol (N Y)* **2021**, *17* (8), 367–376.

(4) McNaughton, A. L.; D'Arienzo, V.; Ansari, M. A.; Lumley, S. F.; Littlejohn, M.; Revill, P.; McKeating, J. A.; Matthews, P. C. Insights From Deep Sequencing of the HBV Genome—Unique, Tiny, and Misunderstood. *Gastroenterology* **2019**, *156* (2), 384–399. https://doi.org/10.1053/j.gastro.2018.07.058.

(5) Seeger, C.; Mason, W. S. Molecular Biology of Hepatitis B Virus Infection. *Virology* **2015**, *479–480*, 672–686. https://doi.org/10.1016/j.virol.2015.02.031.

(6) Mitra, B.; Thapa, R. J.; Guo, H.; Block, T. M. Host Functions Used by Hepatitis B Virus to Complete Its Life Cycle: Implications for Developing Host-Targeting Agents to Treat Chronic Hepatitis B. *Antiviral Research* **2018**, *158*, 185–198. https://doi.org/10.1016/j.antiviral.2018.08.014.

(7) Zheng, C.; Fu, Y.; Xu, Z.; Zou, Y.; Deng, K. Hepatitis B Virus Core Protein Dimer-dimer Interface Is Critical for Viral Replication. *Mol Med Report* **2018**. https://doi.org/10.3892/mmr.2018.9620.

(8) Zlotnick, A.; Venkatakrishnan, B.; Tan, Z.; Lewellyn, E.; Turner, W.; Francis, S. Core Protein: A Pleiotropic Keystone in the HBV Lifecycle. *Antiviral Research* **2015**, *121*, 82–93. https://doi.org/10.1016/j.antiviral.2015.06.020.

(9) Yang, S.; Shen, Z.; Kang, Y.; Sun, L.; Viswanathan, U.; Guo, H.; Zhou, T.; Dai, X.; Chang, J.; Zhang, J.; Guo, J.-T. A Putative Amphipathic Alpha Helix in Hepatitis B Virus Small Envelope Protein Plays a Critical Role in the Morphogenesis of Subviral Particles. *J Virol* **2021**, *95* (8), e02399-20. https://doi.org/10.1128/JVI.02399-20.

(10) Yan, H.; Zhong, G.; Xu, G.; He, W.; Jing, Z.; Gao, Z.; Huang, Y.; Qi, Y.; Peng, B.; Wang, H.; Fu, L.; Song, M.; Chen, P.; Gao, W.; Ren, B.; Sun, Y.; Cai, T.; Feng, X.; Sui, J.; Li, W. Sodium Taurocholate Cotransporting Polypeptide Is a Functional Receptor for Human Hepatitis B and D Virus. *eLife* **2012**, *1*, e00049. https://doi.org/10.7554/eLife.00049.

(11) Revill, P. A.; Chisari, F. V.; Block, J. M.; Dandri, M.; Gehring, A. J.; Guo, H.; Hu, J.; Kramvis, A.; Lampertico, P.; Janssen, H. L. A.; Levrero, M.; Li, W.; Liang, T. J.; Lim, S.-G.; Lu, F.; Penicaud, M. C.; Tavis, J. E.; Thimme, R.; Zoulim, F.; Arbuthnot, P.; Boonstra, A.; Chang, K.-M.; Chen, P.-J.; Glebe, D.; Guidotti, L. G.; Fellay, J.; Ferrari, C.; Jansen, L.; Lau, D. T. Y.; Lok, A. S.; Maini, M. K.; Mason, W.; Matthews, G.; Paraskevis, D.; Petersen, J.; Rehermann, B.; Shin, E.-C.; Thompson, A.; Van Bömmel, F.; Wang, F.-S.; Watashi, K.; Yang, H.-C.; Yuan, Z.; Yuen, M.-F.; Block, T.; Miller, V.; Protzer, U.; Bréchot, C.; Locarnini, S.; Peters, M. G.; Schinazi, R. F. A Global Scientific Strategy to Cure Hepatitis B. *The Lancet Gastroenterology & Hepatology* **2019**, *4* (7), 545–558. https://doi.org/10.1016/S2468-1253(19)30119-0.

(12) Scaglioni, P. P.; Melegari, M.; Wands, J. R. Posttranscriptional Regulation of Hepatitis B Virus Replication by the Precore Protein. *J Virol* **1997**, *71* (1), 345–353. https://doi.org/10.1128/jvi.71.1.345-353.1997.

(13) Revill, P.; Yuen, L.; Walsh, R.; Perrault, M.; Locarnini, S.; Kramvis, A. Bioinformatic Analysis of the Hepadnavirus E-Antigen and Its Precursor Identifies Remarkable Sequence Conservation in All Orthohepadnaviruses. *J. Med. Virol.* **2010**, *82* (1), 104–115. https://doi.org/10.1002/jmv.21645.

(14) Ito, K.; Kim, K.-H.; Lok, A. S.-F.; Tong, S. Characterization of Genotype-Specific Carboxyl-Terminal Cleavage Sites of Hepatitis B Virus e Antigen Precursor and Identification of Furin as the Candidate Enzyme. *J Virol* **2009**, *83* (8), 3507–3517. https://doi.org/10.1128/JVI.02348-08.

(15) Hu, J.; Cheng, J.; Tang, L.; Hu, Z.; Luo, Y.; Li, Y.; Zhou, T.; Chang, J.; Guo, J.-T. Virological Basis for the Cure of Chronic Hepatitis B. *ACS Infect. Dis.* **2019**, *5* (5), 659–674. https://doi.org/10.1021/acsinfecdis.8b00081.

(16) Ruan, P.; Zhou, R.; He, C.; Huang, C.; Lin, M.; Yin, H.; Dai, X.; Sun, J. Two Fragments of HBV DNA Integrated into chrX: 11009033 and Its Genetic Regulation in HepG2.2.15. *Mol Med Rep* **2023**, *27* (5), 98. https://doi.org/10.3892/mmr.2023.12985.

(17) Sebaugh, J. L. Guidelines for Accurate EC50/IC50 Estimation. *Pharm Stat* **2011**, *10* (2), 128–134. https://doi.org/10.1002/pst.426.

(18) Higa, L. M.; Caruso, M. B.; Canellas, F.; Soares, M. R.; Oliveira-Carvalho, A. L.; Chapeaurouge, D. A.; Almeida, P. M.; Perales, J.; Zingali, R. B.; Da Poian, A. T. Secretome of HepG2 Cells Infected with Dengue Virus: Implications for Pathogenesis. *Biochimica et Biophysica Acta (BBA) - Proteins and Proteomics* **2008**, *1784* (11), 1607–1616. https://doi.org/10.1016/j.bbapap.2008.06.015.

(19) Liaci, A. M.; Förster, F. Take Me Home, Protein Roads: Structural Insights into Signal Peptide Interactions during ER Translocation. *IJMS* **2021**, *22* (21), 11871. https://doi.org/10.3390/ijms222111871.

(20) Lin, Y.; Zhao, Z.; Huang, A.; Lu, M. Interplay between Cellular Autophagy and Hepatitis B Virus Replication: A Systematic Review. *Cells* **2020**, *9* (9), 2101. https://doi.org/10.3390/cells9092101.

(21) Hu, Q.; Zhang, F.; Duan, L.; Wang, B.; Ye, Y.; Li, P.; Li, D.; Yang, S.; Zhou, L.; Chen, W. E-Cadherin Plays a Role in Hepatitis B Virus Entry Through Affecting Glycosylated Sodium-Taurocholate Cotransporting Polypeptide Distribution. *Front. Cell. Infect. Microbiol.* **2020**, *10*, 74. https://doi.org/10.3389/fcimb.2020.00074.

(22) Baietti, M. F.; Zhang, Z.; Mortier, E.; Melchior, A.; Degeest, G.; Geeraerts, A.; Ivarsson, Y.; Depoortere, F.; Coomans, C.; Vermeiren, E.; Zimmermann, P.; David, G. Syndecan–Syntenin–ALIX Regulates the Biogenesis of Exosomes. *Nat Cell Biol* **2012**, *14* (7), 677–685. https://doi.org/10.1038/ncb2502.

(23) Hou, X.; Wei, H.; Rajagopalan, C.; Jiang, H.; Wu, Q.; Zaman, K.; Xie, Y.; Sun, F. Dissection of the Role of VIMP in Endoplasmic Reticulum-Associated Degradation of CFTRΔF508. *Sci Rep* **2018**, *8* (1), 4764. https://doi.org/10.1038/s41598-018-23284-8.

(24) Elangovan, M.; Chong, H. K.; Park, J. H.; Yeo, E. J.; Yoo, Y. J. The Role of Ubiquitin-Conjugating Enzyme Ube2j1 Phosphorylation and Its Degradation by Proteasome during Endoplasmic Stress Recovery. *J. Cell Commun. Signal.* **2017**, *11* (3), 265–273. https://doi.org/10.1007/s12079-017-0386-6.

(25) Christianson, J. C.; Shaler, T. A.; Tyler, R. E.; Kopito, R. R. OS-9 and GRP94 Deliver Mutant A1-Antitrypsin to the Hrd1–SEL1L Ubiquitin Ligase Complex for ERAD. *Nat Cell Biol* **2008**, *10* (3), 272–282. https://doi.org/10.1038/ncb1689.

(26) Cui, X. A.; Zhang, H.; Palazzo, A. F. P180 Promotes the Ribosome-Independent Localization of a Subset of mRNA to the Endoplasmic Reticulum. *PLoS Biol* **2012**, *10* (5), e1001336. https://doi.org/10.1371/journal.pbio.1001336.

(27) Radons, J. The Human HSP70 Family of Chaperones: Where Do We Stand? *Cell Stress and Chaperones* **2016**, *21* (3), 379–404. https://doi.org/10.1007/s12192-016-0676-6.

(28) Seo, H. W.; Seo, J. P.; Jung, G. Heat Shock Protein 70 and Heat Shock Protein 90 Synergistically Increase Hepatitis B Viral Capsid Assembly. *Biochemical and Biophysical Research Communications* **2018**, *503* (4), 2892–2898. https://doi.org/10.1016/j.bbrc.2018.08.065.

(29) Higashio, H.; Kohno, K. A Genetic Link between the Unfolded Protein Response and Vesicle Formation from the Endoplasmic Reticulum. *Biochemical and Biophysical Research Communications* **2002**, *296* (3), 568–574. https://doi.org/10.1016/S0006-291X(02)00923-3.

(30) Jiang, X.; Zhang, B.; Zhao, J.; Xu, Y.; Han, H.; Su, K.; Tao, J.; Fan, R.; Zhao, X.; Li, L.; Li, M. D. Identification and Characterization of SEC24D as a Susceptibility Gene for Hepatitis B Virus Infection. *Sci Rep* **2019**, *9* (1), 13425. https://doi.org/10.1038/s41598-019-49777-8.

(31) Zhang, R.-N.; Pan, Q.; Zhang, Z.; Cao, H.-X.; Shen, F.; Fan, J.-G. Saturated Fatty Acid Inhibits Viral Replication in Chronic Hepatitis B Virus Infection With Nonalcoholic Fatty Liver Disease by Toll-Like Receptor 4-Mediated Innate Immune Response. *Hepat Mon* **2015**, *15* (5). https://doi.org/10.5812/hepatmon.15(5)2015.27909.

(32) Qiu, X.-B.; Shao, Y.-M.; Miao, S.; Wang, L. The Diversity of the DnaJ/Hsp40 Family, the Crucial Partners for Hsp70 Chaperones. *Cell. Mol. Life Sci.* **2006**, *63* (22), 2560–2570. https://doi.org/10.1007/s00018-006-6192-6.

(33) Synofzik, M.; Haack, T. B.; Kopajtich, R.; Gorza, M.; Rapaport, D.; Greiner, M.; Schönfeld, C.; Freiberg, C.; Schorr, S.; Holl, R. W.; Gonzalez, M. A.; Fritsche, A.; Fallier-Becker, P.; Zimmermann, R.; Strom, T. M.; Meitinger, T.; Züchner, S.; Schüle, R.; Schöls, L.; Prokisch, H. Absence of BiP Co-Chaperone DNAJC3 Causes Diabetes Mellitus and Multisystemic Neurodegeneration. *The American Journal of Human Genetics* **2014**, *95* (6), 689–697. https://doi.org/10.1016/j.ajhg.2014.10.013.

(34) Rosam, M.; Krader, D.; Nickels, C.; Hochmair, J.; Back, K. C.; Agam, G.; Barth, A.; Zeymer, C.; Hendrix, J.; Schneider, M.; Antes, I.; Reinstein, J.; Lamb, D. C.; Buchner, J. Bap (Sil1) Regulates the Molecular Chaperone BiP by Coupling Release of Nucleotide and Substrate. *Nat Struct Mol Biol* **2018**, *25* (1), 90–100. https://doi.org/10.1038/s41594-017-0012-6.

(35) Daverkausen-Fischer, L.; Draga, M.; Pröls, F. Regulation of Translation, Translocation, and Degradation of Proteins at the Membrane of the Endoplasmic Reticulum. *IJMS* **2022**, *23* (10), 5576. https://doi.org/10.3390/ijms23105576.

(36) Pauwels, E.; Rutz, C.; Provinciael, B.; Stroobants, J.; Schols, D.; Hartmann, E.; Krause, E.; Stephanowitz, H.; Schülein, R.; Vermeire, K. A Proteomic Study on the Membrane Protein Fraction of T Cells Confirms High Substrate Selectivity for the ER Translocation Inhibitor Cyclotriazadisulfonamide. *Molecular & Cellular Proteomics* **2021**, *20*, 100144. https://doi.org/10.1016/j.mcpro.2021.100144.

(37) Pauwels, E.; Provinciael, B.; Camps, A.; Hartmann, E.; Vermeire, K. Reduced DNAJC3 Expression Affects Protein Translocation across the ER Membrane and Attenuates the Down-Modulating Effect of the Translocation Inhibitor Cyclotriazadisulfonamide. *IJMS* **2022**, *23* (2), 584. https://doi.org/10.3390/ijms23020584.

(38) Pobre, K. F. R.; Poet, G. J.; Hendershot, L. M. The Endoplasmic Reticulum (ER) Chaperone BiP Is a Master Regulator of ER Functions: Getting by with a Little Help from ERdj Friends. *Journal of Biological Chemistry* **2019**, *294* (6), 2098–2108. https://doi.org/10.1074/jbc.REV118.002804.

(39) Olivari, S.; Cali, T.; Salo, K. E. H.; Paganetti, P.; Ruddock, L. W.; Molinari, M. EDEM1 Regulates ER-Associated Degradation by Accelerating de-Mannosylation of Folding-Defective Polypeptides and by Inhibiting Their Covalent Aggregation. *Biochemical and Biophysical Research Communications* **2006**, *349* (4), 1278–1284. https://doi.org/10.1016/j.bbrc.2006.08.186.

(40) Shen, Y.; Hendershot, L. M. ERdj3, a Stress-Inducible Endoplasmic Reticulum DnaJ Homologue, Serves as a CoFactor for BiP's Interactions with Unfolded Substrates. *MBoC* **2005**, *16* (1), 40–50. https://doi.org/10.1091/mbc.e04-05-0434.

(41) Yamamoto, Y.; Kimura, T.; Momohara, S.; Takeuchi, M.; Tani, T.; Kimata, Y.; Kadokura, H.; Kohno, K. A Novel ER J-Protein DNAJB12 Accelerates ER-Associated Degradation of Membrane Proteins Including CFTR. *Cell Struct. Funct.* **2010**, *35* (2), 107–116. https://doi.org/10.1247/csf.10023.

(42) Ligat, G.; Verrier, E. R.; Nassal, M.; Baumert, T. F. Hepatitis B Virus–Host Interactions and Novel Targets for Viral Cure. *Current Opinion in Virology* **2021**, *49*, 41–51. https://doi.org/10.1016/j.coviro.2021.04.009.

(43) Boulon, R.; Blanchet, M.; Lemasson, M.; Vaillant, A.; Labonté, P. Characterization of the Antiviral Effects of REP 2139 on the HBV Lifecycle in Vitro. *Antiviral Research* **2020**, *183*, 104853. https://doi.org/10.1016/j.antiviral.2020.104853.

(44) Dobrica, M.-O.; Lazar, C.; Branza-Nichita, N. N-Glycosylation and N-Glycan Processing in HBV Biology and Pathogenesis. *Cells* **2020**, *9* (6), 1404. https://doi.org/10.3390/cells9061404.

(45) Strasser, R. Protein Quality Control in the Endoplasmic Reticulum of Plants. *Annu. Rev. Plant Biol.* **2018**, *69* (1), 147–172. https://doi.org/10.1146/annurev-arplant-042817-040331.

(46) Simsek, E.; Lu, X.; Ouzounov, S.; Block, T. M.; Mehta, A. S. α-Glucosidase Inhibitors Have a Prolonged Antiviral Effect against Hepatitis B Virus through the Sustained Inhibition of the Large and Middle Envelope Glycoproteins. *Antivir Chem Chemother* **2006**, *17* (5), 259–267. https://doi.org/10.1177/095632020601700503.

(47) Arnold, S. M.; Fessler, L. I.; Fessler, J. H.; Kaufman, R. J. Two Homologues Encoding Human UDP-Glucose:Glycoprotein Glucosyltransferase Differ in mRNA Expression and Enzymatic Activity. *Biochemistry* **2000**, *39* (9), 2149–2163. https://doi.org/10.1021/bi9916473.

(48) Lu, L.; Zhou, J.; Shi, J.; Peng, X.; Qi, X.; Wang, Y.; Li, F.; Zhou, F.-Y.; Liu, L.; Liu, Z.-Q. Drug-Metabolizing Activity, Protein and Gene Expression of UDP-Glucuronosyltransferases Are Significantly Altered in Hepatocellular Carcinoma Patients. *PLoS ONE* **2015**, *10* (5), e0127524. https://doi.org/10.1371/journal.pone.0127524.

(49) Yan, T.; Gao, S.; Peng, X.; Shi, J.; Xie, C.; Li, Q.; Lu, L.; Wang, Y.; Zhou, F.; Liu, Z.; Hu, M. Significantly Decreased and More Variable Expression of Major CYPs and UGTs in Liver Microsomes Prepared from HBV-Positive Human Hepatocellular Carcinoma and Matched Pericarcinomatous Tissues Determined Using an Isotope Label-Free UPLC-MS/MS Method. *Pharm Res* **2015**, *32* (3), 1141–1157. https://doi.org/10.1007/s11095-014-1525-x.

(50) Hu, S.; Jiang, L.-B.; Zou, X.-J.; Yi, W.; Tian, D.-Y. Hepatitis B Virus Upregulates Host Expression of α-1,2-Mannosidases *via* the PPARα Pathway. *WJG* **2016**, *22* (43), 9534. https://doi.org/10.3748/wjg.v22.i43.9534.

(51) Wang, L.; Zhu, L.; Wang, C. The Endoplasmic Reticulum Sulfhydryl Oxidase Ero1β Drives Efficient Oxidative Protein Folding with Loose Regulation. *Biochemical Journal* **2011**, *434* (1), 113–121. https://doi.org/10.1042/BJ20101357.

(52) Mezghrani, A. Manipulation of Oxidative Protein Folding and PDI Redox State in Mammalian Cells. *The EMBO Journal* **2001**, *20* (22), 6288–6296. https://doi.org/10.1093/emboj/20.22.6288.

(53) Zeyen, L.; Döring, T.; Prange, R. Hepatitis B Virus Exploits ERGIC-53 in Conjunction with COPII to Exit Cells. *Cells* **2020**, *9* (8), 1889. https://doi.org/10.3390/cells9081889.

(54) Iguchi, K.; Sada, R.; Matsumoto, S.; Kimura, H.; Zen, Y.; Akita, M.; Gon, H.; Fukumoto, T.; Kikuchi, A. DKK1-CKAP4 Signal Axis Promotes Hepatocellular Carcinoma Aggressiveness. *Cancer Sci* **2023**, *114* (5), 2063–2077. https://doi.org/10.1111/cas.15743.

(55) Das, P.; Dudley, J. P. How Viruses Use the VCP/P97 ATPase Molecular Machine. *Viruses* **2021**, *13* (9), 1881. https://doi.org/10.3390/v13091881.

(56) Jiao, B.-Y.; Lin, W.-S.; She, F.-F.; Chen, W.-N.; Lin, X. Hepatitis B Virus X Protein Enhances Activation of Nuclear Factor κB through Interaction with Valosin-Containing Protein. *Arch Virol* **2011**, *156* (11), 2015–2021. https://doi.org/10.1007/s00705-011-1099-4.

(57) Liu, D.; Wu, A.; Cui, L.; Hao, R.; Wang, Y.; He, J.; Guo, D. Hepatitis B Virus Polymerase Suppresses NF-κB Signaling by Inhibiting the Activity of IKKs via Interaction with Hsp90β. *PLoS ONE* **2014**, *9* (3), e91658. https://doi.org/10.1371/journal.pone.0091658.

(58) Liu, Y.; Testa, J. S.; Philip, R.; Block, T. M.; Mehta, A. S. A Ubiquitin Independent Degradation Pathway Utilized by a Hepatitis B Virus Envelope Protein to Limit Antigen Presentation. *PLoS ONE* **2011**, *6* (9), e24477. https://doi.org/10.1371/journal.pone.0024477.

(59) Lumangtad, L. A.; Bell, T. W. The Signal Peptide as a New Target for Drug Design. *Bioorganic & Medicinal Chemistry Letters* **2020**, *30* (10), 127115. https://doi.org/10.1016/j.bmcl.2020.127115.
(60) Chen, J.; Bao, Z.; Huang, Y.; Wang, Z.; Zhao, Y. Selection of Suitable Reference Genes for qPCR Gene Expression Analysis of HepG2 and L02 in Four Different Liver Cell Injured Models. *Biomed Res Int* **2020**, *2020*, 8926120. https://doi.org/10.1155/2020/8926120.
(61) Dyer, B. W.; Ferrer, F. A.; Klinedinst, D. K.; Rodriguez, R. A Noncommercial Dual Luciferase Enzyme Assay System for Reporter Gene Analysis. *Analytical Biochemistry* **2000**, *282* (1), 158–161. https://doi.org/10.1006/abio.2000.4605.

Chapter 4: Developing 96-well Assays for ACE2, CX43, and MTT

Section 1: Introduction

1.1 Screening, toxicity and validation of potential Covid-19 antivirals

Covid-19 caused a global pandemic, a huge number of deaths and enormous economic consequences. Early in the outbreak the lack of known and effective drugs was a major issue; scientists raced to find solutions. The causative agent, SARS-CoV-2, enters cells through interaction with the cell surface ACE2 protease. This protein quickly became a target of interest for novel therapeutic approaches.[1] The protease contains a signal peptide with a serine residue in the hydrophobic region which could be a h-bond donor to interact with the sulfonamide group of CADA analogues causing down-modulation (**Fig. 4.1A**). Previous studies had developed assays to detect ACE2 activity using a commercially available fluorogenic ACE2 substrate (**Fig. 4.1B**).[2,3] These assays were adapted to a 96-well plate drug screening platform for CADA analogues.

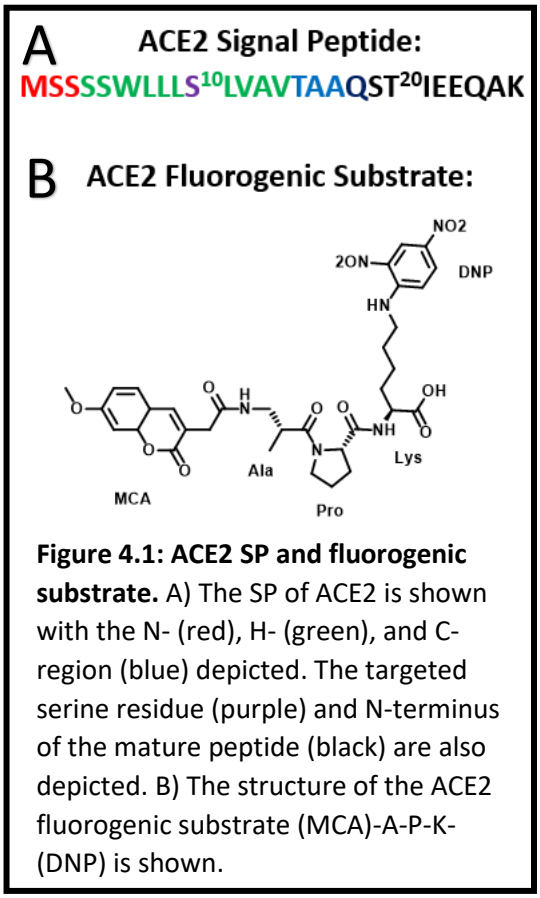

Figure 4.1: ACE2 SP and fluorogenic substrate. A) The SP of ACE2 is shown with the N- (red), H- (green), and C-region (blue) depicted. The targeted serine residue (purple) and N-terminus of the mature peptide (black) are also depicted. B) The structure of the ACE2 fluorogenic substrate (MCA)-A-P-K-(DNP) is shown.

We used Calu-3 cells because they are lung cells with high levels of ACE2 expression which makes them relevant for COVID-19 infections.[3] A major difference between the literature and our assay was that in the literature they used compounds which almost instantly inhibited ACE2 enzymatic activity while our compounds work by reducing protein levels over time. The reason it takes time to see a reduction in protein levels is that CADA analogues prevent the synthesis of new proteins, but the proteins already

present must turnover by being degraded by cellular proteases before a decrease can be detected. Due to the slow turnover rate of ACE2, this required an extended treatment time. The cells were grown in 96-well plates, then treated by incubation with compound or vehicle control (DMSO), the cells were washed with PBS and the ACE2 fluorogenic substrate was added. After a 30-minute incubation, the supernatant was removed and added to a black 96-well plate for fluorescent measurement. The long treatment period created the potential for toxic compounds to kill cells and reduce ACE2 levels in a non-specific fashion, producing false positives. As such an MTT based viability screen was developed to screen out toxic compounds. Compounds with promising ACE2 down-modulatory activity were checked by qRT-PCR to confirm that the down-modulatory mechanism was not due to reduced mRNA levels. Furthermore, the assay was validated by western blot to confirm the down-modulation of ACE2 by active compounds.

1.2 Developing a Screening Assay for Cx43 Down-modulation

There is an unmet need in the realm of therapeutics for preventing preterm birth.[4,5] Connexin 43 (Cx43) forms channels between two cells which allow for ion and small molecule exchange.[6] Cx43 has been identified as a potential therapeutic target in connection with transmission of contractile signals in uterine smooth muscle cells (USMCs). Inhibition of Cx43 reduces myometrial contractions; however, known inhibitors are toxic or nonspecific.[7] While Cx43 does not have a SP it is targeted to the Sec61 channel by its 1st TMD which must undergo a flip-turn in a similar fashion to SPs during channel gating. The TMD contains two serine residues that could be targeted by H-bonding as well as a positively charged arginine and negatively charged glutamic acid residue that are separated by nine amino acids and would be on the same face of an alpha-helix. Western blots reveled several compounds reduced cellular levels of Cx43 after treatment and that RK006 and TK047 were the most potent. RK006 is capable of producing a

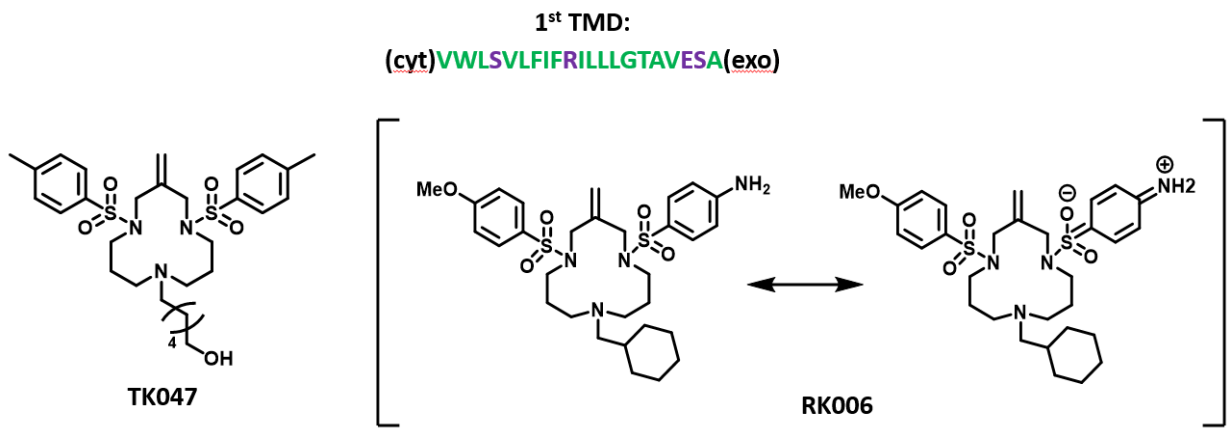

Figure 4.2: Cx43 1st TMD and potent inhibitors. The amino acid sequence of the 1st TMD is depicted with the potentially targetable polar and charged residues (purple). The structures of CADA analogues shown to have strong down-modulatory activity are shown below the 1st TMD.

resonance structure that contains both positive and negative charges separated by a distance sufficient to match the distance which separates the charges on Cx43's 1st TMD. While TK047 has an extended aliphatic tail ending in a hydroxyl group capable of H-bonding with one serine while the sulfonamide group of one side-arm H-bonds with the other serine (**Fig. 4.2**). Previous studies using fluorescence microscopy had shown cells expressing different levels of Cx43 could be identified based on uptake and subsequent fluorescence of ethidium bromide (EtBr) due to the ability of EtBr to pass through the channels.[8,9] The procedures in these previous studies were modified and adapted to develop a novel higher throughput procedure to screen for the ability of CADA analogues to reduce Cx43 levels in pregnant human USMCs (phUSMCs) grown in 96-well plates. This assay was capable of correctly identifying the most potent Cx43 inhibitory CADA analogue as determined by Western blot.

1.3 Determining the CC_{50} for VGD040 on HEK293 Cells

The thyroid-stimulating hormone receptor (TSHR) is a GPCR cell surface glycoprotein expressed as a single subunit that undergoes cleavage during maturation to become two subunits held together by disulfide bonds.[10,11] TSHR is the receptor for the thyroid-stimulating hormone

(TSH) and when TSHR binds TSH a signaling cascade occurs that results in the proliferation of thyrocytes and increased production of thyroid hormone (TH).[12] Graves's disease is a common condition that affects about 1% of the American population.[13] This condition occurs when autoantibodies bind to TSHR and over stimulate TH production.[12] This manifests in a variety of symptoms including sensitivity to heat, weight loss, anxiety, goiter, frequent bowel movements, and loss of sexual desire.[14] Currently there are multiple treatment options, but all have serious limitations such as relapse, requirement of life-long medication regimens, or risk of serious complications.[15–17]

New approaches to treatment are desired. A CADA analogue, VGD040, was shown by a collaborators Dr. Christine Krieger and Dr. Marvin Gershengorn to selectively down-modulate TSHR to a moderate degree, which in turn reduced TH production in mice with no observed toxicity. Flow cytometry experiments were conducted to measure TSHR levels in response to drug treatment in HEK293 cells overexpressing TSHR. A follow-up experiment on the potential toxicity of VGD040 on HEK293 cells was desired for the publication of the results. I conducted dose response experiments by treatment of HEK293 cells with VGD040 in order to calculate the CC50 of VGD040 on HEK293 cells. The results showed that the compound was not toxic at the concentration required to down-modulate TSHR expression levels. TSHR has a SP and the mechanism of down-modulation may be SP-dependent via interaction with Sec61 to block entry into the ER. The SP of TSHR has two negatively charged aspartic acid residues and VGD040 has a single side-arm giving it a secondary amine which could be protonated to give it a positive charge, making it capable of forming a salt-bridge with one of the aspartic acid residues (**Fig. 4.3**). However, glycosylation is also important to the maturation and trafficking of TSHR so it's

down-modulation by VGD040 could be linked to the broad disturbances observed for TL020 on protein processing in the ER related to glycosylation and maturation of glycoproteins. Further validation of the mechanism of action of TSHR down-modulation is warranted.

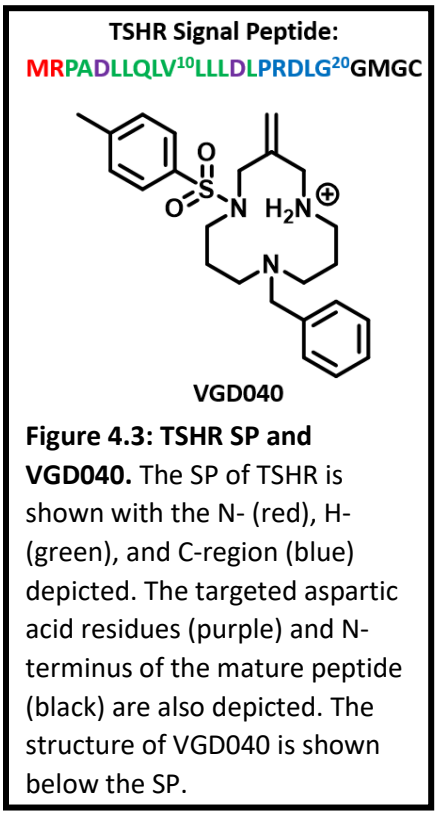

Figure 4.3: TSHR SP and VGD040. The SP of TSHR is shown with the N- (red), H- (green), and C-region (blue) depicted. The targeted aspartic acid residues (purple) and N-terminus of the mature peptide (black) are also depicted. The structure of VGD040 is shown below the SP.

1.4 Stability of novel 4-hydroxycoumarin imines

Myosins are proteins which cause movement in a concerted fashion by hydrolysis of ATP which causes a ratcheting-like movement along actin filaments. The three standard subdomains are the ATP binding motor domain, the bridging neck domain, and the tail domain which can act as an anchor or attachment point for cargo or other functional domains. This diverse superfamily of proteins comes in 15 classes. Class II myosins come in a large variety of isoforms which are found in muscles and the cytoplasm of animal cells (non-muscle myosin) and were the first class to be discovered.[18] Beyond their breadth of diversity found in this protein superfamily the importance of myosins can also be demonstrated by the breadth of essential functions from cellular division, cellular movement, tissue movement, communication, sensors, metabolism, cytoplasmic streaming, and more.[19] Inhibition of myosin could have medicinal value, but due to the importance of myosin for so many functions it is important to be able to selectively target a single isoform to avoid undesirable and potentially lethal side effects. Blebbistatin is a research chemical that broadly inhibits class II myosin but lacks medicinal value due to the lack of selectivity. Jhonnathan Brawley synthesized a series of 4-hydroxycoumarin imines and the laboratory of Dr. Christine Cremo determined the activities of these compounds towards non-

muscle myosin, cardiac muscle myosin, skeletal muscle myosin, and smooth muscle myosin isoforms of myosin II. Some of these compounds have very strong selectivity profiles such as JB100 which has an IC_{50} of 3.3 μM against skeletal muscle myosin, but no activity against the other tested isoforms. Interestingly, two very similar compounds have very dissimilar activities. Compound JB104 has no activity for any of the tested muscle isoforms while JB002 has IC_{50}s of 8 μM (cardiac muscle isoform) and 1 μM (skeletal muscle isoform). The only difference is that JB104 has an aldimine whereas JB002 has a ketimine group.[20]

To follow up on this work I performed an experiment to determine whether the difference in observed activity between JB104 and JB002 was due to stability. It is known that aldimines hydrolyze more rapidly than ketimines in aqueous media such as that used in the assay for determining IC_{50} values. This made it worthwhile to determine whether rapid hydrolysis was responsible for the lack of activity for JB104. Furthermore, MTT assays to determine the CC_{50} values for compounds with interesting activity were performed to demonstrate medicinal potential.

Section 2: Results and Discussion

2.1 Screening, toxicity and validation of potential Covid-19 antivirals

In screening for Covid-19 lead compounds it was important to find compounds capable of down-modulating ACE2 while demonstrating minimal cellular toxicity. First a screen for down-modulation of ACE2 was developed based of a review of the literature which revealed the use of a fluorogenic substrate capable of detecting ACE2 enzymatic activity.[2,3] It was reasoned that ACE2 enzymatic activity could be used as a way to determine the amount of ACE2 expressed on the cell surface. A previous study revealed the activity of ACE2 was strong in

Calu-3 cells when probed with the same substrate.[3] Calu-3 cells, human lung epithelial cancer cells, were determined to be an appropriate choice considering Covid-19 is known to infect the lungs. Initial testing involved simultaneously varying the number of Calu-3 cells plated per well as well as varying the concentration of substrate to determine the optimal concentration for each cell density. The initial test involved plating the cells at 0, 5 X 10^4, 1 X 10^5, 5 X 10^5, and 1 X 10^6 cells/well in a 96-well plate with 200 µL of media. After an overnight incubation in a 37 ºC incubator with 5% CO_2, the assay buffer was used to make 0, 2, 6, 10, 20, 60, or 100 µM dilutions of the fluorogenic substrate. The media was removed from the cells, the wells washed with 100 µL of PBS twice, and 100 µL of the appropriate substrate dilution was added to the wells. After a 20-minute incubation at 37 ºC, 95 µL of the solution was transferred to a black 96-well plate and the fluorescent intensity was read with excitation of 320 nm and emission of 405 nm (**Fig. 4.4**). Being the first assay that was developed in this lab there were some mistakes made in this assay such as not doing sufficient replicates. Only 20 µM and 60 µM substrate concentrations were tested in duplicate while everything else had no replicates. The two highest

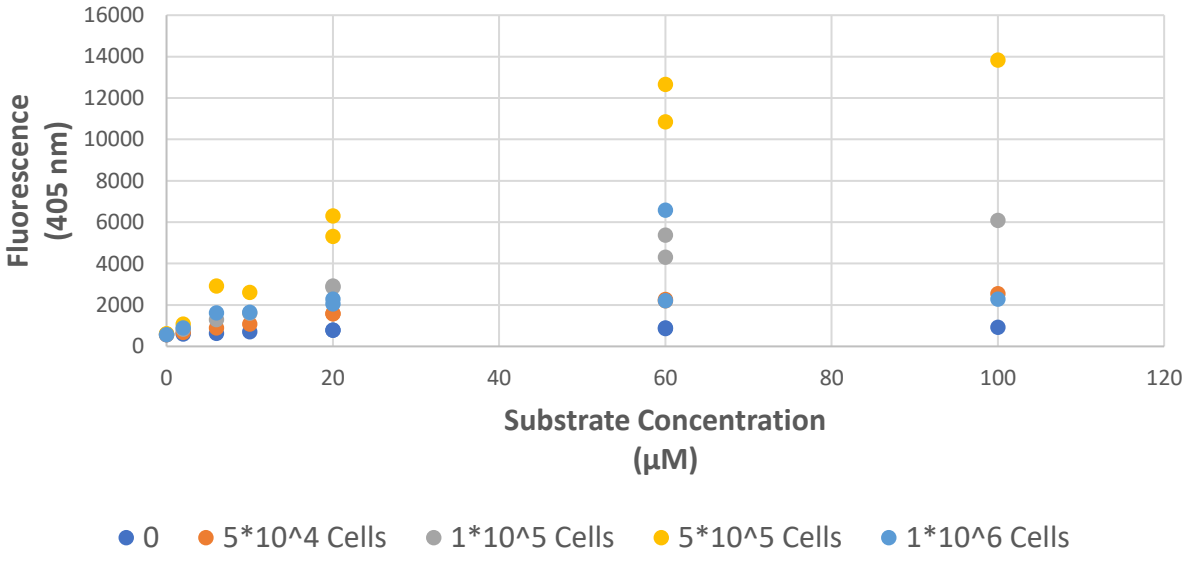

Figure 4.4: Fluorescence of ACE2 assay. The fluorescence intensity produced using excitation of 320 nm and emission of 405 nm for varying concentrations of fluorogenic substrate and varying number of cells per well.

cell densities tested, 5 X 10^5 and 1 X 10^6 cells/well, turned the media yellow after the overnight incubation and the 1 X 10^6 cells/well concentration subsequently produced poor fluorescent intensity, likely due to cell death. The fluorescent intensity hit a plateau around 100 μM of substrate. It was determined that a cell density of 1 X 10^5 cells/well with 60 μM substrate concentration would produce sufficient signal in subsequent assays. This cell concentration is high, but it is consistent with a literature assay that used the same number of cells/well when seeding and doing an overnight incubation before probing for ACE2 activity.[3] An initial set of screening assays were performed following this initial test. The assay followed the same general procedure, using the parameters chosen in the initial test (1 X 10^5 cells/well with 60 μM substrate concentration). The only other change was that during the cell plating procedure, the test compounds were added at 20 μM concentrations to an aliquot of cells before plating the mixture of cells with compound in triplicate wells. Three sets of compounds (54 in total) were screened using this assay. After subtracting the average no cell control signal as background from each well, the DMSO control (no compound) wells for each assay was used as a reference to normalize for 100% ACE2 activity (**Fig. 4.5**). Analysis of these three different assays reveals that the average intensity for the DMSO control for assay 1 (8,557 units) was significantly higher than the DMSO controls for assays 2 and 3 (6,080 and 5,638 units). This makes the results from the first assay somewhat questionable due to the unusually high absorbance of the DMSO control. Additionally, a no cell control background reading was not taken in the first screen and so the background for assay 1 was estimated from using the average background from assay 2. The average background for assays 2 and 3 (2,655 and 2,976 units) were similar. It is notable that on assays 2 and 3 the error bars for several of the compounds were unacceptably large. Nonetheless the results were promising as a large number of compounds showed strong

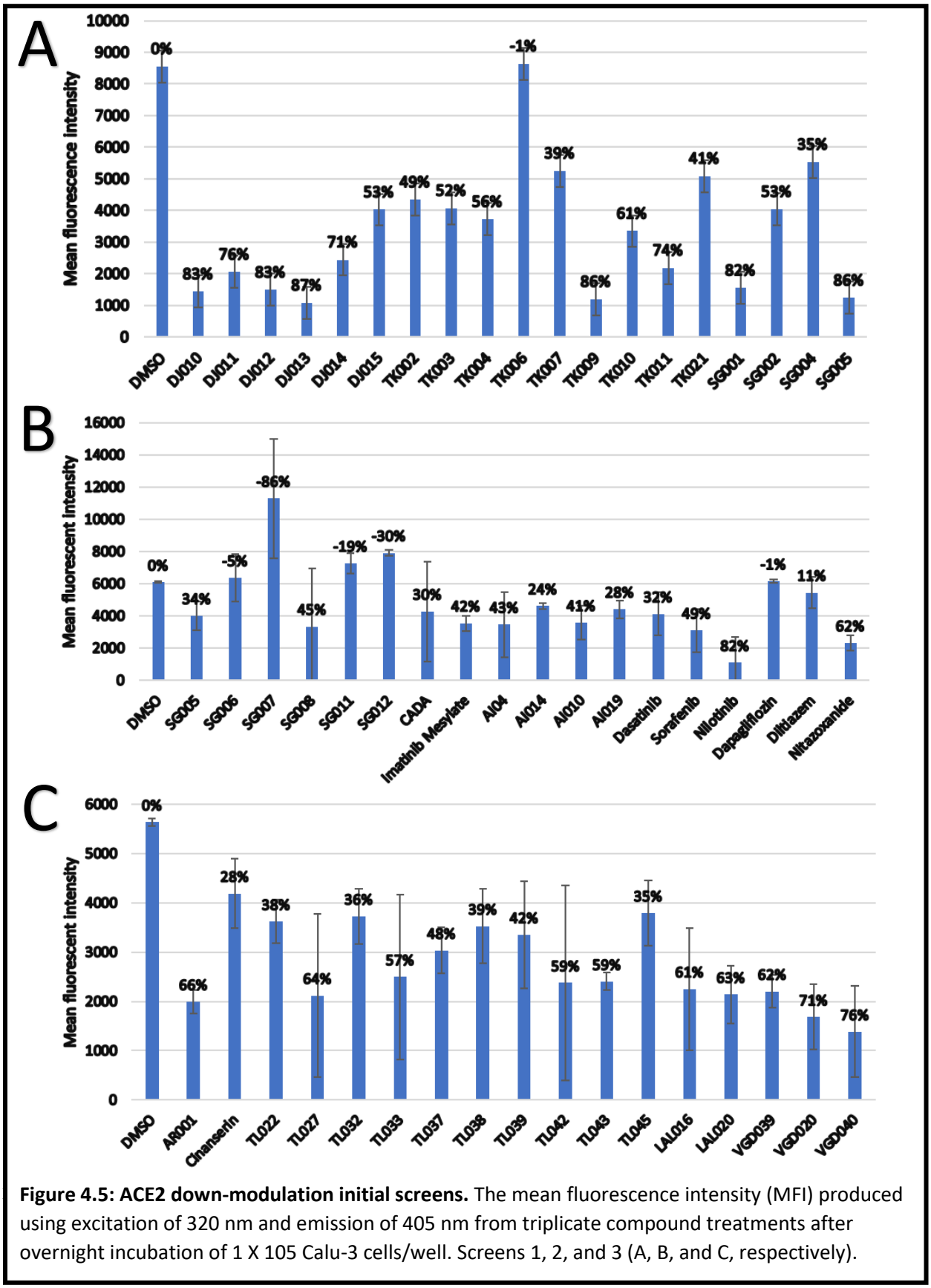

Figure 4.5: ACE2 down-modulation initial screens. The mean fluorescence intensity (MFI) produced using excitation of 320 nm and emission of 405 nm from triplicate compound treatments after overnight incubation of 1 X 105 Calu-3 cells/well. Screens 1, 2, and 3 (A, B, and C, respectively).

reductions in ACE2 activity. Because assay 1 had an unusually high control it also appeared to have a large number of compounds with high activity; however, looking simply at the MFI for all the compounds revealed AR001, DJ010, DJ012, DJ013, Nilotinib, Nitazoxanide, SG001, SG005, TK009, TK011, TL027, VGD020, and VGD040 as promising targets. Due to the time constraints of bringing a new drug to market during an on-going pandemic, several FDA approved drugs for other indications were tested in assays 2 and 3 as an attempt at drug repurposing. The activity of Nilotinib and Nitazoxanide made them particularly promising candidates. One major concern was the potential for these compounds to be toxic which would show up as false positives of down-modulatory activity by killing cells.

To determine the effect of each compound on cellular viability an MTT assay was developed. MTT is a compound that is converted to formazan, a purple compound, by cellular enzymes. Importantly the cells must be viable for this conversion to occur. The MTT assay was modeled on the ACE2 activity assay, but instead of adding 100 µL of the fluorogenic substrate for detection of ACE2 activity, 100 µL of a solution of MTT in media was added and the cells were incubated at 37 ºC with 5% CO_2 for 2 hours in the dark. The insoluble formazan product was solubilized by the adding 200 µL of acidified isopropanol and thoroughly mixing with a pipette. The absorbance was measured at 570 nm (**Fig. 4.6**). The DMSO controls showed some variation between the two assays (0.389 and 0.497 units for assays 1 and 2, respectively). An additional concern was that the no cell background was high and also showed variability (0.211 and 0.167 units for assays 1 and 2, respectively). The results of this screen revealed that all the compounds tested exhibited moderate to high toxicity levels when compared with the DMSO controls. Cinanserin, Nitazoxanide, and TL045 had the highest viability (69%, 56%, and 53%,

respectively), but they also produced the largest error bars. When doing the washing step for the MTT assay it was noticed that a large number of cells were being removed with the PBS used to

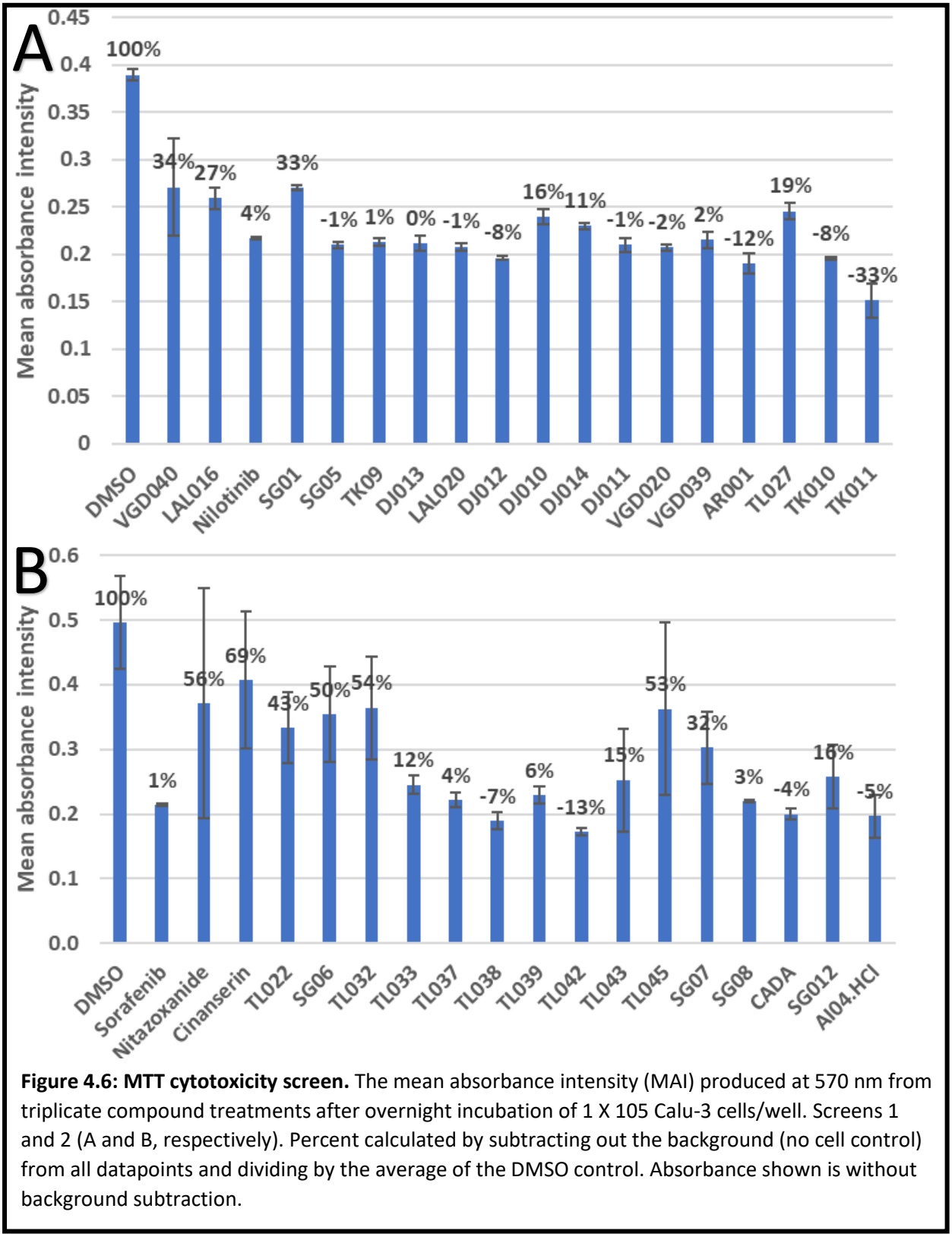

Figure 4.6: MTT cytotoxicity screen. The mean absorbance intensity (MAI) produced at 570 nm from triplicate compound treatments after overnight incubation of 1 X 105 Calu-3 cells/well. Screens 1 and 2 (A and B, respectively). Percent calculated by subtracting out the background (no cell control) from all datapoints and dividing by the average of the DMSO control. Absorbance shown is without background subtraction.

wash the wells, and this was suspected as a potential cause for the large error bars. In addition, it was discovered that other labs typically plate the cells and incubate them for a day prior to drug treatment, which allows them to attach properly to the plate and begin growing, before doing the drug treatment. This was in contrast to the above procedure which treated the cells at the time of seeding. As a result, the assay was further optimized by introducing an overnight incubation before treatment, but this presented a new and unique problem in the case of ACE2 down-modulatory screening.

In the original screen, trypsinization prior to treatment and seeding in the 96-well plate, removed ACE2 from the surface of the cell. Treatment with an active compound would prevent replenishment of ACE2, while the DMSO control (no compound) or a non-active compound allowed for ACE2 levels to return to normal. This made the assay sensitive to ACE2 down-modulating drugs. By delaying drug treatment, the detection of reduced ACE2 levels would be dependent on the slow ACE2 depletion due to its degradation in the absence of new ACE2 synthesis. Md Azizul Islam worked on further optimizing this assay and determined that the best results were obtained when retreating the cells with trypsin without EDTA (EDTA helps detach the cells) after the initial overnight incubation and immediately prior to treatment. He also made improvements by minimizing or removing unnecessary wash steps. This new procedure was also adapted to the ACE2 screen and a large number of compounds were screened for both ACE2 activity as well as toxicity (data not shown). The most promising compounds were selected for further testing to investigate the mechanism of action and validate their activity. First, qRT-PCR was used to determine if the mRNA transcripts for ACE2 were also being down-modulated, as discussed previously down-modulation by CADA analogues does not necessarily correlate with a change in mRNA levels, as opposed to other cellular regulatory mechanisms. For this

experiment cells were incubated in 24-well plates at 5 X 10^5 cells/mL overnight before treatment with trypsin immediately prior to compound treatment. After treatment, the cells were given to Dr. Timsy Uppal in Dr. Subhash Verma's lab for mRNA extraction and qRT-PCR analysis which revealed that the ACE2 mRNA was not being reduced. To verify that the ACE2 enzyme was actually being reduced and to validate the results from the screening assay, the assay conditions used for the qRT-PCR experiment were replicated for performing Western blots on protein extracts. The difference was that at the end of the treatment period the media was removed and the cells were incubated with a PBS-EDTA solution for 30 minutes to detach the cells without cleaving the ACE2 surface expressed protein. The cell suspension was centrifuged to pellet the cells and the cells were frozen at -20 ºC until they could be processed by Kabita Adhikari in Dr. Subhash Verma's lab. This testing confirmed that some of the compounds were truly down-modulating ACE2 expression. Further testing in Dr. Subhash Verma's lab verified activity against the virus in a viral replication assay as well as a second mechanism of viral inhibition by showing activity against the viral RNA dependent RNA polymerase (RdRp).

2.2 Developing a Screening Assay for Cx43 Down-modulation

Working closely with Dr. Amarawan Intasiri, an assay was developed for detection of Cx43 down-modulation in a 96-well plate format using the entry and subsequent fluorescence of ethidium bromide (EtBr) in phUSMCs. EtBr entered the cells through the Cx43 cell surface channels. Western blots performed by Dr. Scott Barnett in the laboratory of Dr. Ian Buxton revealed that several CADA analogues were capable of down-modulating Cx43 levels in phUSMCs. RK006 and TK047 were the most potent of the small subset of compounds tested by western blot, but it was desirable to be able to screen a much larger number of compounds in a

relatively short time by using a 96-well plate assay. Previous work, including work done by Dr. Scott Barnett and Dr. Ian Buxton, had revealed the potential for using EtBr fluorescence to detect decreased levels of Cx43, but this involved the use of fluorescence microscopy and was labor intensive.[8] A preliminary assay was developed by growing phUSMCs in T75 flasks and plating either 2.5 X 10^3 or 5.0 X 10^3 cells/well in a 96-well plate. The cells were incubated for 48 hours and then the media was removed. The cells were washed twice with 200 µL of PBS and treated with 200 µL of media containing 10 µM of the desired compound and 0.5% DMSO. The cells were incubated with the compound for another 24 hours and then the treatment media was removed, the cells were washed twice and treated with 100 µL of 0, 2, 5, or 10 µM EtBr solutions for 5 or 10 minutes. The EtBr solution was removed and the cells were washed three times. The fluorescence intensity was measured every 10 minutes for an hour using excitation and emission wavelengths of 285 nm and 605 nm, respectively. This produced very little signal and a subsequent assay tested 1.0 X 10^4 or 1.5 X 10^4 cells/well, 26.7 or 266.7 µM EtBr concentrations, and 15-, 40-, or 60-minute EtBr incubation times. This assay also did away with the removal of the treatment media before addition of the EtBr solution. This testing revealed the feasibility of such an assay and detected a reduction in fluorescence in the presence of both RK006 and TK047. The best results were obtained from using 1.5 X 10^4 cells/well, 266.7 µM EtBr, and a 60-minute EtBr incubation time. The assay also revealed that the fluorescent intensity remained relatively consistent for up to 60 minutes after washing out the EtBr solution.

At a later time, this assay was further optimized with a different batch of phUSMCs. It is not clear whether it is due to variability between the cells or due to an error in the cell counting procedure, but later testing revealed that seeding at 1.5 X 10^4 cells/well consistently produced overly confluent wells and high background signals which was not responsive to drug treatment.

Discussions with Dr. Ian Buxton's lab revealed that this seeding density was too high in their experience and it was suggested to reduce the number of cells to either 2.5 X 10^3 or 5.0 X 10^3

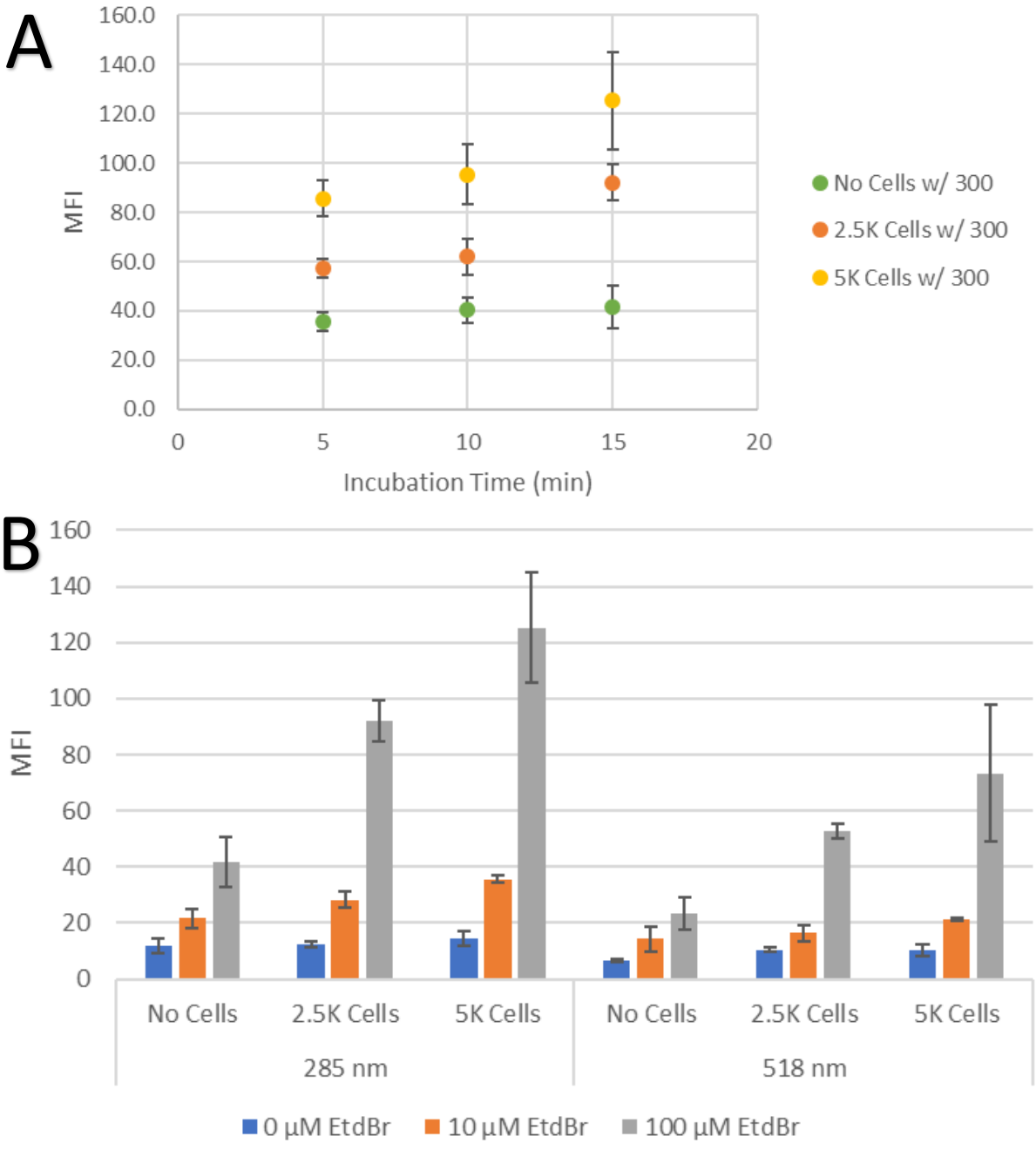

Figure 4.7: EtBr assay optimization. The MFI produced from phUSMC uptake of EtBr. Each condition was tested in triplicate and error bars show the standard deviation. A) Graph shows the trend of increasing MFI with increasing EtBr incubation times. The fluorescence was measured with an excitation of 285 nm and emission of 605 nm. B) Graph shows the stronger signal produced by excitation at 285 nm compared with excitation at 518 nm. The EtBr incubation time was 15 minutes.

cells/well. Additionally, there was concern that the high EtBr concentration and long incubation time would be detrimental to cellular morphology, cause apoptosis, or cause issues with Cx43 independent uptake of EtBr into the cells. The next experiment tested final EtBr concentrations of 10 and 100 µM with 5-, 10-, and 15- minute EtBr incubation times. Additionally, EtBr has an alternative excitation peak at 518 nm which may be gentler on the cells due to the lower energy of the light at this wavelength so this was tested as a possible alternative wavelength for excitation (**Fig 4.7**). Looking at the EtBr incubation time there was a clear trend of increasing MFI with increasing EtBr incubation time; however, whether this trend was linear or exponential and whether a plateau would be reached was unclear with the short incubation times used in this assay. Looking at longer incubation times to better understand the kinetics of EtBr entry into phUSMCs would be explored in the next assay. The higher 5.0 X 10^3 cells/well seeding density produced a better signal to noise ratio when looking at the no cell control as the background noise in the assay. The 10 µM EtBr concentration produced signal that was barely above background. Focusing on 100 µM EtdBr (although the same trend follows for 0µM and 10 µM), 518 nm produced slightly less signal with no cell background, 42 units at 285 nm compared to 23 units at 518 nm; however, with 5 X 10^3 cells/well there was a much higher signal with 285 nm excitation (125 units) compared to 518 nm (73 units). For 5 X 10^3 cells/well, the ratio between background to signal for each was as follows: 0.336 at 285 nm and 0.315 at 518 nm. For 2.5 X 10^3 cells/well, the ratio between background to signal for each was as follows: 0.453 at 285 nm and 0.488 at 518 nm. The difference between these values is likely not significant, but the stronger signal produced by 285 nm excitation was preferred and chosen as the excitation wavelength moving forward.

In a follow-up assay, a broader range of EtBr incubation times (up to 100 minutes) was assessed for both 2.5 X 10^3 cells/well and 5.0 X 10^3 cells/well seeding densities (**Fig. 4.8**). The results gave a linear trend of increasing intensity with EtBr incubation time up to 60 minutes (linear trend line has an R^2 of 0.9966 for 2.5 X 10^3 cells/well and an R^2 of 0.9851 for 5.0 X 10^3 cells/well when removing the 100 min time point). The decrease in signal at 100 minutes for 2.5 X 10^3 cells/well is hard to explain and may be due to experimental error. Degradation by cellular metabolism is another possibility, but it is inconsistent with the lack of decrease with 5.0 X 10^3 cells/well. Nonetheless, it does not appear that the cells are beginning to lyse and release their DNA as it is expected that this would produce a deviation from the linear trend. The cells were checked with an inverted microscope after the reading which also seemed to show the cells were

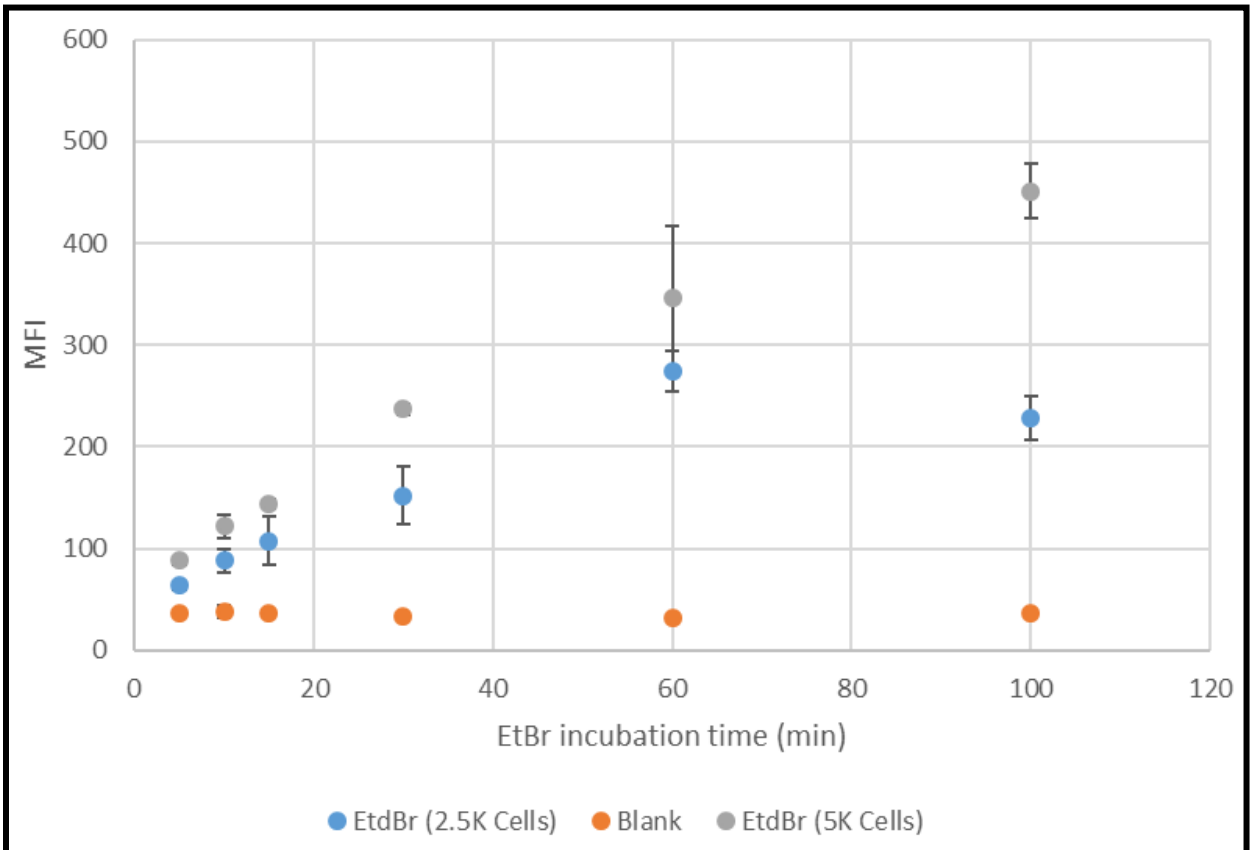

Figure 4.8: Kinetics of EtBr uptake. The MFI produced from phUSMC uptake of EtBr. Each condition was tested in triplicate and error bars show the standard deviation. Graph shows a linear trend of increasing MFI with increasing EtBr incubation times up to 60 minutes. The fluorescence was measured with an excitation of 285 nm and emission of 605 nm.

mostly intact and there was not much difference between no EtBr blanks and EtBr treatment wells; however, the quality phUSMCs grow as extended and very thin cells which makes it difficult to see with a standard cell culture microscope. The same conditions were repeated and the cells were visualized and imaged with a phase-contrast microscope which confirmed there were no visibly negative effects on the cells even after a 60-minute EtBr incubation (**Fig. 4.9**). The 30-minute incubation produced a good difference between signal and noise while also

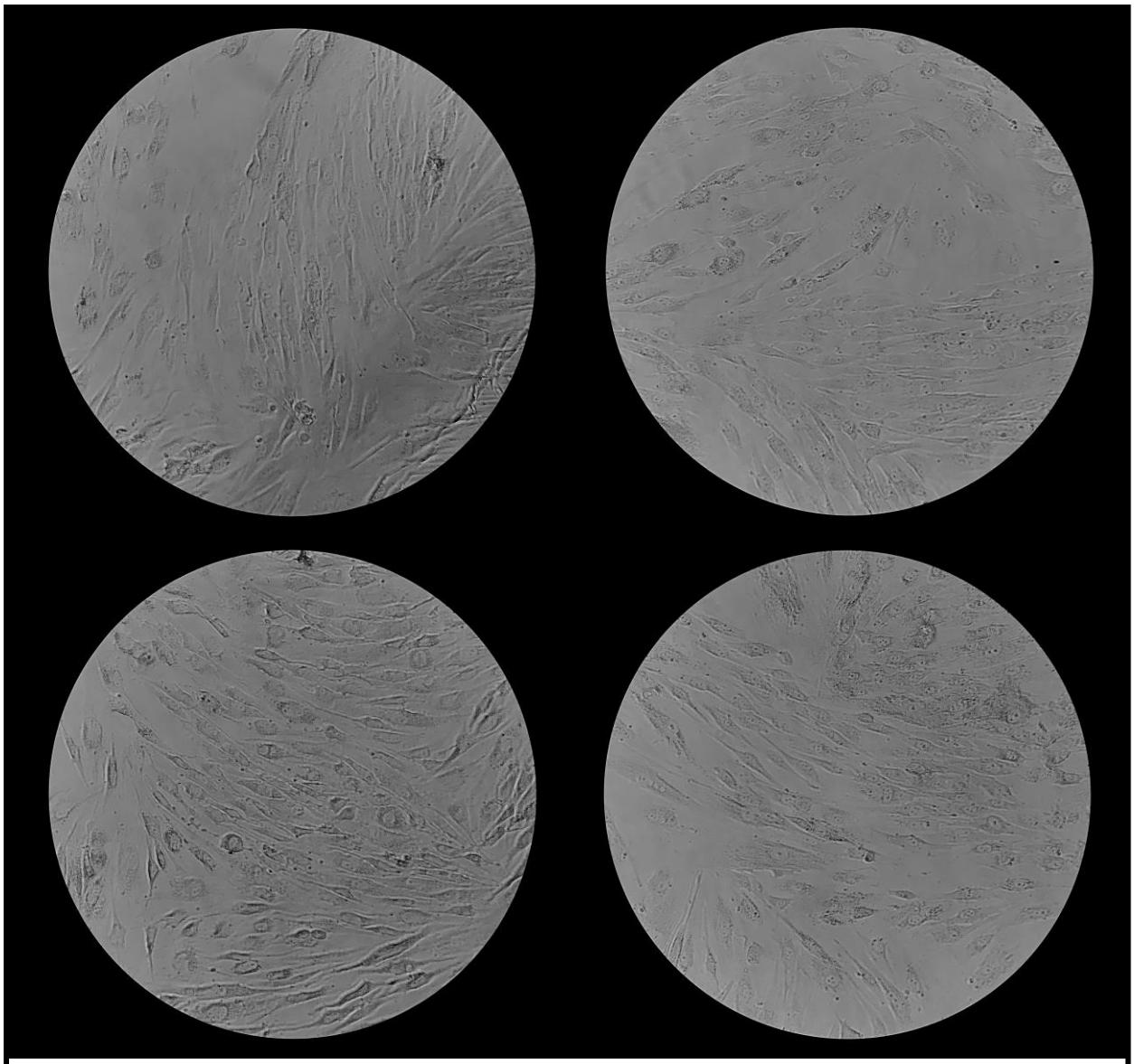

Figure 4.9: 60-minute incubation of 100 µM EtBr with phUSMCs. The two upper images show the phUSMCs after 60-minute incubation with a blank control while the two lower images show the cells after 60-minute incubation with 100 µM EtBr.

having the appeal of having a low chance that the EtBr had begun to negatively affect the cells in a way that would compromise the results of the assay.

Next, a small-scale screening assay was attempted using 2.5 X 10^3 cells/well and a 3-day incubation period prior to treatment, which was seen as a compromise between giving the better well to well consistency seen previously when seeding smaller number of cells yet giving a stronger signal by allowing the cells to grow an extra day (**Fig. 4.10**). The cells were observed to be at about 70% confluency at the time of treatment. The result gave a strong signal for the DMSO control, but the error bar was somewhat larger than desired. It was concerning that RK006 which is known to have strong activity, was causing an increase in fluorescence. The YM series of compounds showed promising activity, and TK047 was confirmed to be one of the most potent compounds in this screen. Looking at the wells with a microscope after treatment showed

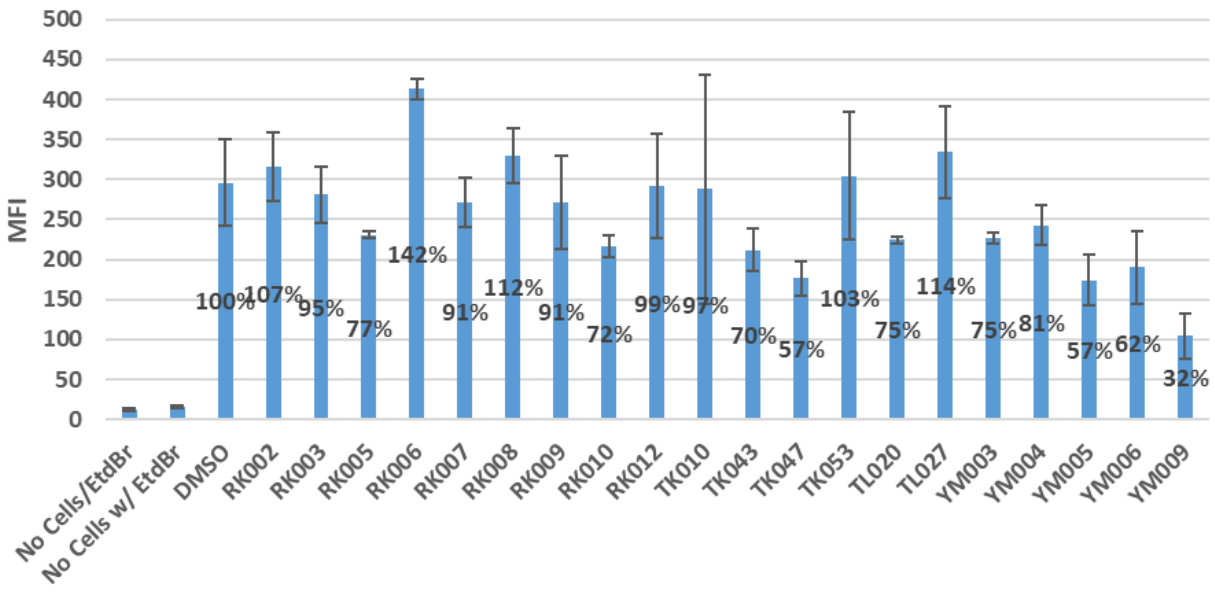

Figure 4.10: Trial Cx43 screening assay. A sterile, black 96-well plate was seeded with 2.5 X 10^3 cells/well and incubated for three days before treatment with 10 mM compound in hTRT media with 0.5% DMSO. Percentage of DMSO control after background subtraction shown. Error bars represent standard deviation.

that YM009 was likely having toxic effects on the cells which was responsible for the apparently strong Cx43 down-modulatory activity.

One suspected cause for the large error bars seen in the assay was the washing step at the end of the assay to remove the residual EtBr. In this step the EtBr containing media was removed and the wells were washed with 300 µL of HPKR solution followed by addition of 100 µL of HPKR solution and removal of just 90 µL of HPKR solution. The thought behind leaving behind some of the solution was that it could prevent cells from drying out and that it would leave a more consistent volume of liquid in the wells, as opposed to trying to take out all the solution which might leave behind unequal volumes of residual liquid. In practice it appeared that after removal of 90 µL of the HPKR solution the wells often had uneven liquid levels left behind. Additionally, there was a concern that the more stringent the washing step the more potential for dislodging cells from the plate in unequal proportions, causing a higher amount of variability in the assay. As such an assay was performed where four different washing techniques were attempted: 1) no wash and leave behind 10 µL, 2) wash once with 300 µL and leave behind 10 µL, 3) wash once with 300 µL then once with 100 µL and leave nothing behind, 4) wash once with 300 µL then once with 100 µL and leave behind 10 µL (**Fig. 4.11**). The results show that at least one wash is necessary to reduce background to acceptable levels. There is little difference in terms of the controls on whether 10 µL or nothing left behind in the well after the first wash. It also revealed that the second wash gave little improvement on decreasing background, but that it was decreasing the signal for the DMSO control which is likely from detachment of cells from plate. Interestingly, regardless of all the different techniques the error bars were relatively consistent in size (even with the no wash technique). This indicates that the size of the error bars is not dependent on the washing technique. An unexpected result was seen with the results with

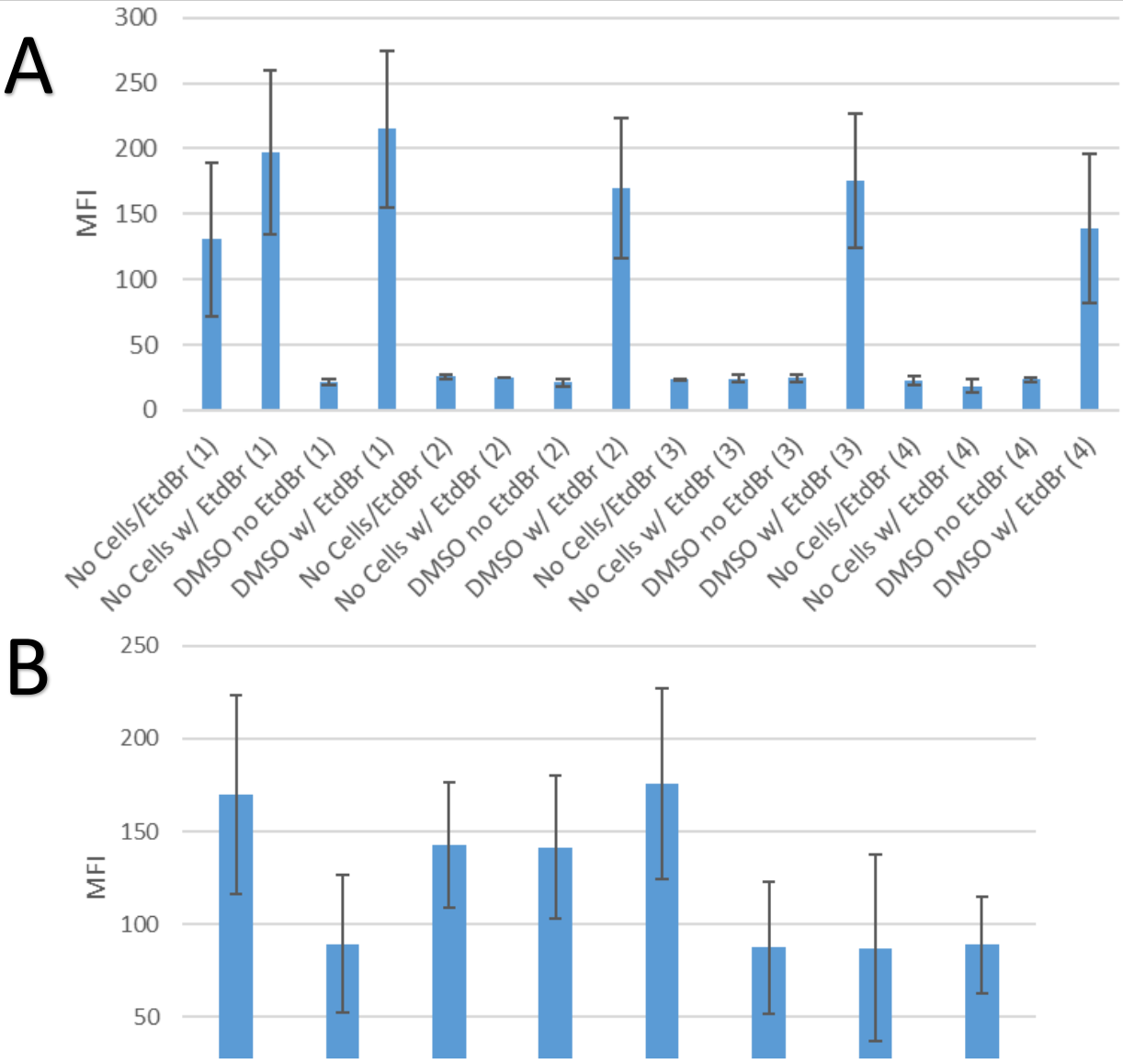

Figure 4.11: Exploring different washing techniques. After incubation with EtBr the plates were washed in four different ways: 1) no wash and leave behind 10 µL, 2) wash once with 300 µL and leave behind 10 µL, 3) wash once with 300 µL then once with 100 µL and leave nothing behind, 4) wash once with 300 µL then once with 100 µL and leave behind 10 µL. Error bars represent standard deviation. A) Shows no cell and DMSO only treatment controls. B) Shows comparison of the 2nd and 3rd washing technique which either leaves 10 µL or nothing behind after washing, respectively.

treatment of RK006 or TK047 when looking at the difference between wash techniques 2 and 3. When 10 µL was left behind in the well, RK006 treatment gave a fluorescent intensity much higher than the TK047 treatment, but when all the HPKR solution was removed after washing the result was almost identical to the TK047 treatment which was unchanged between the two

washing techniques. Of note is the fact that RK006 has a peak absorption at 269 nm and still absorbs light strongly at 285 nm which was the excitation wavelength used in the assay. Similarities in the structures of EtBr and RK006 (presence of aniline groups and a positively charged nitrogen) and the results of this assay suggest that RK006 could be interfering with the fluorescent output of the assay.

The other concern was that the compounds could have toxic effects that produced false positives. One way to counteract that is with a counter screen for viability using the MTT reagent. While the treatment with EtBr is an obvious concern for down-stream applications with the cells it was attempted to perform an MTT assay on the cells after reading for fluorescence. It would be highly beneficial to be able to assess the viability of cells in the same well that the EtBr assay was performed on so that the results could be correlated in a very meaningful way. After reading the fluorescence the 100 µL of MTT solution was added to the wells that had 10 µL of HPKR solution left after washing. Another plate treated with the same compounds which never received the EtBr treatment simply had the treatment media removed and 100 µL of MTT solution added to the wells (**fig. 4.12**). Using the MTT assay after doing the EtBr assay was able to correctly identify YM009 as a toxic compound and the overall trend was similar with the exception of a few outliers, such as RK005 and RK010, but the assay was far less sensitive. It was decided not to pursue this technique further; however, it could be a useful technique to help explain erroneous results. It does show that the signal was also decreased when doing the MTT in series with the EtBr assay as is evident when looking at the absorbance of the DMSO controls (0.910 units and 0.620 units for MTT alone and EtBr/MTT assays, respectively). This is likely an

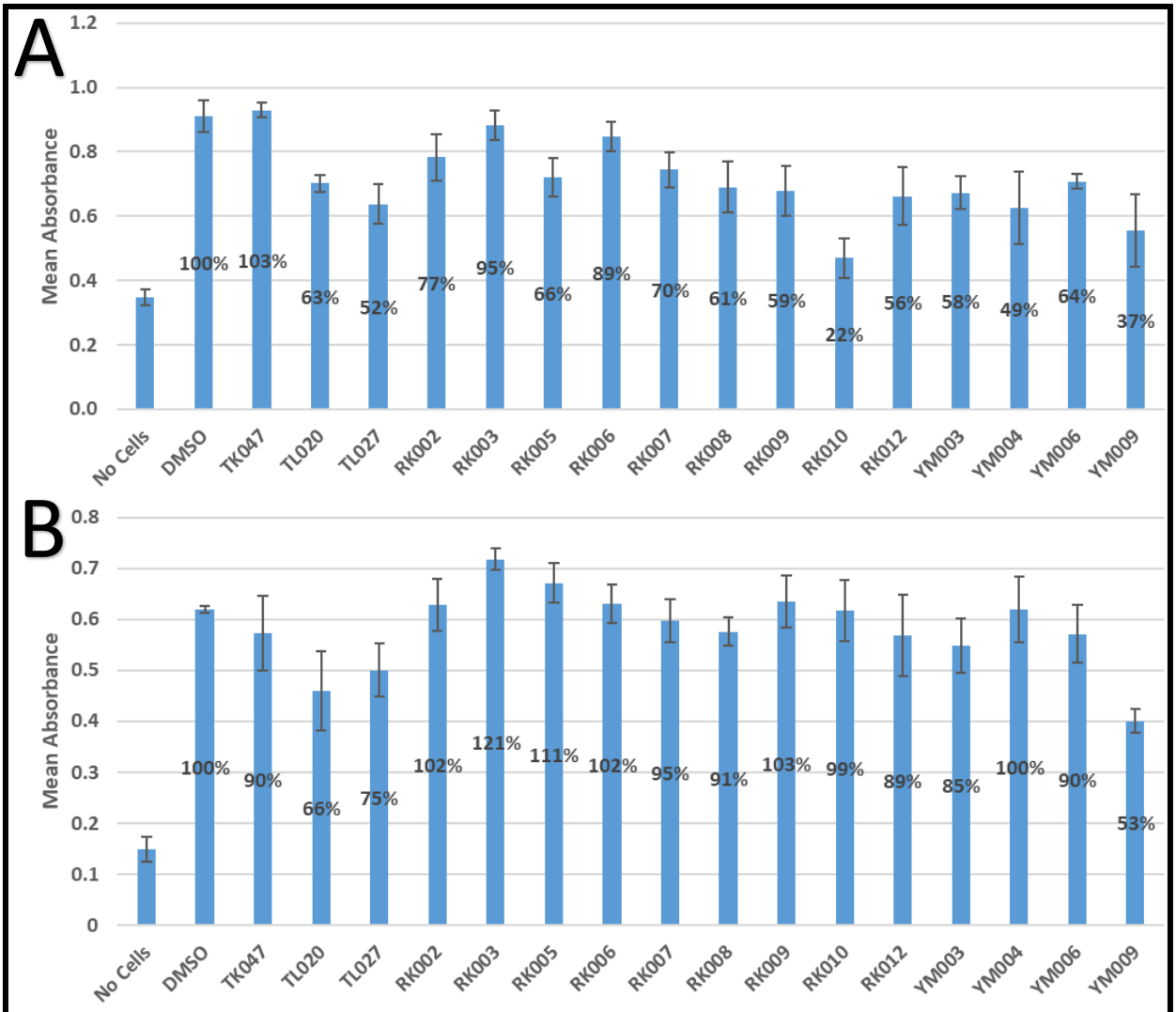

Figure 4.12: Testing of the MTT assay. A) MTT assay was performed on a subset of compounds to test their viability. On another plate the same compounds were tested for activity with the EtBr assay and after incubation with EtBr the plates were washed and read for fluorescence then the MTT reagent was added and the plates were treated in the same manner as the regular MTT assay from that point on. Error bars represent standard deviation. Percentages represent the percent of the average for the DMSO control after the no cells average was subtracted from every well.

indication of toxicity of the EtBr treatment, but it is also likely that it is partly the result of the extra washing steps needed in the EtBr assay. Overall, it is a good sign that cells are still healthy enough after the EtBr treatment that they were able to produce signal in the MTT assay albeit with an obvious reduction in signal.

Another option besides doing the MTT assay to help reduce false positives due to toxicity is to use a shorter incubation time to reduce the potential for toxicity. Fortunately, the literature shows that Cx43 has a rapid turnover rate.[21] This means that the effects of reducing the cell surface expression would manifest rather quickly and a shortened incubation period should be sufficient to reveal the down-modulatory activity of active compounds. However, compounds may exhibit different kinetics so a second small scale screen was attempted with a variety of compounds on three replicate plates. Each plate was incubated for either 2, 6, or 24 hours with the compounds prior to addition of the EtBr (**Fig. 4.13**). The 2-hour incubation with compound was sufficient to start to see Cx43 downmodulation as TK047 had only 70% of the signal compared to the DMSO control. Interestingly, this screen resulted in almost all compounds showing some degree of activity and several compounds with stronger activity than TK047 (RK007, 69%; YM005, 48%; YM006, 59%; TK018, 56%; and TK053, 53%). For the 6-hour incubation with compound, the TK047 signal had dropped to 54% of the control. Compounds YM006 went up to 70% and TK053 to 85%. It is not clear if this is due to inaccuracy of the assay or perhaps it could be the result of degradation of compound or compensatory effects by the cell. There are likely several factors at play that would be difficult to separate out. Several RK compounds which showed little activity at 2 hours (RK003, 83%; RK008, 80%; and RK009, 113%) were starting to show improved activity (RK003, 62%; RK008, 62%; and RK009, 65%). While RK003 had good viability in an MTT assay (96%), RK008 (64%) and RK009 (62%) had shown similar levels of toxicity in the MTT assay which may explain the apparent activity. At 24 hour all but one compound (RK012) showed some level of activity and 13 of 18 showed less than 70% the signal of DMSO control. For compounds such as YM009, which is known to be toxic, reduced cellular viability is likely the cause for the apparent activity. A shorter incubation

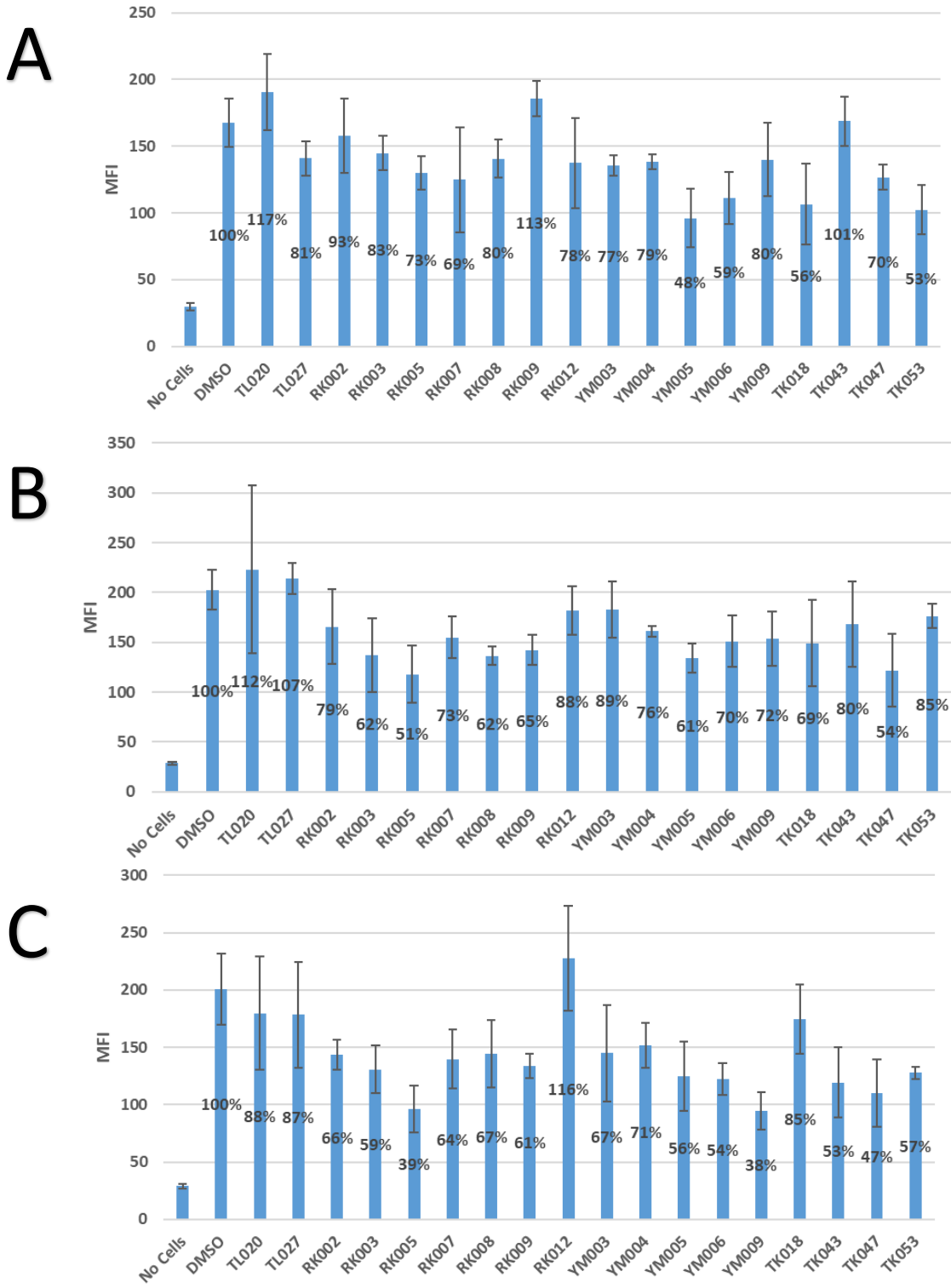

Figure 4.13: Testing compound incubation times. Cells were treated with 10 mM compound in hTRT media with 0.5% DMSO for 2, 6, or 24 hours for A, B, or C, respectively. Percentage of DMSO control after background subtraction shown. Error bars represent standard deviation.

time seems preferable to avoid false positives due to toxicity. TK047 went from 70% (2 h) to 54% (6 h) to 47% (24 h) while RK003 went from 83% (2 h) to 62% (6 h) to 59% (24 h). This indicates that somewhere between 2 to 6 hours compound incubation times would be ideal as there is little increase in activity past 6 hours, but 2 hours is not yet showing very strong effects. From these assays RK003, RK005, RK008, RK009, YM005, YM006, TK047, and TK053 warrant further investigation.

At the same time, that those plates were set up it was also decided that the assay was functioning well enough to do a screen of a larger set of compounds to look for other compounds with strong activity. Three plates were screened with using a 24-hour treatment time (**Fig. 4.14**). This set compounds did not tend to show as much activity in general. The top compounds from those plates were selected for further testing and included in the plates with the above compounds when doing the next assays with 3-, 4.5-, & 6-hour treatment times (**Fig. 4.15**). These compounds are CADA (74%), AI037 (70%), Dasatinib (76%), Lycorine (61%), SG001 (66%), VGD023 (84%), VGD027 (81%), VGD029 (82%), VGD040 (79%), and VGD049 (68%).

The results of the 3-, 4.5-, & 6-hour treatment time, indicated that TK047 activity is apparent after just 3 h, along with YM006 and SG001. However, the results are not very consistent in terms of producing trends of decreasing signal with increasing treatment times. The 4.5 h incubation is particularly concerning where TK047 is close to 100% of the control, while the 3 h and 6 h timepoints show very strong activity for TK047. Looking across all three time points only 6 of the 18 compounds show a reduction in signal from both 3 to 4.5 hours and 4.5 to 6 hours. From 3 to 6 hours 12 compounds show a reduction in activity (although for CADA it is less than 1%). Interestingly, from 4.5 to 6 hours all but 3 of the compounds (15 compounds) show a

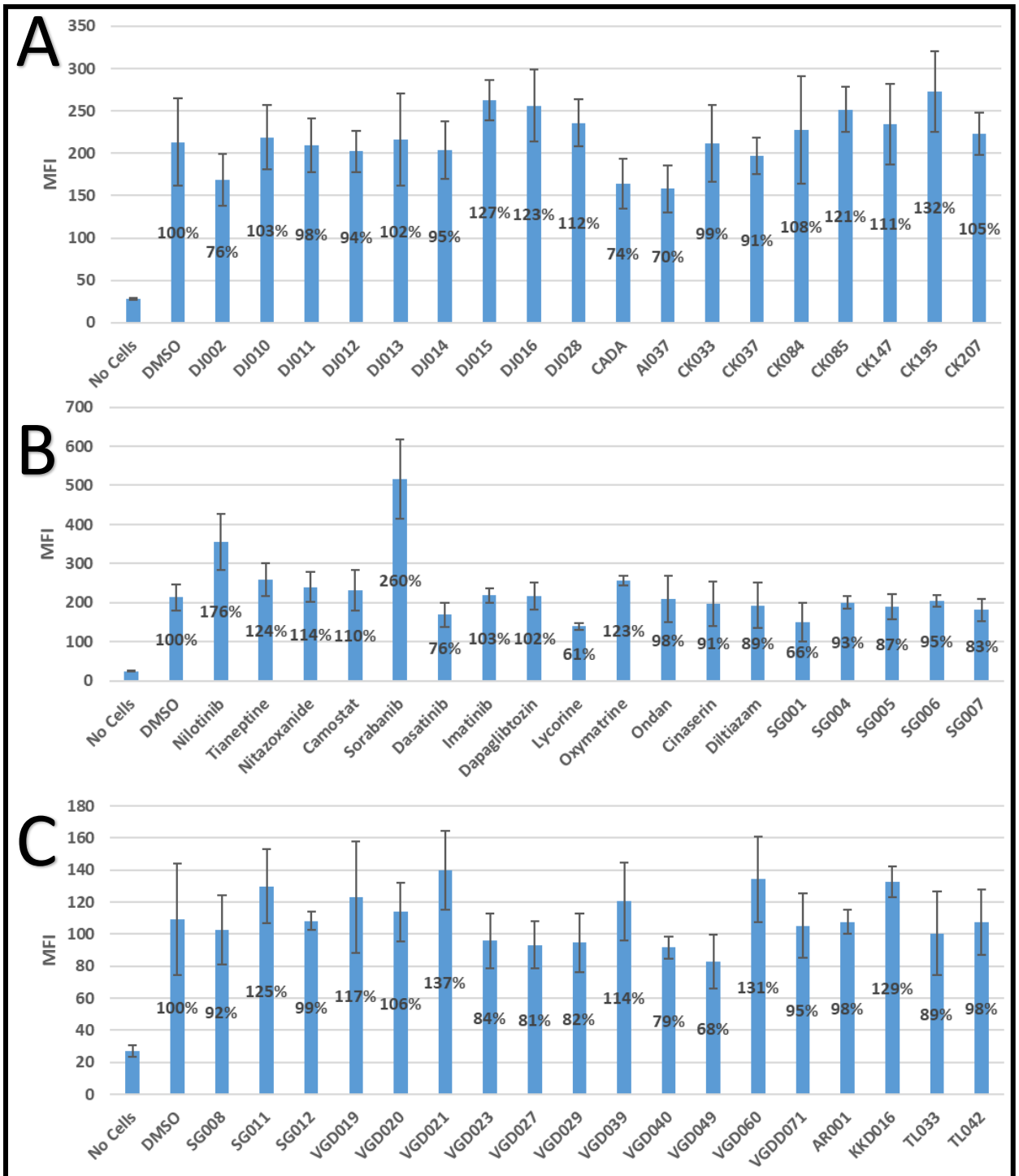

Figure 4.14: Cx43 down-modulation screen. All plates were treated equally, treatment times were 24 hours with 10 µM compound in hTRT media with 0.5% DMSO. Percentage of DMSO control after background subtraction shown. Error bars represent standard deviation. A, B, and C each represent individual plates.

reduction in activity. Both the 3- and 4.5-hour time points have only 3 compounds below 70% while the 6-hour time point has 6 compounds below 70%. When taking the average of all three

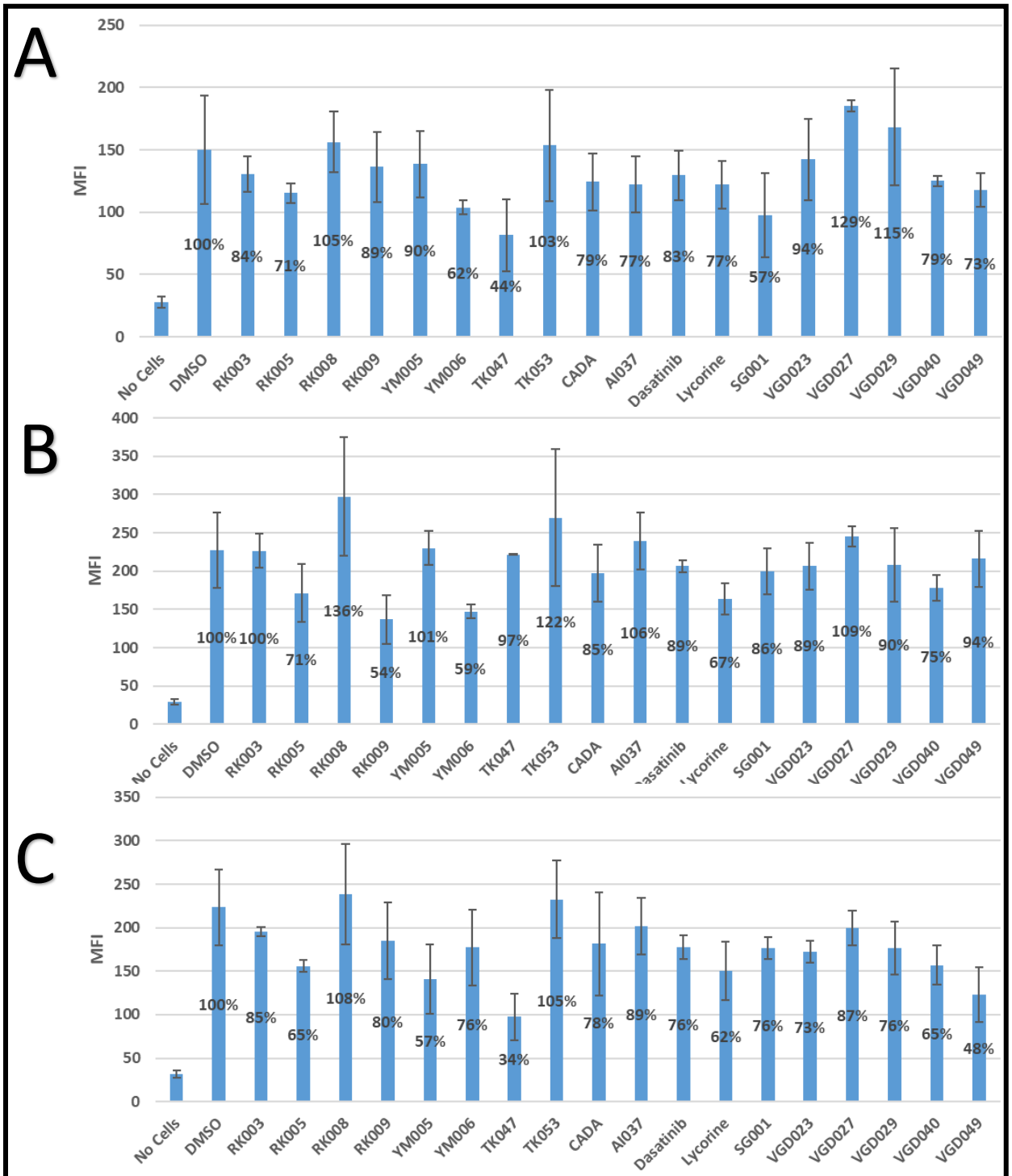

Figure 4.15: Retesting compound incubation times. All plates were treated equally, treatment times were 3, 4.5, and 6 hours (A, B, and C, respectively) with 10 µM compound in hTRT media with 0.5% DMSO. Percentage of DMSO control after background subtraction shown. Error bars represent standard deviation.

time points there are 4 compounds with an average below 70%: TK047 (58.3%), YM006 (65.7%), Lycorine (68.7%), and RK005 (69.1%). It is quite impressive that TK047 achieved a much lower

average than all other compounds despite having the 4.5 h time point give 97.1% (every other test up to that point had showed good activity for TK047).

More work needs to be done to reduce the SD of the assay and improve consistency to make it a more valuable tool for screening. A screen with 4-replicates was not accurate enough to be used to screen compounds as the results for the compounds tends to fluctuate too much between tests. TK047 could have been missed if the test performed was the one that returned a result of 97.1% and other compounds with slightly less activity are even more likely to missed. To

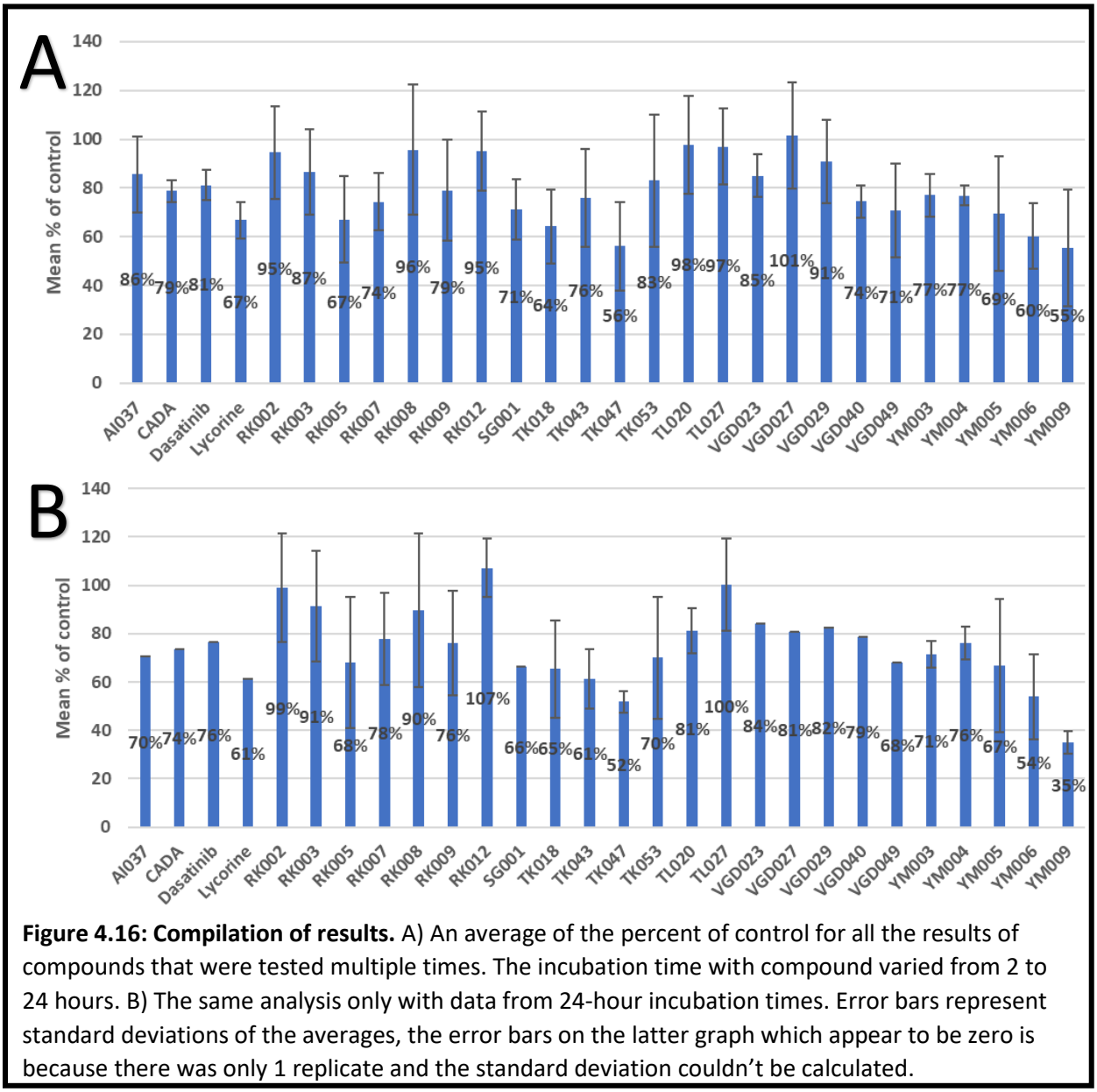

Figure 4.16: Compilation of results. A) An average of the percent of control for all the results of compounds that were tested multiple times. The incubation time with compound varied from 2 to 24 hours. B) The same analysis only with data from 24-hour incubation times. Error bars represent standard deviations of the averages, the error bars on the latter graph which appear to be zero is because there was only 1 replicate and the standard deviation couldn't be calculated.

determine the accuracy of the screen across multiple tests I compiled all the results for compounds that were tested multiple times (**Fig. 4.16**). The incubation time with compound varied from 2 to 24 hours, but the compilation of the results revealed the compounds with consistently strong activity. To ensure that this wasn't favoring compounds which were screened more often at 24 hours than shorter time periods, the analysis was repeated with only data from 24-hour incubation times.

When including the shorter incubation times the compounds with averages below 70% are: YM009 (55.5%, N=4), TK047 (56.2%, N=9), YM006 (60.2%, N=9), TK018 (64.2%, N=4), Lycorine (66.8%, N=4), RK005 (67.0%, N=9), YM005 (69.4%). When only including 24-hour incubation times the compounds with averages below 70% are: YM009 (35.0%, N=2), TK047 (51.8%, N=4), YM006 (53.9%, N=4), Lycorine (61.1%, N=1), TK043 (61.2%, N=2), TK018 (65.3%, N=3), SG001 (66.4%, N=1), YM005 (66.8%, N=4), RK005 (67.9%, N=4), & VGD049 (68.1%, N=1). It is likely that the 24-hour incubations tend to favor toxic compounds. Compounds with a large decrease in percentage between the former and latter (YM009, 20.5%; and TK043, 14.7%) are suspected to be toxic.

While it is clear that 3 hours is sufficient to see a large decrease in percentage such that TK047 produced 43.8% activity which was the second lowest percentage observed for TK047 (only 6 hours from the same date showed lower activity with 34.1%). In one of the time-course studies TK047 showed a large decrease from 2 (70.2%) to 6 hours (53.5%). As such, a 6-hour compound treatment time was determined to be optimal for giving sufficient time to reduce levels of Cx43 while producing minimal false positives from toxicity.

Further attempts were made to improve the consistency of the assay. It was reasoned that if the cells were fully confluent prior to treatment there would be less variation introduced from

inconsistencies in the actual number of cells plated per well when seeding. To test this the seeding density was increased to 5.0 X 10^3 cells/well and the plate was incubated for 6 days (with a media change after 3 days) prior to treatment (**Fig. 4.17**). The results failed to reduce the size of error bars and additionally, TK047 was tested in four separate sets of replicates of four and each set was treated separately. This produced average values of 82.9%, 73.6%, and 64.2%, 58.7% of the control for the different sets of replicates which indicated that the variability was not due to differences in seeding density caused by pipetting error. Another attempt to reduce the variability was to try mixing the EtBr in the well after addition to try to get a more equal exposure, but this actually increased the variability likely because it dislodged cells from the bottom of the plate during the mixing process (data not shown).

There were some general patterns in the results depending on where on the plate the well was, which raised concerns about the effects of the position of each well within the plate. An assay was performed where the plate was treated with only media with 0.5% DMSO and no compound to get a sense of the variability and if there were any affects related to the position of

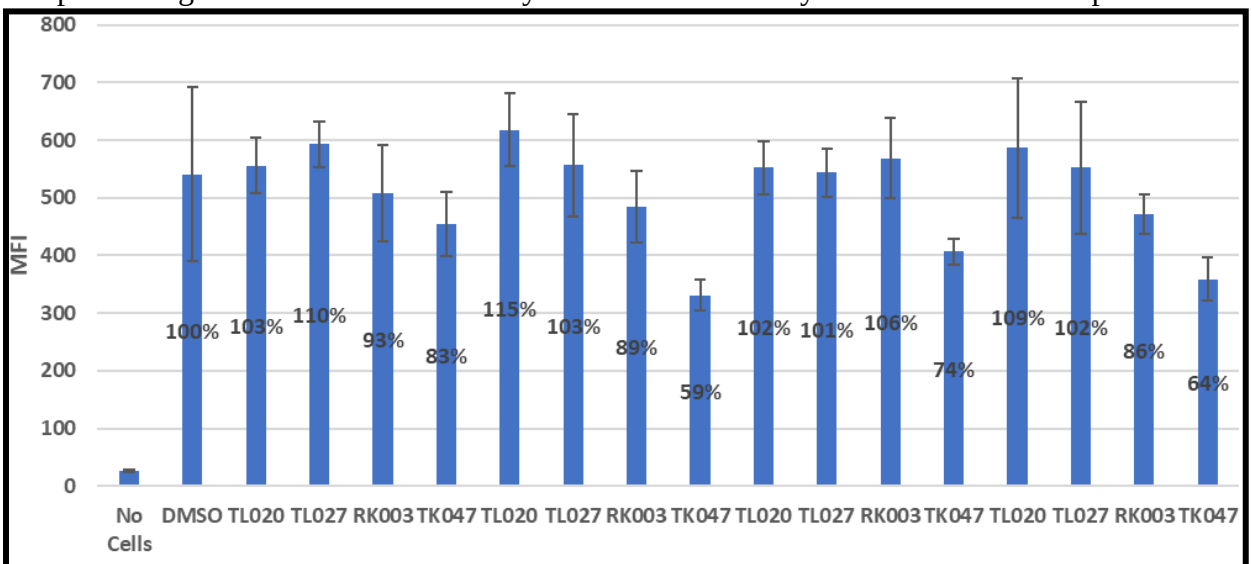

Figure 4.17: Testing treatment on fully confluent wells. Plate was seeded with 5.0 X 10^3 cells/well and cells were grown for 3 days had the media changed and grown for 3 more days in the plate prior to treatment with compound. Percentage of DMSO control after background subtraction shown. Error bars represent standard deviation. A, B, and C each represent individual plates.

a well in the plate. Suspecting it could also be related to the order of addition of the reagents/washing for the top half of the plate I worked from left to right and I worked in the opposite direction for the bottom half of the plate. This assay was repeated on two different plates and the order of addition of EtBr did not have a significant impact. Previously, the compounds were screened in replicates of four, plated in a vertical manner with respect to each other. To replicate this scenario in the analysis, the plate was analyzed by treating each group of four as a set of replicates (**Fig. 4.18A**). The average absorbance for each set was graphed in the order in which it received EtBr and was washed (**Fig. 4.18B**). What this produced is a continuous wave-like pattern that appeared symmetrical around the point where it switched from the top to the bottom of the plate (set 10 was on top and set 11 was on bottom). Seeing this symmetry, I graphed the same points depending on the column they were in on the plate as opposed to the

A

	1	2	3	4	5	6	7	8	9	10	11	12
A	No EtBr/No Cells	No Cells	1	2	3	4	5	6	7	8	9	10
B	No EtBr/No Cells	No Cells	1	2	3	4	5	6	7	8	9	10
C	No EtBr/No Cells	No Cells	1	2	3	4	5	6	7	8	9	10
D	No EtBr/No Cells	No Cells	1	2	3	4	5	6	7	8	9	10
E	No EtBr		21	20	19	18	17	16	15	14	13	12	11
F	No EtBr		21	20	19	18	17	16	15	14	13	12	11
G	No EtBr		21	20	19	18	17	16	15	14	13	12	11
H	No EtBr		21	20	19	18	17	16	15	14	13	12	11

B

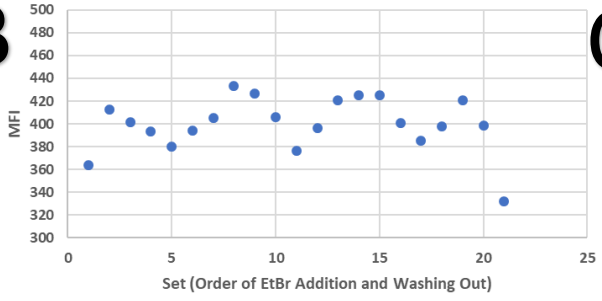

C

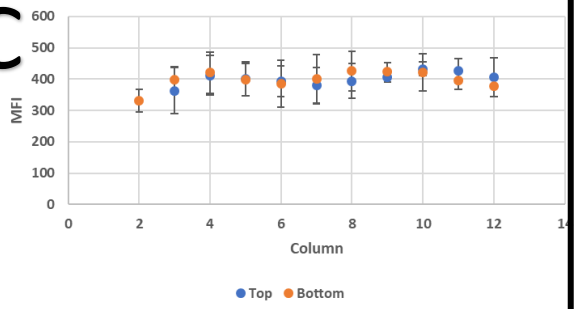

Figure 4.18: Effects of column position on MFI. A) Shows the plate map where the controls with background levels of signal were wells in column 1, A-H and column 2, A-D. Column 1 does not receive EtBr, whereas the rest of the plate does. Column 2, A-D is the "No Cells" control that is used for subtraction of background when calculating the percent of control. The whole plate was treated with media with 0.5% DMSO. Sets 1-21 all received cells and EtBr which was added and washed out starting with set 1 and working up to set 21. B) Shows the MFI for each set which revealed a symmetrical wave-like pattern. C) Shows the MFI for each set based on which column the well was in. This revealed that both the top and bottom set had similar values for every column which produced a smooth and flat "M" like pattern. For both B and C, only the data for the first plate shown but both plates were similar.

order of EtBr addition. This revealed a smooth and shallow "M" shaped wave-like pattern where the points had similar values depending on the row they were in on the plate (**Fig. 4.18C**). Both plates exhibit a similar pattern. What this indicates is that there is a considerable amount of variability introduced simply by the column that a compound is tested in. Setting the same sets of replicates as the "DMSO control" wells used in previous screens and calculating the percent of control in the same fashion as previous screens revealed the percentages ranged from 93% to 113% which gives a range of 20%. This indicates that the percent of control found for any given compound could vary up to 20% simply based on its location in the plate! The pattern revealed that intensities were lowest on the ends and middle two columns of plate and higher in between these points. A similar analysis was done by looking at the rows instead. Both plates also had wave-like patterns for the intensity of the signal based on the position of the well in respect to the row; however, in this case the waves did not align with each other in the same manner as when looking at the columns (**Fig. 4.19**). The reason for this pattern is unknown, but it doesn't seem to be consistent with procedural errors. The trend going across the columns or down the rows for both plates is for a tendency for the edges to be some of the lowest points which may have to do with the fact that evaporation from the plate occurs more at the edges of the plate as can be visually noted in the level of liquid left in the wells when removing the plate after a 3-day incubation period. Inconsistent with this hypothesis is the fact that set 21 is actually set column 2

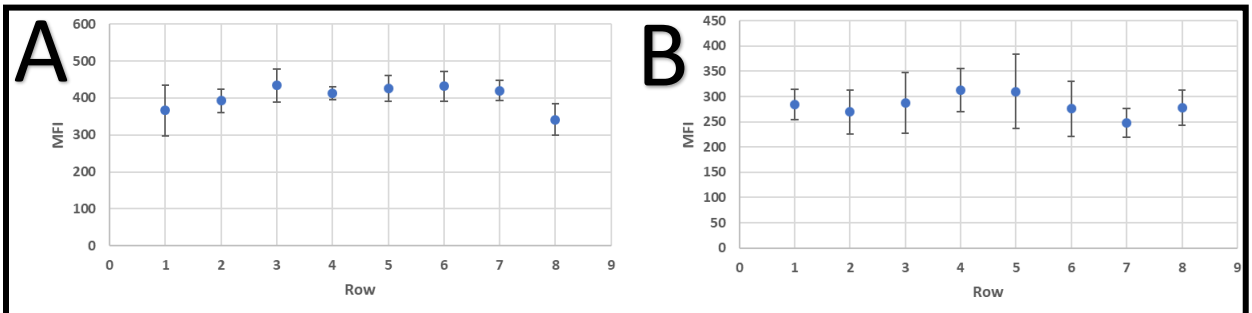

Figure 4.19: Effects of column position on MFI. Shows the MFI for each set based on which row the well was in A and B represent plates 1 and 2, respectively.

(lowest MFI) and set 1 is in column 3 (second lowest MFI) whereas set 10 and 11 are truly on the edge in column 12 and have higher MFI values. The dip seen in the center of the plate for 3 of the 4 graphs is harder to explain. Regardless, of the explanation it is clear that this is an major issue that affects the reproducibility of the assay and needs to be either controlled for or fixed in future assays. It may be difficult to determine the cause of the issue and even if the cause is determined it may be unavoidable or difficult to resolve. If the same pattern (particularly for the columns) can be reliable reproduced and quantified then it is possible to control for this in the calculations which would be recommended. Further recommendations would to be to reduce the EtBr wash volume to the minimal volume necessary. Lastly, while more cells and longer growth periods before treatment has increased the signal to noise ratio it has not improved on the well to well variability and smaller error bars were seen in some of the preliminary assays with smaller number of cells. It may be worth exploring seeding less cells and shorter growth periods to see if the error bars can be reliably reduced. Shorter growth times may also cut down on the variability introduced by evaporation at the edges of the plate. Another option could be to spread replicates out across the plates in different columns and also potentially increasing the number of replicates. However, the assay is capable of detecting compounds that reduce Cx43 expression, and it can be used as a screening tool to rapidly screen through the entire Bell lab library as is.

2.3 Determining the CC_{50} for VGD040 on HEK293 Cells

To determine the CC_{50} for VGD040 on HEK293 Cells three replicate MTT assays were performed by plating cells and growing overnight until the confluency was 70-80%. The cells were then treated with VD040 in a 1:3 serial dilution with 9 points plus a DMSO only control. One point was dropped in one of the experiments because it failed to pass Dixon's Q-test at 95%

confidence. Four parameter nonlinear regression curves of three independent experiments were generated in GraphPad Prism V8.0.1 which were used to determine the CC_{50} of VGD040 (**Fig. 4.20**). The average CC_{50} of three experiments was calculated to be 44 ± 1 µM.

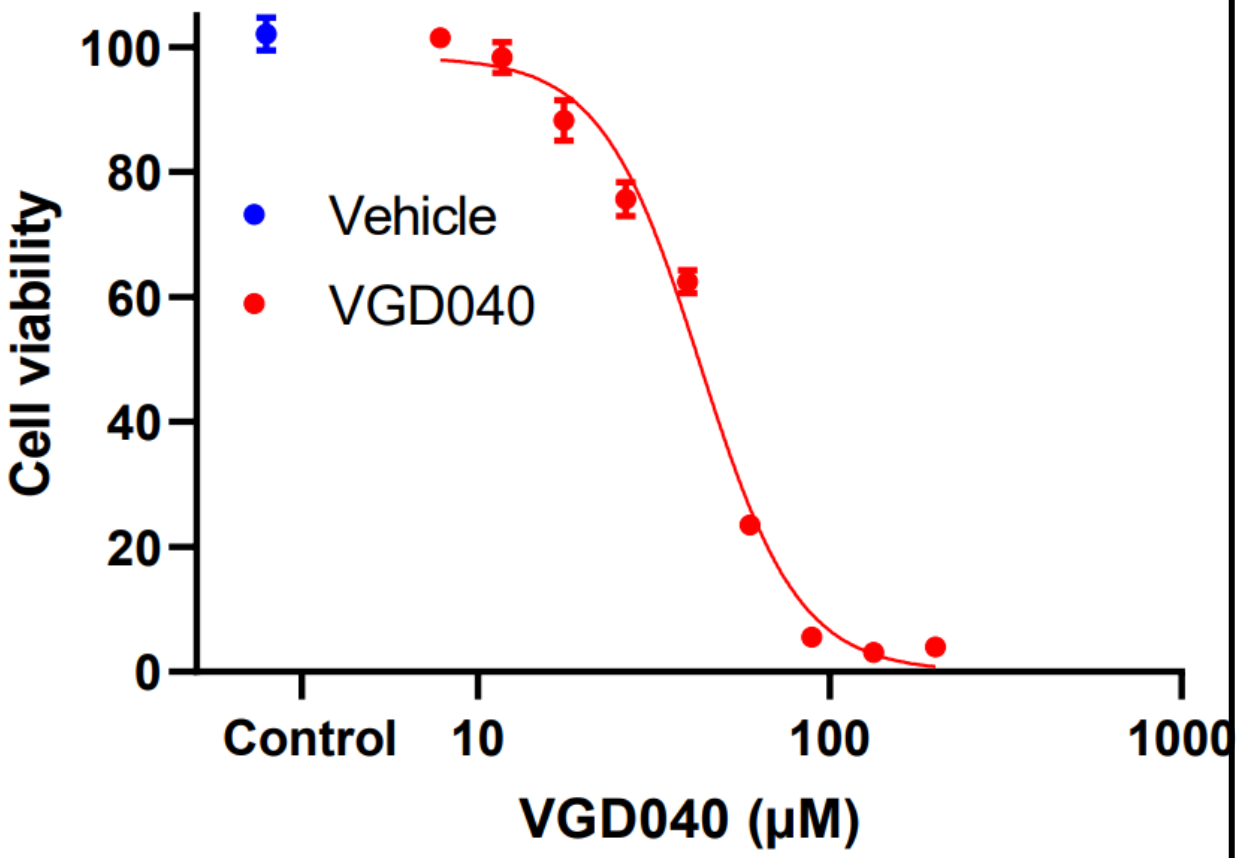

Figure 4.20: Dose-response curve for VGD040 on HEK293 cells. HEK 293 cells were treated with VGD040 for 48 h then cell viability was determined by MTT assay. VGD040 (red circles) at each concentration represents the mean ± SD of 4 wells, while the vehicle control (blue circle) represents the mean ± SD of 8 wells. Curve is a four-parameter nonlinear regression normalized to the bounds of this dose response curve. The viability was tested in 3 independent experiments performed on different days. The graph shown is of one representative experiment.

2.4 Stability of novel 4-hydroxycoumarin imines

The goal was to determine whether the aldimine group in JB104 was causing rapid hydrolysis in the aqueous assay buffer used to determine the IC_{50}s for compounds against various myosin isoforms. The small change from ketimine to aldimine surprisingly caused a complete

loss of activity compared with the analogous compound JB002. The stability of JB104 and JB002 were tested in the assay buffer over the course of 6 days. The predicted hydrolysis reactions for JB104 and JB002 are shown (**Fig. 4.21**).

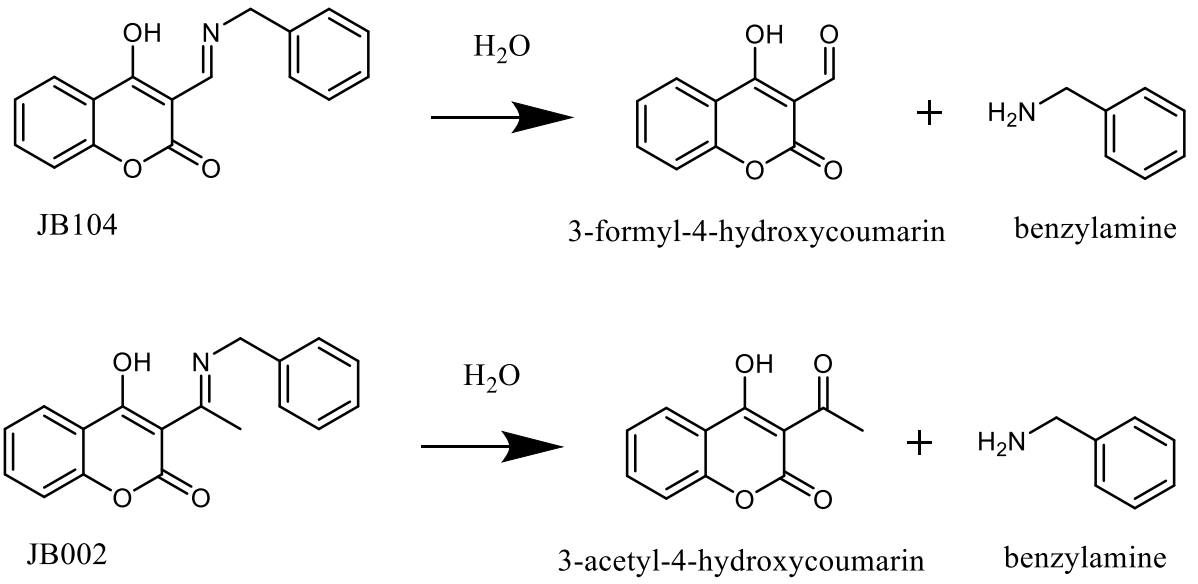

Figure 4.21: Proposed hydrolysis reactions for JB104 and JB002. The products of each are predicted to be benzylamine and either 3-formyl-4-hydroxycoumarin or 3-acetyl-4-hydroxycoumarin, respectively.

Hydrolysis experiments were performed at 30 ºC by mixing JB compounds in ATPase assay buffer at a final concentration 8 µM compound and 2% DMSO. Immediately after preparation a 3 mL aliquot was removed, and the UV spectrum was recorded. The remaining solution was kept at 30 ºC in a glass vial sealed with parafilm and every 24 hours another aliquot was removed and used to record the UV spectrum. The UV spectrum of each compound was graphed for each day of the experiment, and the UV spectrum of the combined predicted hydrolysis products for each compound was graphed (8 µM 3-acetyl-4-hydroxycoumarin + 8 µM benzylamine for JB104, and 8 µM 3-formyl-4-hydroxycoumarin + 8 µM benzylamine for JB002) (**Fig. 4.22**). The half-life was estimated by graphing the weighted average at each wavelength of the initial UV spectrum of the compound and the UV spectrum of the hydrolysis products. This weighted average

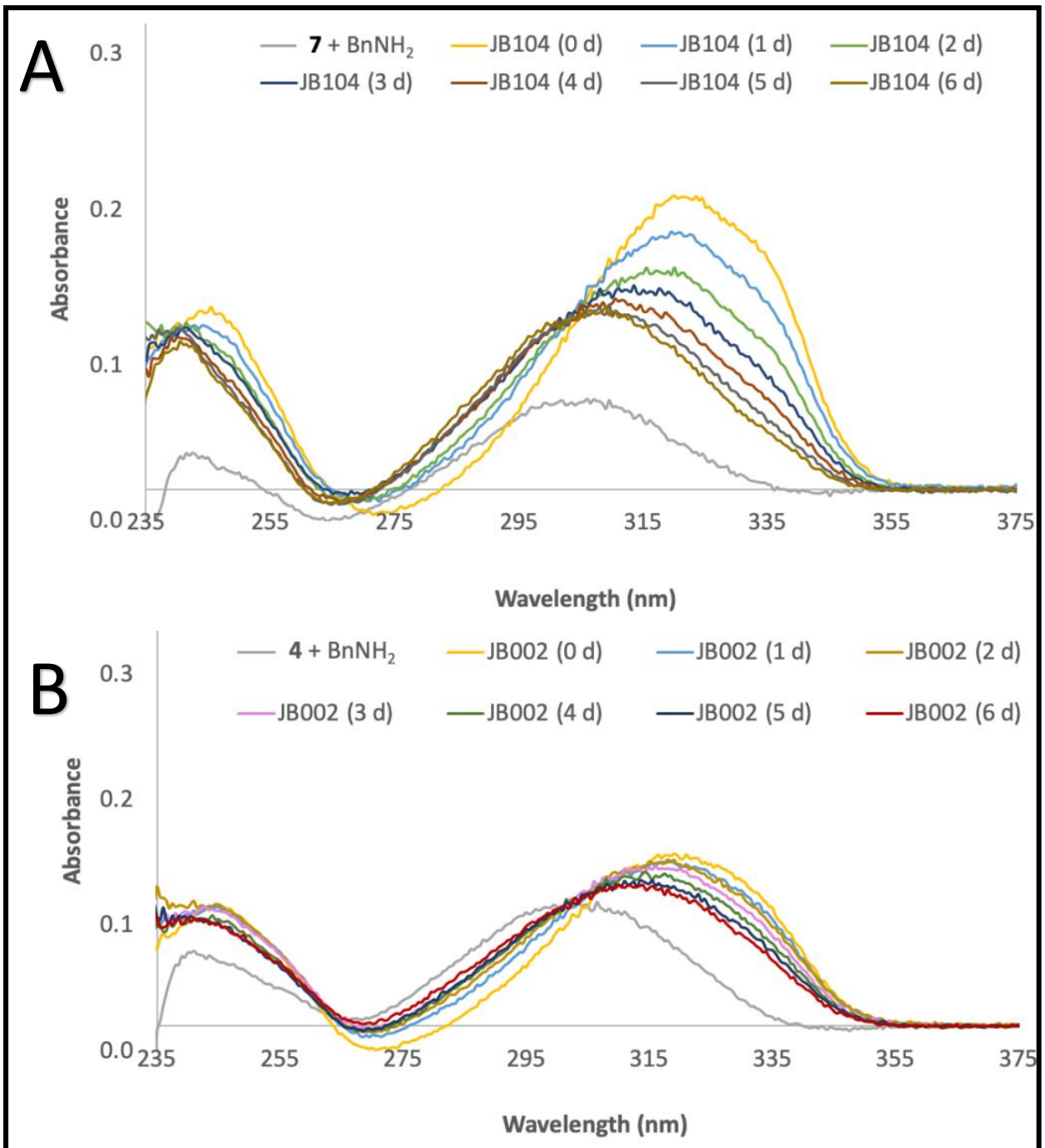

Figure 4.22: Daily spectrums of JB104 and JB002. The spectrum from 375 to 235 nm for JB104 (A) and JB002 (B) was taken immediately and every day after mixing with the assay buffer. Additionally, a spectrum of the predicted degradation products for the respective compounds is shown.

spectrum was compared with the experimental spectra for the compounds on each day of the experiment to determine how many days it took to reach a spectrum with similar absorbance values to the weighted average spectrum (**Fig. 4.23**).

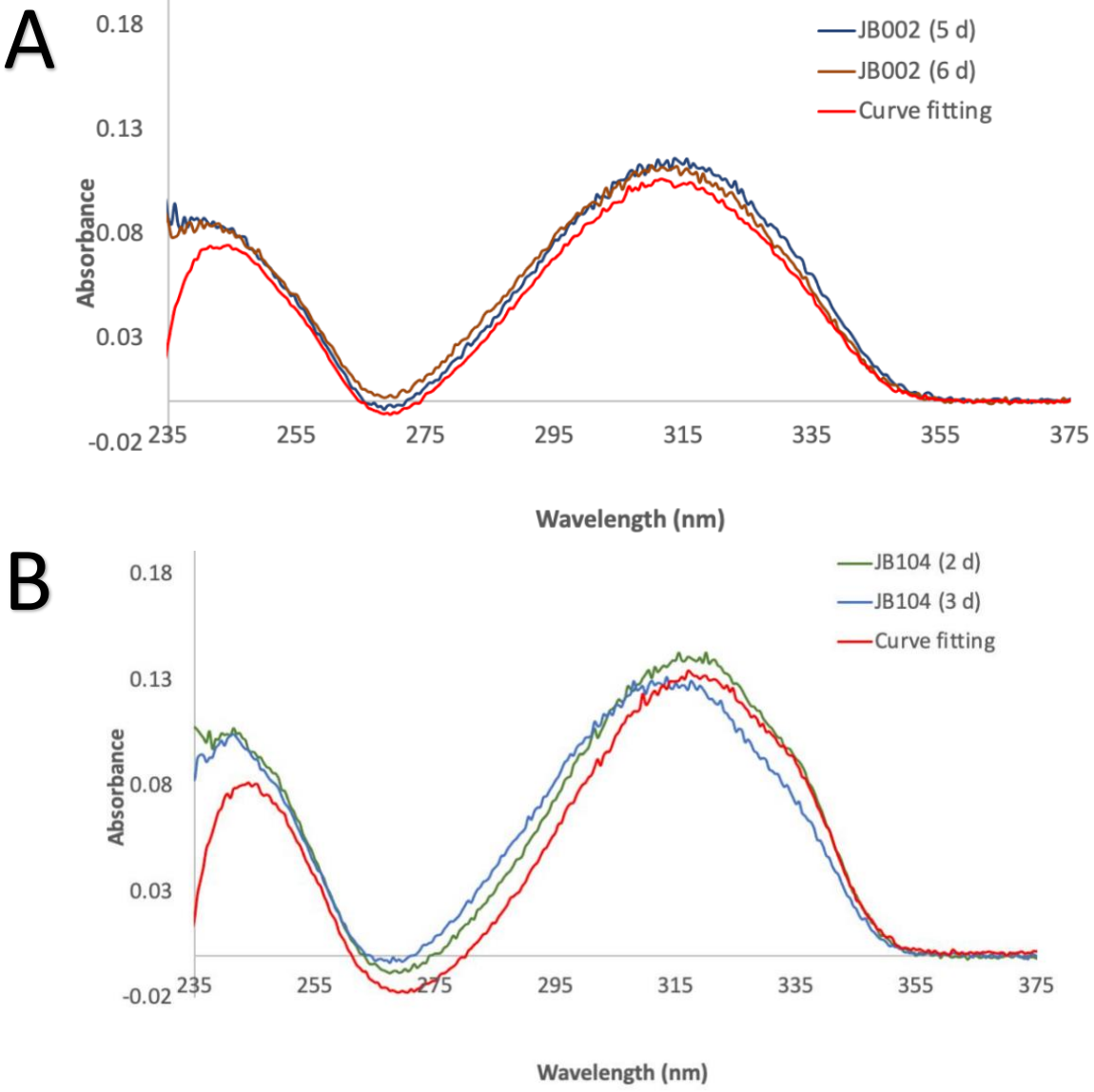

Figure 4.23: Estimated half-lives of JB104 and JB002. Weighted average of the spectra of the starting material and predicted degradation products shown with the matched spectra for the compound after incubation.

By taking the weighted average of the spectrum of the starting material and the degradation products it was possible to predict the spectrum of the solution containing a 50/50 mix of starting material and degradation products. In hindsight it may be more prudent to make this mixture containing 4 µM of starting material and 4 µM of each degradation product and take the spectrum directly as a reference instead of using a mathematical estimation. As expected, the

results indicate that the aldimine JB104 was less stable than the ketimine JB002, with half-lives of 2-3 days and greater than 6 days, respectively. However, the ATPase assay used to calculate IC_{50}s exposed the compounds to the buffer for less than 2 h. The aldimine hydrolysis rate was thus concluded to not be responsible for the complete loss of activity.

Several JB compounds were also tested for viability in Cos7 cells and dose response curves were produced. The solubility of the compounds limited them to the highest concentration tested with one set being tested up to 1,000 µM and another set only being tested up to 200 µM. On the first day after plating, the cells were observed to be about 40-50% confluent in the DMSO control wells. Precipitates were observed in the 200 µM solutions for JB061, JB062 and JB080. On the second day right before addition of MTT, the cells were observed to be about 60-70% confluency in DMSO control wells. A mistake was made when making the treatment solution for 0.1 µM for JB008 so these points were dropped from the analysis. Dose response curves were generated using GraphPad Prism 9.4.0 (**Fig. 4.24**). The background was subtracted using the average of the no cell (media only) control wells. The viability was normalized to average of DMSO (no compound) control wells. The compounds showed very little toxicity and only JB058 produced toxicity greater than 50% at the highest concentration, making calculations of CC_{50}s not practical. Instead CC_{10}s were calculated for each compound (JB008 = 286 ± 28 µM, JB057 = 184 ± 85 µM, JB058 = 57 ± 27 µM, JB059 = 339 ± 91 µM, JB061 = 39 ± 38 µM, JB062 = 36 ± 35 µM, JB080 = 46 ± 9 µM, JB092 = 110 ± 54 µM, JB100 = 135 ± 28 µM). The low toxicity and selective nature of these compounds makes them great drug candidates for further development as well as useful research compounds.

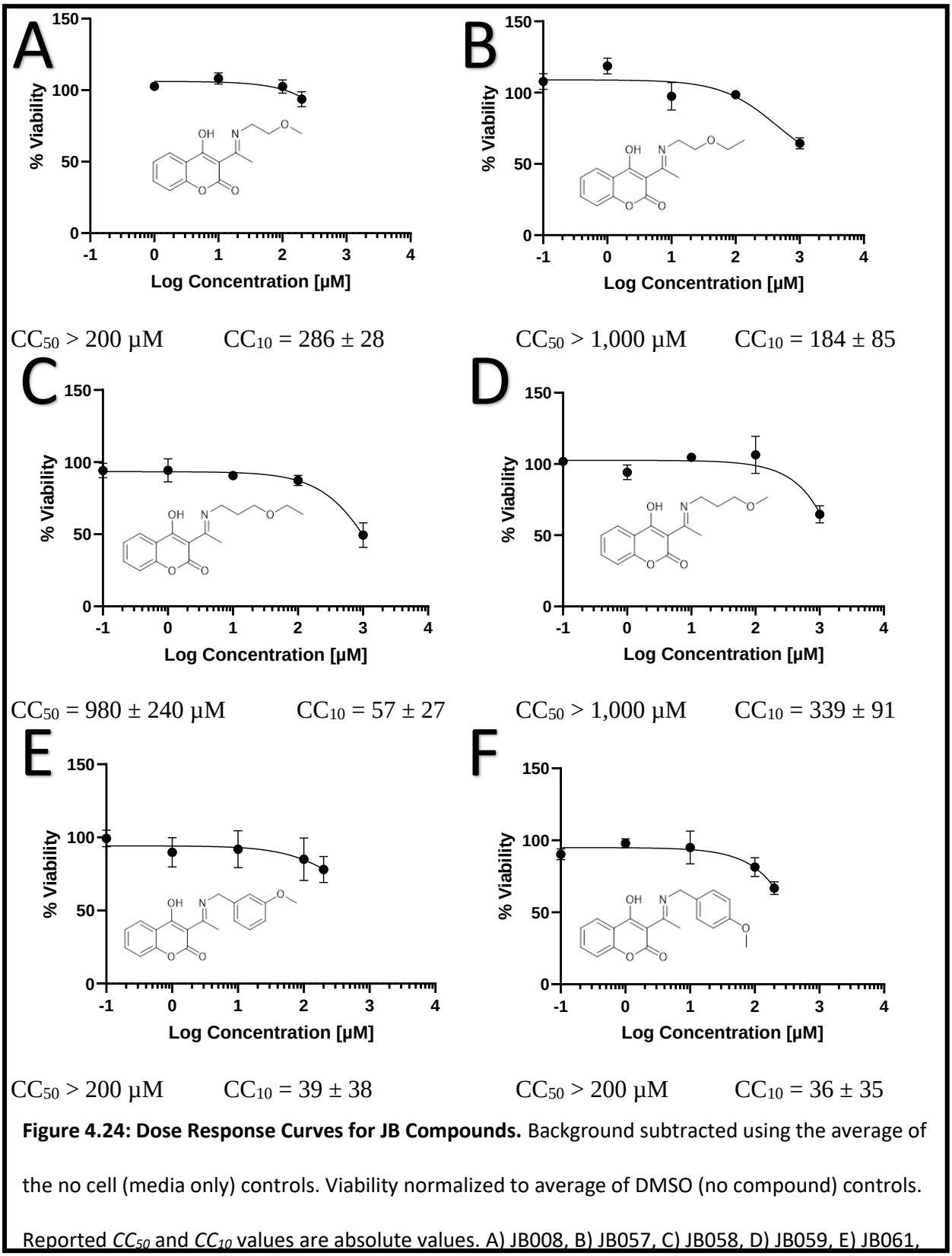

Figure 4.24: Dose Response Curves for JB Compounds. Background subtracted using the average of the no cell (media only) controls. Viability normalized to average of DMSO (no compound) controls. Reported CC_{50} and CC_{10} values are absolute values. A) JB008, B) JB057, C) JB058, D) JB059, E) JB061, F) JB062. Figure continued on next page.

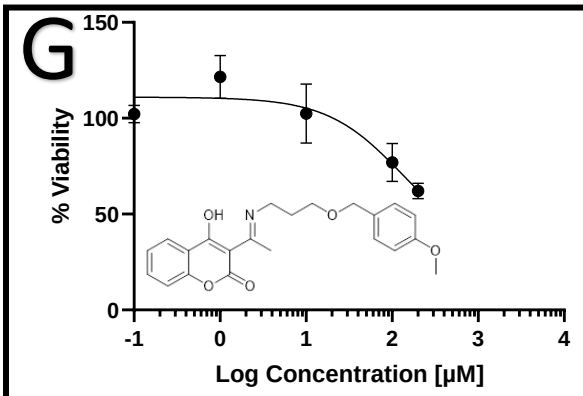

CC_{50} > 200 µM CC_{10} = 46 ± 9

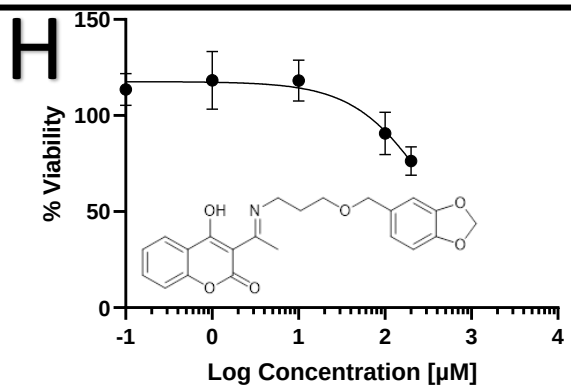

CC_{50} > 200 µM CC_{10} = 110 ± 54

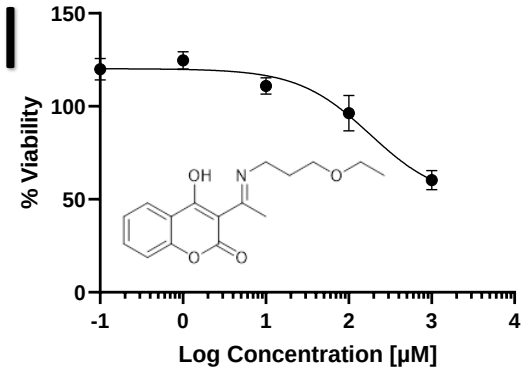

CC_{50} > 1,000 µM CC_{10} = 135 ± 28

Figure 4.24: Dose Response Curves for JB Compounds (cont.). Continued from previous page. G) JB080, H) JB092, I) JB100

Section 3: Experimental

Note: Special thanks to Dr. Subhash Verma and Dr. Ian Buxton for their guidance and support, and for allowing me to work in their laboratories and use their reagents and equipment. Special thanks to Dr. Amarawan Intasiri and Dr. Scott Barnett for their dedication and help with the development of assay protocols. Special thanks to Kabita Adhikari and Dylan Saxon for their patience, guidance, and help with growing cells. Special thanks to Md Azizul Islam for his hard work and devotion to the ACE2 project. Without the help of these individuals I would not have been able to do this work.

3.1 General Methods

Calu-3 were purchased from ATCC. The phUSMCs were originally isolated and telomerized in the laboratory of Dr. Ian Buxton and were donated by Dr. Ian Buxton. HEK293 cells, originally from ATCC, were donated from the cells maintained by Kabita Adhikari in Dr. Subhash Verma's laboratory. Cos7 cells, originally from ATCC, were donated from Dr. Christine Cremo's laboratory. All these cells were worked with under BSLII conditions taking all appropriate precautions. All work involving the growth of cells was performed under strict aseptic conditions working in a class II BSC and wearing appropriate PPE including gloves, lab coat, and safety glasses. All surfaces were cleaned before and after work with 70% ethanol. All materials in contact with the cells or culture media were purchased as sterile equipment or sterilized via autoclave. After use, all materials in contact with the cells or culture media were decontaminated by treatment with freshly prepared 20% bleach for a minimum of 15 minutes or sterilized in an autoclave. The care of HEK293 cells was previously described in the general methods section of chapter 3. Calu-3 and Cos7 cells were grown in a complete media that was prepared by mixing 440 mL of Dulbecco's Modified Eagle Medium (DMEM), with 50 mL of

FBS, 5 mL of 100X NEAA, and 5 mL of 200X PEST. phUSMCs were grown in a hTRT media that was prepared by mixing 450 mL of DMEM, 50 mL of FBS, 5 mL of 200X PEST, 50 µL of 0.15 mg/mL estrogen in ethanol (E2), and 50 µL of 2 mg/mL progesterone in ethanol (P4). The HEPES-buffered Krebs-Ringer (HPKR) solution (120 mM NaCl, 5 mM KCl, 1 mM $MgCl_2$, 25 mM $NaHCO_3$, 1 mM D-glucose, HEPES pH 7.4) used in phUSMC assays was prepared by mixing 3.5064 g NaCl, 0.1864 g KCl, 0.1017 g $MgCl_2$ heptahydrate, 1.0501 g $NaHCO_3$, 0.0901 g D-glucose in a beaker with 500 mL of water and the pH was adjusted to 7.40 by addition of approximately 10 mL of HEPES buffer. Calu-3, Cos7, and phUSMCs were grown in treated T75 flasks incubated in a 37 ºC incubator with a 5% CO_2 atmosphere alternating between media changes and splitting every three days. The cells were split by decanting the media, washing with 5 mL of PBS (pH 7.4), and adding of 2 mL of 0.25% Trypsin-EDTA. The Calu-3 and Cos7 cells were incubated with the trypsin solution for up to 10 minutes in a 37 ºC incubator with a 5% CO_2 atmosphere checking periodically for detachment with an inverted microscope, while a 5-minute incubation was sufficient for phUSMC detachment. Once cells detached 8 mL of fresh media was added to the flask and the suspension was transferred to a sterile 15 mL conical tube which was centrifuged at 100 rcf for 5 min. The supernatant was decanted and the pellet was resuspended in 2 mL of fresh media for Calu-3 and Cos7 cells or 0.5 mL for phUSMCs. The cells were seeded back into a T75 flask by adding 1 mL of the Calu-3 or Cos7 cell suspension or 200 µL of the phUSMC suspension and 9 mL of fresh media. To perform a cell count, 20 µL of the cell suspension was removed and mixed with 60 µL of PBS. A 10 µL aliquot of this was mixed with 10 µL of 0.2% trypan blue and 15 µL was added to a cell counting slide. The cells were counted on a Nexcelom Cellometer Auto T4, by selecting a dilution factor of eight and selecting either Calu-3 or HASMC under cell type. Water used for making solutions was distilled

diH_2O, unless otherwise noted. All reagents were warmed to 37 ºC in a bead bath prior to being used for live cell culture experiments, unless otherwise noted.

3.2 Screening, toxicity and validation of potential Covid-19 antivirals

Determining Optimal Cell Density and Fluorogenic Substrate Concentration

Materials and Reagents

Table 4.1: Materials and reagents for determining optimal cell density.

0.2% trypan blue solution	Gibco 0.25% Trypsin-EDTA	phenylmethylsulfonyl fluoride
Calu-3 cells	Gibco 200X NEAA	Sigma Aldrich 200X PEST
Cell counter	Gibco DMEM	Sterile 96-well plates
Cell counting slides	Gibco FBS	Sterile PBS (pH 7.4)
Class II BSC	Mca-APK-Dnp	Sterile pipette tips
CO_2 incubator	N-ethylmaleimide	Sterile T75 Flask
Fluorescent plate reader	NH_4OH	$ZnCl_2$

Preparation of Essential Solutions

The **Mca-APK-Dnp fluorogenic substrate** (1 mg) was reconstituted in 100 µl of 1% NH_4OH in H_2O and mixed with 1.335 mL of PBS and stored at -20 ºC.

A **100 mM N-ethylmaleimide (NEM)** solution was made by dissolving 0.0125 g NEM in 1 mL of H_2O.

A **100 mM phenylmethylsulfonyl fluoride (PMSF)** solution was made by dissolving 0.0174 g PMSF in 1 mL of ethanol.

A **2 mM $ZnCl_2$** solution was made by dissolving 0.0136 g $ZnCl_2$ in 1 mL of PBS.

Procedure

Calu-3 cells were grown in T75 flasks, split, and counted. For 5.5 x 10^6 cells/mL, 100 µL of cell suspension was mixed with 2,100 µL of media to get a working concentration of 2.5 x 10^5 cell/mL. To nine individual wells, 200 µL of this suspension was added to get 5 x 10^4 cells/well.

In a similar fashion, wells were seeded in sets of nine with concentrations of 1 x 10^5, 5 x 10^5, and 1 x 10^6 cells/well. Additionally, a set of nine wells was seeded with 200 µL of media and no cells. The plate was incubated at 37 °C with 5% CO_2 for 24 h. After incubation, the media was removed by aspiration, and the wells were washed twice with 100 µL of sterile PBS. The fluorogenic substrate solution was prepared by mixing 525 µL of PBS, 6 µL of 100 mM of NEM, 6 µL of PMSF, 3 µL of Zn_2Cl and 60 µL of substrate for a final substrate concentration of 100 µM. In a similar way 60, 20, 10, 6, 2, and 0 µM substrate solutions were prepared. When using smaller volumes of substrate an equivalent volume of PBS was used to keep the final volume consistent. For 60 and 20 µM concentrations a total volume twice that of the other concentrations was made. For each substrate concentration, 100 µL of the solution was added to five separate wells each with a different cell concentration (0, 5 x 10^4, 1 x 10^5, 5 x 10^5, and 1 x 10^6 cells/well). The 20 and 60 µM substrate concentrations, were tested in duplicate for each cell concentration. The plate was placed in the incubator for 20 minutes. Then 95 µL of solution was transferred to black 96-well plates and the fluorescence was measured by using an excitation wavelength of 320 nm and an emission wavelength of 405 nm.

Initial Screening for ACE2 Down-modulation

Materials and Reagents

Table 4.2: Materials and reagents for initial screen.

0.2% trypan blue solution	Gibco 0.25% Trypsin-EDTA	Sigma Aldrich 200X PEST
20 mM compound stock in DMSO	Gibco 200X NEAA	Sterile 2 mL tubes
Calu-3 cells	Gibco DMEM	Sterile 96-well plates
Cell counter	Gibco FBS	Sterile PBS (pH 7.4)
Cell counting slides	Mca-APK-Dnp	Sterile pipette tips
Class II BSC	N-ethylmaleimide	Sterile T75 Flask
CO_2 incubator	NH_4OH	$ZnCl_2$
Fluorescent plate reader	phenylmethylsulfonyl fluoride	

Preparation of Essential Solutions

A 1 mg vial of **Mca-APK-Dnp fluorogenic substrate** was reconstituted in 100 µl of 1% NH_4OH in H_2O and mixed with 1.335 mL of PBS and stored at -20 ºC.

A **100 mM N-ethylmaleimide (NEM)** solution was made by dissolving 0.0125 g NEM in 1 mL of H_2O.

A **100 mM phenylmethylsulfonyl fluoride (PMSF)** solution was made by dissolving 0.0174 g PMSF in 1 mL of ethanol.

A **2 mM $ZnCl_2$** solution was made by dissolving 0.0136 g $ZnCl_2$ in 1 mL of PBS.

Procedure

Calu-3 cells were grown in T75 flasks, split, and counted. For 2.62 x 10^6 cells/mL, 2.9 mL of cell suspension was mixed with 4.6 mL of media to make a working cell suspension with a concentration of 1.0 x 10^6 cells/mL. For each compound to be tested (18 total), 350 µL of a solution of media containing 40 µM compound and 2% DMSO, 343 µL media, 6.3 µL DMSO, and 0.7 µL of 20 mM compound stock solution in DMSO were mixed in sterile 1.5 mL tubes. For use as the vehicle control (media containing 2% DMSO), 343 µL of media and 7 µL of DMSO were mixed in a sterile 1.5 mL tube. For use as a no cell control (media containing 1% DMSO), 693 µL media and 7 µL of DMSO were mixed in a sterile 1.5 mL tube. Next 350 µL of working cell suspension (1.0 x 10^6 cells/mL) was mixed with each of the compound and vehicle control tubes. The final concentration of the compounds was 20 µM and DMSO was 1%. Next 200 µL from each tube was added to each of three separate wells in a sterile 96-well culture plate (giving 1.0 x 10^5 cells/well for the wells with cells). The plate was incubated at 37 °C with 5% CO_2 for 24 h. After incubation, the assay buffer was prepared by mixing 13,725 µl of PBS, 900 µl of 1 mM Mca-APK-Dnp, 150 µl of 100 mM NEM, 150 µl of 100 mM PMSF, and 75 µl of 2 mM Zn_2Cl. Then the media was removed, and the wells were washed with two times with 100

µL of sterile PBS. Next 100 µl of assay buffer was added to every well and the plate was placed in the incubator for 20 minutes. After incubation, 95 µL of the assay buffer solution was transferred to a black 96-well plate and the fluorescence was measured by using an excitation wavelength of 320 nm and an emission wavelength of 405 nm. The fluorescent intensity was taken as a measure of ACE2 expression.

Calculation

$$\%\ Activity\ (relative\ to\ vehicle\ control) = \left\{\frac{(\text{fluorescence for test well} - \text{average fluorescence for no cell control})}{(\text{average fluorescence for vehicle control} - \text{average fluorescence for no cell control})}\right\} \times 100$$

MTT Assay Used in Initial Screening

Materials and Reagents

Table 4.3: Materials and reagents for initial MTT assay.

0.2% trypan blue solution	Concentrated HCl	Sigma Aldrich 200X PEST
20 mM compound stock in DMSO	Gibco 0.25% Trypsin-EDTA	Sterile 2 mL tubes
Absorbance plate reader	Gibco 200X NEAA	Sterile 96-well plates
Calu-3 cells	Gibco DMEM	Sterile PBS (pH 7.4)
Cell counter	Gibco FBS	Sterile pipette tips
Cell counting slides	Isopropanol	Sterile T75 Flask
Class II BSC	MTT	
CO_2 incubator	Multichannel micropipette	

Preparation of Essential Solutions

Prepare 10 mL of sterile **12 mM (5 mg/mL) MTT stock solution** by adding 50 mg of MTT and 10 mL of PBS in glass vial. Vortex until all MTT powder is dissolved. Use a syringe to pass the solution through a sterile (autoclaved) 0.2 µm HPTFE filter and into a sterile 15 mL centrifuge tube wrapped in aluminum foil to prevent exposure to light. Store at -20 ºC.

At the time of addition, prepare 4.8 mL of sterile **1.2 mM (0.5 mg/mL) MTT working solution** in complete growth media in a sterile reagent reservoir by adding 480 µL of 12 mM (5

mg/mL) MTT stock solution and 4,320 µL of complete media. Pipette 1 mL of the solution up and down 15 times to mix. Turn the light off in the BSC while working with MTT to prevent degradation.

Prepare 11.2 mL of **stop solution (0.04 M HCl in isopropanol)** in a plastic reagent reservoir by adding 11.163 mL of isopropanol and 37.0 µL of conc. HCl to a reagent reservoir. Pipette 1 mL of the solution up and down 15 times to mix.

Procedure

Calu-3 cells were grown in T75 flasks, split, and counted. For 5.03 x 10^6 cells/mL, 1.42 mL of cell suspension was mixed with 5.73 mL of media to make a working cell suspension with a concentration of 1.0 x 10^6 cells/mL. For each compound to be tested (18 total), 350 µL of a solution of media containing 40 µM compound and 2% DMSO, 343 µL media, 6.3 µL DMSO, and 0.7 µL of 20 mM compound stock solution in DMSO were mixed in sterile 1.5 mL tubes. For use as the vehicle control (media containing 2% DMSO), 343 µL of media and 7 µL of DMSO were mixed in a sterile 1.5 mL tube. For use as a no cell control (media containing 1% DMSO), 693 µL media and 7 µL of DMSO were mixed in a sterile 1.5 mL tube. Next 350 µL of working cell suspension (1.0 x 10^6 cells/mL) was mixed with each of the compound and vehicle control tubes. The final concentration of the compounds was 20 µM and DMSO was 1%. Next 200 µL from each tube was added to each of three separate wells in a sterile 96-well culture plate (giving 1.0 x 10^5 cells/well for the wells with cells). The plate was incubated at 37 °C with 5% CO_2 for 24 h. After incubation, the media was removed, and the wells were washed with two times with 100 µL of sterile PBS. The MTT stock solution was diluted to 0.5 mg/mL in media and 100 µL was added to each well. The plate was then incubated at 37 °C with 5% CO_2 for 2 h. To stop the reaction, 200 µL of prewarmed (37 °C) HCl in isopropanol was added to each well

and the formazan crystals were dissolved by pipetting up and down. Absorbance was read at 570 nm.

Calculation

$$\%\ Viability\ (relative\ to\ vehicle\ control) = \left\{\frac{(\text{absorbance for test well} - \text{average absorbance for no cell control})}{(\text{average absorbance for vehicle control} - \text{average absorbance for no cell control})}\right\} \times 100$$

Treatment for qRT-PCR to Validate ACE2 Down-modulatory Mechanism

Materials and Reagents

Table 4.4: Materials and reagents for qRT-PCR treatment.

0.2% trypan blue solution	CO_2 incubator	Sigma Aldrich 200X PEST
20 mM compound stock in DMSO	Gibco 0.25% Trypsin	Sterile 2 mL tubes
Absorbance plate reader	Gibco 0.25% Trypsin-EDTA	Sterile 24-well plates
Calu-3 cells	Gibco 200X NEAA	Sterile PBS (pH 7.4)
Cell counter	Gibco DMEM	Sterile pipette tips
Cell counting slides	Gibco FBS	Sterile T75 Flask
Class II BSC	Multichannel micropipette	

Procedure

Calu-3 cells were grown in T75 flasks, split, and counted. At 5.89 x 10^6 cells/mL, 2.04 mL of the cell suspension was mixed with 21.96 mL of media to make a working cell suspension with a concentration of 5.01 x 10^5 cells/mL. Each well in the sterile 24-well plate received 1 mL of this solution except for two wells which received 1 mL of media without cells. The plate was incubated at 37 °C with 5% CO_2 for 24 h. After incubation, the media was removed, and 200 µL of EDTA-free trypsin solution was added to each well. The plate was incubated at 37 °C with 5% CO_2 for 20 minutes. Two replicate solutions for each compound to be tested was prepared by mixing 1,185.6 µL of media, 12.96 µL of DMSO, and 1.44 µL of the 20 mM stock solution in DMSO in 1.5 mL tubes to give a solution of media containing 24 µM of compound and 1.2% DMSO. Additionally, four vehicle control solutions were prepared made by mixing 1185.6 µL of

media and 14.4 μL of DMSO in 1.5 mL tubes to give a solution of media containing 1.2% DMSO. After the 20-minute trypsin incubation, 1.0 mL of each solution of media containing 24 μM of compound and 1.2% DMSO was added to duplicate wells with cells, and 1.0 mL of each solution of media containing 1.2% DMSO was added to quadruplicate wells with cells. The plate was incubated at 37 °C with 5% CO_2 for 24 h. After incubation the RNA was extracted by Dr. Verma's lab.

Treatment for Western Blot to Validate ACE2 Down-modulation

Materials and Reagents

Table 4.5: Materials and reagents for Western blot treatment.

0.2% trypan blue solution	CO_2 incubator	PBS-EDTA (pH 7.4)
20 mM compound stock in DMSO	Gibco 0.25% Trypsin	Sigma Aldrich 200X PEST
Absorbance plate reader	Gibco 0.25% Trypsin-EDTA	Sterile 2 mL tubes
Calu-3 cells	Gibco 200X NEAA	Sterile 24-well plates
Cell counter	Gibco DMEM	Sterile PBS (pH 7.4)
Cell counting slides	Gibco FBS	Sterile pipette tips
Class II BSC	Multichannel micropipette	Sterile T75 Flask

Procedure

Calu-3 cells were grown in T75 flasks, split, and counted. At 5.54 x 10^6 cells/mL, 2.256 mL of the cell suspension was mixed with 22.744 mL of media to make a working cell suspension with a concentration of 5.0 x 10^5 cells/mL. Each well in the sterile 24-well plate received 1 mL of this solution except for two wells which received 1 mL of media without cells. The plate was incubated at 37 °C with 5% CO_2 for 24 h. After incubation, the media was removed, and 200 μL of EDTA-free trypsin solution was added to each well. The plate was incubated at 37 °C with 5% CO_2 for 20 minutes. Two replicate solutions for each compound to be tested was prepared by mixing 1,185.6 μL of media, 12.96 μL of DMSO, and 1.44 μL of the 20 mM stock solution in DMSO in 1.5 mL tubes to give a solution of media containing 24 μM of compound and 1.2% DMSO. Additionally, four vehicle control solutions were prepared made by mixing 1185.6 μL of

media and 14.4 µL of DMSO in 1.5 mL tubes to give a solution of media containing 1.2% DMSO. After the 20-minute trypsin incubation, 1.0 mL of each solution of media containing 24 µM of compound and 1.2% DMSO was added to duplicate wells with cells, and 1.0 mL of each solution of media containing 1.2% DMSO was added to quadruplicate wells with cells. The plate was incubated at 37 °C with 5% CO_2 for 24 h. After incubation, the media was removed and a 0.2 mL solution of PBS-EDTA was added to each well and the plate was incubated for 30 minutes. The cells were then resuspended, and the suspensions were placed in 2 mL tubes, that were then centrifuged at 100 rcf for 10 minutes. The supernatant was decanted, and the cell pellets were frozen at -20 °C.

3.3 Developing a Screening Assay for Cx43 Down-modulation

1st Attempt Ethidium Bromide Assay

Materials and Reagents

Table 4.6: Materials and reagents for initial EtBr assay.

0.2% trypan blue solution	CO_2 incubator	Sigma Aldrich 200X PEST
10 mg/mL EtdBr Stock	Fluorescent plate reader	Sterile 15 mL plastic tube
20 mL glass vial	Gibco 0.25% Trypsin-EDTA	Sterile 2 mL tubes
20 mM compound stock in DMSO	Gibco DMEM	Sterile, black 96-well plates
Calu-3 cells	Gibco FBS	Sterile DMSO
Cell counter	HPKR solution	Sterile PBS (pH 7.4)
Cell counting slides	hTERT media	Sterile pipette tips
Centrifuge	Inverted Microscope	Sterile Reagent reservoirs
Class II BSC	Multichannel micropipette	Sterile T75 Flask

Preparation of essential solutions

Prepare 2 mL of **10 mM compound of interest in hTRT media containing 0.5% DMSO** by pipetting 1 µL of 20 mM compound of interest stock solution in DMSO into a 15-mL sterile centrifuge tube containing 1,980 µL of sterile hTRT media and 19 µL of sterile DMSO. Mix well.

Prepare 12 mL of **hTRT media containing 0.5% DMSO** by pipetting 60 µL of sterile DMSO into a 15-mL sterile centrifuge tube containing 11.94 mL of sterile hTRT media.

Prepare 12 mL of **HPKR diluted buffer** by pipetting 96 µL of water into a 20 mL glass vial containing 11.904 mL of HPKR solution.

Prepare the different concentrations of **EtBr in HPKR solution** in a 5-mL glass vial by mixing 21.7, 93.7, or 108.5 µL of 10 mg/mL EtBr stock with 2,178.3, 3,703.4, or 2,091.6 µL of HPKR diluted buffer for 2, 5, or 10 µM final concentrations of EtBr, respectively.

Procedure:

The phUSMCs were grown in T75 flasks, split, and counted. Two cell suspensions at 1.25 X 10^4 and 2.5 X 10^4 cells/mL in hTRT media were prepared in 15-mL sterile centrifuge tubes. 200 µL of the cell suspensions or 200 µL of PBS (as a control) were added to the appropriate wells of 2 sterile, black 96-well plate to give 2.5 X 10^3 or 5.0 X 10^3 cells/well which were incubated at 37 ºC for 48 hours. After incubation the cells were washed twice with 200 µL of sterile PBS, followed by 200 µL of a solution of hTRT media containing 10 mM compound and 0.5% DMSO or 200 µL of a solution of hTRT media containing 0.5% DMSO as a no compound control. The plate was incubated at 37 ºC with 5% CO_2 for 24 hours. After incubation, the media was removed and the cells were washed with 200 µL of HPKR solution twice. Each well received 100 µL of a solution of HPKR containing EtBr at the varying concentrations or a HPKR solution without EtBr as a control. The plates were incubated in the dark at 37 ºC for either 5 or 10 minutes. The cells were rinsed with 100 µL of HPKR solution three times to remove the extracellular EtBr and the fluorescence intensity was measured using a plate reader with an excitation of 285 nm and an emission of 605 nm. Readings were taken immediately and every 10 minutes for up to 1 hour.

Ethidium Bromide Assay with Increased Cell and EtBr Concentration and Increased EtBr Incubation Time

Materials and Reagents

Table 4.7: Materials and reagents for further optimization of EtBr assay.

0.2% trypan blue solution	CO_2 incubator	Sigma Aldrich 200X PEST
10 mg/mL EtdBr Stock	Fluorescent plate reader	Sterile 15 mL plastic tube
20 mL glass vial	Gibco 0.25% Trypsin-EDTA	Sterile 2 mL tubes
20 mM compound stock in DMSO	Gibco DMEM	Sterile, black 96-well plates
Calu-3 cells	Gibco FBS	Sterile DMSO
Cell counter	HPKR solution	Sterile PBS (pH 7.4)
Cell counting slides	hTERT media	Sterile pipette tips
Centrifuge	Inverted Microscope	Sterile Reagent reservoirs
Class II BSC	Multichannel micropipette	Sterile T75 Flask

Preparation of essential solutions

Prepare 15 mL of **10 mM compound of interest in hTRT media containing 0.5 % DMSO** by pipetting 7.5 µL of 20 mM compound of interest stock solution in DMSO into a 15-mL sterile centrifuge tube containing 14,925 µL of sterile hTRT media and 67.5 µL of sterile DMSO. Mix well.

Prepare 15 mL of **hTRT media containing 0.5 % DMSO** by pipetting 75 µL of sterile DMSO into a 15-mL sterile centrifuge tube containing 14,925 µL of sterile hTRT media.

Prepare of different concentration of EtBr in HPKR solution in a 5-mL glass vial by mixing 0, 26, or 253 µL of **10 mg/mL** EtBr stock with 253, 227, or 0 µL of water and 7,747 µL of HPKR buffer for 0, 80, or 800 µM final concentrations of EtBr, respectively.

Procedure

The phUSMCs were grown in T75 flasks, split, and counted. Two cell suspensions at 5.0 X 10^4 and 7.5 X 10^4 cells/mL in hTRT media were prepared in 15-mL sterile centrifuge tubes. 200 µL of the cell suspensions were added to the appropriate wells of 3 sterile, black 96-well plate to

give 1.0 X 10^4 or 1.5 X 10^4 cells/well which were incubated at 37 ºC for 48 hours. The cells were washed with 200 µL of sterile PBS once followed by 200 µL of a solution of hTRT media containing 10 mM test compound and 0.5% DMSO or a solution of hTRT media containing 0.5% DMSO as a no compound control. The plate was incubated at 37 ºC with 5% CO_2 for 24 hours. After incubation, each well received 100 µL of a solution of HPKR containing EtBr at the varying concentrations (0, 80, or 800 µM to give final concentrations of 0, 26.7, or 266.7 µM). The plates were incubated in the dark at 37 ºC with 5% CO_2 for 15, 30, or 60 minutes. The cells were rinsed with 300 µL of HPKR solution once followed by a 100 µL wash to remove the extracellular EtBr and the fluorescence intensity was measured using a plate reader with an excitation of 285 nm and an emission of 605 nm. Readings were taken immediately and every ten minutes for up to 1 hour.

Ethidium Bromide Assay Testing for Milder EtBr Conditions

Materials and Reagents

Table 4.8: Materials and reagents for testing milder conditions.

0.2% trypan blue solution	CO_2 incubator	Sigma Aldrich 200X PEST
10 mg/mL EtdBr Stock	Fluorescent plate reader	Sterile 15 mL plastic tube
20 mL glass vial	Gibco 0.25% Trypsin-EDTA	Sterile 2 mL tubes
20 mM compound stock in DMSO	Gibco DMEM	Sterile DMSO
Calu-3 cells	Gibco FBS	Sterile PBS (pH 7.4)
Cell counter	HPKR solution	Sterile pipette tips
Cell counting slides	hTERT media	Sterile Reagent reservoirs
Centrifuge	Inverted Microscope	Sterile T75 Flask
Class II BSC	Multichannel micropipette	Sterile, black 96-well plates

Preparation of essential solutions

Prepare 25 mL of **30 µM EtBr in HPKR solution** by pipetting 30 µL of EtBr stock into a 25 mL volumetric flask. Add HPKR buffer up to the bottom of the neck of the flask and swirl to mix. Add HPKR buffer to the fill line, cap, and invert to mix. Store in 25 mL glass vial covered with aluminum foil.

Prepare 25 mL of **300 µM EtBr in HPKR solution** by pipetting 300 µL of EtBr stock into a 25 mL volumetric flask. Add HPKR buffer up to the bottom of the neck of the flask and swirl to mix. Add HPKR buffer to the fill line, cap, and invert to mix. Store in 25 mL glass vial covered with aluminum foil.

Prepare 25 mL of **0 µM EtBr in HPKR solution** by pipetting 30 µL of water into a 25 mL volumetric flask. Add HPKR buffer up to the bottom of the neck of the flask and swirl to mix. Add HPKR buffer to the fill line, cap, and invert to mix. Store in 25 mL glass vial covered with aluminum foil.

Prepare 17 mL of **hTRT media containing 0.5 % DMSO** by pipetting 85 µL of sterile DMSO into a sterile reagent resevoir containing 16,915 µL of hTRT media.

Procedure

The phUSMCs were grown in T75 flasks, split, and counted. Two cell suspensions at 1.25 X 10^4 and 2.5 X 10^4 cells/mL in hTRT media were prepared in 15-mL sterile centrifuge tubes. 200 µL of the cell suspensions were added to the appropriate wells of a sterile 96-well plate to give 2.5 X 10^3 or 5.0 X 10^3 cells/well which were incubated at 37 ºC for 48 hours. The cells were washed with 200 µL of sterile PBS once followed by 200 µL of a solution of hTRT media containing 0.5% DMSO. The plate was incubated at 37 ºC with 5% CO_2 for 24 hours. After incubation, each well received 100 µL of a solution of HPKR containing EtBr at the varying concentrations (0, 30, or 300 µM to give final concentrations of 0, 10, or 100 µM, respectively). The wells were incubated for 5, 10, or 15 minutes prior to being rinsed with 300 µL of HPKR solution followed by the addition of 100 µL of HPKR. Then, 90 µL of the HPKR solution was removed and the fluorescence intensity was measured using a plate reader with an excitation of 285 nm and an emission of 605 nm. Readings were taken immediately and every 10 minutes for up to 1 hour.

Kinetics of Ethidium Bromide Uptake by phUSMCs

Materials and Reagents

Table 4.9: Materials and reagents for EtBr uptake kinetics.

0.2% trypan blue solution	CO_2 incubator	Sigma Aldrich 200X PEST
10 mg/mL EtdBr Stock	Fluorescent plate reader	Sterile 15 mL plastic tube
20 mL glass vial	Gibco 0.25% Trypsin-EDTA	Sterile 2 mL tubes
20 mM compound stock in DMSO	Gibco DMEM	Sterile DMSO
Calu-3 cells	Gibco FBS	Sterile PBS (pH 7.4)
Cell counter	HPKR solution	Sterile pipette tips
Cell counting slides	hTERT media	Sterile Reagent reservoirs
Centrifuge	Inverted Microscope	Sterile T75 Flask
Class II BSC	Multichannel micropipette	Sterile, black 96-well plates

Preparation of essential solutions

Prepare 25 mL of **300 µM EtBr in HPKR solution** by pipetting 300 µL of EtBr stock into a 25 mL volumetric flask. Add HPKR buffer up to the bottom of the neck of the flask and swirl to mix. Add HPKR buffer to the fill line, cap, and invert to mix. Store in 25 mL glass vial covered with aluminum foil.

Prepare 25 mL of **300 µM EtBr blank in HPKR solution** by pipetting 300 µL of water into a 25 mL volumetric flask. Add HPKR buffer up to the bottom of the neck of the flask and swirl to mix. Add HPKR buffer to the fill line, cap, and invert to mix. Store in 25 mL glass vial covered with aluminum foil.

Prepare 17 mL of **hTRT media containing 0.5 % DMSO** by pipetting 85 µL of sterile DMSO into a sterile reagent resevoir containing 16,915 µL of hTRT media.

Procedure

The phUSMCs were grown in T75 flasks, split, and counted. Two cell suspensions at 1.25 X 10^4 and 2.5 X 10^4 cells/mL in hTRT media were prepared in 15-mL sterile centrifuge tubes. 200 µL of the cell suspensions were added to the appropriate wells of a sterile 96-well plate to give 2.5 X 10^3 or 5.0 X 10^3 cells/well which were incubated at 37 ºC for 48 hours. The cells were

washed with 200 µL of sterile PBS once followed by 200 µL of a solution of hTRT media containing 0.5% DMSO. The plate was incubated at 37 ºC with 5% CO_2 for 24 hours. After incubation each well received 100 µL of a solution of HPKR containing 300 µM EtBr or a blank HPKR solution. The solution of HPKR containing EtBr and the blank solution of HPKR without EtBr were then added to the wells in appropriate intervals such that at the time of reading there would be incubations of 5, 10, 15, 30, 60, or 100 minutes. The plate was incubated in the dark at 37 ºC with 5% CO_2 between additions. The cells were then rinsed with 300 µL of HPKR solution followed addition of 100 µL of HPKR. Then, 90 µL of the HPKR was removed and the fluorescence intensity was measured using a plate reader with an excitation of 285 nm and an emission of 605 nm.

Cx43 Down-modulation Trial Screen

Materials and Reagents

Table 4.10: Materials and reagents for trial screen.

0.2% trypan blue solution	CO_2 incubator	Sigma Aldrich 200X PEST
10 mg/mL EtdBr Stock	Fluorescent plate reader	Sterile 15 mL plastic tube
20 mL glass vial	Gibco 0.25% Trypsin-EDTA	Sterile 2 mL tubes
20 mM compound stock in DMSO	Gibco DMEM	Sterile DMSO
Calu-3 cells	Gibco FBS	Sterile PBS (pH 7.4)
Cell counter	HPKR solution	Sterile pipette tips
Cell counting slides	hTERT media	Sterile Reagent reservoirs
Centrifuge	Inverted Microscope	Sterile T75 Flask
Class II BSC	Multichannel micropipette	Sterile, black 96-well plates

Preparation of essential solutions

Prepare 25 mL of **300 µM EtBr in HPKR solution** by pipetting 300 µL of EtBr stock into a 25 mL volumetric flask. Add HPKR buffer up to the bottom of the neck of the flask and swirl to mix. Add HPKR buffer to the fill line, cap, and invert to mix. Store in 25 mL glass vial covered with aluminum foil.

Prepare 25 mL of **300 µM EtBr blank in HPKR solution** by pipetting 300 µL of water into a 25 mL volumetric flask. Add HPKR buffer up to the bottom of the neck of the flask and swirl to mix. Add HPKR buffer to the fill line, cap, and invert to mix. Store in 25 mL glass vial covered with aluminum foil.

Prepare 1.6 mL of sterile **hTRT media containing 10 µM compound in 0.5% DMSO**. Pipette 7.2 µL of sterile DMSO followed by 0.8 µL of 20 mM compound stock into sterile 2 mL plastic tubes containing 1,592 µL of hTRT media.

Prepare 3.2 mL of **hTRT media containing 0.5 % DMSO** by pipetting 16 µL of sterile DMSO into a sterile reagent resevoir containing 3,184 µL of hTRT media.

Procedure

The phUSMCs were grown in T75 flasks, split, and counted. A cell suspension of 1.25 X 10^4 cells/mL in hTRT media was prepared in a 15-mL sterile centrifuge tube. 200 µL of the cell suspension was added to the wells a sterile, black 96-well plate to give 2.5 X 10^3 cells/well which was incubated at 37 ºC for 72 hours. The cells were washed with 200 µL of sterile PBS followed by 200 µL of a solution of hTRT media containing 10 mM compound and 0.5% DMSO or 200 µL of a solution of hTRT media containing 0.5% DMSO. The plate was incubated at 37 ºC with 5% CO_2 for 24 hours. After incubation each well received 100 µL of a solution of HPKR containing 300 µM EtBr or a blank HPKR solution. The plate was incubated in the dark at 37 ºC with 5% CO_2 for 30 minutes. The cells were then rinsed with 300 µL of HPKR solution followed by the addition of 100 µL of HPKR solution. Then, 90 µL of the HPKR was removed and the fluorescence intensity was measured using a plate reader with an excitation of 285 nm and an emission of 605 nm.

Exploring Cx43 Assay EtBr Washing Technique

Materials and Reagents

Table 4.11: Materials and reagents for exploring washing technique.

0.2% trypan blue solution	CO_2 incubator	Sigma Aldrich 200X PEST
10 mg/mL EtdBr Stock	Fluorescent plate reader	Sterile 15 mL plastic tube
20 mL glass vial	Gibco 0.25% Trypsin-EDTA	Sterile 2 mL tubes
20 mM compound stock in DMSO	Gibco DMEM	Sterile DMSO
Calu-3 cells	Gibco FBS	Sterile PBS (pH 7.4)
Cell counter	HPKR solution	Sterile pipette tips
Cell counting slides	hTERT media	Sterile Reagent reservoirs
Centrifuge	Inverted Microscope	Sterile T75 Flask
Class II BSC	Multichannel micropipette	Sterile, black 96-well plates

Preparation of essential solutions

Prepare 25 mL of **300 µM EtBr in HPKR solution** by pipetting 300 µL of EtBr stock into a 25 mL volumetric flask. Add HPKR buffer up to the bottom of the neck of the flask and swirl to mix. Add HPKR buffer to the fill line, cap, and invert to mix. Store in 25 mL glass vial covered with aluminum foil.

Prepare 25 mL of **300 µM EtBr blank in HPKR solution** by pipetting 300 µL of water into a 25 mL volumetric flask. Add HPKR buffer up to the bottom of the neck of the flask and swirl to mix. Add HPKR buffer to the fill line, cap, and invert to mix. Store in 25 mL glass vial covered with aluminum foil.

Prepare 4.0 mL of sterile **hTRT media containing 10 µM compound in 0.5% DMSO** by pipetting 18 µL of sterile DMSO followed by 2.0 µL of 20 mM compound stock into sterile reagent reservoir containing 3,980 µL of hTRT media.

Prepare 4.0 mL of sterile **hTRT media containing 20 µM RK006 in 0.5% DMSO** by pipetting 16.0 µL of sterile DMSO followed by 4.0 µL of 20 mM compound stock into a sterile 4 mL glass vial containing 3,980 µL of sterile hTRT media.

Prepare 4.0 mL of sterile **hTRT media containing 5 µM RK006 in 0.5% DMSO** by pipetting 19.0 µL of sterile DMSO followed by 1.0 µL of 20 mM compound stock into a sterile 4 mL glass vial containing 3,980 µL of sterile hTRT media.

Prepare 3.2 mL of **hTRT media containing 0.5 % DMSO** by pipetting 16 µL of sterile DMSO into a sterile reagent resevoir containing 3,184 µL of hTRT media.

Procedure

The phUSMCs were grown in T75 flasks, split, and counted. A cell suspension of 1.25 X 10^4 cells/mL in hTRT media was prepared in a 15-mL sterile centrifuge tube. 200 µL of the cell suspension was added to the wells of a sterile, black 96-well plate to give 2.5 X 10^3 cells/well which was incubated at 37 ºC for 72 hours. The cells were washed with 200 µL of sterile PBS once followed by 200 µL of a solution of hTRT media containing the appropriate compound and 0.5% DMSO or 200 µL of a solution of hTRT media containing 0.5% DMSO. The plate was incubated at 37 ºC with 5% CO_2 for 24 hours. After incubation, each well received 100 µL of a solution of HPKR containing 300 µM EtBr or a blank HPKR solution. The plate was incubated in the dark at 37 ºC with 5% CO_2 for 30 minutes. The assay was performed using four different washing techniques: 1) no wash and leave behind 10 µL, 2) wash once with 300 µL and leave behind 10 µL, 3) wash once with 300 µL then once with 100 µL and leave nothing behind, 4) wash once with 300 µL then once with 100 µL and leave behind 10 µL. The fluorescent intensity was measured using a plate reader with an excitation of 285 nm and an emission of 605 nm.

Testing EtBr Assay Compatibility with MTT Assay

Materials and Reagents

Table 4.12: Materials and reagents for testing EtBr followed by MTT assay.

0.2% trypan blue solution	Concentrated HCl	Multichannel micropipette
10 mg/mL EtdBr Stock	Fluorescent plate reader	Sigma Aldrich 200X PEST
20 mL glass vial	Gibco 0.25% Trypsin-EDTA	Sterile 15 mL plastic tube
20 mM compound stock in DMSO	Gibco DMEM	Sterile 2 mL tubes
Calu-3 cells	Gibco FBS	Sterile DMSO
Cell counter	HPKR solution	Sterile PBS (pH 7.4)
Cell counting slides	hTERT media	Sterile pipette tips
Centrifuge	Inverted Microscope	Sterile Reagent reservoirs
Class II BSC	Isopropanol	Sterile T75 Flask
CO_2 incubator	MTT	Sterile, black 96-well plates

Preparation of essential solutions

Prepare 25 mL of **300 µM EtBr in HPKR solution** by pipetting 300 µL of EtBr stock into a 25 mL volumetric flask. Add HPKR buffer up to the bottom of the neck of the flask and swirl to mix. Add HPKR buffer to the fill line, cap, and invert to mix. Store in 25 mL glass vial covered with aluminum foil.

Prepare 25 mL of **300 µM EtBr blank in HPKR solution** by pipetting 300 µL of water into a 25 mL volumetric flask. Add HPKR buffer up to the bottom of the neck of the flask and swirl to mix. Add HPKR buffer to the fill line, cap, and invert to mix. Store in 25 mL glass vial covered with aluminum foil.

Prepare 1.6 mL of sterile **hTRT media containing 10 µM compound in 0.5% DMSO** by pipetting 7.2 µL of sterile DMSO followed by 0.8 µL of 20 mM compound stock into sterile 2 mL plastic tubes containing 1,592 µL of hTRT media.

Prepare 3.2 mL of **hTRT media containing 0.5 % DMSO** by pipetting 16 µL of sterile DMSO into a sterile reagent resevoir containing 3,184 µL of hTRT media.

Prepare 10 mL of sterile **12 mM (5 mg/mL) MTT stock solution** by adding, adding 50 mg of MTT and 10 mL of PBS in glass vial. Vortex until all MTT powder is dissolved. Use a syringe to pass the solution through a sterile (autoclaved) 0.2 µm HPTFE filter and into a sterile

15 mL centrifuge tube wrapped in aluminum foil to prevent continued exposure to light. Store at -20 ºC.

At the time of addition, prepare 7.6 mL of sterile **1.2 mM (0.5 mg/mL) MTT working solution** in complete growth media in a sterile reagent reservoir by adding 760 µL of 12 mM (5 mg/mL) MTT stock solution and 6,840 µL of complete media. Pipette 1 mL of the solution up and down 15 times to mix. Turn the light off in the BSC while working with MTT to prevent degradation.

Prepare 22.4 mL of **stop solution (0.04 M HCl in isopropanol)** in a plastic reagent reservoir by adding 22.326 mL of isopropanol and 74.0 µL of conc. HCl to a reagent reservoir. Pipette 1 mL of the solution up and down 15 times to mix.

Procedure

The phUSMCs were grown in T75 flasks, split, and counted. A cell suspension of 1.25 X 10^4 cells/mL in hTRT media was prepared in a 15-mL sterile centrifuge tube. 200 µL of the cell suspension was added to the wells of a sterile, black 96-well plate to give 2.5 X 10^3 cells/well which was incubated at 37 ºC for 72 hours. The cells were washed with 200 µL of sterile PBS followed by 200 µL of a solution of hTRT media containing compound and 0.5% DMSO or 200 µL of a solution of hTRT media containing 0.5% DMSO. The plate was incubated at 37 ºC with 5% CO_2 for 24 hours. After incubation, one plate was treated for the EtBr assay while the other was left in the incubator. For the EtBr plate, each well received 100 µL of 37 ºC 300 µM EtBr in HPKR solution or a blank HPKR solution. The plate was incubated in the dark at 37 ºC with 5% CO_2 for 30 minutes. The plate was washed with 300 µL of HPKR solution, then with 100 µL of HPKR solution (removing only 90 µL from the 100 µL wash). The fluorescent intensity was measured using a plate reader with an excitation of 285 nm and an emission of 605 nm. After

reading, this plate had 100 µL of MTT working solution added to each well and was incubated in the dark at 37°C in a 5% CO2 atmosphere for 3 hours. The other plate then had the media removed and 100 µL of MTT working solution added to each well and was incubated in the dark at 37°C in a 5% CO2 atmosphere for 3 hours. After the incubation period both plates were treated the same, 200 µL of 37 °C isopropanol containing 0.04 M HCl was added to each well and mixed thoroughly by pipetting up and down until the dark blue formazan crystals were fully dissolved. The absorbance was read at 564 nm.

Testing Shorter Compound Treatment Times for the Cx43 Down-modulation Assay

Materials and Reagents

Table 4.13: Materials and reagents for testing shorter treatment incubations.

0.2% trypan blue solution	CO_2 incubator	Sigma Aldrich 200X PEST
10 mg/mL EtdBr Stock	Fluorescent plate reader	Sterile 15 mL plastic tube
20 mL glass vial	Gibco 0.25% Trypsin-EDTA	Sterile 2 mL tubes
20 mM compound stock in DMSO	Gibco DMEM	Sterile DMSO
Calu-3 cells	Gibco FBS	Sterile PBS (pH 7.4)
Cell counter	HPKR solution	Sterile pipette tips
Cell counting slides	hTERT media	Sterile Reagent reservoirs
Centrifuge	Inverted Microscope	Sterile T75 Flask
Class II BSC	Multichannel micropipette	Sterile, black 96-well plates

Preparation of essential solutions

Prepare 25 mL of **300 µM EtBr in HPKR solution** by pipetting 300 µL of EtBr stock into a 25 mL volumetric flask. Add HPKR buffer up to the bottom of the neck of the flask and swirl to mix. Add HPKR buffer to the fill line, cap, and invert to mix. Store in 25 mL glass vial covered with aluminum foil.

Prepare 25 mL of **300 µM EtBr blank in HPKR solution** by pipetting 300 µL of water into a 25 mL volumetric flask. Add HPKR buffer up to the bottom of the neck of the flask and swirl to mix. Add HPKR buffer to the fill line, cap, and invert to mix. Store in 25 mL glass vial covered with aluminum foil.

Prepare 2.6 mL of sterile **hTRT media containing 10 µM compound in 0.5% DMSO** by pipetting 11.3 µL of sterile DMSO followed by 1.3 µL of 20 mM compound stock into sterile 4 mL glass vial containing 2,588.3 µL of hTRT media.

Prepare 15 mL of **hTRT media containing 0.5 % DMSO** by pipetting 75 µL of sterile DMSO into a sterile reagent resevoir containing 14,925 µL of hTRT media.

Procedure

The phUSMCs were grown in T75 flasks, split, and counted. A cell suspension of 1.25 X 10^4 cells/mL in hTRT media was prepared in a 15-mL sterile centrifuge tube. 200 µL of the cell suspension was added to the wells of three sterile, black 96-well plates to give 2.5 X 10^3 cells/well which were incubated at 37 ºC for 72 hours. The cells were washed with 200 µL of sterile PBS once followed by 200 µL of a solution of hTRT media containing compound and 0.5% DMSO or 200 µL of a solution of hTRT media containing 0.5% DMSO. The plate was incubated at 37 ºC with 5% CO_2 for 2, 6, or 24 hours (later 3, 4.5, and 6 hours were tested). After each incubation time, one of the plates was removed and processed in accordance with the rest of the procedure. Each well received 100 µL of a solution of HPKR containing 300 µM or a blank HPKR solution. The plate was incubated in the dark at 37 ºC with 5% CO_2 for 30 minutes. The plate was washed by removing the media, adding 300 µL of HPKR solution, and removing only 290 µL from each well. The fluorescent intensity was measured using a plate reader with an excitation of 285 nm and an emission of 605 nm.

A 24-hour Treatment Incubation Screen

Materials and Reagents

Table 4.14: Materials and reagents for 24-hour treatment screen.

0.2% trypan blue solution	CO_2 incubator	Sigma Aldrich 200X PEST
10 mg/mL EtdBr Stock	Fluorescent plate reader	Sterile 15 mL plastic tube
20 mL glass vial	Gibco 0.25% Trypsin-EDTA	Sterile 2 mL tubes
20 mM compound stock in DMSO	Gibco DMEM	Sterile DMSO
Calu-3 cells	Gibco FBS	Sterile PBS (pH 7.4)
Cell counter	HPKR solution	Sterile pipette tips
Cell counting slides	hTERT media	Sterile Reagent reservoirs
Centrifuge	Inverted Microscope	Sterile T75 Flask
Class II BSC	Multichannel micropipette	Sterile, black 96-well plates

Preparation of essential solutions

Prepare 25 mL of **300 µM EtBr in HPKR solution** by pipetting 300 µL of EtBr stock into a 25 mL volumetric flask. Add HPKR buffer up to the bottom of the neck of the flask and swirl to mix. Add HPKR buffer to the fill line, cap, and invert to mix. Store in 25 mL glass vial covered with aluminum foil.

Prepare 25 mL of **300 µM EtBr blank in HPKR solution** by pipetting 300 µL of water into a 25 mL volumetric flask. Add HPKR buffer up to the bottom of the neck of the flask and swirl to mix. Add HPKR buffer to the fill line, cap, and invert to mix. Store in 25 mL glass vial covered with aluminum foil.

Prepare 1.0 mL of sterile **hTRT media containing 10 µM compound in 0.5% DMSO** by pipetting 4.5 µL of sterile DMSO followed by 0.5 µL of 20 mM compound stock into sterile 2 mL plastic tubes containing 995 µL of hTRT media.

Prepare 15 mL of **hTRT media containing 0.5 % DMSO** by pipetting 75 µL of sterile DMSO into a sterile reagent resevoir containing 14,925 µL of hTRT media.

Procedure

The phUSMCs were grown in T75 flasks, split, and counted. A cell suspension of 1.25 X 10^4 cells/mL in hTRT media was prepared in a 15-mL sterile centrifuge tube. 200 µL of the cell

suspension was added to the wells of 3 sterile, black 96-well plates to give 2.5 X 10^3 cells/well which were incubated at 37 ºC for 72 hours. The cells were washed with 200 µL of sterile PBS followed by 200 µL of a solution of hTRT media containing compound with 0.5% DMSO or 200 µL of a solution of hTRT media containing 0.5% DMSO. The plates were incubated at 37 ºC with 5% CO_2 for 24 hours. After incubation, each well received 100 µL of a solution of HPKR containing 300 µM EtBr or a blank HPKR solution. The plates were incubated in the dark at 37 ºC with 5% CO_2 for 30 minutes. The plates were washed by removing the media, adding 300 µL of HPKR solution, and removing 290 µL from each well. The fluorescent intensity was measured using a plate reader with an excitation of 285 nm and an emission of 605 nm.

Testing Order of EtBr Addition and Wash

Materials and Reagents

Table 4.15: Materials and reagents for testing order of EtBr addition.

0.2% trypan blue solution	CO_2 incubator	Sigma Aldrich 200X PEST
10 mg/mL EtdBr Stock	Fluorescent plate reader	Sterile 15 mL plastic tube
20 mL glass vial	Gibco 0.25% Trypsin-EDTA	Sterile 2 mL tubes
20 mM compound stock in DMSO	Gibco DMEM	Sterile DMSO
Calu-3 cells	Gibco FBS	Sterile PBS (pH 7.4)
Cell counter	HPKR solution	Sterile pipette tips
Cell counting slides	hTERT media	Sterile Reagent reservoirs
Centrifuge	Inverted Microscope	Sterile T75 Flask
Class II BSC	Multichannel micropipette	Sterile, black 96-well plates

Preparation of essential solutions

Prepare 25 mL of **300 µM EtBr in HPKR solution** by pipetting 300 µL of EtBr stock into a 25 mL volumetric flask. Add HPKR buffer up to the bottom of the neck of the flask and swirl to mix. Add HPKR buffer to the fill line, cap, and invert to mix. Store in 25 mL glass vial covered with aluminum foil.

Prepare 25 mL of **300 µM EtBr blank in HPKR solution** by pipetting 300 µL of water into a 25 mL volumetric flask. Add HPKR buffer up to the bottom of the neck of the flask and swirl to

mix. Add HPKR buffer to the fill line, cap, and invert to mix. Store in 25 mL glass vial covered with aluminum foil.

Prepare 40 mL of **hTRT media containing 0.5 % DMSO** by pipetting 200 µL of sterile DMSO into a sterile reagent resevoir containing 39,800 µL of hTRT media.

Procedure

The phUSMCs were grown in T75 flasks, split, and counted. A cell suspension of 2.50 X 10^4 cells/mL in hTRT media was prepared in a 15-mL sterile centrifuge tube. 200 µL of the cell suspension was added to the wells of 2 sterile, black 96-well plates to give 5.0 X 10^3 cells/well which were incubated at 37 ºC for 72 hours. Then 180 µL of media was removed from each well and replaced with 180 µL of fresh hTRT media followed by another incubation at 37 ºC for 72 hours. The cells were washed with 200 µL of sterile PBS followed by 200 µL of a solution of hTRT media containing 0.5% DMSO. The plates were incubated at 37 ºC with 5% CO_2 for 24 hours. After incubation, each well received 100 µL of a solution of HPKR containing 300 µM EtBr or a blank HPKR solution working from left to right for the top half of the plate, then working right to left for the bottom half of the plate. The plates were incubated in the dark at 37 ºC with 5% CO_2 for 30 minutes. The plates were washed by removing the media, adding 200 µL of HPKR solution, and removing all liquid from each well (each step was performed in series working from left to right for the top half of the plate, then working right to left for the bottom half of the plate). The fluorescent intensity was measured using a plate reader with an excitation of 285 nm and an emission of 605 nm.

3.4 Determining the CC_{50} for VGD040 on HEK293 Cells

Materials and Reagents

Table 4.16: Materials and reagents for VGD040 CC_{50}.

0.2% trypan blue solution	Cos7 cells	Sigma Aldrich 200X PEST
20 mM compound stock in DMSO	Gibco 0.25% Trypsin-EDTA	Sterile 2 mL tubes
Absorbance plate reader	Gibco 200X NEAA	Sterile 96-well plates
Cell counter	Gibco DMEM	Sterile PBS (pH 7.4)
Cell counting slides	Gibco FBS	Sterile pipette tips
Class II BSC	Isopropanol	Sterile T75 Flask
CO_2 incubator	MTT	
Concentrated HCl	Multichannel micropipette	

Preparation of essential solutions

Prepare **complete growth media containing 0.4% DMSO** by adding 5,976 µL of 37 °C complete media to a sterile 15 mL tube, then add 24 µL of DMSO. Vortex to mix. Store in the incubator at 37 °C until ready to use.

Prepare an **8 mM stock of VGD040 in complete media containing 4% DMSO** by weighing out 0.0037 g of VGD040 and adding into a sterile 2 mL plastic tube. Add 33.2 µL of sterile DMSO to dissolve. Add 796.1 µL of sterile complete media heat to 37 °C and sonicate. Mix thoroughly before use as solution should appear cloudy.

Prepare 1.5 mL of **complete media containing 800 µM VGD040 in 0.4% DMSO** by pipetting 150 µL of the 8 mM stock of VGD040 in complete media containing 4% DMSO into sterile 2 mL plastic tubes containing 1,350 µL of 37 °C hTRT media. Mix thoroughly and immediate proceed with serial dilutions.

Prepare 10 mL of sterile **12 mM (5 mg/mL) MTT stock solution** by adding, adding 50 mg of MTT and 10 mL of PBS in glass vial. Vortex until all MTT powder is dissolved. Use a syringe to pass the solution through a sterile (autoclaved) 0.2 µm HPTFE filter and into a sterile 15 mL centrifuge tube wrapped in aluminum foil to prevent continued exposure to light. Store at -20 ºC.

At the time of addition, prepare 10 mL of sterile **1.2 mM (0.5 mg/mL) MTT working solution** in complete growth media in a sterile reagent reservoir by adding 1.0 mL of 12 mM (5 mg/mL) MTT stock solution and 9.0 mL of complete media. Pipette 1 mL of the solution up and down 15 times to mix. Turn the light off in the BSC while working with MTT to prevent degradation.

Prepare 21 mL of **stop solution (0.04 M HCl in isopropanol)** in a plastic reagent reservoir by adding 20.93 mL of isopropanol and 69.4 µL of conc. HCl to a reagent reservoir. Pipette 1 mL of the solution up and down 15 times to mix.

Procedure

HEK 293 cells grown in 150 µL of media to 70-80% confluency in a 96-well plate. Serial dilutions of 1:3 were performed by adding 500 µL of complete media containing 0.4% DMSO to eitht sterile 2 mL tubes followed by moving 1,000 µL of a solution of media containing 800 µM VGD040 and 0.4% DMSO into the first tube, mixing thoroughly, and then transferring 1,000 µL of this solution into the next tube. This process was continued until all tubes had been mixed with 1,000 µL from the previous tube. Each well received 50 µL of one of these serially diluted solutions or complete media containing 0.4% DMSO without compound (vehicle control). All conditions were tested in quadruplicate, except the vehicle control conditions which were tested in sets of 8. After incubation for 48 h, the treatment media was replaced with 100 µL of MTT working solution (media containing 1.2 mM MTT and 10% PBS) and incubated for 4 h. To dissolve the formazan crystals, 200 µL of 37 ºC isopropanol containing 0.04 M aq. HCl was added to each well and mixed thoroughly by pipetting up and down. Absorbance was measured at 564 nm. CC_{50} values were determined using by nonlinear regression with a four-parameter

curve fitting model in GraphPad Prism V8.0.1. The bounds of the curve were used to normalize the data.

3.5 Stability and *CC_{50}s* of novel 4-hydroxycoumarin imines

Stability Testing

Materials and Reagents

Table 4.17: Materials and reagents for stability testing.

3-morpholinopropane-1-sulfonic acid (MOPS)	HPLC grade DMSO
2 quartz cuvettes	JB002
25 mL volumetric flasks	JB104
37 ˚C incubator	$MgCl_2$
ATP	NaCl
dithiothreitol (DTT)	parafilm
ethylene glycol bis(β-aminoethyl ether)-N,N,N′ ,N’-tetraacetic acid (EGTA)	UV spectrophotometer

Preparation of essential solutions

Reference solutions were prepared in 5 mL volumetric flasks while solutions containing JB002 and JB104 were prepared in 25 mL volumetric flasks. The flasks were initially filled partly with ATP assay buffer (10 mM 3-morpholinopropane-1-sulfonic acid (MOPS), pH 7.0, 50 mM NaCl, 0.1 mM ethylene glycol bis(β-aminoethyl ether)-N,N,N′ ,N’-tetraacetic acid (EGTA), 5 mM $MgCl_2$, 2 mM ATP (Sigma; A3377) and 1 mM dithiothreitol (DTT)), then DMSO was added, followed by addition of desired compound(s) (**Table 4.18**). The flask was then filled to the line with more ATP assay buffer capped and inverted to mix.

Table 4.18: Preparation table for stability testing. Volumes used for making solutions used for hydrolysis testing and analysis.

Solution	JB002 (µL)	JB104 (µL)	3-acetyl-4-hydroxycoumarin (µL)	3-formyl-4-hydroxycoumarin (µL)	benzylamine (µL)	DMSO (µL)	Total Volume (mL)
8 µM 3-acetyl-4-hydroxycoumarin			1			99	5
8 µM 3-formyl-4-hydroxycoumarin				1		99	5
8 µM benzylamine					2	98	5
8 µM 3-acetyl-4-hydroxycoumarin + 8 µM benzylamine			1		2	97	5
8 µM 3-formyl-4-hydroxycoumarin + 8 µM benzylamine				1	2	97	5
8 µM JB002	10					490	25
8 µM JB104		10				490	25

Procedure

Hydrolysis experiments were performed at 30 ºC in a solution of the ATPase assay buffer (10 mM 3-morpholinopropane-1-sulfonic acid (MOPS), pH 7.0, 50 mM NaCl, 0.1 mM ethylene glycol bis(β-aminoethyl ether)-N,N,N′ ,N’-tetraacetic acid (EGTA), 5 mM MgCl2, 2 mM ATP (Sigma; A3377) and 1 mM dithiothreitol (DTT)). A 10 μL aliquot of a solution of DMSO containing 20 mM of the desired compound was mixed thoroughly with 24.5 mL of ATPase assay buffer and 490 μL of DMSO (final concentration 8 μM, 2% DMSO). Immediately after preparation, a 3 mL aliquot was removed, and the UV spectrum was recorded on a Shimadzu UV-2550 UV–visible spectrophotometer in steps of 0.5 nm with a 1 cm pathlength quartz cuvette. The remaining solution was kept at 30 ◦C in a glass vial sealed with parafilm, and every 24 h another aliquot was removed and used to record the UV spectrum. Reference solutions were prepared in ATPase assay buffer containing 8 μM of the compound and 2% DMSO. Immediately after preparation of each reference solution, a UV spectrum was recorded as described above.

*CC_{50}*s of novel 4-hydroxycoumarin imines

Materials and Reagents

Table 4.19: Materials and reagents for *CC_{50}*s of novel 4-hydroxycoumarin imines.

0.2% trypan blue solution	Gibco 0.25% Trypsin-EDTA	Sigma Aldrich 200X PEST
Absorbance Plate Reader	Gibco 200X NEAA	Sterile 2 mL plastic tubes
Cell counter	Gibco DMEM	Sterile 96-well plate
Cell counting slides	Gibco FBS	Sterile PBS (pH 7.4)
Class II BSC	Isopropanol	Sterile pipette tips
CO_2 incubator	Micropipettes	Sterile T75 Flask
Concentrated HCl	MTT	
Cos7 Cells	NP-40	

Preparation of essential solutions

Prepare a **0.1 mM compound solution in DMSO** by pipetting 6 µL of the 20 mM compound stock in DMSO into a sterile 2 mL plastic tube with 1,194 µL of DMSO or by pipetting 1.2 µL of the 100 mM compound stock in DMSO into a sterile 2 mL plastic tube with 1,198.8 µL of DMSO. Vortex to mix.

Prepare a **1.0 mM compound solution in DMSO** by pipetting 60 µL of the 20 mM compound stock in DMSO into a sterile 2 mL plastic tube with 1,140 µL of DMSO or by pipetting 12 µL of the 100 mM compound stock in DMSO into a sterile 2 mL plastic tube with 1,188 µL of DMSO. Vortex to mix.

Prepare **1% DMSO in complete growth media** by pipetting 60 µL of DMSO into a sterile 15 mL plastic tube with 5,940 µL of complete growth media. Cap and invert several times to mix.

Prepare **JB compound treatment solutions** using pre-warmed (37 °C) complete media between 15-30 minutes before addition to the plate and placed in oven (37 °C) until ready for use. Check for the presence of any precipitates in the solutions before use and note if necessary. Dilute compounds JB057, JB058, JB059, and JB100 to 0.1, 1.0, 10, 100, and 1,000 µM in complete media with 1% DMSO. Dilute compounds JB008, JB061, JB062, JB080, and JB092 to 0.1, 1.0, 10, 100, and 200 µM in complete media with 1% DMSO. Add media, DMSO, then stock solutions in that order then vortex and placed in oven at 37 °C.

Prepare 10 mL of sterile **12 mM (5 mg/mL) MTT stock solution** by adding, adding 50 mg of MTT and 10 mL of PBS in glass vial. Vortex until all MTT powder is dissolved. Use a syringe to pass the solution through a sterile (autoclaved) 0.2 µm HPTFE filter and into a sterile 15 mL centrifuge tube wrapped in aluminum foil to prevent continued exposure to light. Store at -20 ºC.

At the time of addition, prepare 21 mL of sterile **1.2 mM (0.5 mg/mL) MTT working solution** in complete growth media in a sterile reagent reservoir by adding 2.1 mL of 12 mM (5 mg/mL) MTT stock solution and 18.9 mL of complete media. Pipette 1 mL of the solution up and down 15 times to mix. Turn the light off in the BSC while working with MTT to prevent degradation.

Prepare 42 mL of **stop solution (0.04 M HCl in isopropanol)** in a plastic reagent reservoir by adding 41.82 mL of isopropanol, 42 µL of NP-40, and 138.8 µL of conc. HCl to a reagent reservoir. Pipette 1 mL of the solution up and down 15 times to mix.

Procedure

Cos7 cells were grown in a 75 cm^2 culture flask to 70-80% confluency. The cells were split and counted. The cells were diluted to 5 x 10^4 cells/mL by mixing the cell suspension with the required volume of complete growth media in a sterile reagent reservoir and pipetting 1 mL of the cell suspension in the reservoir up and down 15 times to mix thoroughly. Then 200 µL of the cell suspension was immediately added to each well in sterile 96-well plates. A total of 192 wells received this cell suspension. During this step the cells were kept in a homogenous suspension by regularly pipetting the cell suspension in the reservoir up and down with the multichannel. The no cell control wells (4 replicate wells on each of the three plates) received 200 µL of complete growth media. The assay plates were incubated for 24 hours at 37˚C in a humidified incubator containing 5% CO_2.

After incubation, the media was removed from each well and 200 µL of a solution of complete media containing 1% DMSO and compound was added to four replicate wells for each of the solutions of diluted compound. Alternatively, the DMSO control (no compound) wells and the no cell control wells (four sets of replicates for each control on each of the three plates), recieved 200

µL of a solution of media containing 1% DMSO. For this step, media was removed from one column of wells at a time and the appropriate media solution was immediately added to that column before moving to the next column. The cells were incubated for 24 h at 37˚C in a humidified incubator containing 5% CO_2.

After the 24 h incubation, the treatment solution was removed from each well and 100 µL of the MTT working solution was added to all the wells. This step was performed with the light in the hood off to prevent excessive exposure of the MTT solution to light. The plates were incubated in the dark at 37°C in a 5% CO_2 atmosphere for 3 h. After the incubation, 200 µL of a freshly prepared 37 °C solution of isopropanol containing 0.04 M HCl and 0.1% NP-40 (v/v) was added to each well and mixed thoroughly by pipetting up and down until the dark blue formazan crystals were fully dissolved. A plate reader was used to measure the absorbance at 564 nm.

Calculations

Processed data for each plate separately. Used Dixon's Q test to mask any outliers with >90% probability (limit value for 4 points = 0.765; if Q < 0.765 the point can be masked). Calculated the percent viability for each data point individually using the equation below. Used these percentages to make CC_{50} curves in GraphPad Prism 9.4.0.

$$\%\,Viability\ (relative\ to\ vehicle\ control) = \left\{\frac{(\text{absorbance for test well} - \text{average absorbance for no cell control})}{(\text{average absorbance for vehicle control} - \text{average absorbance for no cell control})}\right\} \times 100$$

Section 4: References

(1) Li, G.; Hilgenfeld, R.; Whitley, R.; De Clercq, E. Therapeutic Strategies for COVID-19: Progress and Lessons Learned. *Nat Rev Drug Discov* **2023**, *22* (6), 449–475. https://doi.org/10.1038/s41573-023-00672-y.

(2) Xiao, F.; Burns, K. D. Measurement of Angiotensin Converting Enzyme 2 Activity in Biological Fluid (ACE2). In *Hypertension*; Touyz, R. M., Schiffrin, E. L., Eds.; Methods in Molecular Biology; Springer New York: New York, NY, 2017; Vol. 1527, pp 101–115. https://doi.org/10.1007/978-1-4939-6625-7_8.

(3) Liao, K.; Sikkema, D.; Wang, C.; Lee, T. N. Development of an Enzymatic Assay for the Detection of Neutralizing Antibodies against Therapeutic Angiotensin-Converting Enzyme 2 (ACE2). *Journal of Immunological Methods* **2013**, *389* (1–2), 52–60. https://doi.org/10.1016/j.jim.2012.12.010.

(4) Frey, H. A.; Klebanoff, M. A. The Epidemiology, Etiology, and Costs of Preterm Birth. *Seminars in Fetal and Neonatal Medicine* **2016**, *21* (2), 68–73. https://doi.org/10.1016/j.siny.2015.12.011.

(5) Van Vliet, E. O.; Boormans, E. M.; De Lange, T. S.; Mol, B. W.; Oudijk, M. A. Preterm Labor: Current Pharmacotherapy Options for Tocolysis. *Expert Opinion on Pharmacotherapy* **2014**, *15* (6), 787–797. https://doi.org/10.1517/14656566.2014.889684.

(6) Kotini, M.; Barriga, E. H.; Leslie, J.; Gentzel, M.; Rauschenberger, V.; Schambony, A.; Mayor, R. Gap Junction Protein Connexin-43 Is a Direct Transcriptional Regulator of N-Cadherin in Vivo. *Nat Commun* **2018**, *9* (1), 3846. https://doi.org/10.1038/s41467-018-06368-x.

(7) Natha, C. M.; Vemulapalli, V.; Fiori, M. C.; Chang, C.-W. T.; Altenberg, G. A. Connexin Hemichannel Inhibitors with a Focus on Aminoglycosides. *Biochimica et Biophysica Acta (BBA) - Molecular Basis of Disease* **2021**, *1867* (6), 166115. https://doi.org/10.1016/j.bbadis.2021.166115.

(8) Barnett, S. D.; Asif, H.; Anderson, M.; Buxton, I. L. O. Novel Tocolytic Strategy: Modulating Cx43 Activity by *S* -Nitrosation. *J Pharmacol Exp Ther* **2021**, *376* (3), 444–453. https://doi.org/10.1124/jpet.120.000427.

(9) Contreras, J. E.; Sáez, J. C.; Bukauskas, F. F.; Bennett, M. V. L. Gating and Regulation of Connexin 43 (Cx43) Hemichannels. *Proc. Natl. Acad. Sci. U.S.A.* **2003**, *100* (20), 11388–11393. https://doi.org/10.1073/pnas.1434298100.

(10) Rapoport, B.; McLachlan, S. M. TSH Receptor Cleavage Into Subunits and Shedding of the A-Subunit; A Molecular and Clinical Perspective. *Endocr Rev* **2016**, *37* (2), 114–134. https://doi.org/10.1210/er.2015-1098.

(11) Núñez Miguel, R.; Sanders, J.; Furmaniak, J.; Smith, B. R. Structure and Activation of the TSH Receptor Transmembrane Domain. *Auto Immun Highlights* **2017**, *8* (1), 2. https://doi.org/10.1007/s13317-016-0090-1.

(12) Chistiakov, D. A. Thyroid-Stimulating Hormone Receptor and Its Role in Graves' Disease. *Mol Genet Metab* **2003**, *80* (4), 377–388. https://doi.org/10.1016/j.ymgme.2003.09.001.

(13) Akram, S.; Elfenbein, D. M.; Chen, H.; Schneider, D. F.; Sippel, R. S. Assessing American Thyroid Association Guidelines for Total Thyroidectomy in Graves' Disease. *Journal of Surgical Research* **2020**, *245*, 64–71. https://doi.org/10.1016/j.jss.2019.07.029.

(14) Vaidya, B.; Pearce, S. H. S. Diagnosis and Management of Thyrotoxicosis. *BMJ* **2014**, *349* (aug21 7), g5128–g5128. https://doi.org/10.1136/bmj.g5128.
(15) Francis, N.; Francis, T.; Lazarus, J. H.; Okosieme, O. E. Current Controversies in the Management of Graves' Hyperthyroidism. *Expert Review of Endocrinology & Metabolism* **2020**, *15* (3), 159–169. https://doi.org/10.1080/17446651.2020.1754192.
(16) Sjölin, G.; Holmberg, M.; Törring, O.; Byström, K.; Khamisi, S.; De Laval, D.; Abraham-Nordling, M.; Calissendorff, J.; Lantz, M.; Hallengren, B.; Filipsson Nyström, H.; Wallin, G. The Long-Term Outcome of Treatment for Graves' Hyperthyroidism. *Thyroid* **2019**, *29* (11), 1545–1557. https://doi.org/10.1089/thy.2019.0085.
(17) Sundaresh, V.; Brito, J. P.; Thapa, P.; Bahn, R. S.; Stan, M. N. Comparative Effectiveness of Treatment Choices for Graves' Hyperthyroidism: A Historical Cohort Study. *Thyroid* **2017**, *27* (4), 497–505. https://doi.org/10.1089/thy.2016.0343.
(18) Sellers, J. R. Myosins: A Diverse Superfamily. *Biochim Biophys Acta* **2000**, *1496* (1), 3–22. https://doi.org/10.1016/s0167-4889(00)00005-7.
(19) *Encyclopedia of Cell Biology*, Second edition.; Bradshaw, R. A., Hart, G. W., Stahl, P., Eds.; Academic Press, Elsevier: Amsterdam Boston Heidelberg London New York Oxford Paris San Diego San Francisco Singapore Sydney Tokyo, 2023.
(20) Smith, J. D.; Brawley, J.; Bordenave, K. C.; Olsen, R. K.; Intasiri, A.; Cremo, C. R.; Bell, T. W. Isoform Selectivities of Novel 4-Hydroxycoumarin Imines as Inhibitors of Myosin II. *European Journal of Medicinal Chemistry* **2023**, *247*, 115008. https://doi.org/10.1016/j.ejmech.2022.115008.
(21) Beardslee, M. A.; Laing, J. G.; Beyer, E. C.; Saffitz, J. E. Rapid Turnover of Connexin43 in the Adult Rat Heart. *Circ Res* **1998**, *83* (6), 629–635. https://doi.org/10.1161/01.res.83.6.629.

Appendix

Supporting Materials for Synthesis and Pharmacokinetics of New Compounds

1. **^{1}H and ^{13}C NMR Spectra**
2. **UV Absorption Spectra (only cyclized compounds)**
3. **Kinetic Solubility (only cyclized compounds)**

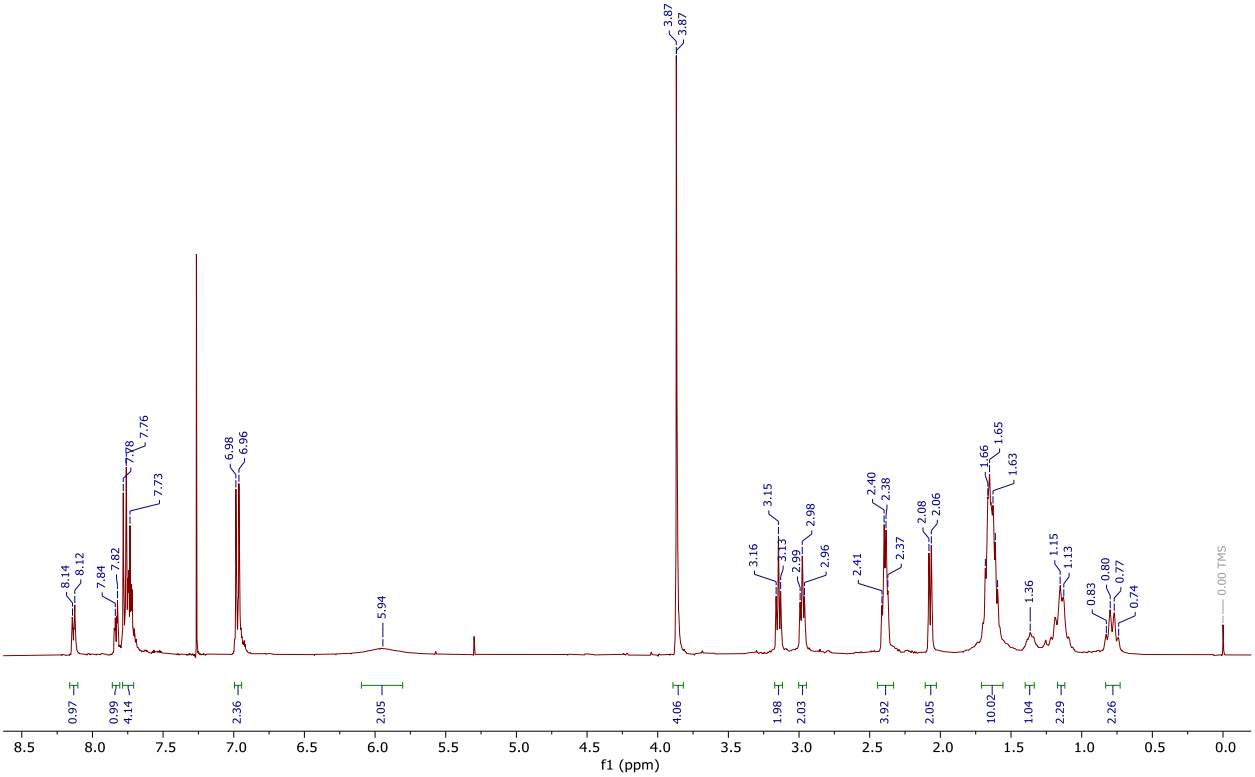

^{1}H NMR for **RK001**

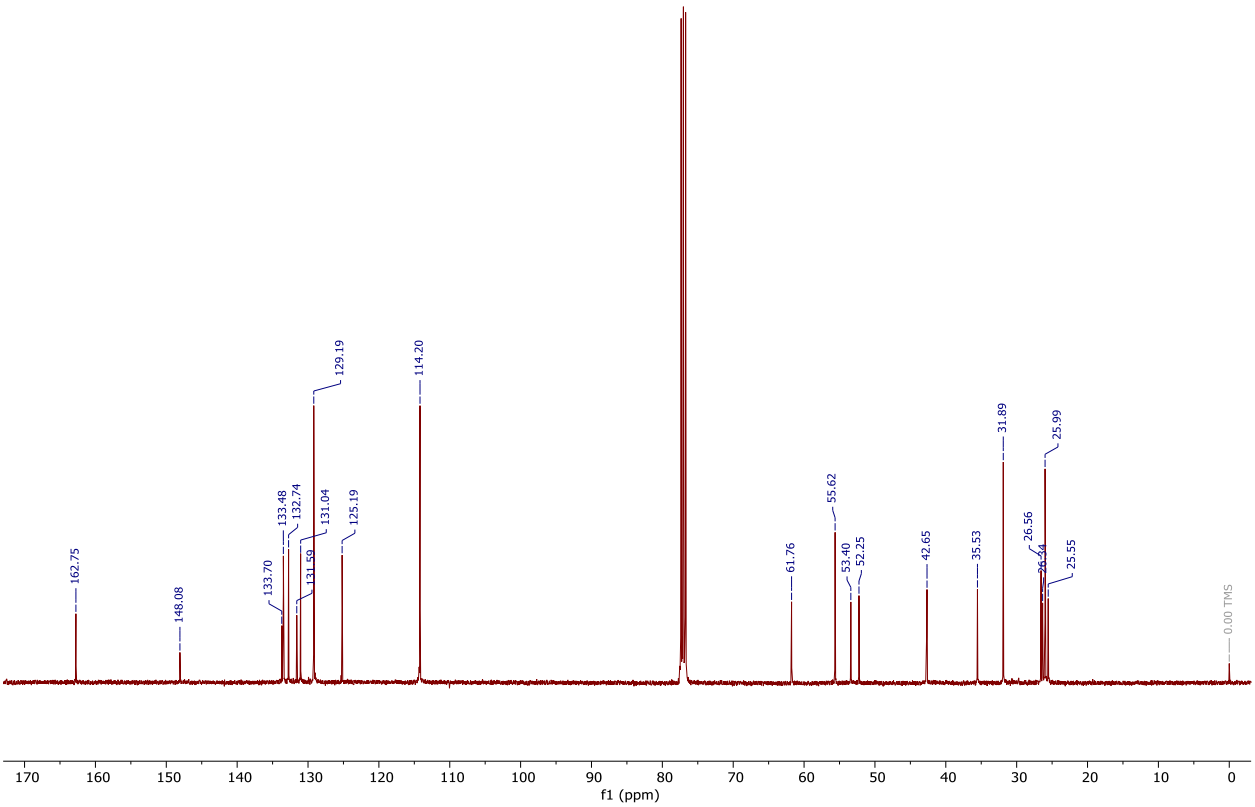

^{13}C NMR for **RK001**

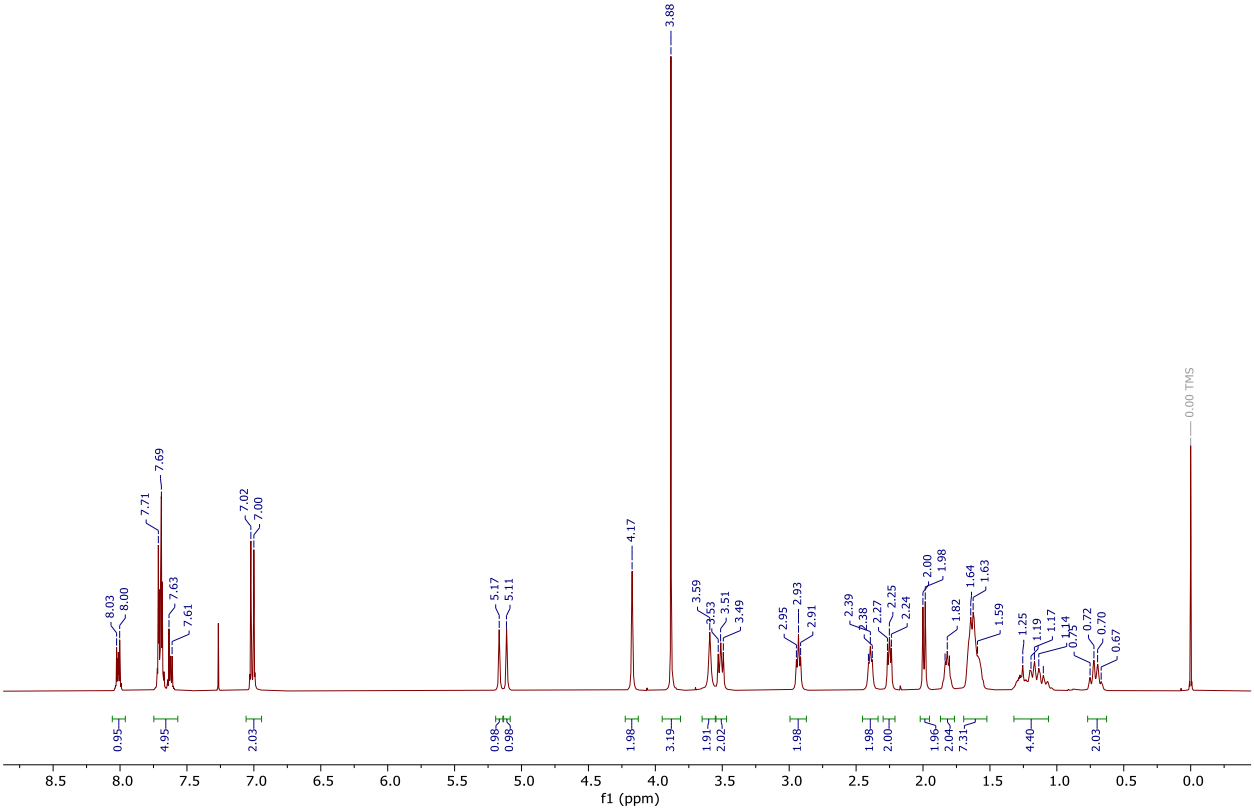

^{1}H NMR for **RK002**

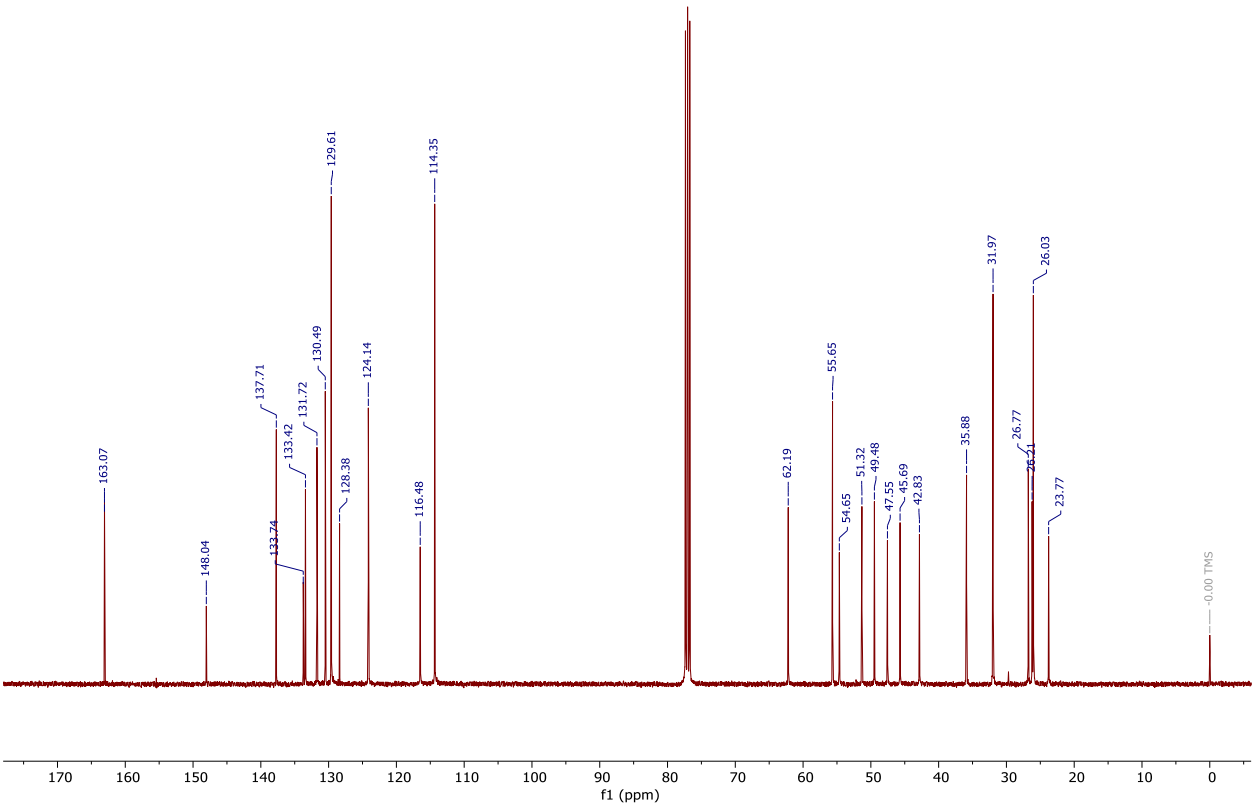

^{13}C NMR for **RK002**

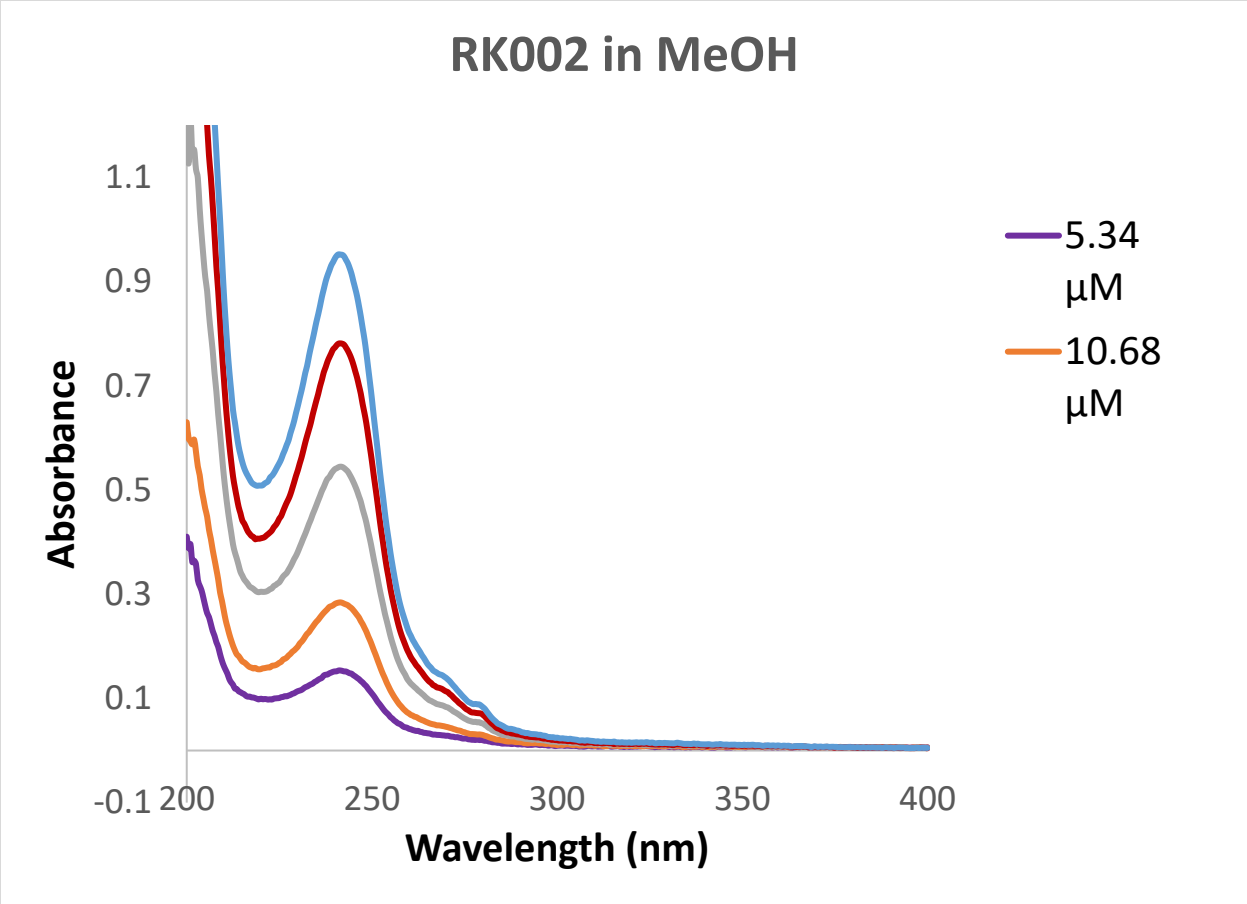

UV Absorption Spectra for **RK002**

Trial	1					2					3				
Measurement	1st	2nd	3rd	average	sd	1st	2nd	3rd	average	sd	1st	2nd	3rd	average	sd
$Abs_{(Blank)}$	0.128	0.13	0.13	0.129	0.001	0.128	0.13	0.13	0.129	0.001	0.128	0.13	0.13	0.129	0.001
$Abs_{(spiking\ soln)}$	0.203	0.219	0.206	0.209	0.009	0.21	0.211	0.209	0.210	0.001	0.23	0.25	0.208	0.229	0.021
$Abs_{(sample)}$	0.176	0.182	0.184	0.181	0.004	0.192	0.178	0.18	0.183	0.008	0.178	0.179	0.187	0.181	0.005
$Abs_{(spiked\ sample)}$	0.332	0.329	0.341	0.334	0.006	0.341	0.339	0.336	0.339	0.003	0.327	0.335	0.337	0.333	0.005
C_{stock} (µM)	20003					20003					20003				
V_{stock} (µL)	0.40					0.40					0.40				
V_{sample} (µL)	400					400					400				
S_{sample}	0.051					0.054					0.052				
$S_{spiked\ sample}$	0.205					0.209					0.204				
$C_{Analyte}$ (µM)	6.70					6.95					6.86				
$C_{analyte\ average}$ (µM)	6.84														
$C_{analyte\ SD}$ (µM)	0.13														
Wavelength = 242 nm															

Kinetic Solubility Results for **RK002**

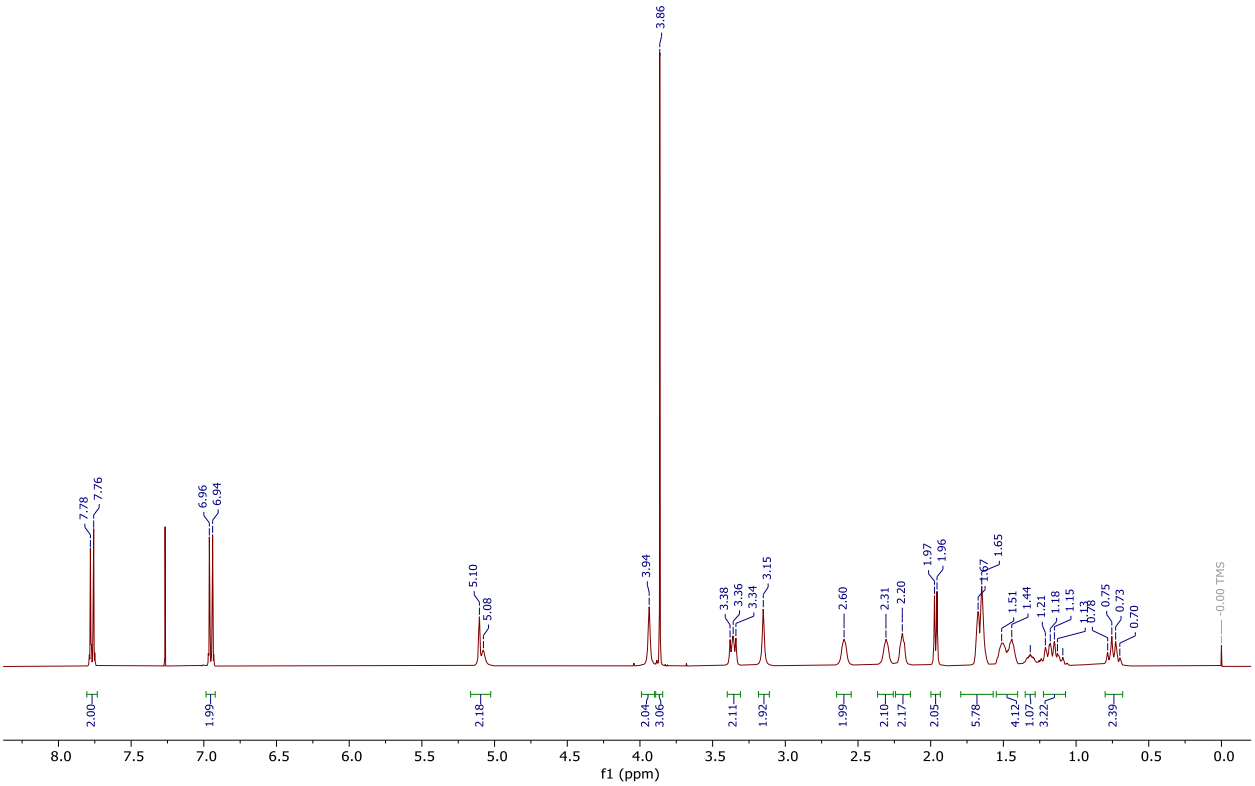

^{1}H NMR for **RK003**

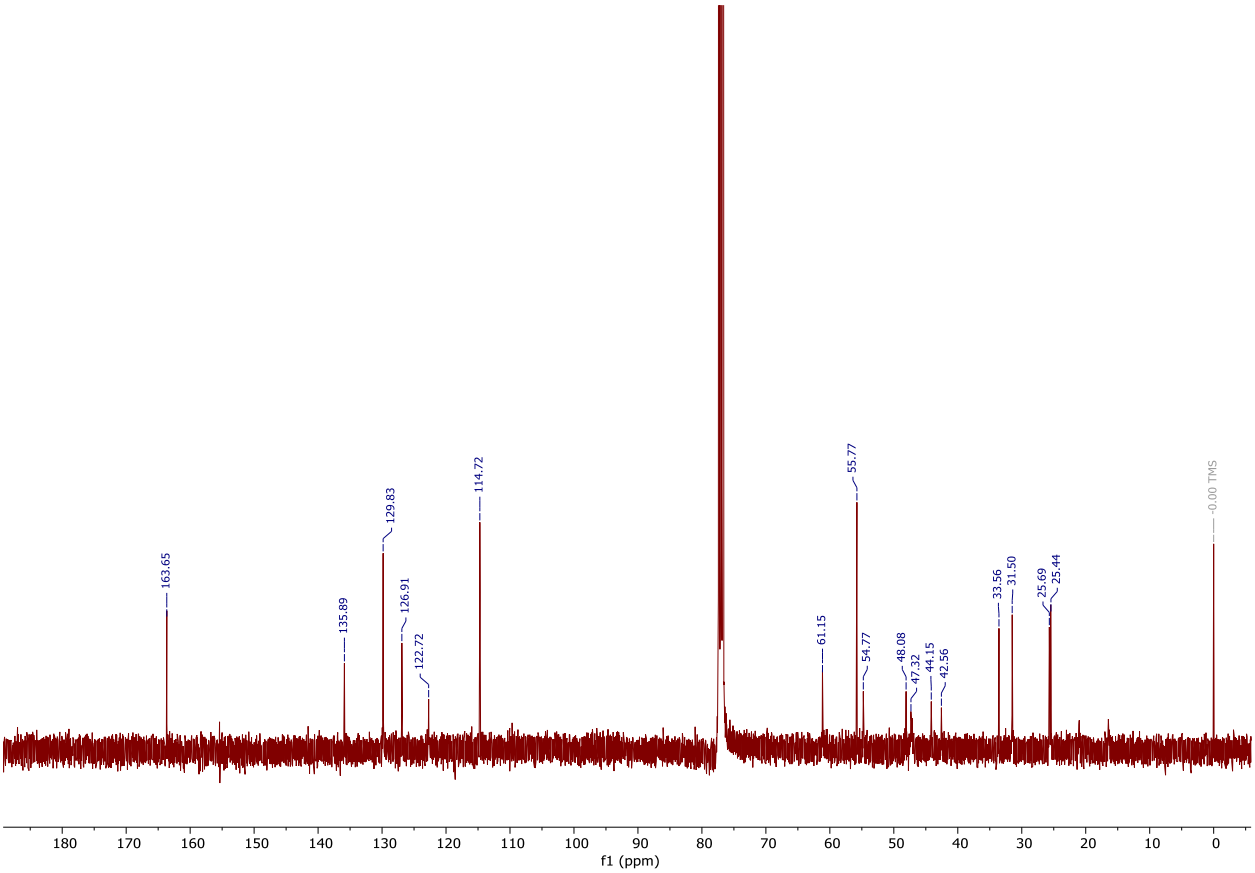

^{13}C NMR for **RK003**

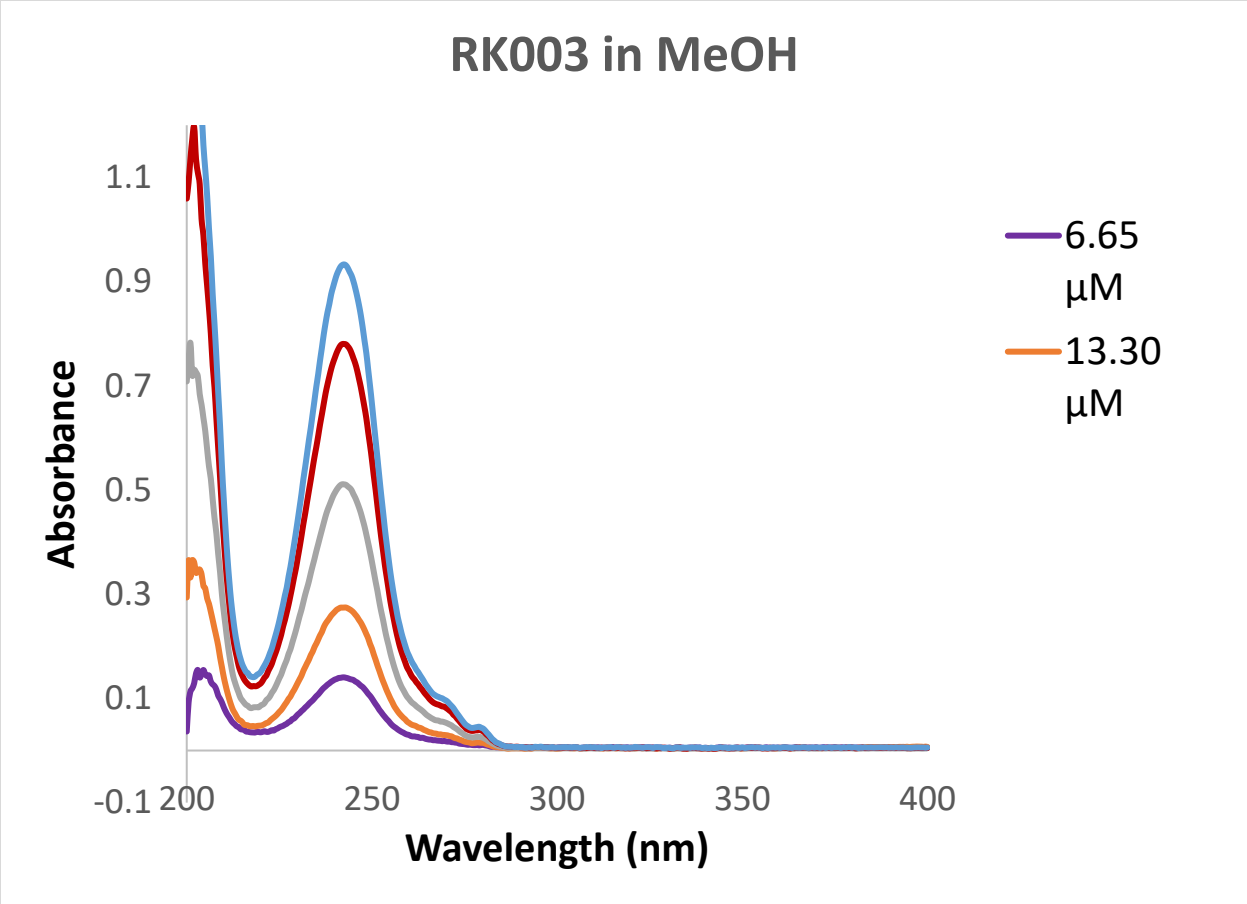

UV Absorption Spectra for **RK003**

Trial	1					2					3				
Measurement	1st	2nd	3rd	average	sd	1st	2nd	3rd	average	sd	1st	2nd	3rd	average	sd
$Abs_{(Blank)}$	0.17	0.169	0.167	0.169	0.002	0.17	0.169	0.167	0.169	0.002	0.17	0.169	0.167	0.169	0.002
$Abs_{(spiking\ soln)}$	0.487	0.504	0.487	0.493	0.010	0.482	0.483	0.494	0.486	0.007	0.483	0.494	0.479	0.485	0.008
$Abs_{(sample)}$	0.684	0.672	0.668	0.675	0.008	0.695	0.677	0.683	0.685	0.009	0.679	0.677	0.692	0.683	0.008
$Abs_{(spiked\ sample)}$	0.999	0.995	0.994	0.996	0.003	0.999	0.981	0.983	0.988	0.010	1.029	0.988	1	1.006	0.021
C_{stock} (µM)	19997					19997					19997				
V_{stock} (µL)	1.00					1.00					1.00				
V_{sample} (µL)	400					400					400				
S_{sample}	0.506					0.516					0.514				
$S_{spiked\ sample}$	0.827					0.819					0.837				
$C_{Analyte}$ (µM)	78.72					85.28					79.55				
$C_{analyte\ average}$ (µM)	81.19														
$C_{analyte\ SD}$ (µM)	3.57														
Wavelength = 242 nm															

Kinetic Solubility Results for **RK003**

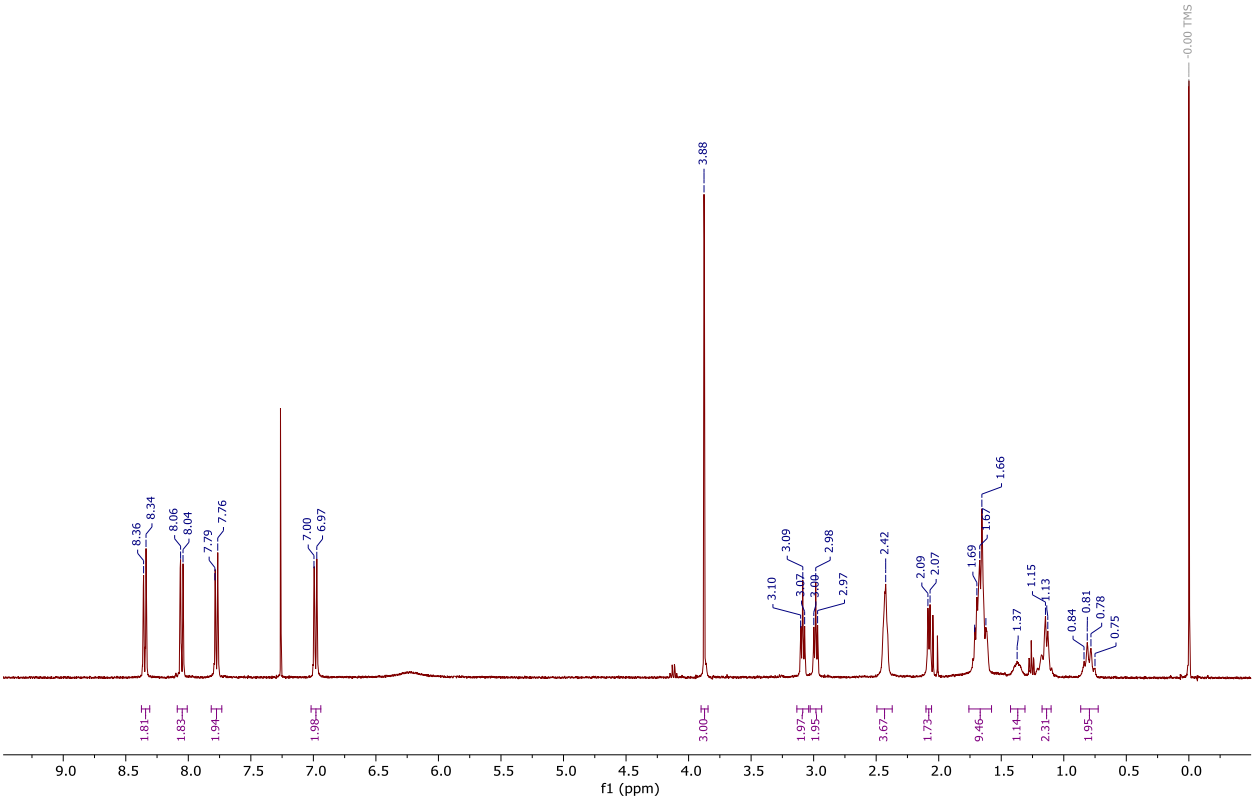

^{1}H NMR for **RK004**

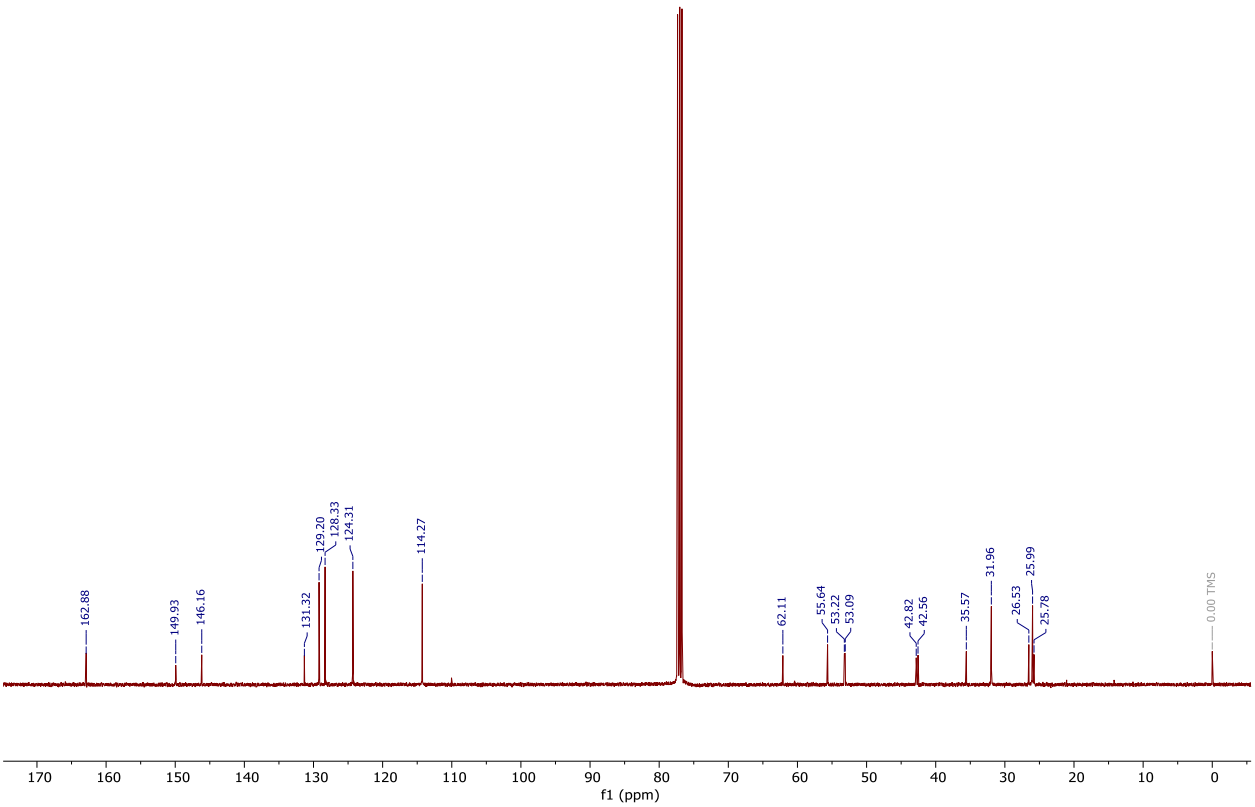

^{13}C NMR for **RK004**

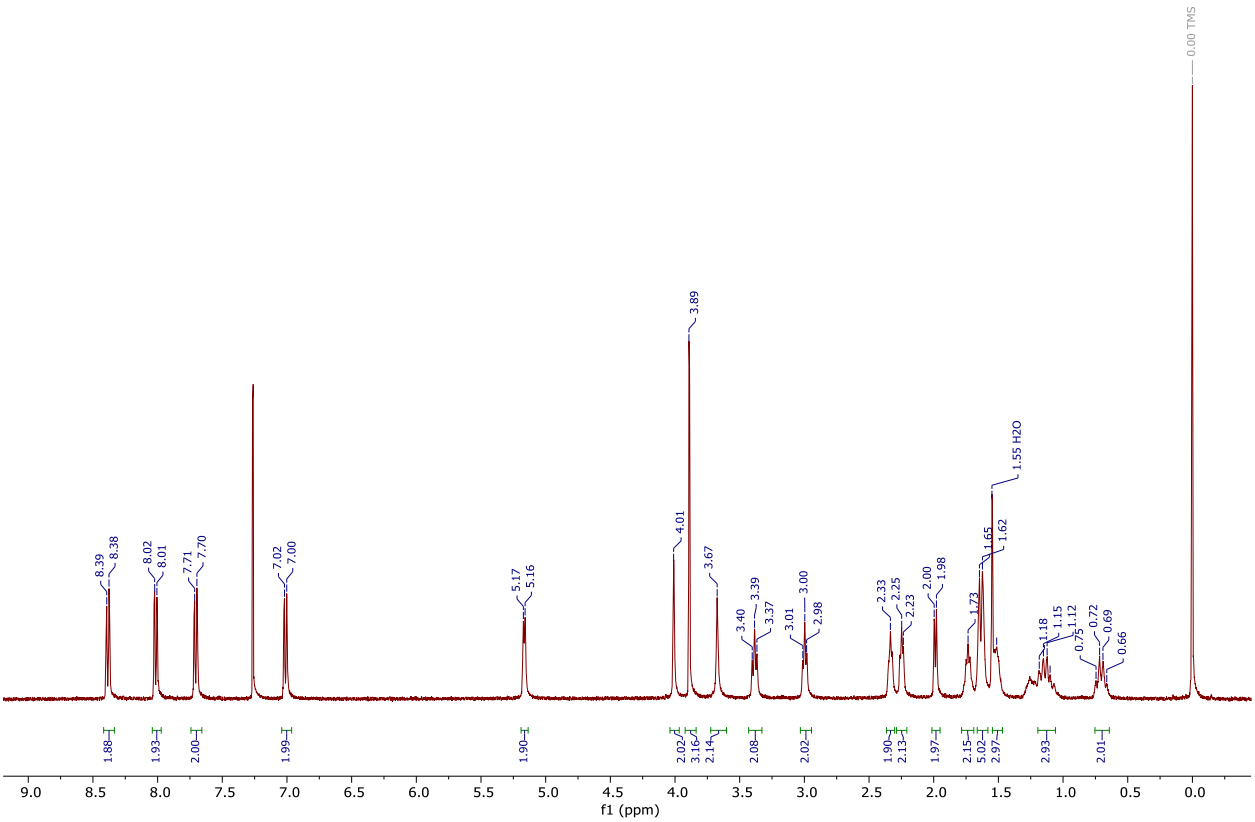

^{1}H NMR for **RK005**

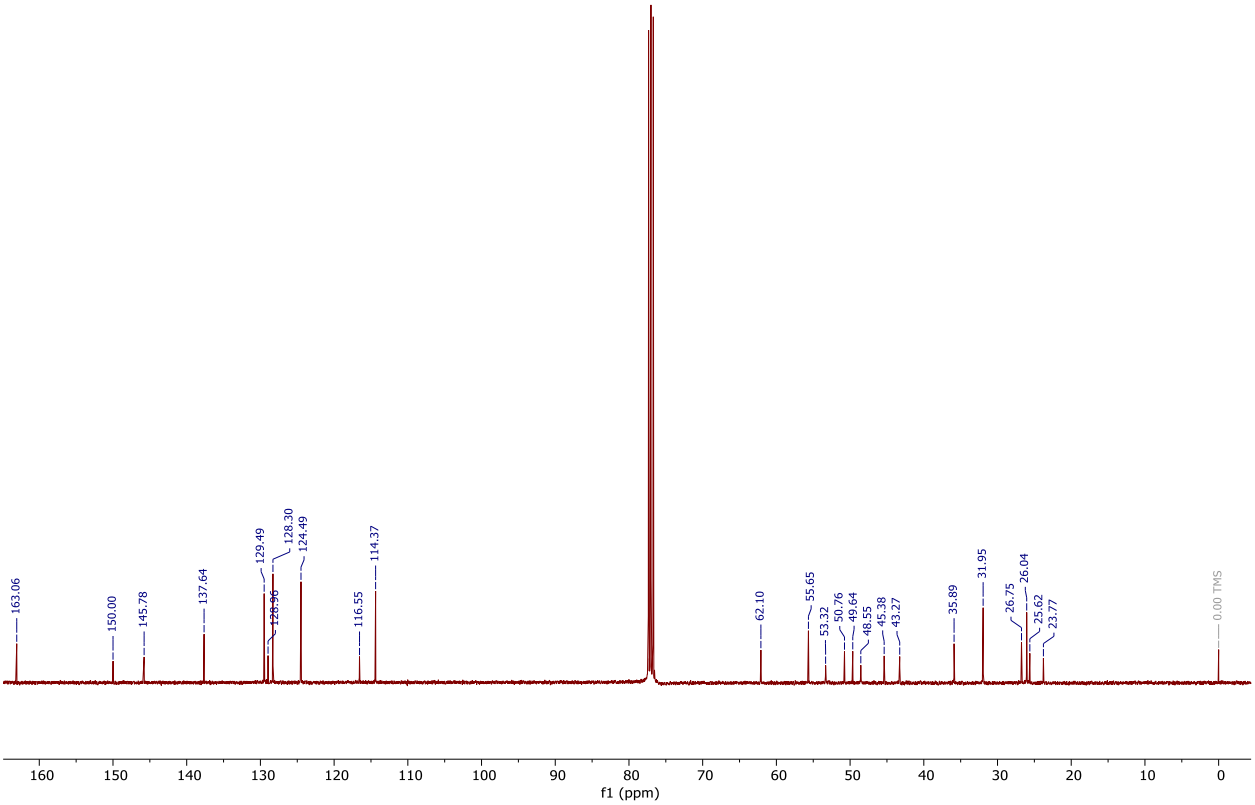

^{13}C NMR for **RK005**

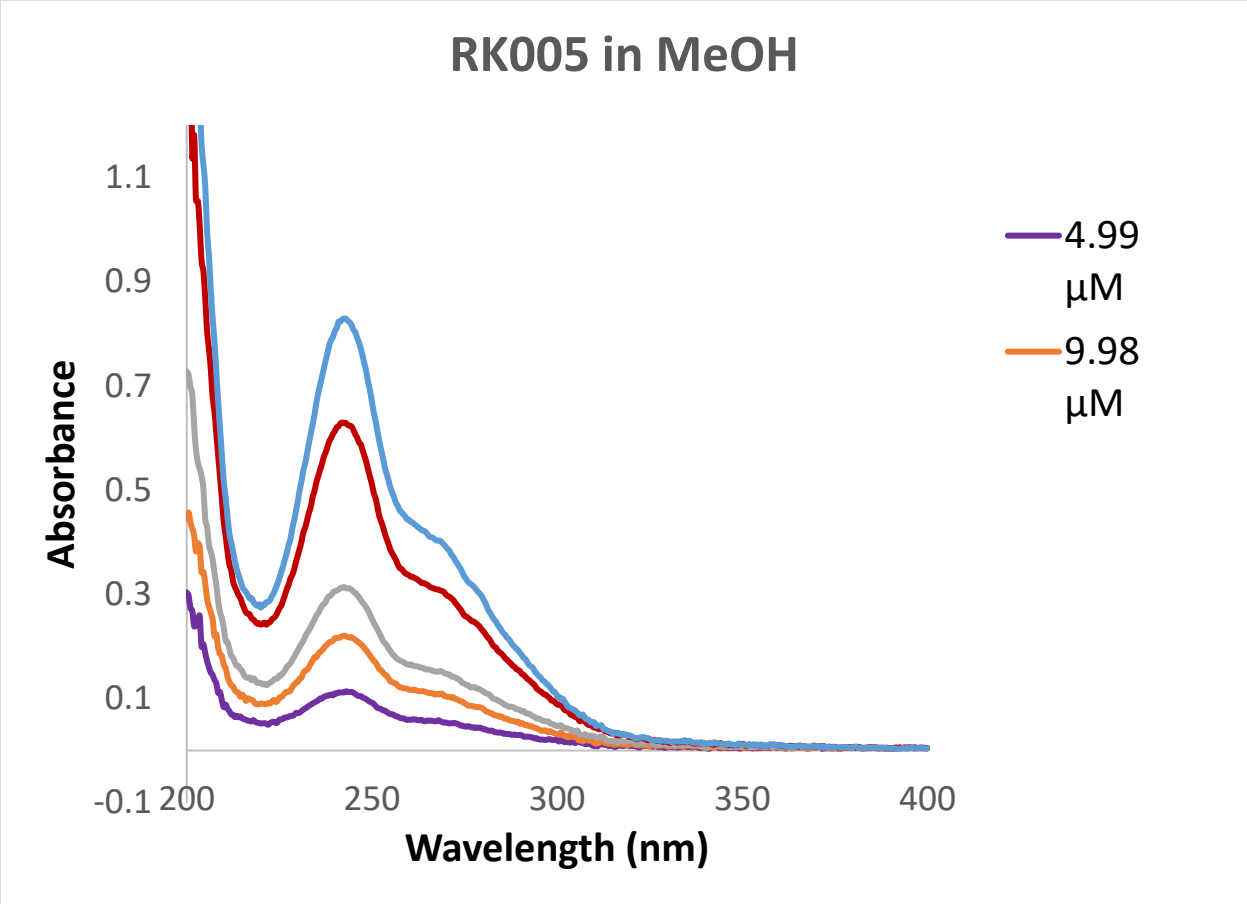

UV Absorption Spectra for **RK005**

Trial	1					2					3				
Measurement	1st	2nd	3rd	average	sd	1st	2nd	3rd	average	sd	1st	2nd	3rd	average	sd
$Abs_{(Blank)}$	0.116	0.118	0.117	0.117	0.001	0.116	0.118	0.117	0.117	0.001	0.116	0.118	0.117	0.117	0.001
$Abs_{(spiking\ soln)}$	0.174	0.168	0.171	0.171	0.003	0.204	0.203	0.208	0.205	0.003	0.194	0.2	0.205	0.200	0.006
$Abs_{(sample)}$	0.16	0.165	0.163	0.163	0.003	0.162	0.164	0.165	0.164	0.002	0.162	0.159	0.166	0.162	0.004
$Abs_{(spiked\ sample)}$	0.314	0.32	0.318	0.317	0.003	0.297	0.3	0.301	0.299	0.002	0.299	0.299	0.335	0.311	0.021
C_{stock} (µM)	19989					19989					19989				
V_{stock} (µL)	0.40					0.40					0.40				
V_{sample} (µL)	400					400					400				
S_{sample}	0.046					0.047					0.045				
$S_{spiked\ sample}$	0.200					0.182					0.194				
$C_{Analyte}$ (µM)	5.90					6.88					6.10				
$C_{analyte\ average}$ (µM)	6.29														
$C_{analyte\ SD}$ (µM)	0.52														
Wavelength = 244 nm															

Kinetic Solubility Results for **RK005**

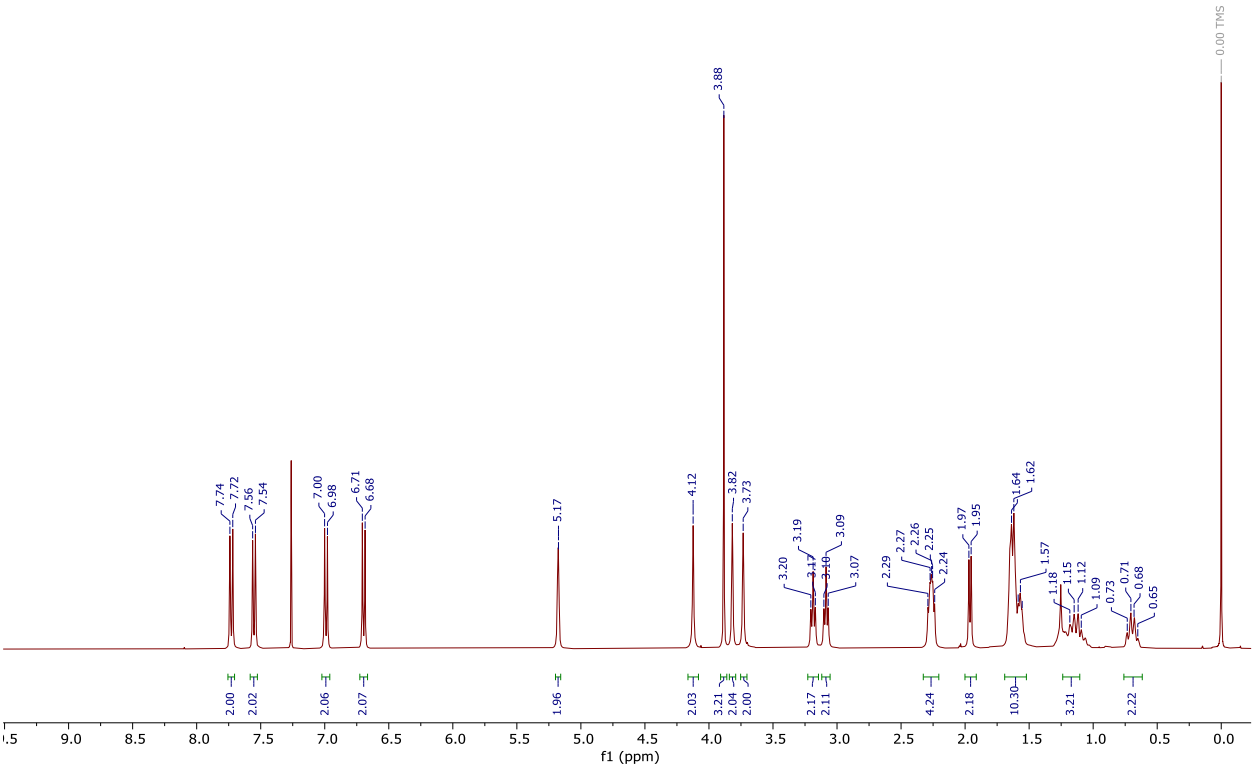

^{1}H NMR for **RK006**

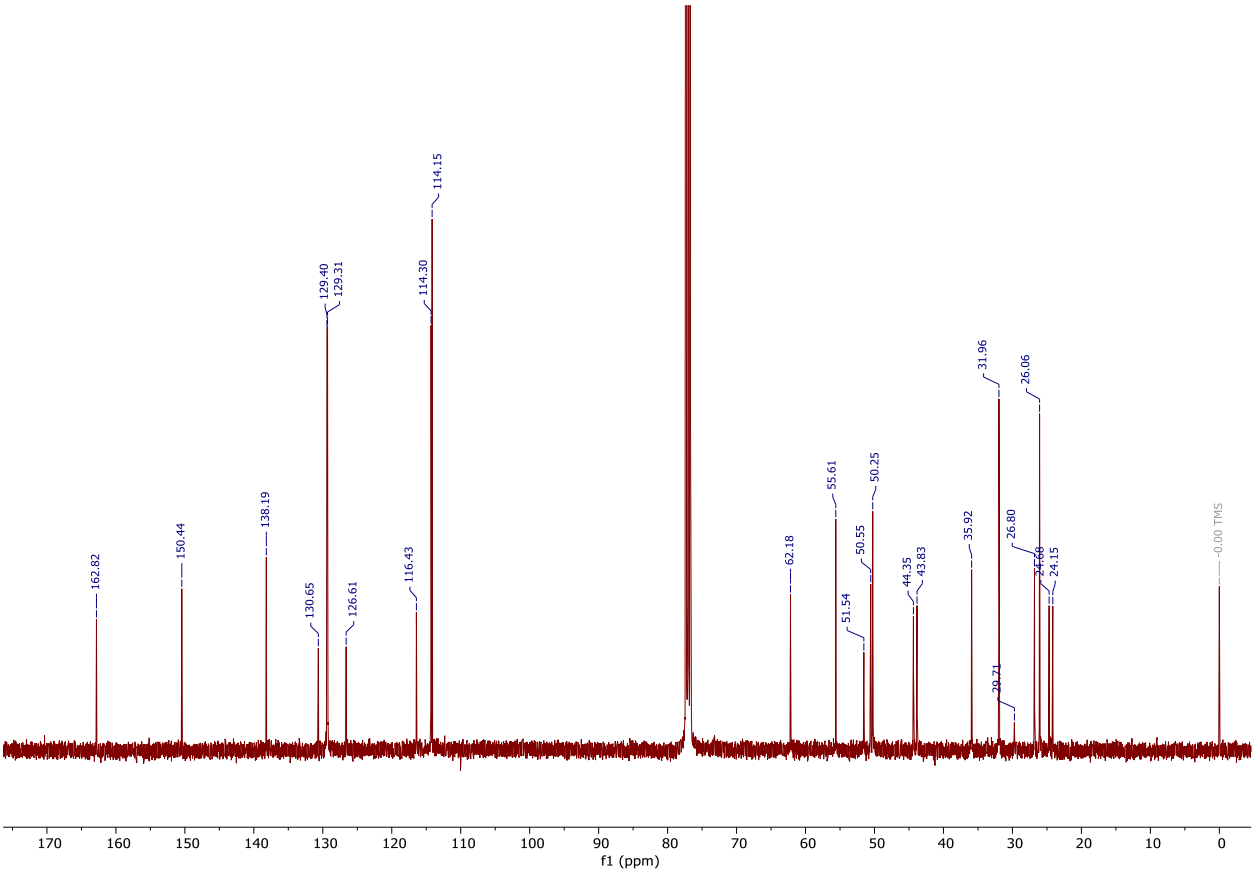

^{13}C NMR for **RK006**

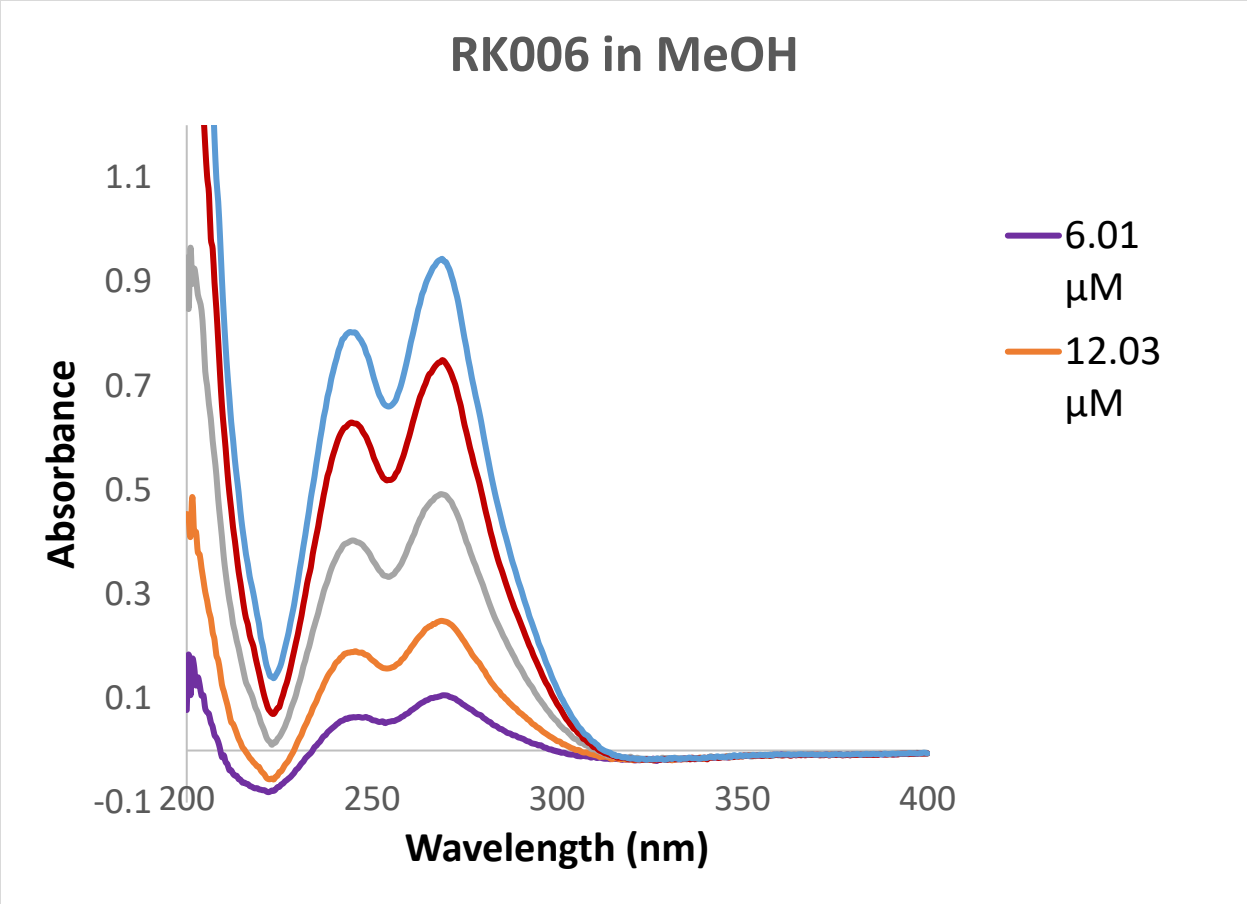

UV Absorption Spectra for **RK006**

Trial	1					2					3				
Measurement	1st	2nd	3rd	average	sd	1st	2nd	3rd	average	sd	1st	2nd	3rd	average	sd
$Abs_{(Blank)}$	0.069	0.074	0.068	0.070	0.003	0.071	0.07	0.07	0.070	0.001	0.068	0.069	0.07	0.069	0.001
$Abs_{(spiking\ soln)}$	0.389	0.39	0.38	0.386	0.006	0.394	0.399	0.397	0.397	0.003	0.378	0.386	0.383	0.382	0.004
$Abs_{(sample)}$	0.106	0.107	0.107	0.107	0.001	0.105	0.107	0.107	0.106	0.001	0.108	0.107	0.107	0.107	0.001
$Abs_{(spiked\ sample)}$	0.413	0.414	0.411	0.413	0.002	0.406	0.415	0.42	0.414	0.007	0.418	0.425	0.422	0.422	0.004
C_{stock} (µM)	21151					21151					21151				
V_{stock} (µL)	1.00					1.00					1.00				
V_{sample} (µL)	400					400					400				
S_{sample}	0.036					0.036					0.038				
$S_{spiked\ sample}$	0.342					0.343					0.353				
$C_{Analyte}$ (µM)	6.28					6.19					6.45				
$C_{analyte\ average}$ (µM)	6.31														
$C_{analyte\ SD}$ (µM)	0.13														
Wavelength = 269 nm															

Kinetic Solubility Results for **RK006**

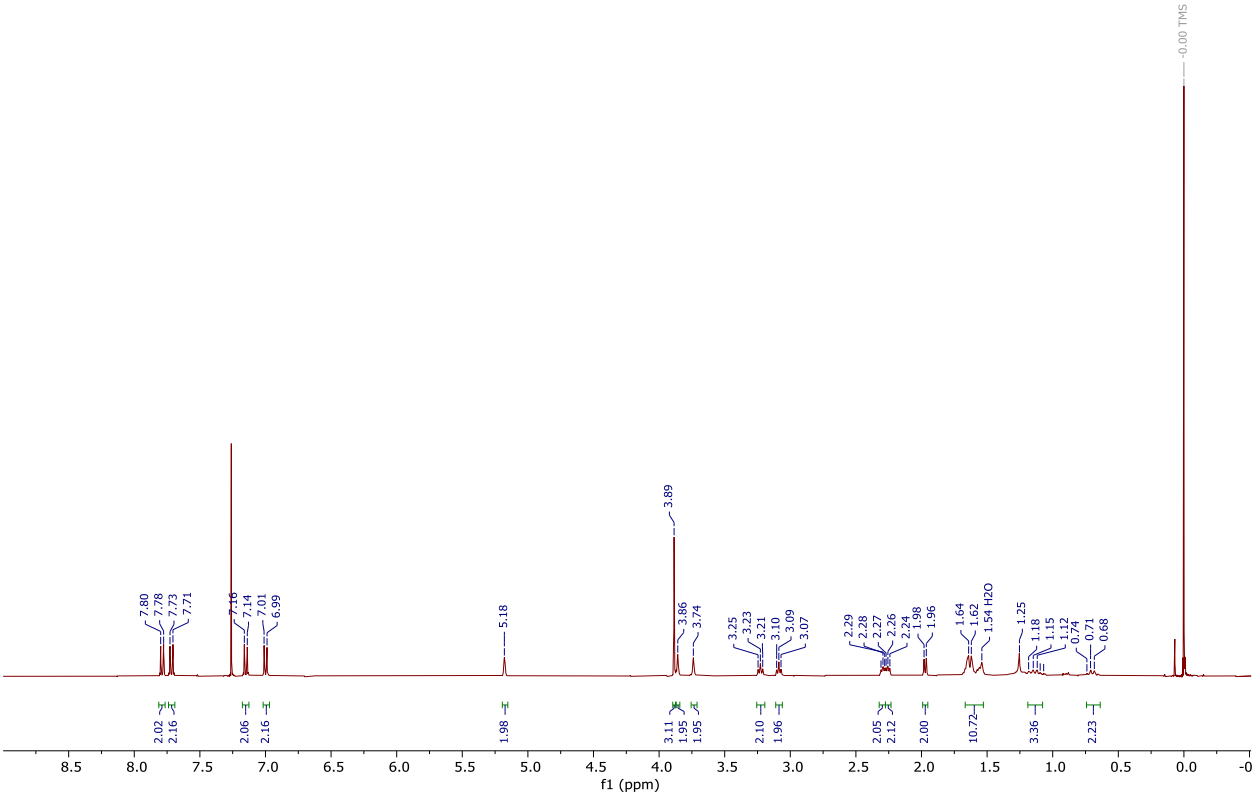

^{1}H NMR for **RK007**

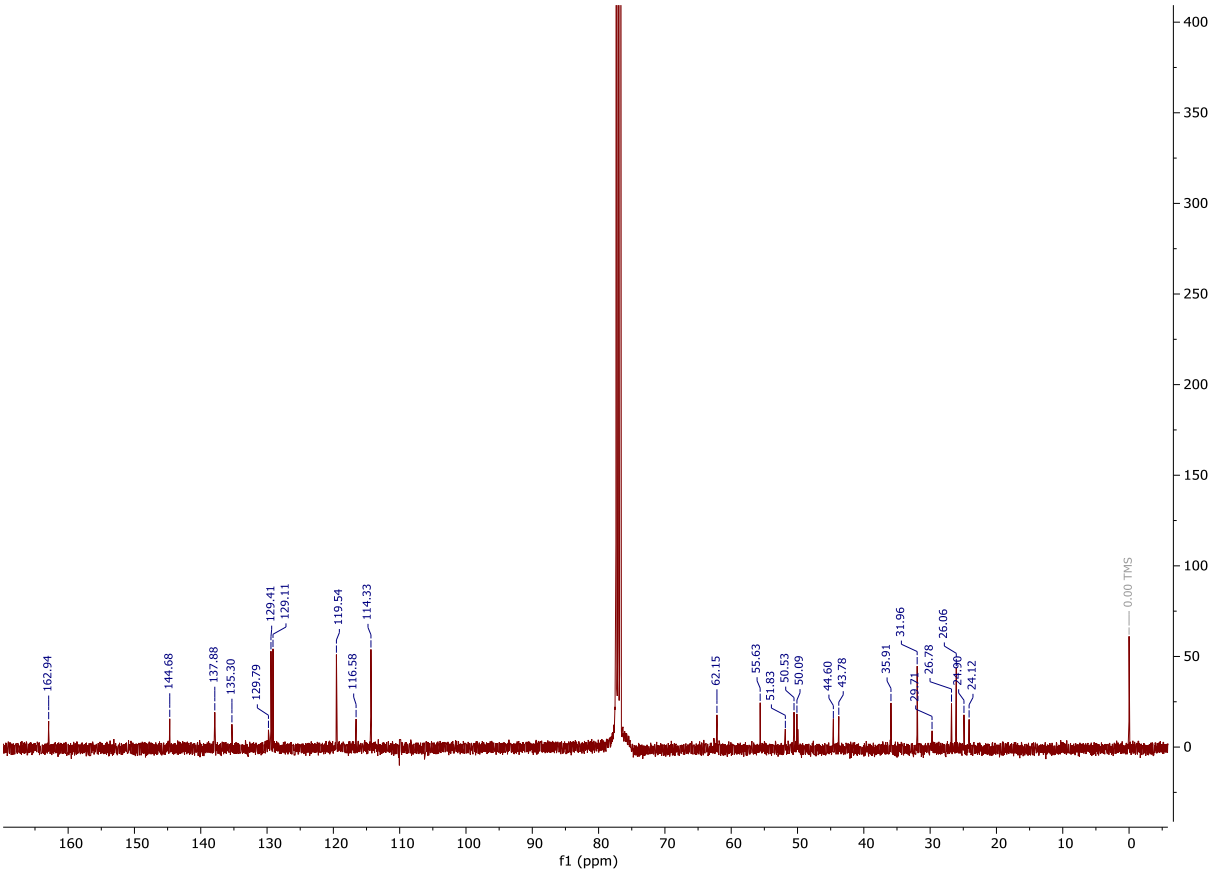

^{13}C NMR for **RK007**

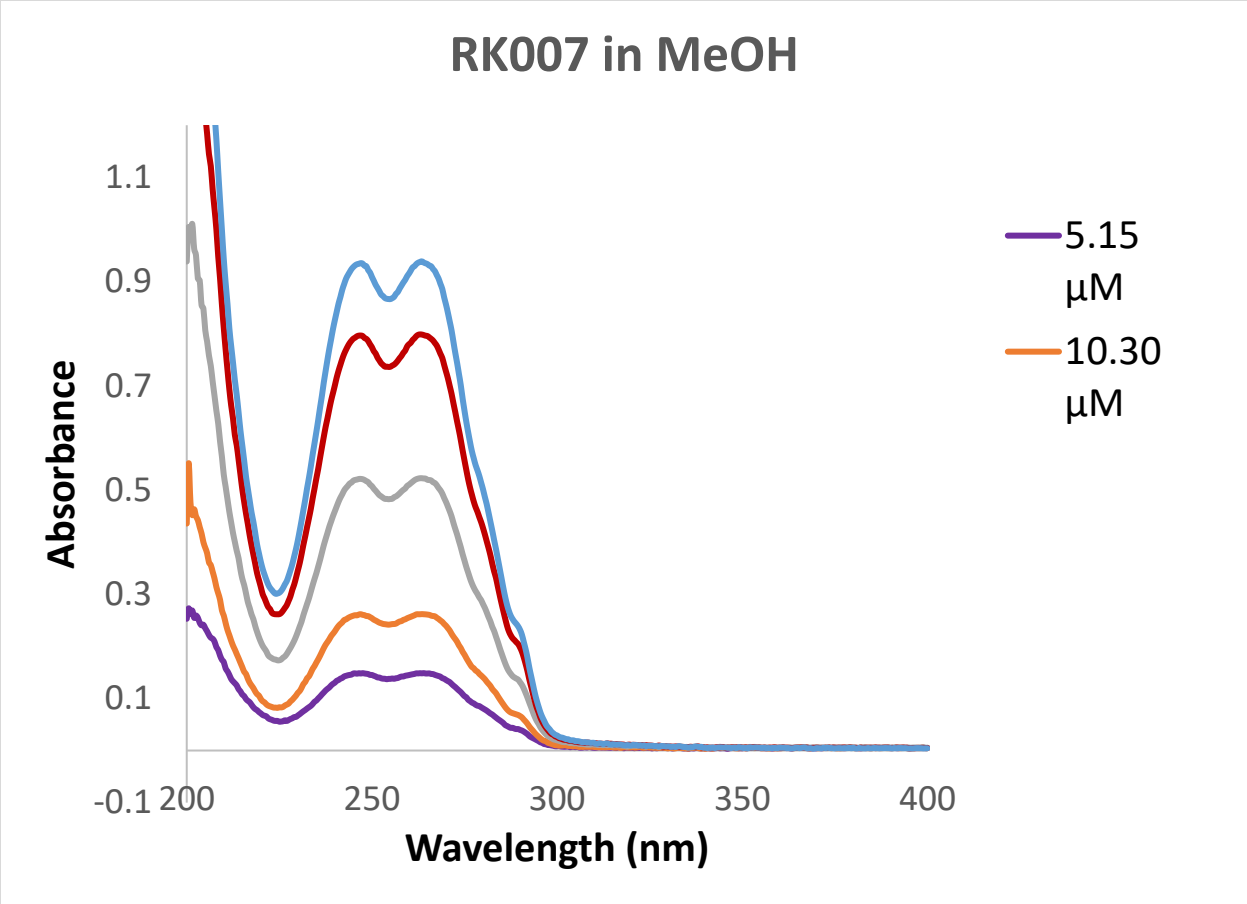

UV Absorption Spectra for **RK007**

Trial	1					2					3				
Measurement	1st	2nd	3rd	average	sd	1st	2nd	3rd	average	sd	1st	2nd	3rd	average	sd
$Abs_{(Blank)}$	0.075	0.071	0.07	0.072	0.003	0.075	0.071	0.07	0.072	0.003	0.075	0.071	0.07	0.072	0.003
$Abs_{(spiking\ soln)}$	0.216	0.216	0.222	0.218	0.003	0.217	0.222	0.236	0.225	0.010	0.223	0.218	0.228	0.223	0.005
$Abs_{(sample)}$	0.112	0.11	0.112	0.111	0.001	0.11	0.111	0.11	0.110	0.001	0.113	0.111	0.113	0.112	0.001
$Abs_{(spiked\ sample)}$	0.277	0.277	0.277	0.277	0.000	0.283	0.272	0.27	0.275	0.007	0.304	0.3	0.288	0.297	0.008
C_{stock} (µM)	20095					20095					20095				
V_{stock} (µL)	0.40					0.40					0.40				
V_{sample} (µL)	400					400					400				
S_{sample}	0.039					0.038					0.040				
$S_{spiked\ sample}$	0.205					0.203					0.225				
$C_{Analyte}$ (µM)	4.77					4.68					4.38				
$C_{analyte\ average}$ (µM)	4.61														
$C_{analyte\ SD}$ (µM)	0.20														
Wavelength = 263 nm															

Kinetic Solubility Results for **RK007**

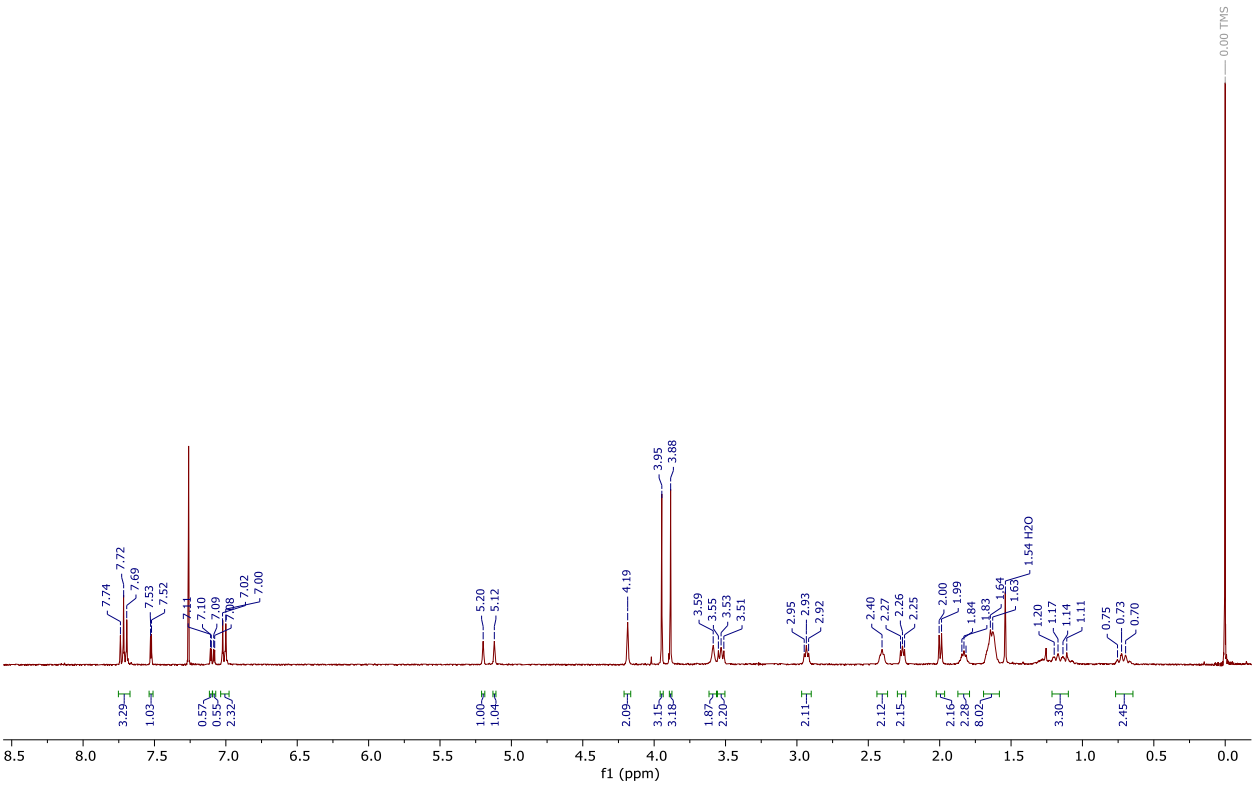

^{1}H NMR for **RK008**

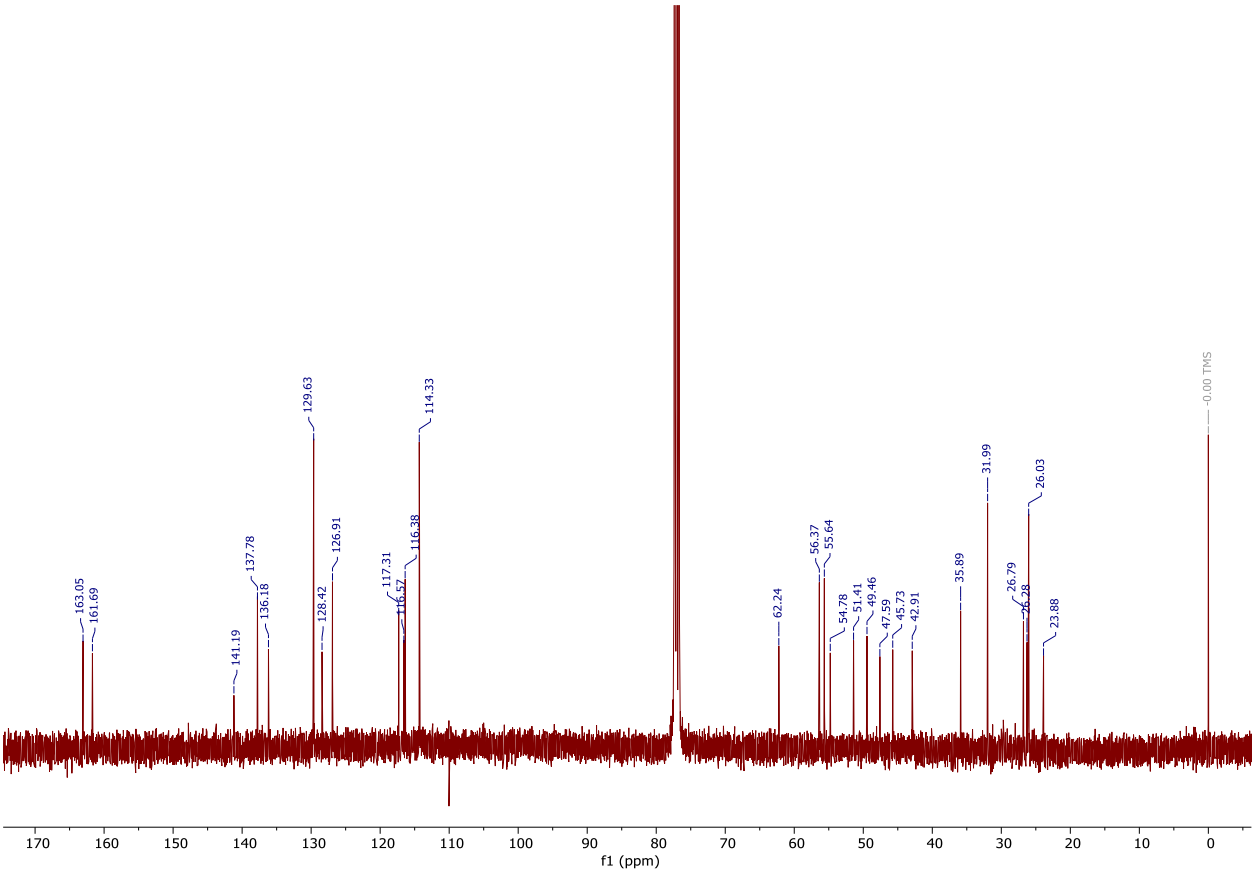

^{13}C NMR for **RK008**

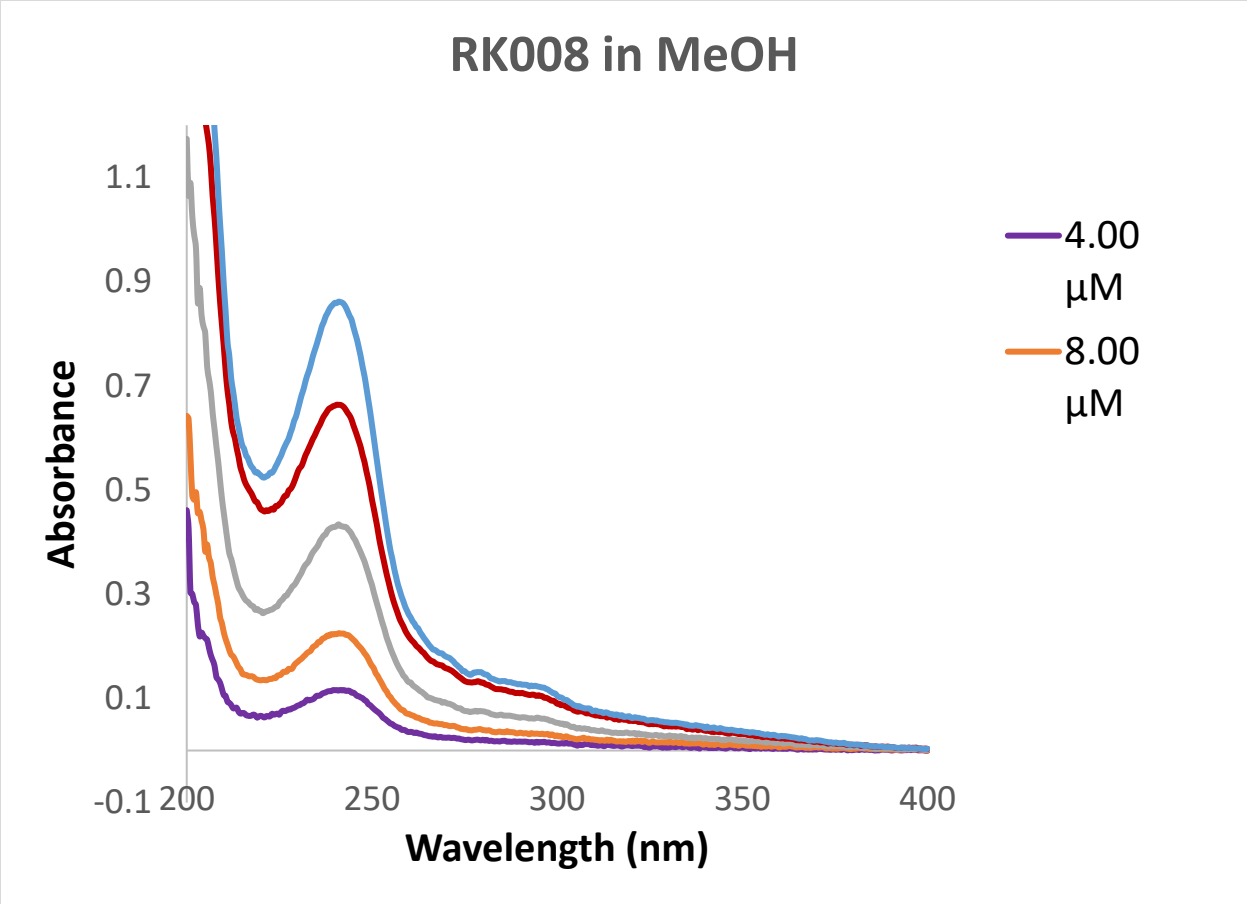

UV Absorption Spectra for **RK008**

Trial	1					2					3				
Measurement	1st	2nd	3rd	average	sd	1st	2nd	3rd	average	sd	1st	2nd	3rd	average	sd
$Abs_{(Blank)}$	0.138	0.134	0.133	0.135	0.003	0.138	0.134	0.133	0.135	0.003	0.138	0.134	0.133	0.135	0.003
$Abs_{(spiking\ soln)}$	0.228	0.23	0.233	0.230	0.003	0.235	0.23	0.237	0.234	0.004	0.232	0.238	0.225	0.232	0.007
$Abs_{(sample)}$	0.202	0.197	0.204	0.201	0.004	0.201	0.196	0.201	0.199	0.003	0.197	0.197	0.198	0.197	0.001
$Abs_{(spiked\ sample)}$	0.338	0.339	0.337	0.338	0.001	0.345	0.34	0.345	0.343	0.003	0.364	0.358	0.355	0.359	0.005
C_{stock} (µM)	19933					19933					19933				
V_{stock} (µL)	0.40					0.40					0.40				
V_{sample} (µL)	400					400					400				
S_{sample}	0.066					0.064					0.062				
$S_{spiked\ sample}$	0.203					0.208					0.224				
$C_{Analyte}$ (µM)	9.60					8.91					7.69				
$C_{analyte\ average}$ (µM)	8.73														
$C_{analyte\ SD}$ (µM)	0.97														
Wavelength = 241 nm															

Kinetic Solubility Results for **RK008**

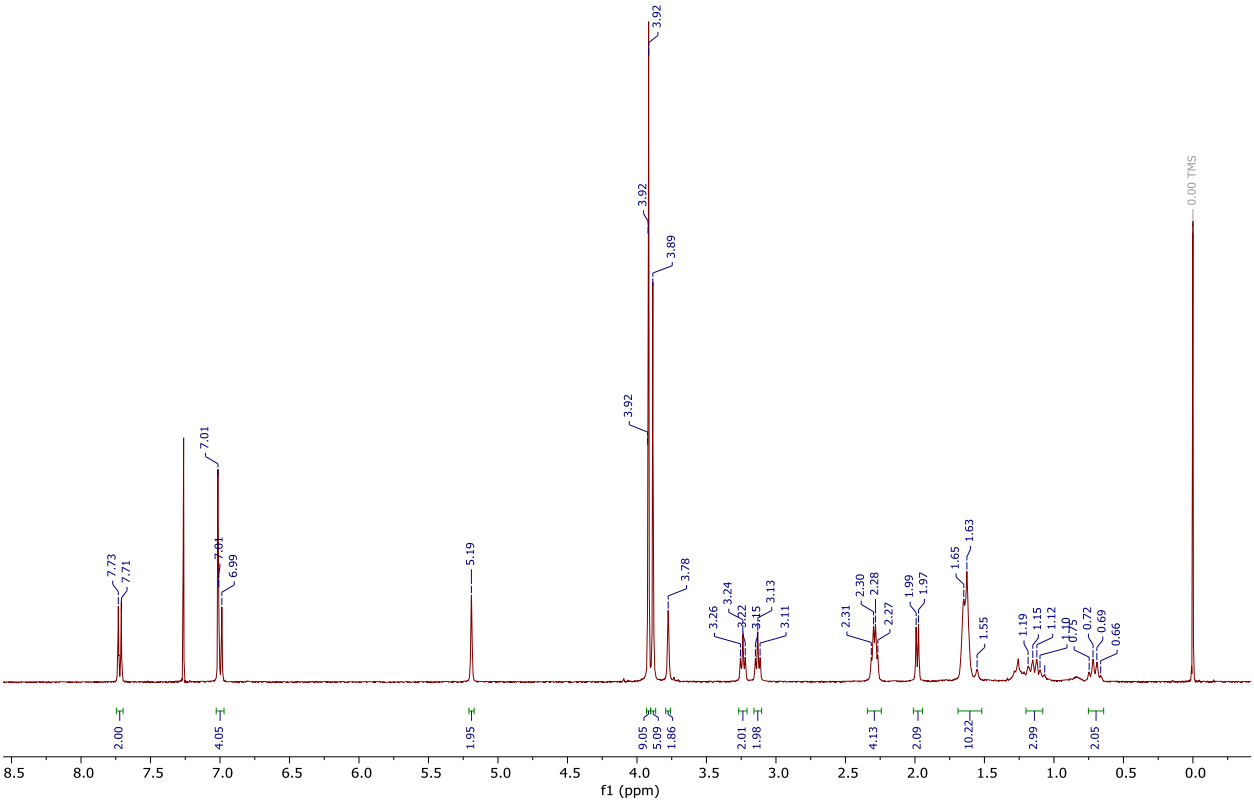

^{1}H NMR for **RK009**

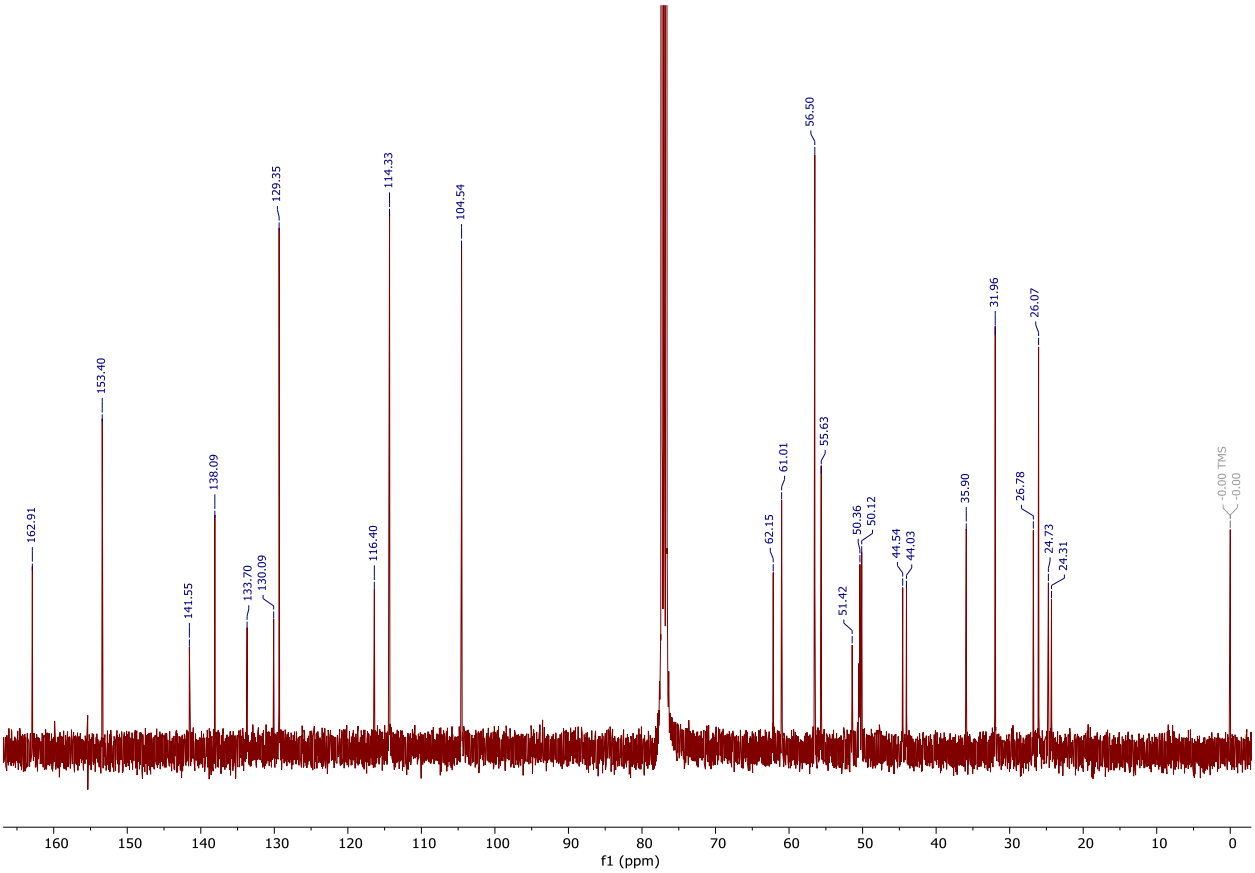

^{13}C NMR for **RK009**

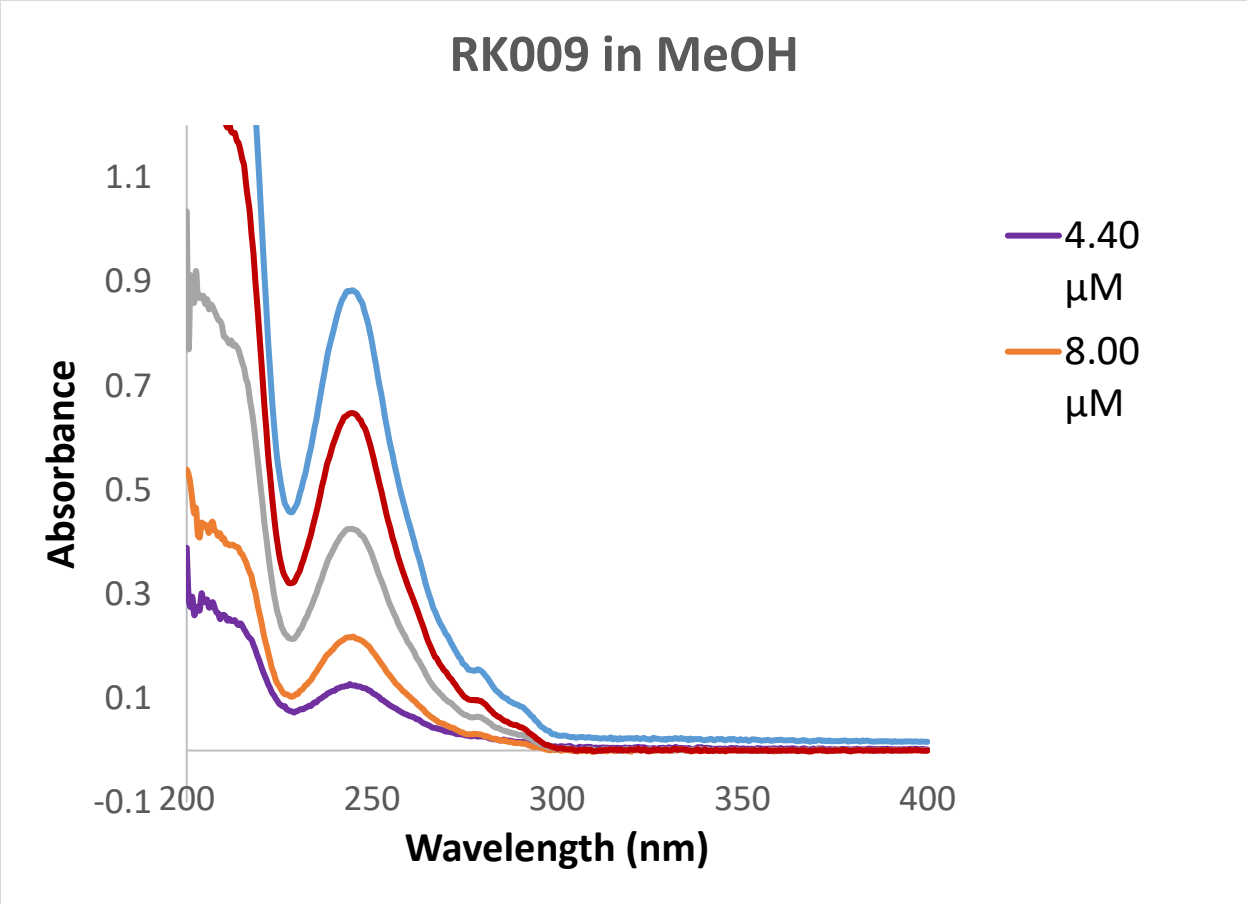

UV Absorption Spectra for **RK009**

Trial	1					2					3				
Measurement	1st	2nd	3rd	average	sd	1st	2nd	3rd	average	sd	1st	2nd	3rd	average	sd
$Abs_{(Blank)}$	0.127	0.13	0.129	0.129	0.002	0.128	0.129	0.129	0.129	0.001	0.121	0.127	0.128	0.125	0.004
$Abs_{(spiking\ soln)}$	0.481	0.496	0.497	0.491	0.009	0.487	0.514	0.514	0.505	0.016	0.497	0.503	0.51	0.503	0.007
$Abs_{(sample)}$	0.163	0.169	0.21	0.181	0.026	0.194	0.201	0.196	0.197	0.004	0.187	0.191	0.187	0.188	0.002
$Abs_{(spiked\ sample)}$	0.505	0.546	0.627	0.559	0.062	0.514	0.653	0.61	0.592	0.071	0.57	0.571	0.575	0.572	0.003
C_{stock} (µM)	19963					19963					19963				
V_{stock} (µL)	1.00					1.00					1.00				
V_{sample} (µL)	400					400					400				
S_{sample}	0.052					0.068					0.063				
$S_{spiked\ sample}$	0.431					0.464					0.447				
$C_{Analyte}$ (µM)	6.85					8.63					8.20				
$C_{analyte\ average}$ (µM)	7.89														
$C_{analyte\ SD}$ (µM)	1.25														
Wavelength=245 nm															

Kinetic Solubility Results for **RK009**

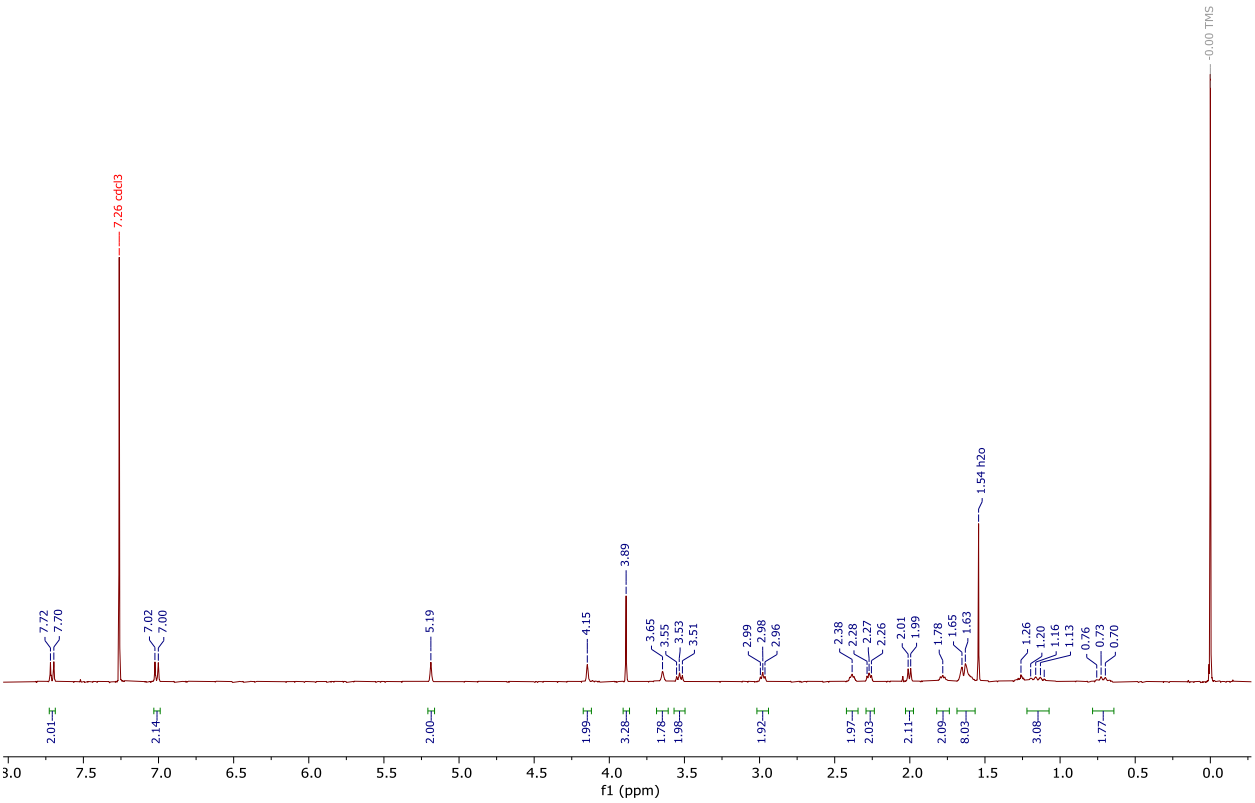

^{1}H NMR for **RK010**

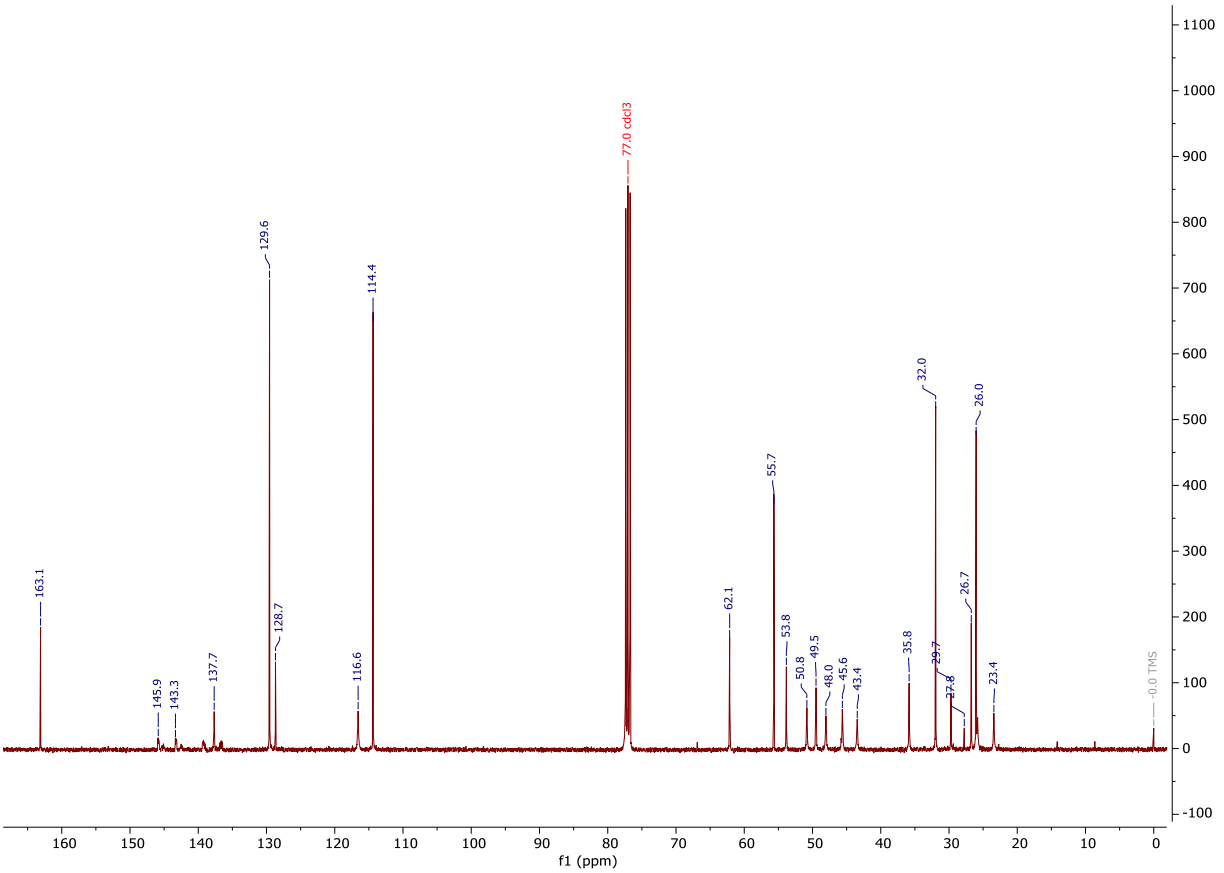

^{13}C NMR for **RK010**

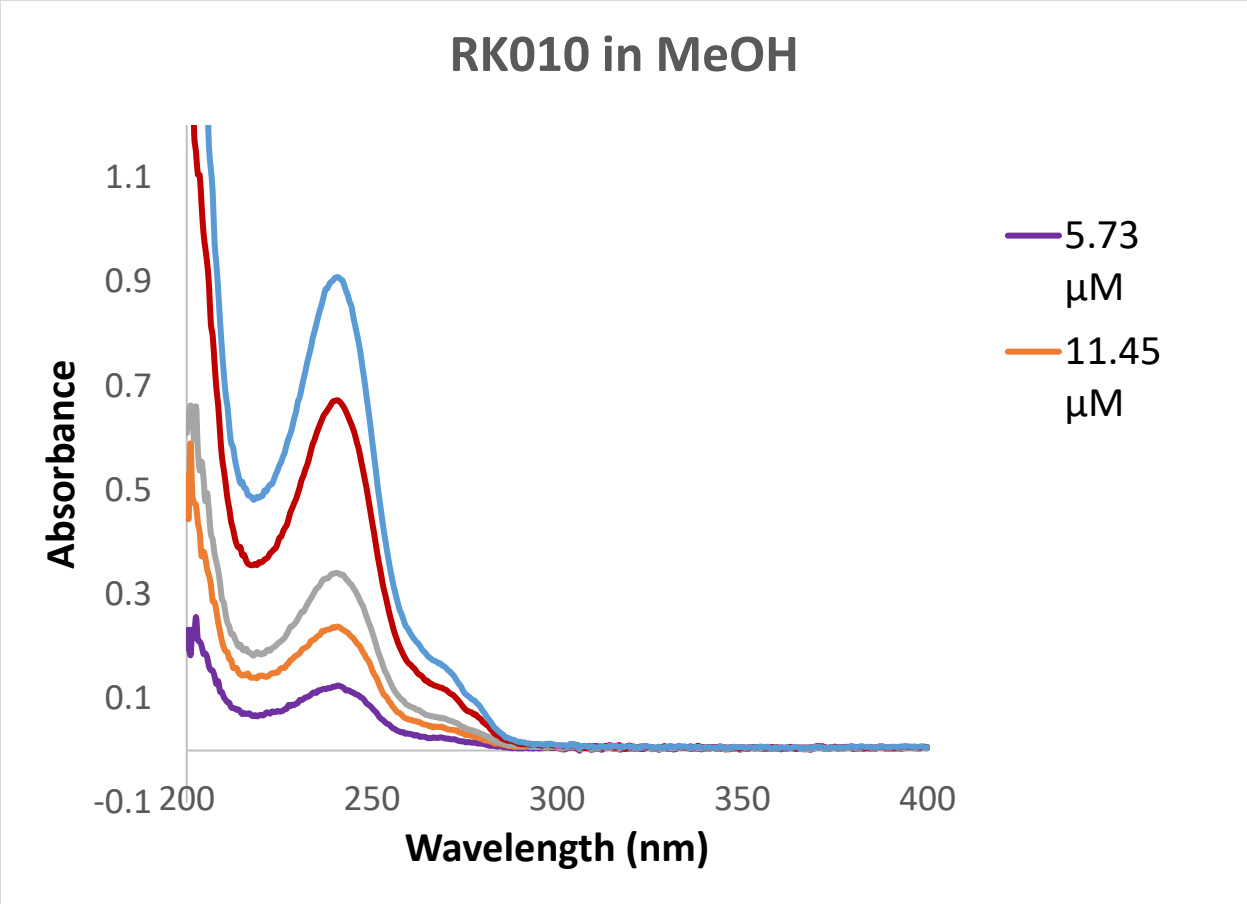

UV Absorption Spectra for **RK010**

Trial	1					2					3				
Measurement	1st	2nd	3rd	average	sd	1st	2nd	3rd	average	sd	1st	2nd	3rd	average	sd
$Abs_{(Blank)}$	0.132	0.131	0.134	0.132	0.002	0.132	0.131	0.134	0.132	0.002	0.132	0.131	0.134	0.132	0.002
$Abs_{(spiking\ soln)}$	0.187	0.183	0.19	0.187	0.004	0.185	0.2	0.189	0.191	0.008	0.177	0.18	0.185	0.181	0.004
$Abs_{(sample)}$	0.175	0.18	0.188	0.181	0.007	0.18	0.18	0.176	0.179	0.002	0.184	0.177	0.18	0.180	0.004
$Abs_{(spiked\ sample)}$	0.305	0.31	0.308	0.308	0.003	0.293	0.297	0.301	0.297	0.004	0.297	0.3	0.283	0.293	0.009
C_{stock} (µM)	19992					19992					19992				
V_{stock} (µL)	0.40					0.40					0.40				
V_{sample} (µL)	400					400					400				
S_{sample}	0.049					0.046					0.048				
$S_{spiked\ sample}$	0.175					0.165					0.161				
$C_{Analyte}$ (µM)	7.68					7.83					8.49				
$C_{analyte\ average}$ (µM)	8.00														
$C_{analyte\ SD}$ (µM)	0.43														
Wavelength = 241 nm															

Kinetic Solubility Results for **RK010**

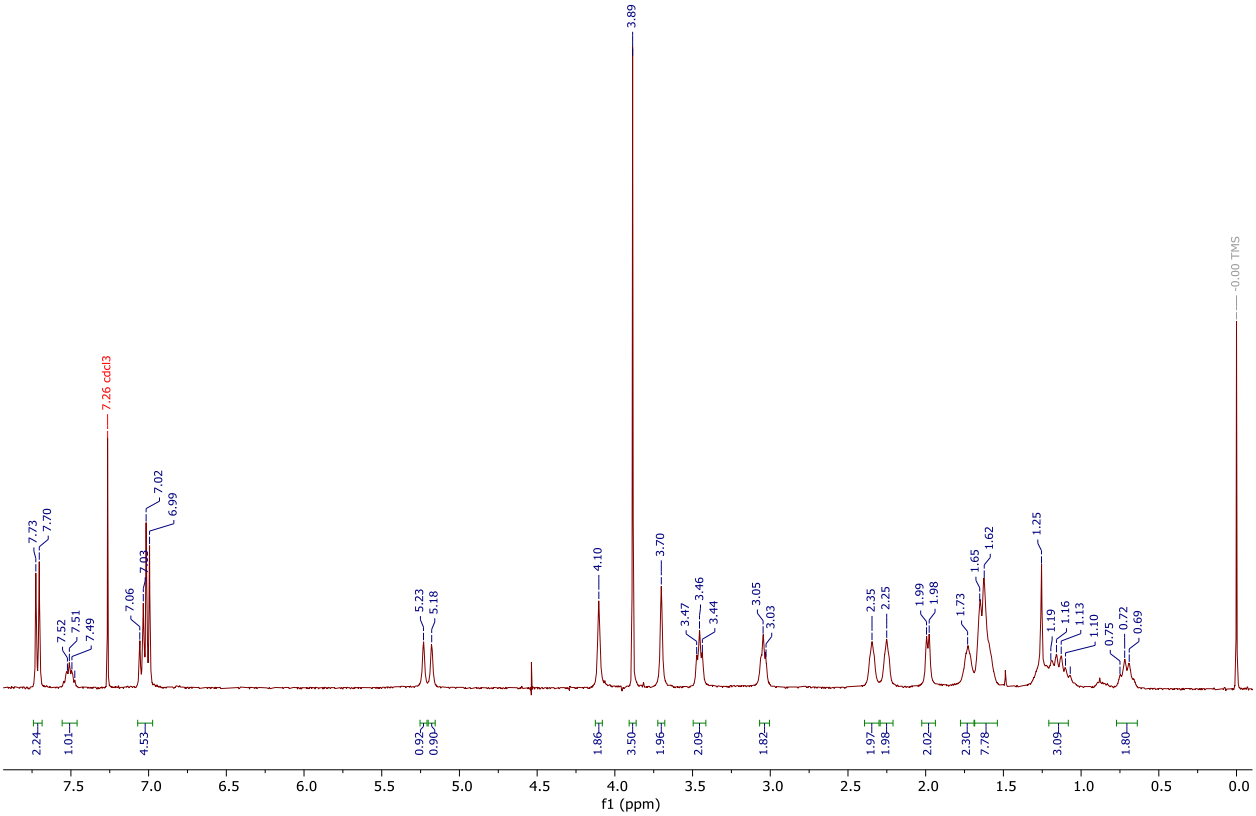

^{1}H NMR for **RK012**

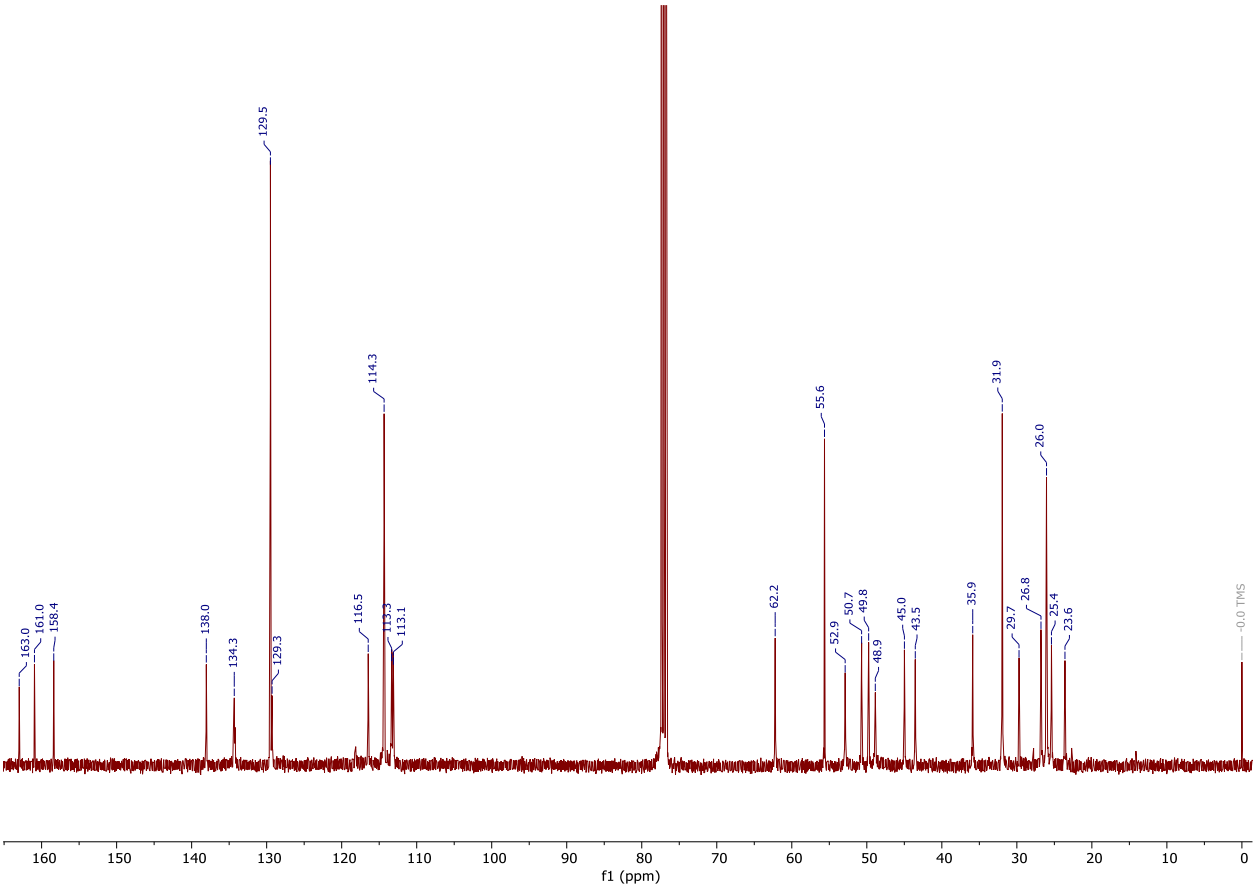

^{13}C NMR for **RK012**

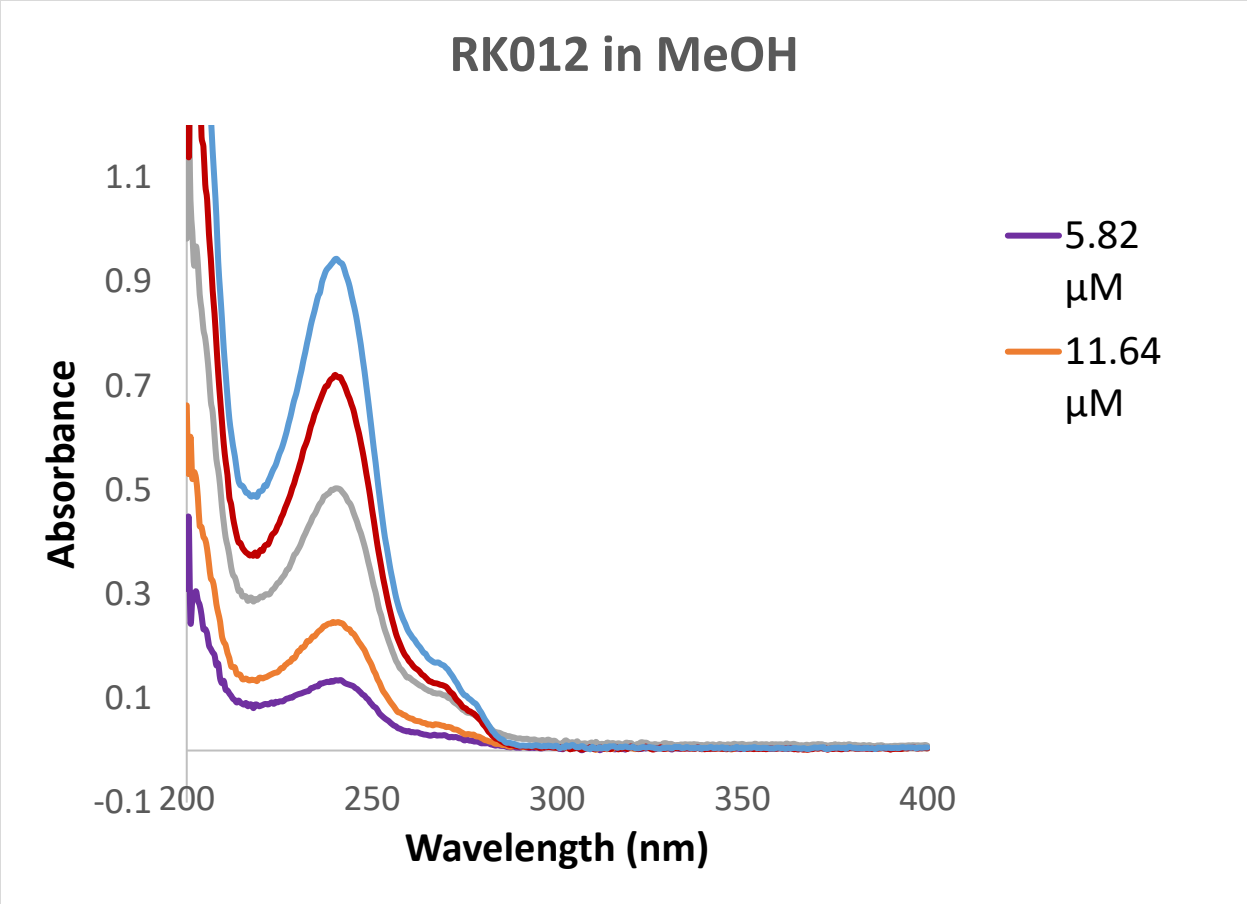

UV Absorption Spectra for **RK012**

Trial	1					2					3				
Measurement	1st	2nd	3rd	average	sd	1st	2nd	3rd	average	sd	1st	2nd	3rd	average	sd
$Abs_{(Blank)}$	0.135	0.135	0.14	0.137	0.003	0.135	0.135	0.14	0.137	0.003	0.135	0.135	0.14	0.137	0.003
$Abs_{(spiking\ soln)}$	0.268	0.283	0.285	0.279	0.009	0.287	0.289	0.292	0.289	0.003	0.244	0.241	0.25	0.245	0.005
$Abs_{(sample)}$	0.177	0.179	0.176	0.177	0.002	0.182	0.183	0.182	0.182	0.001	0.176	0.179	0.179	0.178	0.002
$Abs_{(spiked\ sample)}$	0.357	0.354	0.358	0.356	0.002	0.363	0.368	0.366	0.366	0.003	0.349	0.353	0.355	0.352	0.003
C_{stock} (µM)	19998					19998					19998				
V_{stock} (µL)	0.40					0.40					0.40				
V_{sample} (µL)	400					400					400				
S_{sample}	0.041					0.046					0.041				
$S_{spiked\ sample}$	0.220					0.229					0.216				
$C_{Analyte}$ (µM)	4.54					4.98					4.74				
$C_{analyte\ average}$ (µM)	4.76														
$C_{analyte\ SD}$ (µM)	0.22														
Wavelength = 241 nm															

Kinetic Solubility Results for **RK012**